AD-A031 464 ADAPTRONICS INC MCLEAN VA F/G 20/1
ADAPTIVE NONLINEAR SIGNAL PROCESSING FOR CHARACTERIZATION OF UL--ETC(U)
JUN 76 R SHANKAR, A N MUCCIARDI, D CLEVELAND F33615-74-C-5122
UNCLASSIFIED 687 AFML-TR-76-44 NL

1 OF 2
AD A031464



AD A031464

AFML-TR-76-44

(12)
B.S.

ADAPTIVE NONLINEAR SIGNAL PROCESSING FOR CHARACTERIZATION OF ULTRASONIC NDE WAVEFORMS
TASK 2: MEASUREMENT OF SUBSURFACE FATIGUE CRACK SIZE

ADAPTRONICS, INC.
WESTGATE RESEARCH PARK
7700 OLD SPRINGHOUSE ROAD
MCLEAN, VIRGINIA 22101

BABCOCK&WILCOX, INC.
LYNCHBURG RESEARCH CENTER
LYNCHBURG, VIRGINIA

APRIL 1976

TECHNICAL REPORT AFML-TR-76-44
FINAL REPORT FOR PERIOD 1 MAY 1974 - 1 SEPTEMBER 1975

Approved for public release; distribution unlimited

DDC
RECEIVED
NOV 2 1976
B

AIR FORCE MATERIALS LABORATORY
AIR FORCE WRIGHT AERONAUTICAL LABORATORIES
AIR FORCE SYSTEMS COMMAND
WRIGHT-PATTERSON AIR FORCE BASE, OHIO 45433

NOTICE

When Government drawings, specifications, or other data are used for any purpose other than in connection with a definitely related Government procurement operation, the United States Government thereby incurs no responsibility nor any obligtation whatsoever; and the fact that the government may have formulated, furnished, or in any way supplied the said drawings, specifications, or other data, is not to be regarded by implication or otherwise as in any manner licensing the holder or any other person or corporation, or conveying any rights or permission to manufacture, use, or sell any patented invention that may in any way be related thereto.

This report has been reviewed by the Information Office (OI) and is releasable to the National Technical Information Service (NTIS). At NTIS, it will be available to the general public, including foreign nations.

This technical report has been reviewed and is approved for publication.

Michael J. Buckley

MICHAEL J. BUCKLEY
Project Monitor

DONALD M. FORNEY, JR., ACTG CHIEF
NONDESTRUCTIVE EVALUATION BRANCH
METALS AND CERAMICS DIVISION

Copies of this report should not be returned unless return is required by security considerations, contractual obligations, or notice on a specific document.

AIR FORCE - 17 SEPTEMBER 76 - 400

UNCLASSIFIED

SECURITY CLASSIFICATION OF THIS PAGE (When Data Entered)

REPORT DOCUMENTATION PAGE

READ INSTRUCTIONS BEFORE COMPLETING FORM

1. REPORT NUMBER: AFML-TR-76-44	2. GOVT ACCESSION NO.
3. RECIPIENT'S CATALOG NUMBER	
4. TITLE (and Subtitle): ADAPTIVE NONLINEAR SIGNAL PROCESSING FOR CHARACTERIZATION OF ULTRASONIC NDE WAVEFORMS, TASK 2: MEASUREMENT OF SUBSURFACE FATIGUE CRACK SIZE.	5. TYPE OF REPORT & PERIOD COVERED: Final Technical Report 5/1/74 - 9/30/75
	6. PERFORMING ORG. REPORT NUMBER: 687
7. AUTHOR(s): Ramesh Shankar, Anthony N. Mucciardi, Ph.D., Dixon Cleveland, William E. Lawrie, Henry L. Reeves	8. CONTRACT OR GRANT NUMBER(s): F33615-74-C-5122
9. PERFORMING ORGANIZATION NAME AND ADDRESS: ADAPTRONICS, INC. Westgate Research Park 7700 Old Springhouse Road McLean, Virginia 22101	10. PROGRAM ELEMENT, PROJECT, TASK AREA & WORK UNIT NUMBERS: Project 7351 Task 73510942
11. CONTROLLING OFFICE NAME AND ADDRESS: Air Force Systems Command Aeronautical Systems Division/PPMRA Wright-Patterson AFB, Ohio 45433	12. REPORT DATE: June 1976
	13. NUMBER OF PAGES: 164 (Incl. Appendices)
14. MONITORING AGENCY NAME & ADDRESS (if different from Controlling Office): Final technical rept. 1 May 74 - 1 Sep 75 Com t p iii	15. SECURITY CLASS. (of this report): UNCLASSIFIED
	15a. DECLASSIFICATION/DOWNGRADING SCHEDULE

16. DISTRIBUTION STATEMENT (of this Report): AF-7351

Approved for public release; distribution unlimited

165p. 7351Ø9

17. DISTRIBUTION STATEMENT (of the abstract entered in Block 20, if different from Report)

18. SUPPLEMENTARY NOTES

19. KEY WORDS (Continue on reverse side if necessary and identify by block number)

Nondestructive evaluation; nondestructive testing; ultrasonics; nonlinear signal processing; fastener hole; fatigue crack; pulse echo; waveform parameterization; adaptive learning network; pattern recognition; pattern classification; power spectrum; cepstrum; deconvolution.

20. ABSTRACT (Continue on reverse side if necessary and identify by block number)

A new NDE nonlinear signal processing system has been developed to detect and measure small, subsurface fastener hole fatigue cracks. The system synthesized from nondestructive evaluation (NDE) waveform parameter inputs is capable of detecting and measuring quantitatively subsurface fatigue cracks in the size range of 0 to 279 mils to within 70 percent of their nominally characterized lengths. Previous investigations had achieved

(over)

DD FORM 1 JAN 73 1473 EDITION OF 1 NOV 55 IS OBSOLETE

UNCLASSIFIED

SECURITY CLASSIFICATION OF THIS PAGE (When Data Entered)

003 350 AB

a 50 percent detection rate for cracks larger than 30 mils, and no detection capability for cracks smaller than 30 mils. However, the fatigue crack measurement system reported herein is the first known fatigue crack NDE system capable of detection and measurement for this wide range.

The NDE waveforms were recorded from sixteen aluminum sample specimen cracks under two different experimental conditions. Series 1 was recorded with the ultrasonic transducer wedge at 20 degrees to the plane of the material surface, and Series 2 with the wedge at 30 degrees. A 10 MHz transducer was used for both series.

The Air Force Materials Laboratory acceptable tolerance limits are ±10 mils for cracks nominally characterized less than 30 mils; ±20 mils for cracks greater than 30 mils but less than 100 mils; and ±40 mils for cracks greater than 100 mils. Eighty-one and two-tenths (81.2) percent (13 out of 16) of the sample specimens in Series 1, and 75 percent (12 out of 16) of the specimens in Series 2 nave been correctly classified within the proper tolerance limits. Overall, 78.1 percent (25 out of 32) were correctly classified for both series, in spite of the wide amplitude differences of crack signatures from the same specimen crack.

The major conclusion regarding this new NDE signal processing software system is that subsurface fatigue crack length can be accurately measured from the information contained in the ultrasonic NDE signature. In particular, cracks below 30 mils, heretofore undetectable, can be detected and measured with reasonable accuracy.

ACCESSION for
NTIS White Section ☒
DDC Buff Section ☐
UNANNOUNCED ☐
JUSTIFICATION
BY
DISTRIBUTION/AVAILABILITY CODES
Dist. AVAIL. and/or SPECIAL
A

FOREWORD

This final report documents the materials, methods, results, conclusions and recommendations of the second of two tasks of the project entitled "Research on Adaptive Nonlinear Signal Processing of Ultrasonic Waveforms" sponsored by the Air Force Materials Laboratory (AFML) and Air Force Avionics Laboratory (AFAL) under Contract Number F33615-74-C-5122, Project 7351 and Task 73510942. The research (Tasks I and II) was conducted during the period 5/1/74 to 9/1/75.

Dr. Anthony N. Mucciardi was the Project Manager and Mr. Ramesh Shankar was the Principal Investigator for Adaptronics, Inc., McLean, Virginia; Messrs. William E. Lawrie and Henry L. Reeves of Babcock and Wilcox Lynchburg Research Center, performed the experimental work and the data collection of the ultrasonic waveforms under subcontract to Adaptronics. Section 5 of this report was written by Messrs. Lawrie and Reeves. The fatigue crack specimens were prepared by Metcut Research Associates, Cincinnati, Ohio, under subcontract to Adaptronics.

The authors are indebted to Mr. John Sanders of Adaptronics for his help during the program and to Mses. Linda Flickinger and Janice Sennett of the Adaptronics staff for editorial and typing assistance. Ms. Flickinger served as Contract Administrator.

The authors thank Dr. Michael J. Buckley, AFML/LLP, and Mr. Cecil W. Gwinn, AFAL/DHE-1, for their guidance throughout this project. Dr. Buckley was the Project Monitor. The authors thank him for his encouragement and for the freedom to investigate topics that arose as a natural consequence of conducting a broad and comprehensive research project. Special thanks are due Dr. Buckley, Mr. Gwinn, Dr. Steve Crist, formerly of AFML, and the late Dr. Harry Kirkpatrick for introducing this methodological approach to the NDE field. The results of this project -- ability to detect and measure accurately fatigue cracks over a range of 0 to 279 mils -- justify their foresight.

This report was submitted to the Air Force Materials Laboratory in April, 1976.

TABLE OF CONTENTS

		Page
1.	SUMMARY OF MAJOR RESULTS AND CONCLUSIONS	1
2.	INTRODUCTION	9
	2.1 Objectives	9
	2.2 Report Organization	10
3.	PREPARATION OF FATIGUE CRACK SPECIMENS	11
4.	SUBSURFACE FATIGUE CRACK DETECTION PROCEDURES	19
	4.1 Methods of Crack Detection	19
	4.2 Choice of Ultrasonic Frequencies	20
	4.3 Experimental Arrangement	21
	4.4 Circular Scanning of the Defect	23
5.	DATA COLLECTION PROTOCOL	33
	5.1 Objective	33
	5.2 Design of the Ultrasonic Experiments	33
	5.3 Selection of Ultrasonic Equipment	34
	5.4 Data Acquisition System	36
	5.5 Signal Averaging	40
	5.6 Test Data Listings	42
	5.7 Reproducibility of Test Data	42
6.	THEORETICAL AND PRACTICAL CONSIDERATIONS OF PULSE ECHO WAVEFORM PREPROCESSING	45
	6.1 Introduction	45
	6.2 Mathematical Development	45
	6.3 Deconvolution of Pulse Echo Signals	50
	6.4 Cepstral Analysis	54
	6.5 The Spatial Transform	59
	6.6 Summary and Discussion	68
7.	PULSE ECHO WAVEFORM PARAMETERIZATION	71
8.	SYNTHESIS AND PERFORMANCE OF ADAPTIVE LEARNING NETWORK (ALN) SUBSURFACE FATIGUE CRACK MEASUREMENT MODEL	77
	8.1 ALN Synthesis Procedure	77
	8.2 Resultant ALN Subsurface Fatigue Crack Measurement Model	82
	8.3 Discussion of Results	85
	8.4 Characteristics of ALN Crack Measurement Model.	88

PRECEDING PAGE BLANK-NOT FILMED

9. RECOMMENDATIONS 91

10. REFERENCES 95

APPENDICES

A - Preparation of Fatigue Cracked Fastener Specimens A-1

B - Ultrasonic Test Data Listed by Test Number B-1

Ultrasonic Test Data Listed by Sample Number B-13

C - Amplitude Versus Time Plots of Series 1 and 2 Data C-1

TABLES

Table		Page
3.1	Crack Lengths of Specimens	12
3.2	Relation of Observed Crack Length to Actual Surface Length and Bore Depth	16
7.1	ALN Input Parameters	73
7.2	Parameter List Used as Input to the ALN Fatigue Estimation Crack Model	74
8.1	Distribution of the 192 Data Records Among the Three Data Subsets	78
8.2	Performance of ALN Model in Measuring Crack Size from Ultrasonic NDE Waveform Parameters	86
8.3	Crack Length Sensitivity to Changes in NDE Ultrasonic Parameters	[illegible]

FIGURES

Figure		Page
1.1	Ultrasonic Waveforms Recorded from Two Sample Specimen Cracks Under Different Test Conditions .	2
1.2	Performance of ALN Quantitative Surface/ Subsurface Fatigue Crack Length Measurement System	3
1.3	Reliability of NDE Crack Detection System	5
3.1	Fatigue Crack Specimen Configuration	13
3.2	Precracking Fixture Loaded with Specimen	14
3.3	Photomicrographs of Fatigue Crack Depth at Magnification of 10X	17
4.1	Simplified View of the Ultrasonic Test Procedure .	22
4.2	Illustration of Interference Effects as Function of Transducer Viewing Angle	24
4.3	Fatigue Crack Ultrasonic Recording Equipment . . .	26
4.4	Schematic of Crack Reflection Geometry	28
4.5	Fatigue Crack NDE Waveforms Recorded from Four Specimens at Six Viewing Angles	30
4.6	Response from 14-192 Specimen Viewed at $\theta = 0^{o}$ . .	31
5.1	Block Diagram of Ultrasonic Waveform Acquisition System	35
5.2	Transducers & Wedges Used for Ultrasonic Data Acquisition	37
5.3	Mechanical Fixture to Rotate Transducer About Fastener	37
5.4	Coordinate System for Transducer Location and Orientation	38
5.5	Heading Information Format	39
5.6	Signal-to-Noise Ratio Enhancement Obtained by Signal Averaging	41
6.1	Linear System Model of Reflection from Sub-surface Defects	46
6.2	Schematic of Deconvolution of Crack Response From a Reference Signal	52
6.3	Deconvolution of 279 mil crack (viewed at 0^{o}) From a Reference Signal	53
6.4	Crack Response Under Different Transducer Conditions	57

FIGURES (Continued)

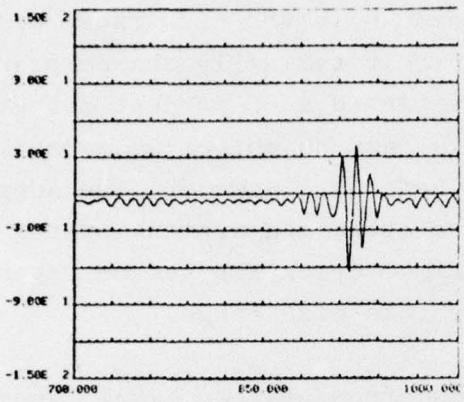
Figure		Page
6.5	Waveform Preprocessing for 279 Mil Crack	58
6.6	Illustration of High Frequency Impersonating a Low Frequency	66
6.7	Plot of Deconvolved Total Spectral Energy Versus Crack Length	69
7.1	Fatigue Crack Length Signal Preprocessing Steps .	76
8.1	Quantitative Surface/Subsurface Fatigue Crack Length Measurement System	80
8.2	ALN Subsurface Fatigue Crack Measurement Model. .	84
8.3	Performance of ALN Quantitative Surface/Subsurface Fatigue Crack Length Measurement System	87

1. SUMMARY OF MAJOR RESULTS AND CONCLUSIONS

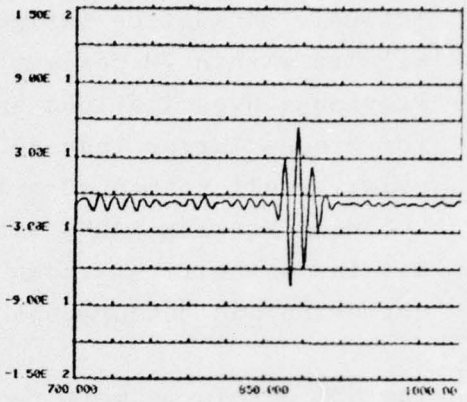
A quantitative subsurface fatigue crack measurement system has been synthesized from nondestructive evaluation (NDE) waveform parameter inputs and is capable of detecting and measuring quantitatively subsurface fatigue cracks in the size range of 0 to 279 mils to within 70 percent of their nominally characterized lengths. Previous investigations had achieved a 50 percent detection rate for cracks larger than 30 mils, and no detection capability for cracks smaller than 30 mils (Ref. 3). However, the Adaptive Learning Network (ALN) fatigue crack measurement system reported herein is the first known fatigue crack NDE system capable of detection and measurement for this wide range.

The NDE waveforms were recorded from sixteen sample specimen fastener hole fatigue cracks under two different experimental conditions. Series 1 was recorded with the ultrasonic transducer wedge at 20 degrees to the plane of the material surface, and Series 2 with the wedge at 30 degrees. Figure 1.1 illustrates the diversity of responses observed between Series 1 and 2. In Series 1 (Figure 1.1(a)), the signature from a 93 mil crack has a larger amplitude than the one from a 192 mil crack. In Series 2, (Figure 1.1(b)), the reverse is true. Among the four signatures in the figure, the 93 mil crack for Series 1 has the largest amplitude, followed by 192 mils for Series 2, 192 mils for Series 1, and lastly, 93 mils for Series 2. If amplitude were the determining factor (as it was in previous investigations), serious errors would be committed in resolving crack sizes under different recording conditions.

Figure 1.2 is a plot of the measured crack size, by the ALN system, and its nominally characterized length for the two series of experiments. The AFML accepted tolerance limits are $\pm$10 mils for cracks nominally characterized less than 30 mils; $\pm$20 mils for cracks greater than 30 mils but less than 100 mils; and $\pm$40 mils for cracks greater than 100 mils. Eighty-one and two-tenths (81.2) percent (13 out of 16) of the sample specimens in Series 1, and 75 percent (12 out of 16) of the specimens in Series 2 are

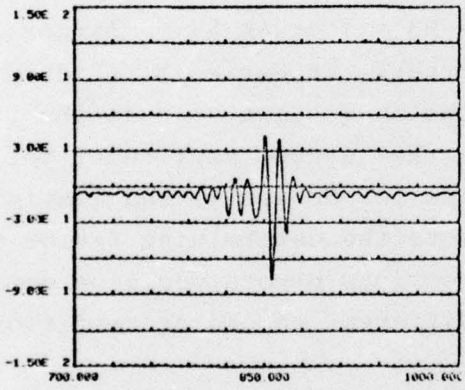


192 Mils

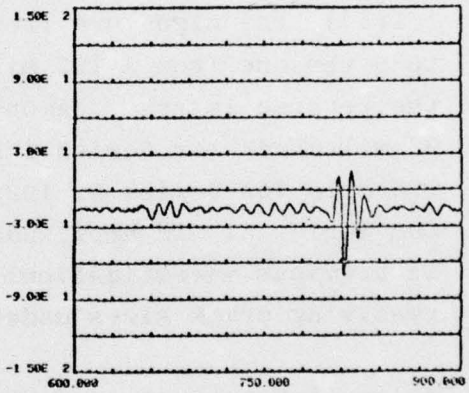


93 Mils

Figure 1.1(a): SERIES 1: 192 and 93 mil crack signatures. Note the larger amplitude of the 93 mil crack. 1/



192 Mils



93 Mils

Figure 1.1(b): SERIES 2: 192 and 93 mil signatures. 93 mil crack signature is considerably smaller.

1/ The abscissa of each plot is time (μsec) and the ordinate is signal amplitude (arbitrary units).

FIGURE 1.1: ULTRASONIC WAVEFORMS RECORDED FROM TWO SAMPLE SPECIMEN CRACKS UNDER DIFFERENT TEST CONDITIONS

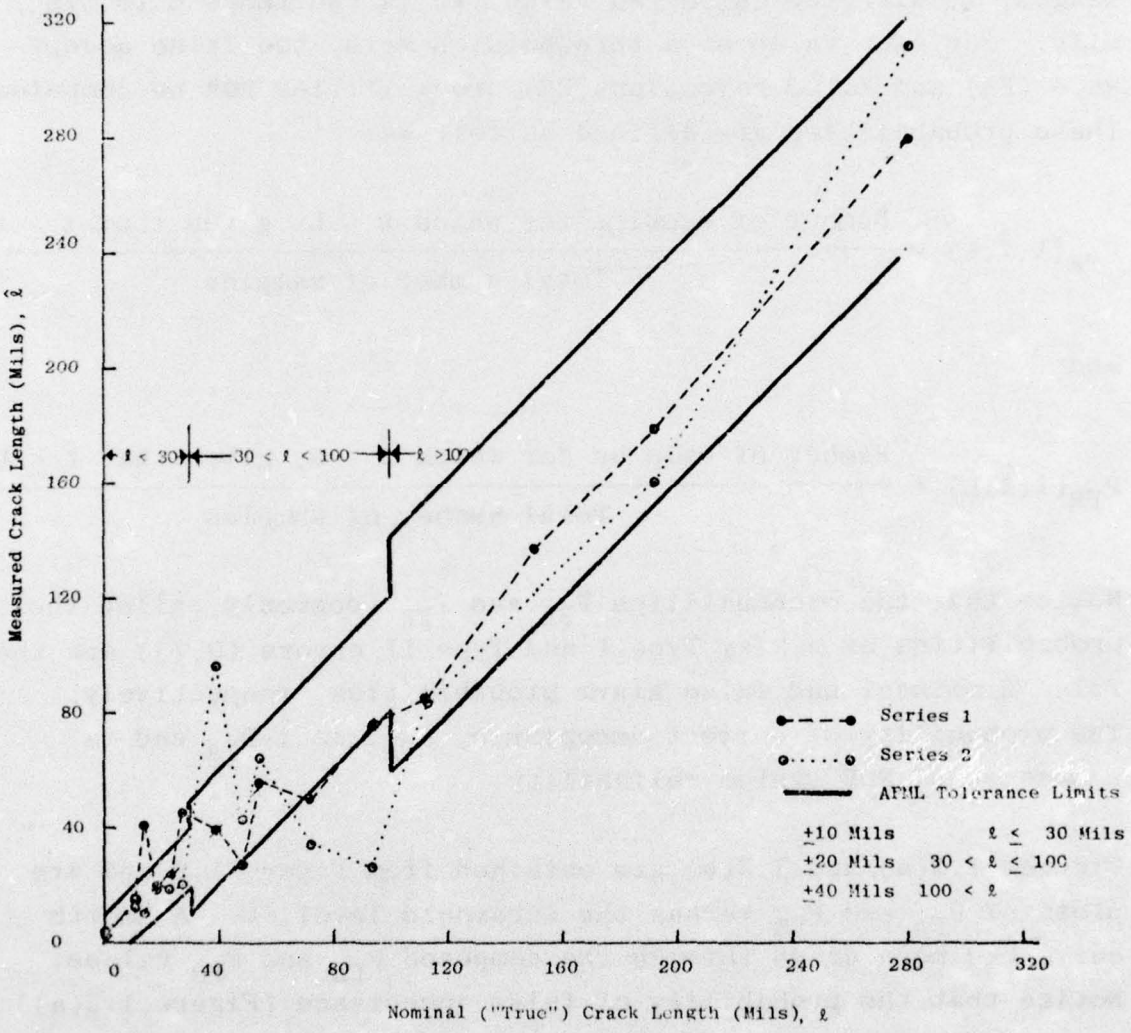


FIGURE 1.2: PERFORMANCE OF ALN QUANTITATIVE SURFACE/SUBSURFACE FATIGUE CRACK LENGTH MEASUREMENT SYSTEM

correctly classified within the proper tolerance limits. Overall 78.1 percent (25 out 32) were correctly classified for both series, in spite of the wide amplitude differences of crack signatures from the same specimen crack.

Another way of assessing the performance of this system is to compare probabilistically the nominally characterized crack length, ℓ, with the estimated value, $\hat{\ell}$, in the range 0 to 279 mils. For each value of a threshold, L mils, the false acceptance (FA) and false rejection (FR) probabilities can be computed. These probabilities are defined as follows:

$$P_{FA}(\ell,\hat{\ell},L) = \frac{\text{Number of samples for which } \hat{\ell} < L, \text{ given that } \ell \geq L}{\text{Total number of samples}}$$

and

$$P_{FR}(\ell,\hat{\ell},L) = \frac{\text{Number of samples for which } \hat{\ell} > L, \text{ given that } \ell \leq L}{\text{Total number of samples}}$$

Notice that the probabilities P_{FA} and P_{FR} (commonly called the probabilities of making Type I and Type II errors (3,7)) are the false dismissal and false alarm probabilities, respectively. The probability of correct acceptance, P_{CA}, is $1-P_{FA}$ and is a measure of NDE system reliability.

Figures 1.3(a) and 1.3(b) are obtained from Figure 1.2 and are plots of P_{FA} and P_{FR} versus the threshold level, L. A smooth curve has been drawn through the computed P_{FA} and P_{FR} values. Notice that the probability of false acceptance (Figure 1.3(a)) is approximately 15 percent for a 30 mil threshold crack and progressively decreases. Current NDE systems cannot detect

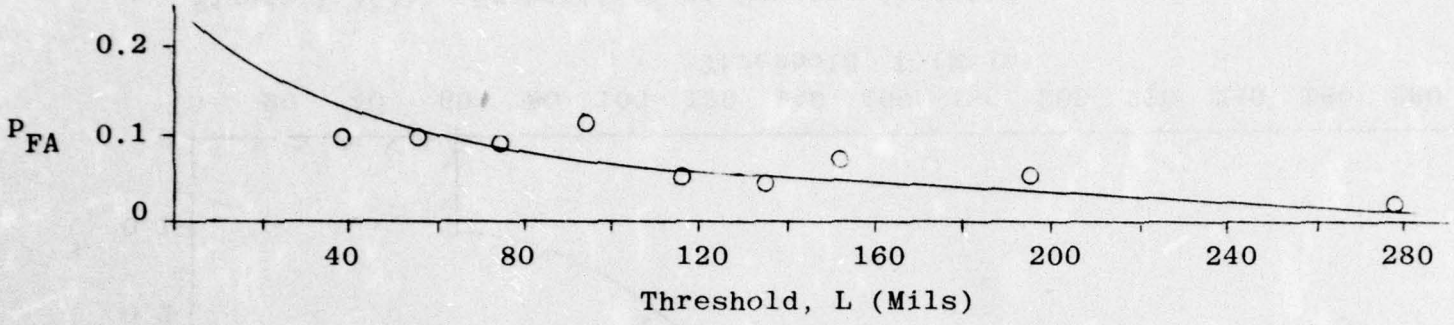


Figure 1.3(a): Probability of False Acceptance

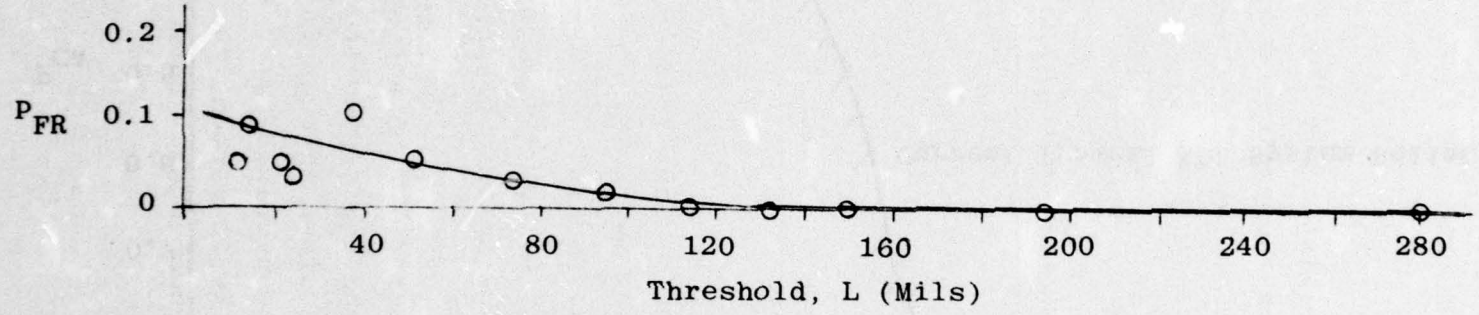


Figure 1.3(b): Probability of False Rejection

FIGURE 1.3: RELIABILITY OF NDE CRACK DETECTION SYSTEM

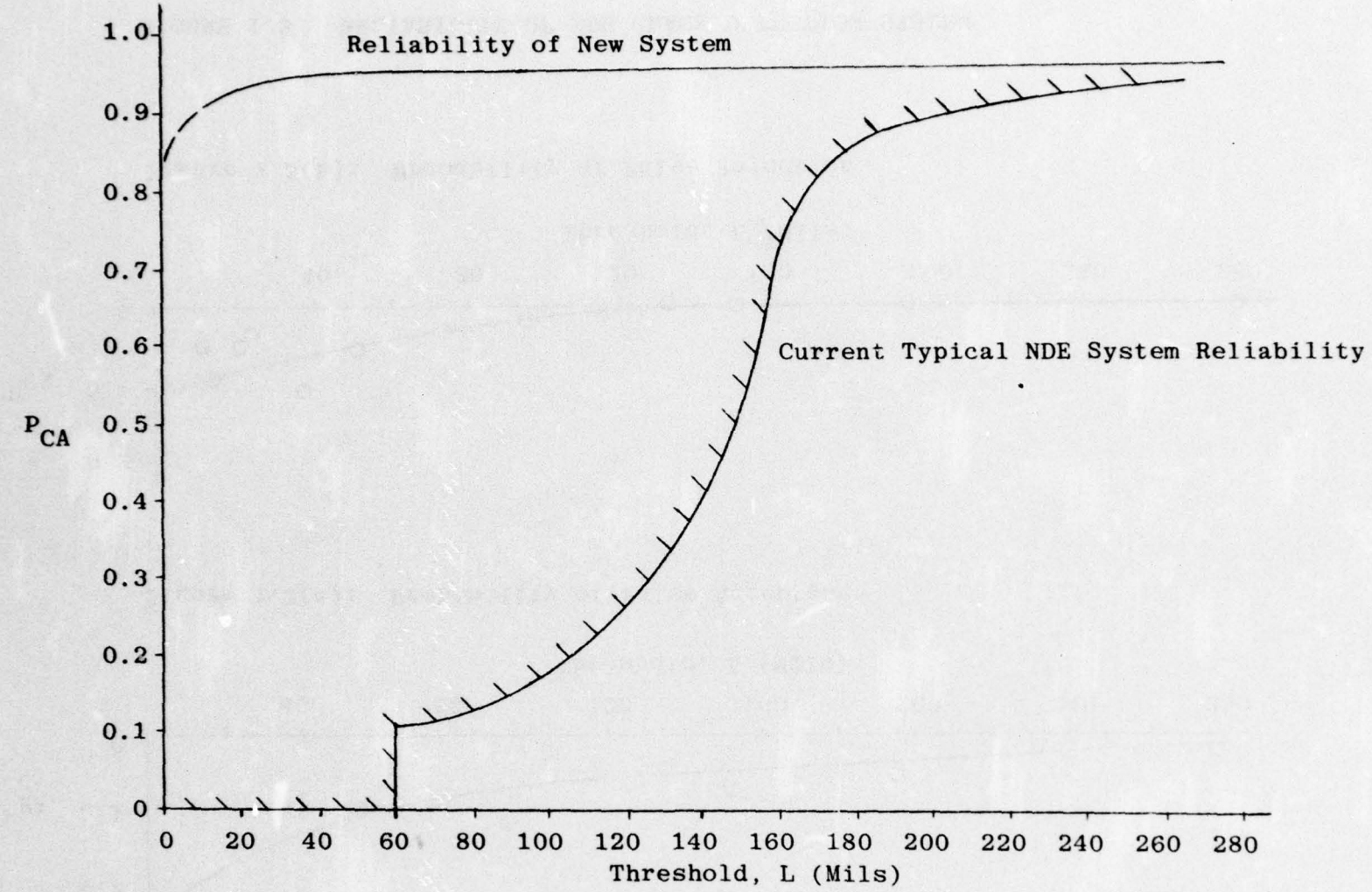


Figure 1.3(c): Probability of Correct Acceptance

FIGURE 1.3: (Continued)

cracks smaller than 30 mils. The probability of false rejection is never more than 11 percent for any crack -- irrespective of size. Finally, the probability of correct acceptance, P_{CA}, is plotted in Figure 1.3(c) for both the new system and the current typical NDE system. The new system is much more uniformly reliable.

In synthesizing the ALN system, sixteen of the 31 candidate ultrasonic parameter inputs were automatically selected by the ALN for identifying the crack length. The 16 parameters were derived from the power spectrum and cepstrum of the NDE amplitude versus time waveform. The fractional power in various bands in the spectrum and cepstrum as well as the overall shape of these two curves were found, as a group, to be key indicators of the crack length, although by themselves they are not capable of resolving its size.

An (incomplete) 16th-order polynomial in the input parameters was realized by the ALN model for measuring subsurface fatigue crack size. New ultrasonic data from unknown crack specimens can be preprocessed to generate the parameter inputs and used to interrogate, in software, the ALN in milliseconds to measure crack size.

The major conclusion is that subsurface fatigue crack length can be accurately measured from the information contained in the ultrasonic NDE signature. In particular, cracks below 30 mils, heretofore undetectable, can be detected and measured with reasonable accuracy.

2. INTRODUCTION

2.1 OBJECTIVES

The identification of subsurface fatigue cracks is an important and difficult problem in the nondestructive evaluation of materials. Such cracks are induced around fastener holes in materials and are known to grow rapidly if the shearing forces on the material exceed a certain threshold. Thus, it is important to identify fatigue cracks on aircraft parts, turbine blades, etc. to develop suitable countermeasures to increase the reliability of these systems.

The main objective of the second half of this program, Task II, was to demonstrate the capability for accurately measuring the size of subsurface fatigue cracks by using adaptive nonlinear signal processing techniques. The cracks, which were induced in aluminum sample blocks via fatigue loading, were ultrasonically tested and the reflected echo signals were available for analysis.

Ancillary objectives included:

- Quantitatively assessing the information content of ultrasonic waveforms relative to modeling the descriptors of crack geometry.
- Identifying the most discriminating subset of parameters derived from such NDE waveforms.
- Determining the sensitivity of the model to variations in the input parameters.

It was stated that the results would provide important information regarding the relationship between the best found ultrasonic NDE waveform parameters and the underlying physical phenomenona.

PRECEDING PAGE BLANK-NOT FILMED

2.2 REPORT ORGANIZATION

The remainder of this report has been divided into the following sections:

Section 3 - Describes the preparation of fatigue crack specimens.

Section 4 - Describes new techniques for the detection of subsurface fatigue cracks. A general philosophy of data collection procedures of ultrasonic waveforms reflected from subsurface fatigue cracks and their analysis is presented. The advantages of scanning the defect at different transducer viewing angles are explained.

Section 5 - Discusses the ultrasonic data collection protocol followed at the Lynchburg Research Center of Babcock & Wilcox under subcontract to Adaptronics, Inc. The data gathering, editing and verification of magnetic tape and computer copies prior to transmittal to Adaptronics are detailed.

Section 6 - Details the signal preprocessing steps performed on the ultrasonic pulse echo data. Both the theoretical aspects and practical limitations of linear signal processing techniques are described. A spatial transform is introduced which, in theory, can be useful in mapping the profile of the subsurface crack. The inability of these signal preprocessing techniques solely to estimate crack length is demonstrated.

Section 7 - Deals with the parameterization of the preprocessed waveforms to generate candidate inputs for the ALN nonlinear subsurface fatigue crack classifier. The reasons and methods for generating such parameters, based particularly on the material in Sections 4 and 6, are detailed.

Section 8 - Describes the synthesis and performance of the ALN classifier. The physical relationships between the synthesized parameter inputs and the crack size are presented.

Section 9 - Recommends research areas for future work.

3. PREPARATION OF FATIGUE CRACK SPECIMENS

Sixteen different sized cracks in aluminum sample specimens were prepared. Table 3.1 shows the size and area of each of the cracks. which ranged in size from 0 to 279 mils. The cracks were induced by creating a notch in the fastener hole and then fatiguing the material to cause crack growth. (See Appendix A for details.)

Crack length versus specimen identification is shown in Table 3.1. The cracked surface is identified in the bottom sketch. If the specimen is held in a manner so that the specimen number can be read, the crack will be on the lower surface. The first two digits of the five digit sample number are a specimen identification code and vary from 00 through 15. The last three digits indicate the size of the crack in mils. For example, 11-093 is specimen 11 in which the subsurface crack is nominally 93 mils in length.

To insure precracking location and to avoid double crack initiation, an EDM starter notch was used on all specimens except 15-279. The depth and width dimensions of the EDM notches are also given in Table 3.1.

The fatigue crack specimens were manufactured in conformance with ASTM Specification E127-64 from 5/8 x 3 inch 7075-T651 aluminum plate. The aluminum conforms to Federal Specification QQ-A-250/13 and was ultrasonically inspected as per American Aluminum Association FBH C1.AA 3/64 inch by Conam Inspection of Columbus, Ohio, a Division of Automation Industries, Inc. Certification of material as to mechanical property and ultrasonic inspection is given in Appendix A.

The specimens were low-stress ground on all surfaces with a single drilled and reamed hole located at one end. Specimen configuration is shown in Figure 3.1. Specimens were then loaded into the precracking fixture shown in Figure 3.2. The precracking

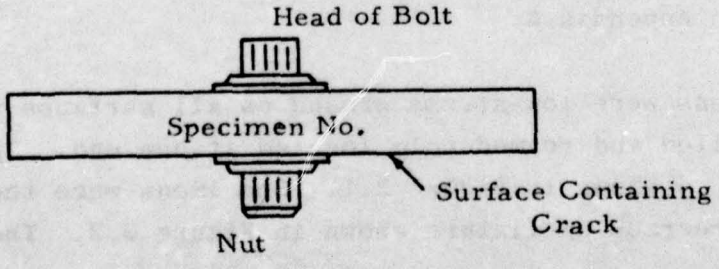
TABLE 3.1

CRACK LENGTHS OF SPECIMENS

Specimen No.	EDM Starter Notch Depth*	EDM Starter Notch Width**	Crack Length
00-000	---	---	0
01-000	---	---	0
02-011	.0026	.0022	.011
3-014	.0016	.0020	.014
4-018	.0016	.0019	.018
5-022	.0035	.0020	.022
6-027	.0020	.0020	.027
7-039	.0014	.0018	.039
8-048	.0019	.0020	.048
9-054	.0016	.0018	.054
10-073	.0019	.0021	.073
11-093	.0020	.0021	.093
12-113	.0024	.0019	.113
13-150	.0015	.0019	.150
14-192	.0017	.0018	.192
15-279	---	---	.279

* Depth along hole radius

** Width tangent to hole circumference



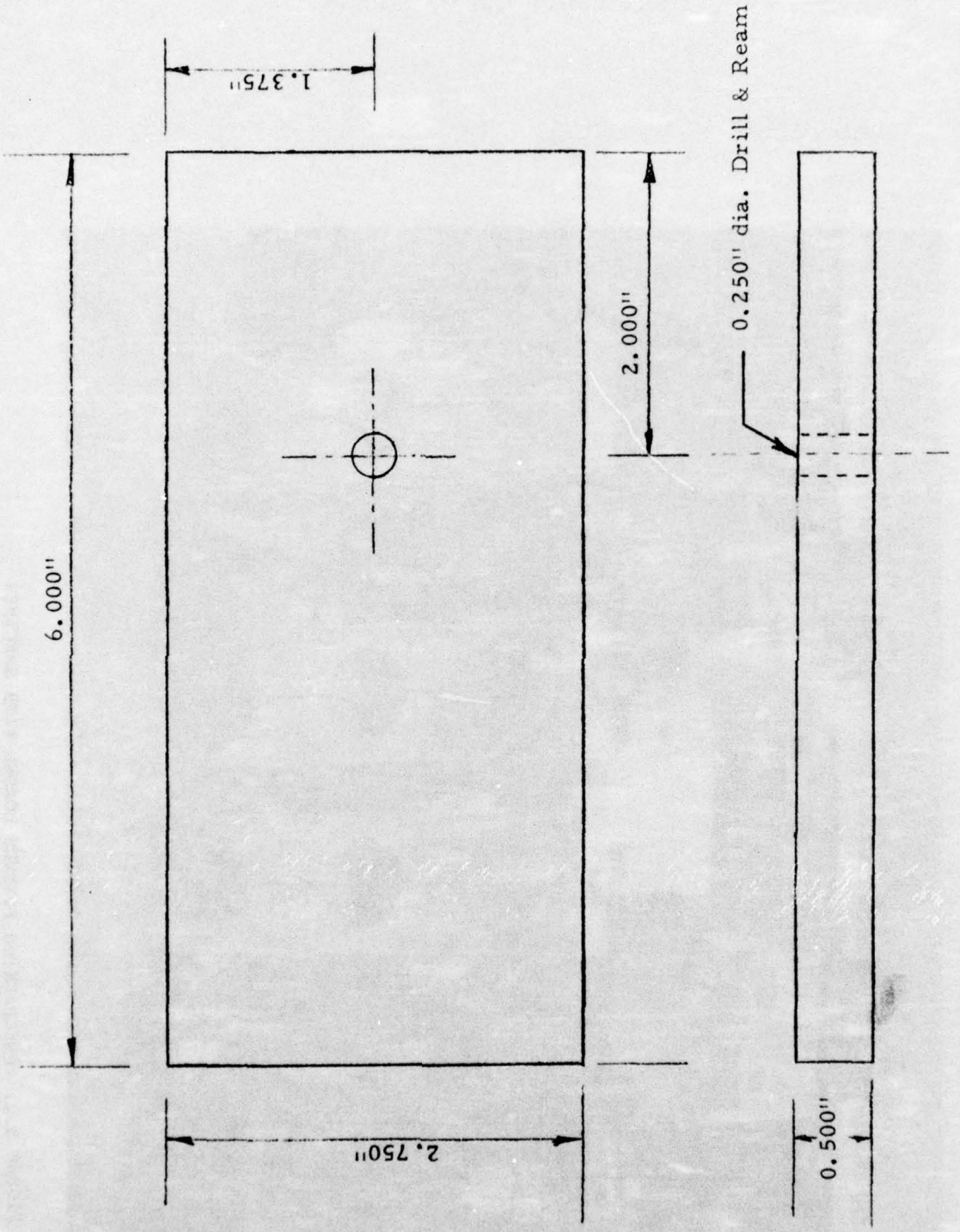


FIGURE 3.1: FATIGUE CRACK SPECIMEN CONFIGURATION

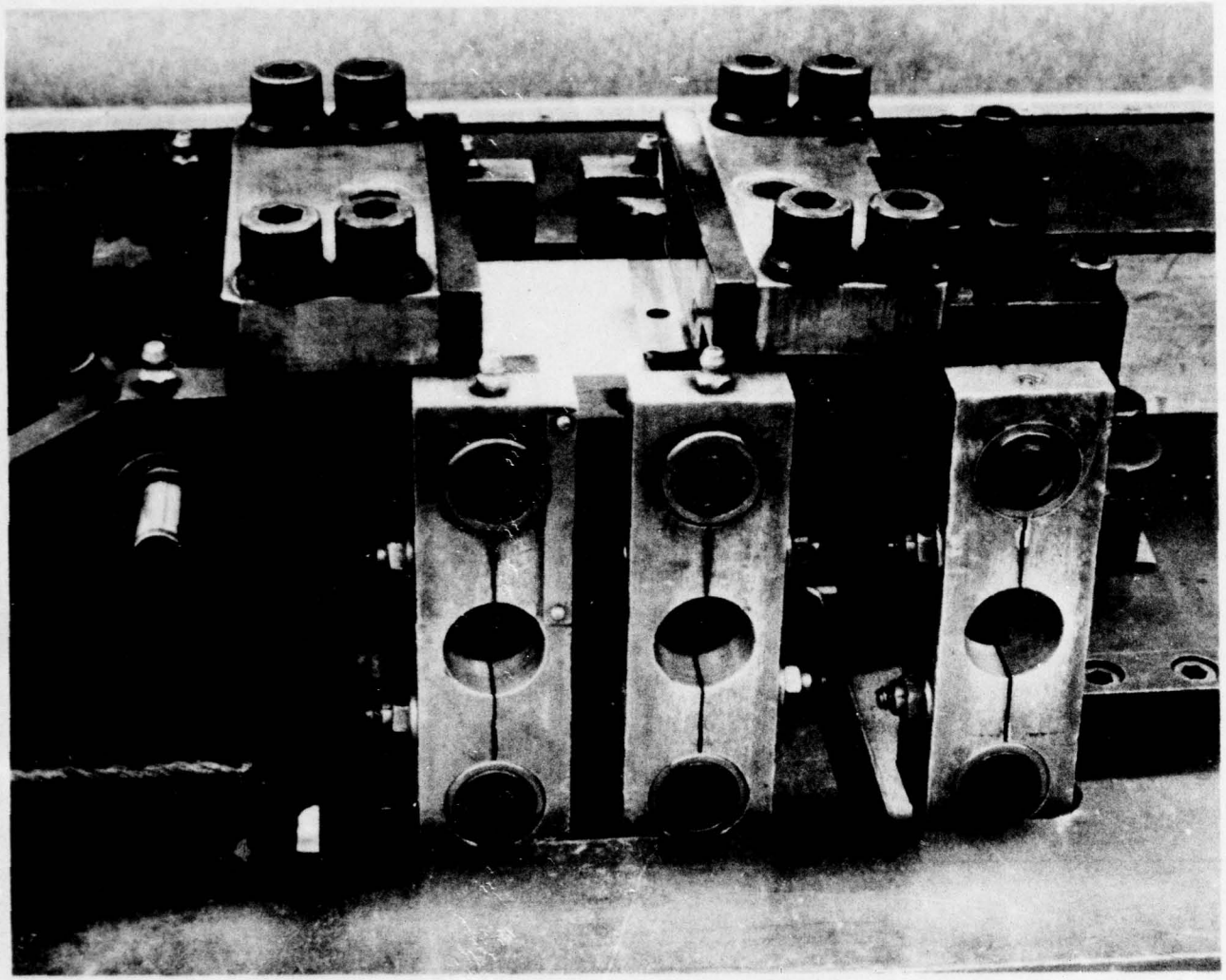


FIGURE 3.2: PRECRACKING FIXTURE LOADED WITH SPECIMEN

was performed in four-point bending on a SF01 Sonntag fatigue machine. This is a constant force machine and has a cycle ratio of 1800 cpm. The specimens were cycled at a surface bending stress of 20 ksi and a ratio of 0.90 (σdyn./σstat. = 0.9 percent). Crack initiation occurred between 20,000 and 50,000 cycles with no specimens requiring more than 400,000 cycles (initation plus growth).

One of the initial concerns in the manufacture of the specimens was to grow cracks with a length-to-depth ratio of approximately 1:1. To verify this ratio, four specimens were precracked and broken to observe the crack shape and also the relation of actual crack length to the observed crack length prior to failure. Table 3.2 gives the crack lengths for the four specimens and Figure 3.3 shows photographs of the crack area at a magnification of 10X.

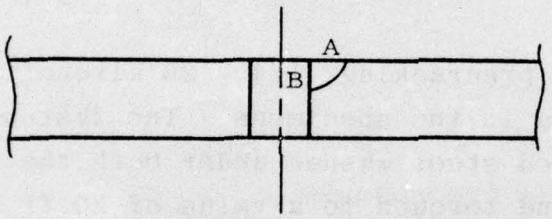
After manufacturing and precracking, 1/4 - 28 aircraft quality fasteners were installed in the specimens. The fasteners were installed with a hardened steel washer under both the nut and the head of the fastener, and torqued to a value of 20 ft.-lbs.

The sealant applied to the fastener assembly was a 3-M product -- EC-1675, Class B -- which is equivalent to MIL-S-8802. (A sketch of the installed fastener is shown at the bottom of Table 3.1.)

TABLE 3.2

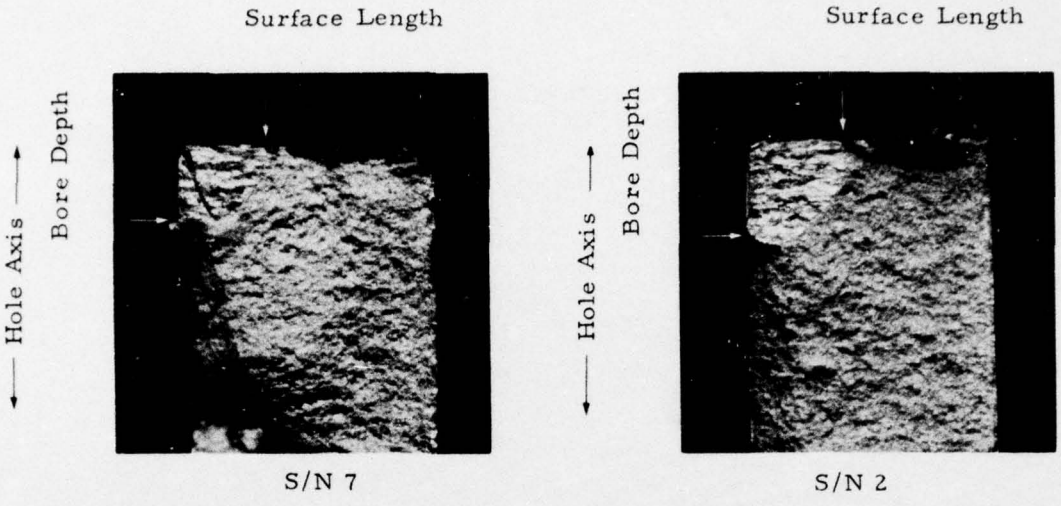
RELATION OF OBSERVED CRACK LENGTH
TO ACTUAL SURFACE LENGTH AND BORE DEPTH

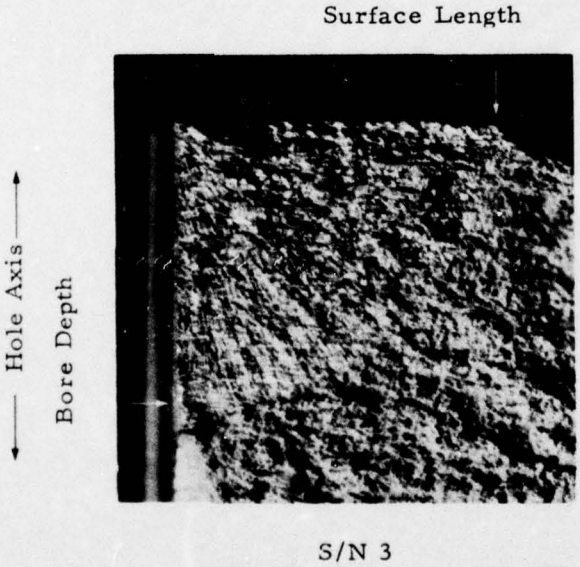
Specimen No.	Surface Crack Length (A) Observed on Surface	Surface Crack Length (A) After Failure	Bore Crack Length (B) After Specimen Failure
7	.057	.055	.035
2	.054	.060	.067
3	.197	.198	.180
10	.196	.201	.185



A = Surface Crack Length

B = Bore Crack Length





Ref. Table 3.2.

Mag. 10X

FIGURE 3.3: PHOTOMICROGRAPHS OF FATIGUE CRACK DEPTH AT MAGNIFICATION OF 10X.

4. SUBSURFACE FATIGUE CRACK DETECTION PROCEDURES

4.1 METHODS OF CRACK DETECTION

Modern techniques for detection of subsurface fatigue cracks in metals rely on the analyses of reflected ultrasonic signals from such defects. The procedure involves directing a beam of ultrasound from an electronic pulser and transducer (which converts electrical pulses to ultrasound) towards the defect and capturing the return signal. The absence of a return signal within a prescribed time interval, that is determined by the velocity of ultrasound in the material and the material thickness, indicates an absence of a defect. The defect acts as a discontinuity to the ultrasound beam and a fraction of its energy is reflected back to the transducer. The return signal constitutes a defect "signature." Assumptions usually made about the defect signature include:

- The larger the defect, the larger the signal amplitude.
- The frequency spectrum of the return signal has essentially the same characteristics as the transmitted signal.

Both of the above statements are subject to qualification (as pointed out in Section 6.5) but they have been key assumptions in previous investigations of the problem (e.g., Ref. 3, 4).

Previous approaches to this problem can be divided into two categories. The first is a linear systems approach. In this case, the return signal from a defect is viewed as a convolutional process between the intervening systems (i.e., transducer, medium and defect) and the transmit signal (Ref. 3, 4). The second is a phased-array approach in which the return signals from an array of transducers situated in the vicinity of the defect are reconstructed, either in software or hardware, to emphasize its characteristics. (Ref. 4).

PRECEDING PAGE BLANK-NOT FILMED

In this study a model was created relating subsurface fatigue crack size to certain parameters of its reflected ultrasonic signature. The crack size is modeled as a nonlinear combination of these parameters. The types of parameters extracted from these ultrasonic signatures were guided, in large part, from the linear systems theoretic point-of-view. For example, the power spectrum and its associated parameters were selected as inputs to the model because these are key indicators of crack size in the linear system analysis (see Section 6.1). Furthermore, ultrasonic signatures were obtained by viewing the defect from various transducer positions in the vicinity of the defect, similar to the phased-array approach of previous investigations. The parameters of these signatures were used to model crack size as a function of the transducer viewing angle.

4.2 CHOICE OF ULTRASONIC FREQUENCIES

Ultrasonic signals in the frequency range of 1 to 15 MHz were used because the associated wavelengths are comparable to the crack sizes being investigated. Assuming a shear wave velocity of 1.26×10^8 mils/second in aluminum, the wavelengths range from 8.4 to 126 mils, and the crack sizes in the sample set were from 0 to 279 mils. Therefore, the wavelength-to-defect size ratio is such that the defect acts as an impediment to the waves in the ultrasound beam and a fraction of its energy will be reflected back to the transducer.

The fraction of energy is functionally dependent on the wavelength, the crack geometry, and the properties of the medium. If the defect is "viewed" at any angle other than normal to its plane, interference effects will be manifested in the return signal spectrum. This is so because the reflections from the two edges of the defect will not arrive at the same instant of time,

and depending on the crack length, the transducer viewing angle, and the wavelength, the consequent phase relationship between the two reflected waves may lead to a constructive or destructive interference pattern. Furthermore, for any particular crack size and viewing angle, the interference effects will occur at multiple frequencies because of the existence of harmonics of those wavelengths for which phase cancellation or enhancement occurs.

4.3 EXPERIMENTAL ARRANGEMENT

A subsurface fatigue crack was assumed to be planar with grain boundaries no larger than the smallest wavelength in the ultrasonic input signal. The length-to-depth (aspect) ratio of the crack was assumed to be unity. (This was verified by destructive testing of specimen cracks discussed in Section 3.) Therefore, a subsurface fatigue crack can be considered a quarter circle planar defect adjacent to the fastener hole bore.

A simplified view of the ultrasonic test procedure is shown in Figure 4.1. It consists of a transducer mounted on a plastic wedge atop the material surface. The plastic wedge converts the longitudinal waves, generated by the transducer, into shear waves at the plastic wedge-metal surface interface. The beam is pointed into the material and toward the defect. The method of operation consists of directing an ultrasonic pulse towards the defect. After a certain time interval, the reflected signal is received at the transducer and is available for analysis.

The normal incident position of the transducer is defined to be in a plane perpendicular to the plane of the crack. In this position, the reflected waves from the two edges of the crack -- the inner edge toward the fastener hole and the outer edge -- arrive in phase at the transducer. This is true for all frequencies because of the normal incident position. Therefore the frequency spectrum of the return signal has essentially the same

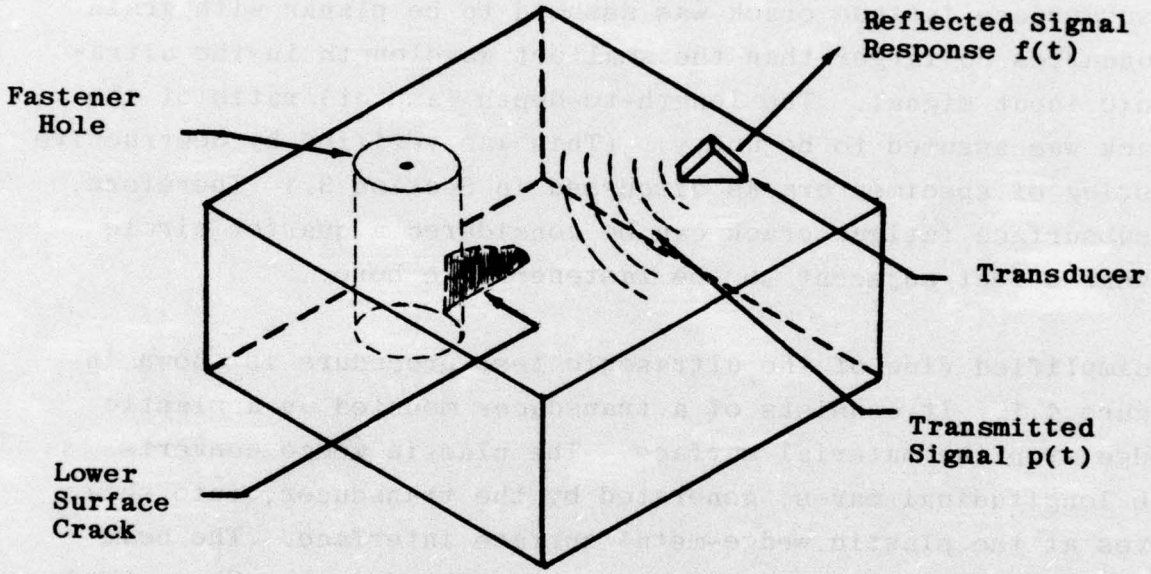


FIGURE 4.1: SIMPLIFIED VIEW OF THE ULTRASONIC TEST PROCEDURE

characteristics as the transmit signal spectrum, except for differences imposed by diffraction. These differences are a function of crack size-wavelength ratios. The amplitude variations of the return signal should be indicative of crack size.

4.4 CIRCULAR SCANNING OF THE DEFECT

Apart from collecting return signals from a subsurface defect at the normal incident position, it is desirable to collect data at various other positions by moving the transducer (either mechanically or manually) in the vicinity of the defect. This is motivated by the fact that a component of the planar crack is "visible" to the transducer at different positions -- that component is a function of both the crack size and the viewing angle with respect to the normal position. Thus the return signal spectrum, at any position, is a function of crack size and position. Different viewing angles can produce marked changes in the interference effects in the return signal spectrum and they can therefore be useful in characterizing crack sizes.

Figure 4.2 illustrates why interference effects may be manifested in the return signal spectrum when a defect is viewed at different angles. At the normal incident position, the transducer's longitudinal axis is perpendicular to the plane of the crack. All waves emanating from the transducer arrive at edges A and B at the same instant of time and are consequently reflected and received in phase at the transducer. Thus the return signal spectrum is essentially the same as the transmit signal spectrum. However, when the crack is viewed at the off-normal position, the reflection from edge A is received prior to the reflection from edge B. An interference pattern (either constructive or destructive) will be observed in the return signal spectrum depending on the wavelength λ of the wave, the differential distance needed for this wave to travel the extra round trip distance to B with respect to edge A, and the viewing angle, θ.

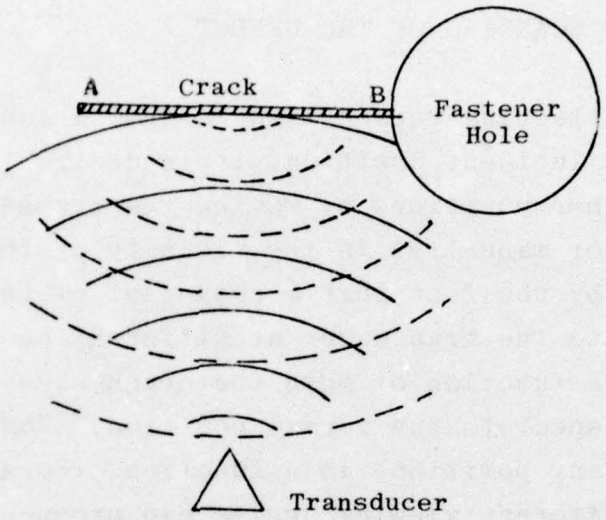


FIGURE 4.2a: WAVE PATTERNS WITH TRANSDUCER AT NORMAL INCIDENT POSITION

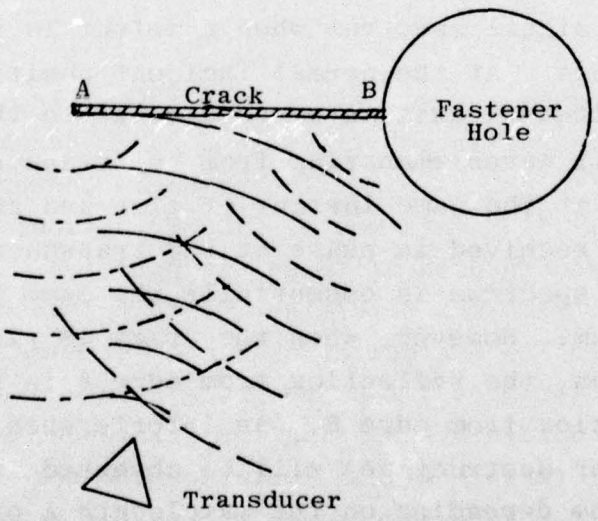


FIGURE 4.2b: WAVE PATTERNS WITH TRANSDUCER AT OFF-NORMAL POSITION

FIGURE 4.2: ILLUSTRATION OF INTERFERENCE EFFECTS AS FUNCTION OF TRANSDUCER VIEWING ANGLE

Therefore, a key parameter that determines the amount of constructive or destructive inference at various frequencies and angles is the crack length AB. This fact was used to advantage in designing the data recording system employed in this project. (The above development is accurate for a line or rectangular crack, but not for the quarter circle shaped defect used in this project. One can imagine the quarter circle to be composed of an infinitely dense stack of lines whose length grow from zero mils at the top of the bore to AB mils at the bottom of the bore (i.e., at the surface). Therefore, a statistical distribution of interference patterns will be recorded rather than one single pattern. The statistical nature of the NDE signal is one of the reasons why an empirical, nonlinear, and statistically-oriented approach is required. This point will be developed more in Sections 6, 7, and 8.)

A recording system was constructed to scan the hole in a circular manner as shown in Figure 4.3. It consists of a transducer positioning device which is free to rotate about a fixed radius from the center of the fastener hole. The transducer is attached to the device and can be manipulated to record data at any desired position.

It was decided to record data at the normal incident position and at five other angular positions in 5.5^{o} increments, in a direction toward the crack. The viewing angle thereby varied from 0^{o} to 27.5^{o} in 5.5^{o} increments. The transducer was moved manually to record data at these six positions. The normal incident (0^{o}) position was determined by that transducer viewing angle which elicited the maximum crack response as determined by visual examination of the oscilloscope trace. In addition, a "reference" signal was recorded by pointing the transducer away from the crack. The reference signal contained the hole response alone and was used for deconvolution purposes (as described in Section 6).

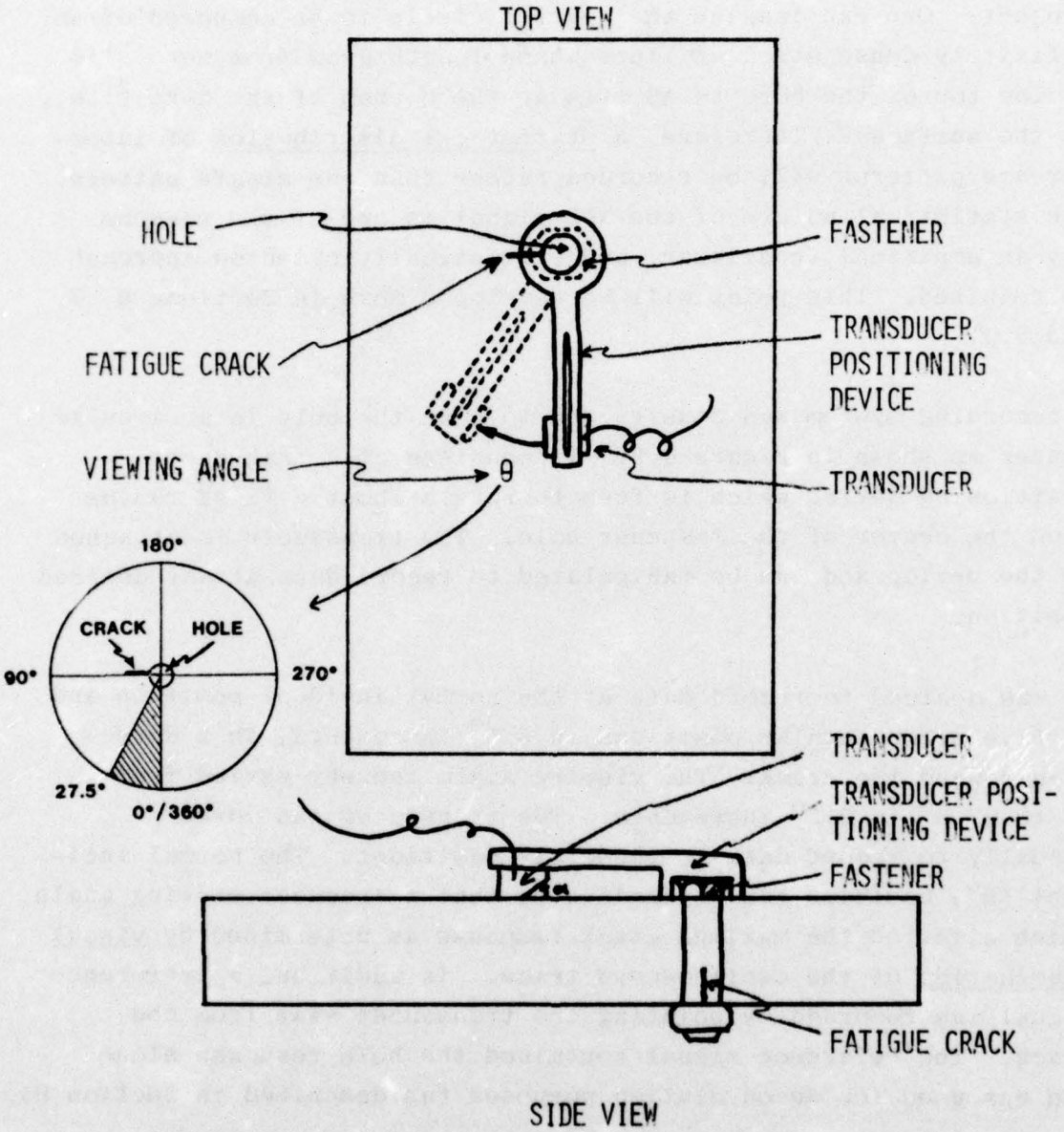


FIGURE 4.3: FATIGUE CRACK ULTRASONIC RECORDING EQUIPMENT

An angular increment of 5.5^{o} was chosen for the following reason. The reflected ultrasonic signal was sampled at a 10 nanosecond/point rate which, by the Nyquist criterion, yielded the theoretical highest observable frequency to be 50 MHz. Assuming that the true highest observable frequency is 30 MHz, the corresponding wavelength is 4.2 mils for a shear wave velocity of 1.26×10^{8} mils/sec.

Figure 4.4 is a schematic of the crack reflection geometry. The bold line AB represents the crack and its plane extends into the paper. The extra round trip distance for a wavefront of wavelength λ, traveling towards corner B with respect to corner A, is $2\ell_{o}\sin\theta$. For <u>destructive</u> interference we require

$$2\,\ell_{o}\,\sin\theta = \lambda/2$$

or

$$\sin\theta = \lambda/4\ell_{o}$$

To observe destructive interference for an 11 mil crack (which is the smallest crack in the sample set) we have:

$$\theta_{min} = \sin^{-1}\left(\frac{\lambda_{min}}{4\ell_{min}}\right) \qquad (4.3)$$

$$= \sin^{-1}\left(\frac{4.2}{4x11}\right) = 5.5^{o} \qquad (4.4)$$

Therefore, 5.5^{o} is the smallest angle required to observe a <u>minimum</u> in the power spectrum of a return signal from the smallest crack in the sample set. So, for an 11 mil crack, minima (i.e., "nulls") should occur in the amplitude versus time waveforms at $\theta = 5.5^{o}$, 16.5^{o} and 27.5^{o}. This result can be used to advantage for an 11 mil crack.

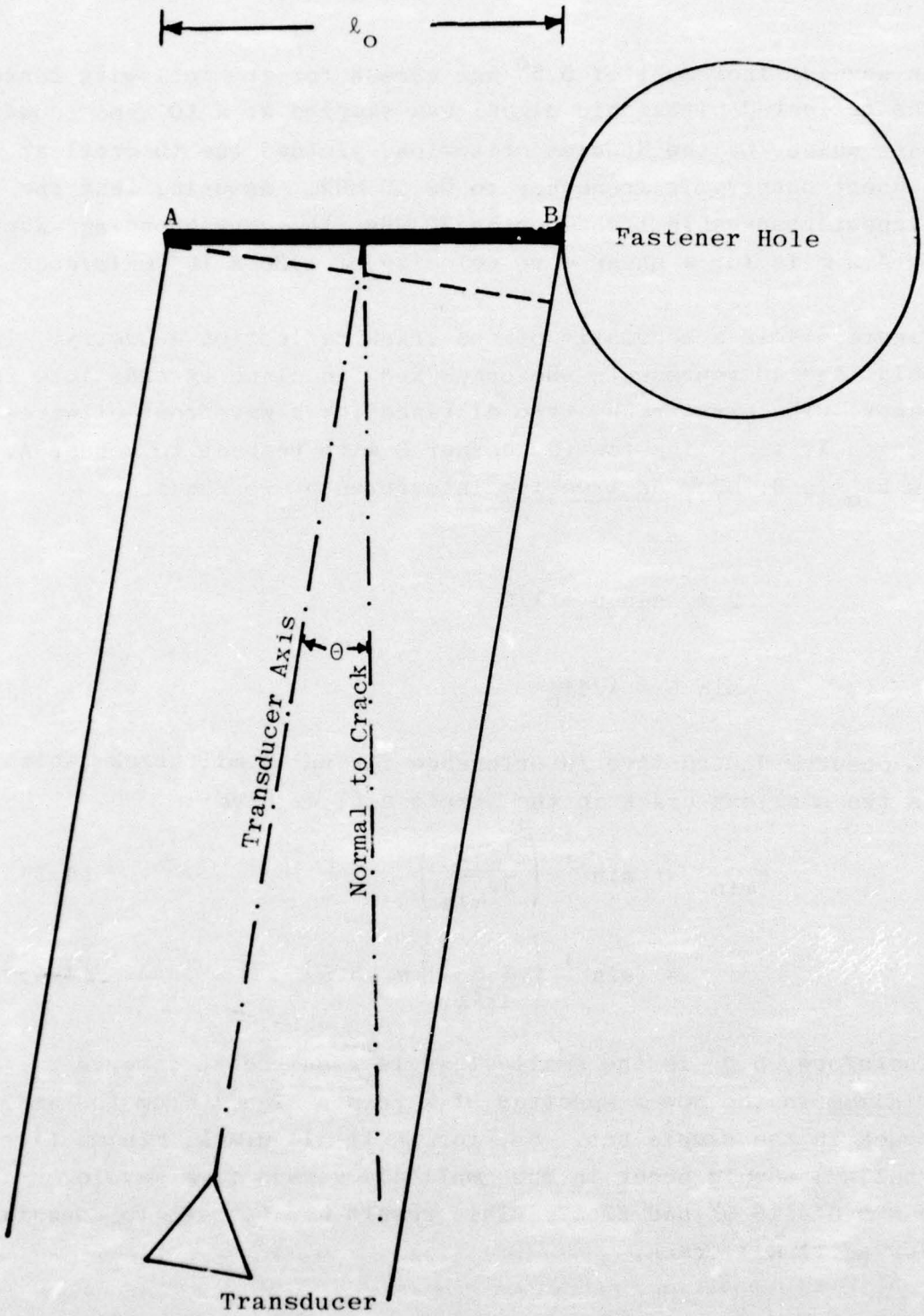


FIGURE 4.4: SCHEMATIC OF CRACK REFLECTION GEOMETRY

Figure 4.5 illustrates the variety of signals obtained from the circular scanning apparatus for the 192 mil, 93 mil, 39 mil, and 14 mil specimens. Each time signal for each crack and viewing angle consists of the reflection from the hole initially, then the response from the inner edge of the crack nearest the hole and, lastly, the response from the outer edge of the crack.

To illustrate the interpretation of each of the plots in Figure 4.5, a single time plot of sample 14-192 viewed at 0^{o} is shown in Figure 4.6. The time window is 4 microseconds. The signal during time interval marked "A", which is approximately 0.5 microseconds in duration, is the response from the outer surface of the fastener hole. The signal during time interval marked "C" is the reflection from the outer and inner edge of the crack. Interval "B" is the time between these two events.

Each plot in Figure 4.5 contains the three time intervals described above, although the duration of each is functionally dependent on the crack length and the viewing angle. The sequence of occurrence of the event is always the same as in Figure 4.6, i.e., the hole response followed by a crack response. As explained above, this is so because the fastener hole is closest to the transducer and its reflection is received initially. Also, as the viewing angle increases, the response from the outer and inner edges of the crack tend to "creep up" on one another because the difference in their physical distances from the transducer decreases. The hole response, however, <u>always occurs at the same instant of time</u>. The time of occurrence of the hole response was used as a reference time for gating the crack response in the data window, because the time of occurrence of the latter varies with crack size and viewing angle, whereas the former is fixed.

Examining Figure 4.5, one can observe the interference phenomenon being manifest. For example, a 192 mil crack has a large response at the 0^{o} position, decreases somewhat at 5.5^{o}, and increases again at 11^{o}. Large responses are elicited from the 93 mil crack at 0^{o} and 16.5^{o}; the preferred viewing angles for a 39 mil crack are 0^{o} and 22^{o}.

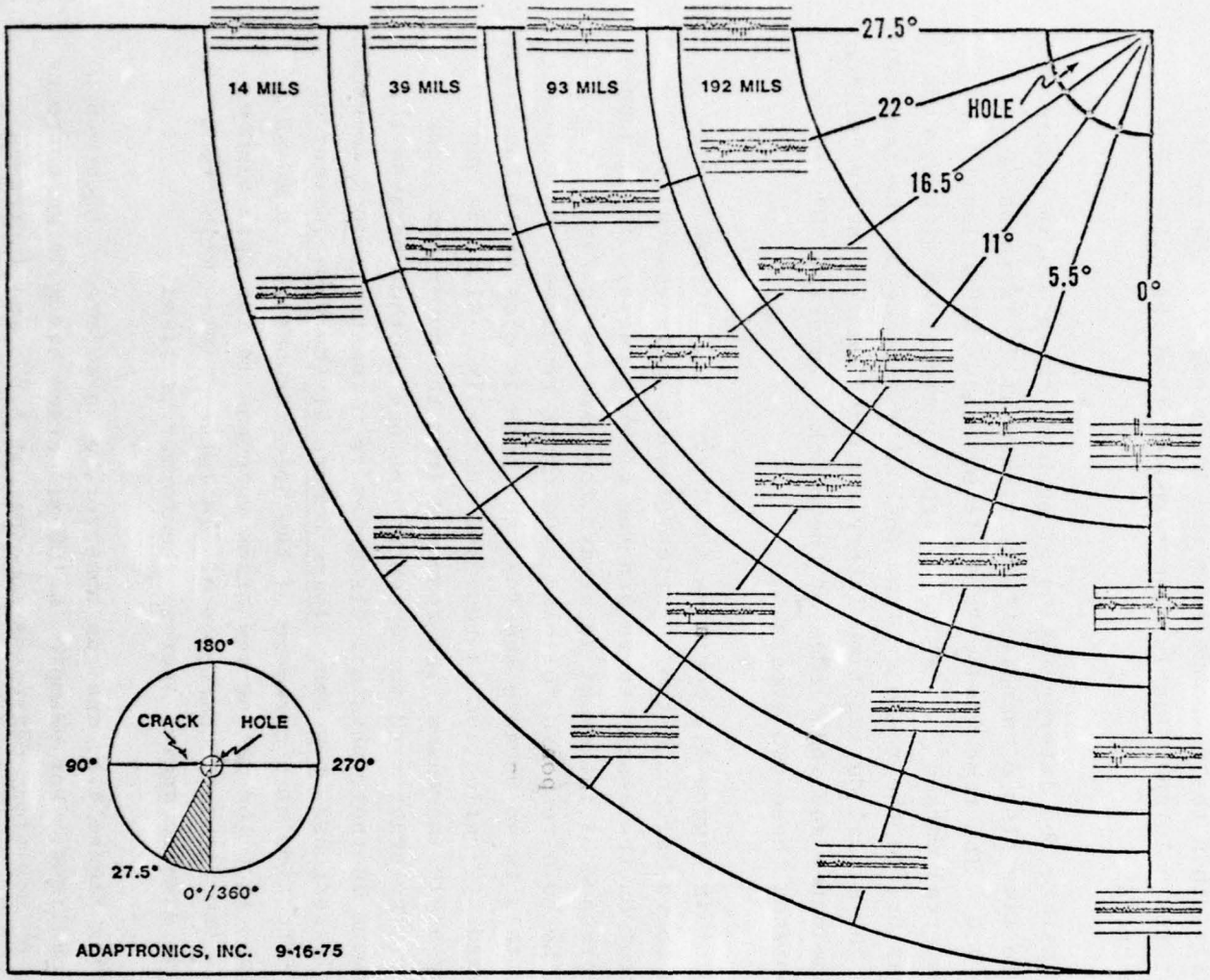
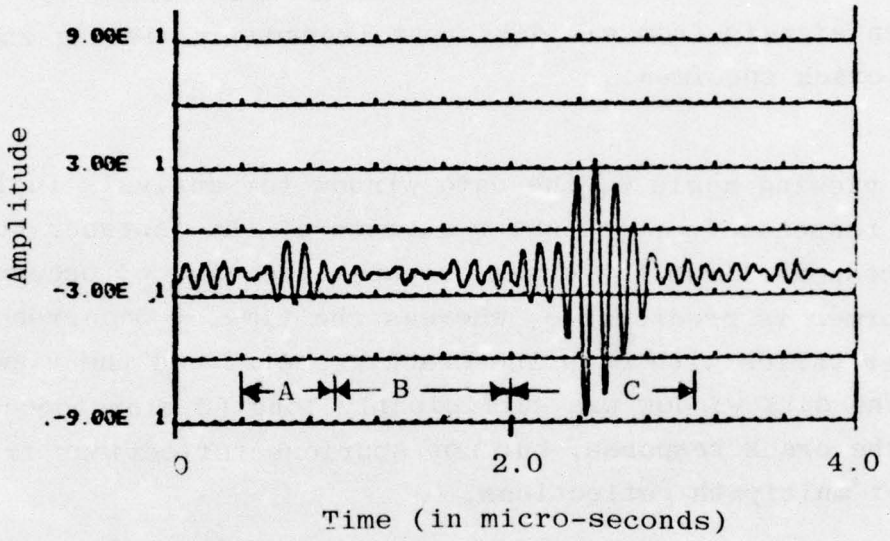


FIGURE 4.5: FATIGUE CRACK NDE WAVEFORMS RECORDED FROM FOUR SPECIMENS AT SIX VIEWING ANGLES



A = Response from hole.

B = Time between responses from hole and crack.

C = Response from crack.

FIGURE 4.6: RESPONSE FROM 14-192 SPECIMEN VIEWED AT $\theta = 0^{o}$.

The smaller cracks -- 39 and especially 14 mils in the figure -- have barely discernible responses and are difficult, if not impossible, to distinguish visually from the background noise (in spite of the fact that signal averaging was performed to minimize equipment noise, see Section 5.5). The information relative to the cracks is, of course, resident in their reflected signals, even though it may not be apparent from visual examination of the amplitude versus time traces. This was another reason for recording return signals from six different transducer viewing angles for each crack specimen.

For each viewing angle θ, the data window for analysis included both the response from the outer surface of the fastener hole and the response from the crack, because the time of occurrence of the former is predictable, whereas the time of occurrence of the latter varies with both the crack geometry and the viewing angle. The data window was sufficiently long (5 microseconds) to include the crack response, but not spurious reflections from other sources or multipath reflections.

In summary, the approach to data collection for the crack detection procedure was an integration of both the "linear systems" and the "phased-array" approaches. The reflection of ultrasonic signals from a subsurface defect was considered as an output from a "black box". The constituents of the black box are the medium, the transducer, and the defect, but the analytical relationship among them is unknown. The problem lies in extracting the characteristics of the defect from the output of the black box. Linear signal processing techniques alone were <u>not</u> capable of resolving defect size, as shown in Section 6. Therefore, the best one can do under the circumstances of lack of knowledge concerning the underlying analytical relationships is to construct an empirical mathematical model based on known <u>parameters</u> of the output response and the intrinsic nature of the defect.

5. DATA COLLECTION PROTOCOL

5.1 OBJECTIVE

The objective of the data collection was to obtain pulse echo ultrasonic data from fatigue cracks guided by the principles outlined in Section 4. As in Task I of this project (Ref. 6), the equipment was specially selected to provide as great a bandwidth as possible so that the ultrasonic waveform would have maximum information content.

5.2 DESIGN OF THE ULTRASONIC EXPERIMENTS

The design of the ultrasonic experiments for Task II of the project was guided, to a large extent, by the results obtained in Task I. In Task I, it was shown that the size of flat-bottomed holes could be determined by parameters other than the amplitude of the reflected ultrasonic pulse. Moreover, the results of Task I demonstrated that differences in the reflected pulses, too subtle to be recognized by a human operator, could in fact be used, with proper signal processing, to elicit much more information than was readily apparent.

In Task I, one of the most important signal parameters was the spectral energy in the 0 to 12.5 MHz band. The transducers produced energy in the frequency range from 3.5 to 8.5 MHz with wavelengths between approximately .064 and .026 inches. The hole diameter ranged from .016 to .125 inches. The diameter-to-wavelength ratio, considering all hole sizes and all wavelengths present, ranged from approximately 4.8 to about 0.24. In this range of diameter-to-wavelength ratios, the radiation pattern of the energy reflected from the hole changed considerably with small changes in hole diameter. The spectrum of the energy detected by the transducer acting as the receiver also changed rapidly with changes in radiation patterns. Although it would be nearly impossible for a human observer to compare the transmitted and received pulses and deduce

hole diameter from a change in observed spectrum shape, parameters descriptive of the spectrum provided significant information in classification of hole diameter.

5.3 SELECTION OF ULTRASONIC EQUIPMENT

The equipment selected for the ultrasonic waveform acquisition system was basically the same as shown in Figure 3.4 of the previous report (Ref. 6). For this task, however, a Panametric 5052PR was substituted for the 5050PR used earlier. The two instruments are almost identical in characteristics. The major advantage of the 5052PR is that instead of having only a 0-20-40 dB attenuator, the latter instrument has an attenuator with a total range of 88 dB in 2 dB steps and a gain selection of either 20 or 40 dB. Pulses reflected by the crack were returned to the transducer and were amplified in the receiver portion of the Pulser/Receiver. The pulses were recorded in digital form in a Biomation 8100 Transient Recorder. The pulse information stored in the Biomation memory was played back through a digital-to-analog converter for examination on an oscilloscope or transmitted to the memory of a Supernova computer for further processing. This capability enabled signal averaging to be performed automatically to enhance the signal-to-noise ratio. The primary function of the processing in the Supernova was to provide several optional means of using the data as input to other computers without further manual preparation. Output data were provided in digital format on magnetic tape, in hardcopy prints from a cathode ray tube display, and as a computer listing from a line printer. (Further details of the data recording equipment can be found in Appendix B of Reference 6.) The data recording equipment are illustrated in Figure 5.1.

Because of the type and orientation of the defects used in this task, the longitudinal-wave normal beam transducer was replaced with a shear-wave transducer. The center frequency of the transducer was 10 MHz to provide a more collimated beam to cope with the rather complex geometry and poor reflecting characteristics

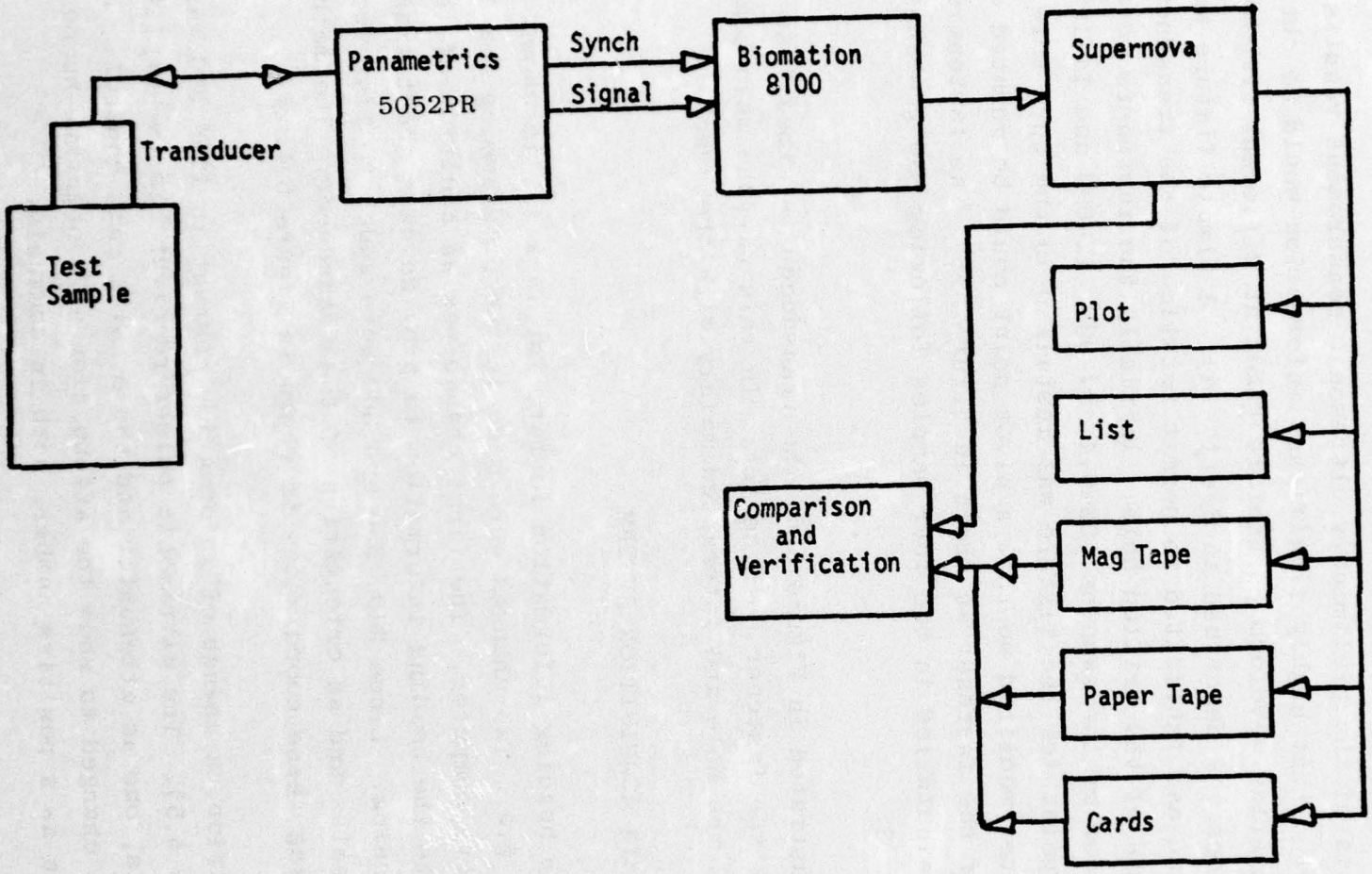


FIGURE 5.1: BLOCK DIAGRAM OF ULTRASONIC WAVEFORM ACQUISITION SYSTEM

of the defects. Transducers and the plastic wedges on which they were mounted are shown in Figure 5.2.

Analysis of the preliminary ultrasonic measurement results indicated that highly significant information would be obtained by comparing waveform parameters taken at different transducer positions (as described in Section 4). A simple fixture was designed and fabricated to permit rotation of the transducer about the axis of the drilled hole. Initially the fasteners were removed from four of the samples (03-014, 07-039, 11-093 and 14-192) and a pivot point for the fixture was installed in the open hole. This was later modified so that a pivot point could be mounted on the head of the fastener as shown in Figure 5.3. The fasteners were then reinstalled in the four samples following the procedure in Section 3.

As illustrated in Figure 5.4, the transducer is aimed just off the axis of the fastener hole center. In this way the main beam avoided the hole and interacted mainly with the crack.

5.4 DATA ACQUISITION SYSTEM

The new heading information format, for Task II, is shown in Figure 5.5. Two changes were made in the programming for the Supernova computer. The first change was an addition of three lines to the heading information to provide data about transducer positioning. Lines 340, 350 and 360 were added to list two coordinates and an orientation of the transducer. The method of measuring these coordinates is shown in Figure 5.4.

In addition, a change of information content in line 560 was made (Figure 5.5). The ultrasonic pulser/receiver has two amplitude controls, one an attenuator and the other a gain control. Line 560 was changed to show the attenuation as a negative number and the gain as a positive number, both in decibels.

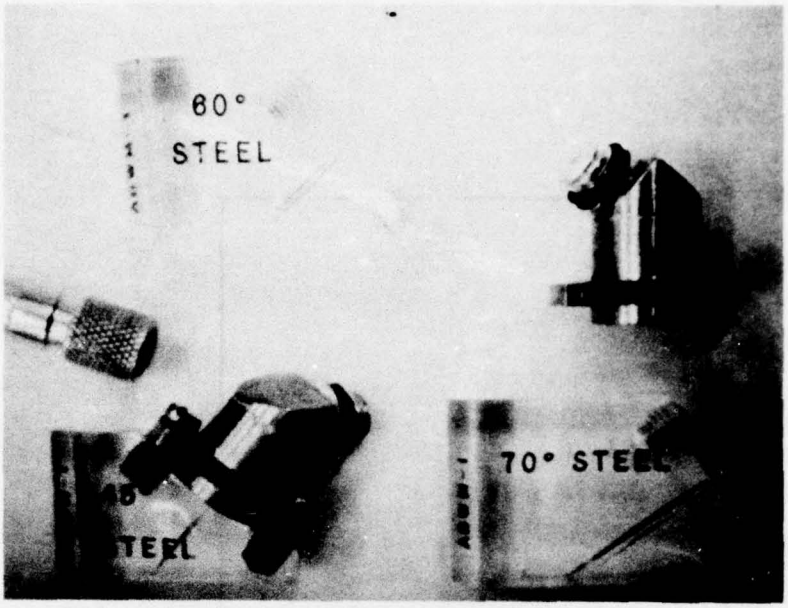


FIGURE 5.2: Transducers & Wedges Used For Ultrasonic Data Acquisition

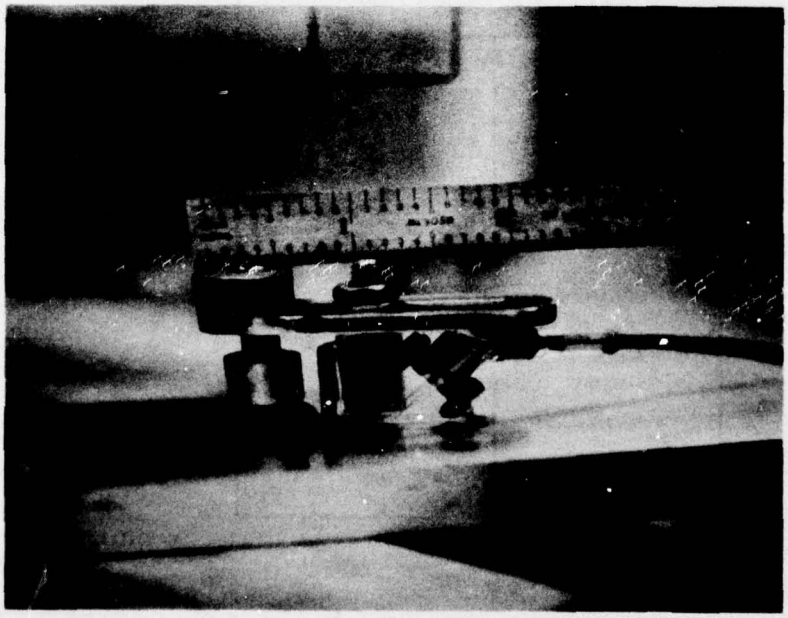


FIGURE 5.3: Mechanical Fixture to Rotate Transducer About Fastener

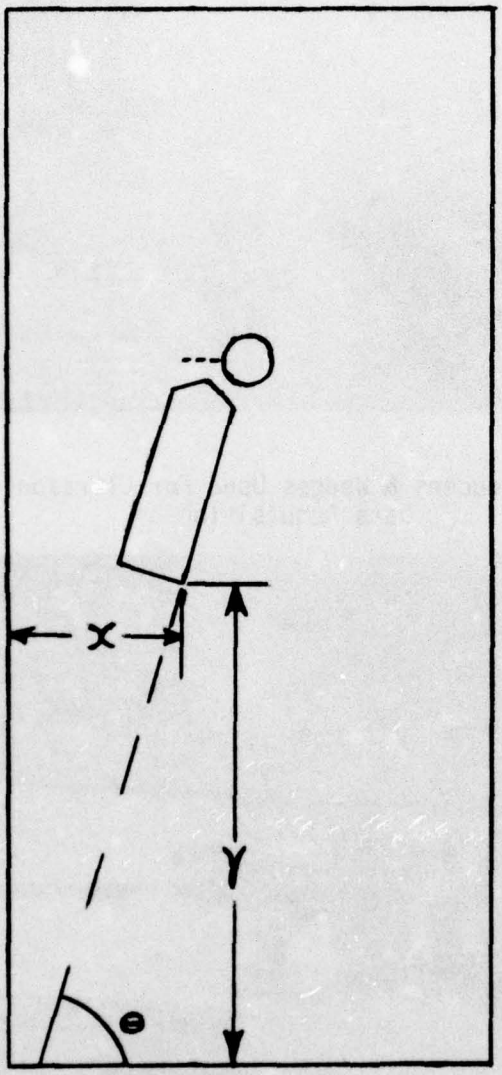


FIGURE 5.4: COORDINATE SYSTEM FOR TRANSDUCER LOCATION AND ORIENTATION.

```
-511      20  BABCOCK AND WILCOX CO                              .
-511      30  LYNCHBURG RESEARCH CENTER          WEL/MLR         .
-511      40  DATE OF TEST                       APR 16, 75      .
-511     310  XDUCER  PANAMETRI SERIAL NO        4081            .
-511     320  XDUCER  PANAMETRI DIAM /ANGLE      0.25/60         .
-511     330  XDUCER  PANAMETRI NOM FREQ         10 MHZ          .
-511     340  XDUCER  POSITION X                 0.94 IN         .
-511     350  XDUCER  POSITION Y                 2.70 IN         .
-511     360  XDUCER  DIRECTION  CCW THETA       65.5 DEG        .
-511     400  SAMPLE  ALUMINUM MFG               METCUT          .
-511     410  SAMPLE  NUMBER                     03-014          .
-511     510  P/R     PANAMETRICS                5052PR          .
-511     520  P/R     PULSER RECVR               1               .
-511     530  P/R     REP RATE                   4               .
-511     540  P/R     ENERGY                     3               .
-511     550  P/R     DAMPING                    8.0             .
-511     560  P/R     ATTENUATION/GAIN           -0/+40 DB       .
-511     610  B8100   CH A      COUPLING         DC DC           .
-511     620  B8100   CH A      INPUT RANGE      .05V-+          .
-511     630  B8100   CH A      INPUT OFFSET     PLUS .00        .
-511     710  B8100   CH B      INPUT/OFF        OFF             .
-511     810  B8100   ARM       FROM             NONE            .
-511     820  B8100   ARM       DELAY            0.00 K SAMPLES  .
-511     830  B8100   ARM       SOURCE           EXT             .
-511     840  B8100   ARM       INTERNAL         CH A            .
-511     870  B8100   ARM       LEVEL            0 X FS INPUT    .
-511     910  B8100   TRIGGER   FROM             5052PR SYNC     .
-511     920  B8100   TRIGGER   DELAY            1.50 K SAMPLES  .
-511     930  B8100   TRIGGER   SOURCE           EXT             .
-511     940  B8100   TRIGGER   INTERNAL         CH A            .
-511     950  B8100   TRIGGER   SLOPE            PLUS            .
-511     960  B8100   TRIGGER   COUPLING         DC              .
-511     970  B8100   TRIGGER   LEVEL            PLUS .10 X FS   .
-511    1010  B8100   TIME BASE SAMPLE INTERV    .01 US          .
-511    1020  B8100   TIME BASE SOURCE           INTERNAL        .
-511    1040  B8100             RECORD MODE      NORMAL          .
-511    1200  COMMENT COUPLANT                   HAMIKLEER       .
-511    1210  COMMENT  ALL OTHER SW OBVIOUS      CRACK ECHO      .
-511    1220  COMMENT TEMP DEG F/R HUMIDITY      73/40           .
-511    1300    0    1    2    3    4    5    6    7    8       .
 511       0   -2    0    0   -1   -1    0    0    0    0   -1
 511      10   -1   -1   -1   -2   -2   -1   -1   -1   -1   -1
 511      20   -1   -1   -1   -1   -1   -1   -2   -1   -2   -2
 511      30   -3   -2   -1   -1   -1   -2   -2   -1   -1   -3

 511    1980  -21  -19  -18  -20  -21  -20  -20  -20  -20  -20
 511    1990  -19  -19  -18  -17  -19  -19  -21  -22  -22  -20
 511    2000  -21  -21  -20  -19  -21  -23  -21  -21  -22  -22
 511    2010  -22  -21  -20  -20  -21  -21  -22  -21  -20  -20
 511    2020  -19  -18  -19  -20  -23  -21  -21  -21  -21  -21
 511    2030  -21  -19  -19  -20  -21  -22  -21  -23  -21  -13
 511    2040   -9   -1    0    0    0    0   -1 1111 1111   10
```

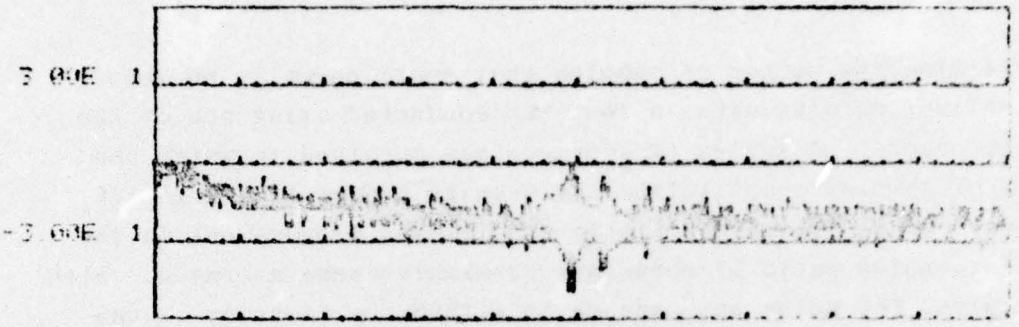
FIGURE 5.5: HEADING INFORMATION FORMAT

5.5 SIGNAL AVERAGING

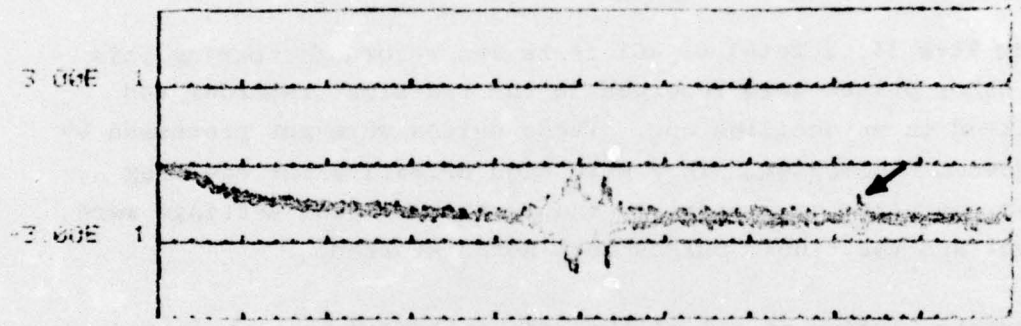
A second and more significant change was made in the programming to allow signal averaging to reduce electronic noise. For most defects, the instrumentation was operated at maximum sensitivity. The total gain was high enough for electronic noise to become apparent on the hardcopy printout as well as in the listed data. For small defects, the signal-to-noise ratio was relatively low. In normal operation, the pulser/receiver is continuously pulsing and a manual trigger was applied to obtain a recorded set of data in the Biomation. These data were examined on the oscilloscope before being transmitted to the computer for permanent recording. Multiple samples could be obtained and the amplitude at corresponding points in each sample averaged in the computer. Because of its randomness, the electronic noise tended to average to zero and the averaged signal data tended to be stripped of the electronic noise. The number of samples that was averaged was listed as the last word in the data listing.

Typical results of signal averaging are shown in Figure 5.6 Hardcopy plots of the same test conditions are shown in which a single sample was used and where 10 and 25 samples were averaged. With a single sample, the signal-to-noise ratio was about 8.6 dB; with the average of 10 samples, the signal-to-noise ratio increased by 10 dB to 18.6 dB. With 25 samples averaged, an additional 2.7 dB in signal-to-noise ratio was obtained.

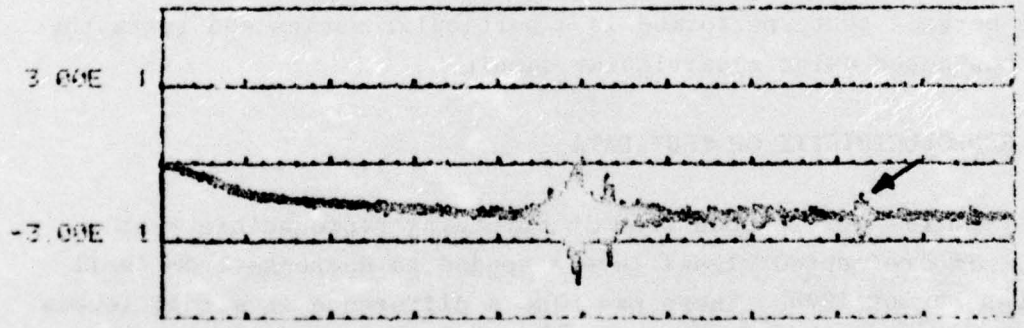
With some of the smaller defects, the true signal could be recognized after signal averaging. A pulse is obvious (indicated by an arrow), in Figures 5.6 (b) and 5.6 (c), that cannot be discerned in Figure 5.6 (a). In some cases, however, even with increased averaging, a recognizable signal on the display could not be produced for the smallest defects (less than 30 mils). For example, note the lack of a visually apparent defect signal for all six viewing angles for the 14 mil crack in Figure 4.5.



A SINGLE DATA SAMPLE: 8.6 dB S/N



B AVERAGE OF 10 SAMPLES: 18.6 dB S/N



C AVERAGE OF 25 SAMPLES: 21.3 dB S/N

FIGURE 5.6: SIGNAL-TO-NOISE RATIO ENHANCEMENT OBTAINED BY SIGNAL AVERAGING.

To determine the number of samples that would normally be averaged while recording data, a test was conducted using one of the smaller cracks. A series of averages was obtained in which the number of samples constituting the average ranged from 2 to 128, in powers of 2. There was little significant improvement in the signal-to-noise ratio if more than 32 samples were averaged. With 32 samples, the noise was reduced to within the accuracy of the integer averaging in the transient recorded (which uses 8 bits/word).

5.6 TEST DATA LISTINGS

During Task II, a total of 401 tests was recorded. During this task other pulses were recorded in the transient recorder and displayed on an oscilloscope. These pulses were not processed by the Nova minicomputer. They were used primarily for checking system operating parameters to insure that control settings were correct and that their pulses were not distorted.

A complete listing of all of the data collected appears in Appendix B1 and shows the tests in chronological order. Appendix B2 has been revised to include, as a group, all of the tests conducted on each sample. A combination of the two listings permits a rapid determination between tests performed in a particular series and tests that were conducted using a particular sample.

5.7 REPRODUCIBILITY OF TEST DATA

Some problems were encountered in obtaining reproducible test data. The reflected signal levels tended to decrease from April through August 1975. There was also a difference in signal levels apparent between the four blocks[1/] that were used for a large number of preliminary tests with their fasteners removed, and from the remainder of the test samples. Some of the early data were taken with 10 MHz, 70° shear wave transducers.

1/ These four blocks were: 03-014, 07-039, 11-093, 14-192.

A number of tests was conducted in an effort to determine the exact cause of the decreased signal level. Although the fatigue cracks in the blocks were protected by washers under the fastener, the possibility of contaminants entering the fatigue crack and reducing reflectivity was considered. An effort was made to remove possible contaminants by placing each block in vacuum, by baking it at a relatively low temperature to drive off any volatile material, and by a combination of vacuum and baking. None of these processes produced any significant change in signal amplitude.

Instrumentation used for the ultrasonic tests was completely checked by comparing the performance to the original (manufacturer) specification. In all cases, electronic instrumentation performed in complete accordance with the original requirements.

Transducers were obtained and, judging by the serial numbers, were produced from the same batch as the ones that had been used for the test. A direct comparison of two transducers (a new one and the one used) showed no significant difference in performance. Although (soft) plastic wedges were used to generate the shear wave, the aluminum surface was subject to marking by the constant motion of the wedge. Fasteners were removed from the samples and the surface refinished using very fine emory paper on a flat surface. Although some increase in the signal amplitude was noted, the signals were still lower than obtained earlier. Finally the same transducer that had previously been used was mounted on a 60^{o} wedge in place of the previously used 70^{o} wedge and data were obtained although the signal amplitudes were still somewhat low.

Thus, the two series of experimental data, Series 1 and Series 2, have <u>significant amplitude differences</u> as shown in the amplitude versus time waveform plots of Appendix C. The cause for the decrease in signal amplitude has still not been determined. It is significant, however, that the data were still usable for determining fatigue crack size even though amplitude varied considerably with time. (See Section 6.6.)

6. THEORETICAL AND PRACTICAL CONSIDERATIONS OF PULSE-ECHO WAVEFORM PREPROCESSING

6.1 INTRODUCTION

This section presents a mathematical description of the reflection of ultrasonic signals from subsurface fatigue cracks and equations relating the crack size to parameters of the input signal. A linear systems theory approach to the analysis of reflected signals from subsurface defects is discussed in Section 6.2. The rationale of the approach was not to derive a complete set of analytical closed-form solutions to the crack detection problem; rather, it served as a guide to the general preprocessing techniques of ultrasonic waveforms. These preprocessing techniques, with their theoretical and practical limitations, are outlined in Sections 6.3 through 6.7.

Three waveforms--power spectrum, power cepstrum, and spatial transform--were computed from the recorded amplitude versus time waveforms. This section of the report develops the mathematical basis for using parameters of these three waveforms as key descriptors of crack length and, hence, as inputs to the ALN crack length model.

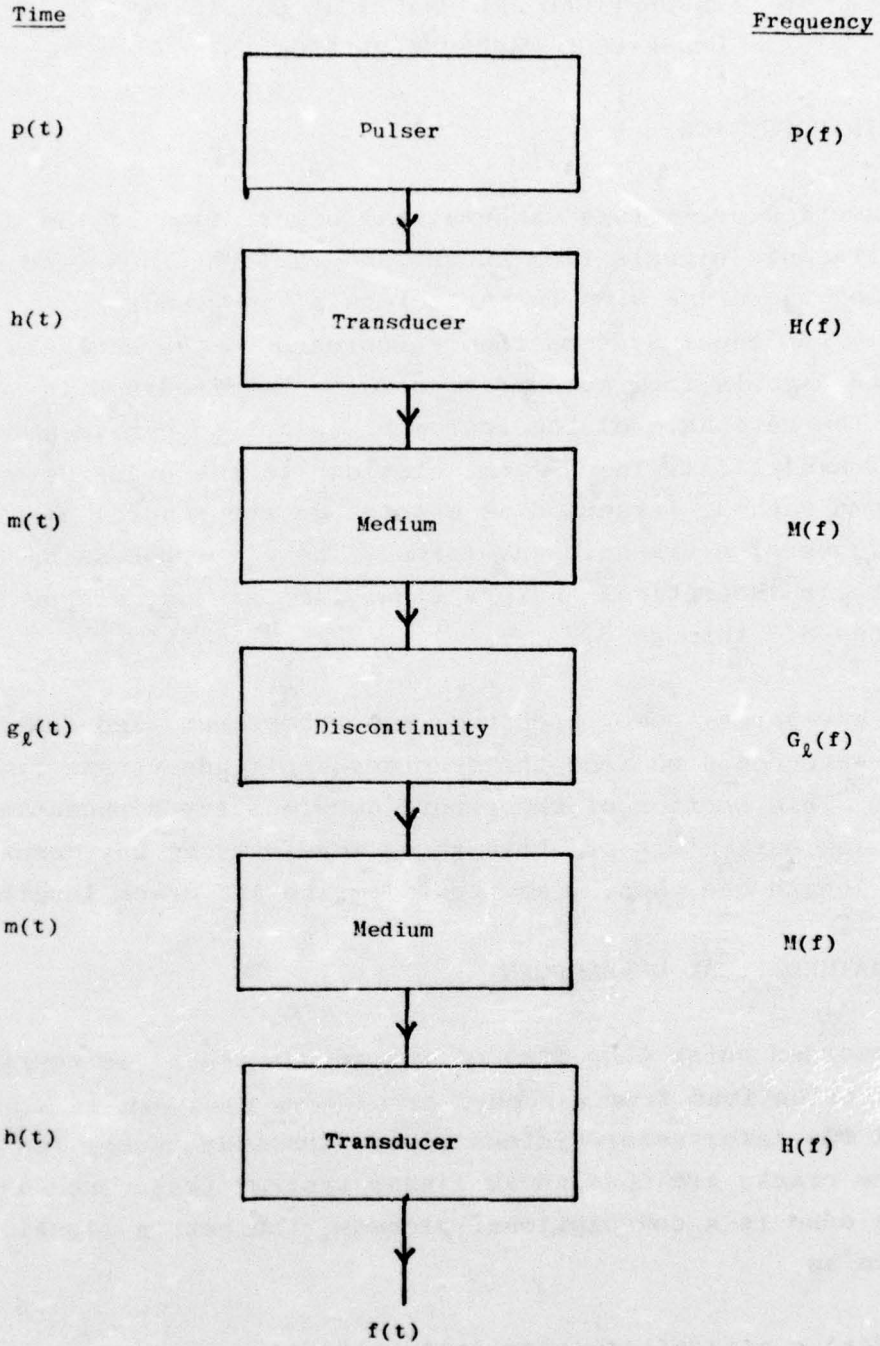
6.2 MATHEMATICAL DEVELOPMENT

The recorded pulse echo f(t) of the return signal is composed of the contributions from a number of systems as shown in Figure 6.1. If all the intervening systems (i.e., the transducer, the medium and the crack) are modeled as linear systems (Reference 4) and the return echo is a convolutional process, the return signal is written as,

$$f(t) = p(t)*h(t)*m(t)*g_{\ell}(t)*m(t)*h(t) \qquad (6.1)$$

where the asterisk denotes the convolution operator. Equation 6.1 can be conveniently written in the frequency domain as

PRECEDING PAGE BLANK-NOT FILMED



Time Response: $f(t) = p(t)*h(t)*m(t)*g_\ell(t)*m(t)*h(t)$

Frequency Response: $F(f) = P(f)H^2(f)M^2(f)G_\ell(f)$

FIGURE 6.1: LINEAR SYSTEM MODEL OF REFLECTION FROM SUB-SURFACE DEFECTS (from Ref. 4)

$$F(f) = P(f)H^2(f)M^2(f)G_{\ell}(f) \qquad (6.2)$$

where the upper case letters indicate (Fourier) frequency transforms of the individual systems.

If the pulser emits a perfect impulse and the transducer is sufficiently broadband to pass all the frequencies of the pulser, and if the medium characteristics do not change from one subsurface crack to another, the return pulse echo from any crack is

$$F(f) = M^2(f)\, G_{\ell}(f) \qquad (6.3)$$

where $M(f)$ is the frequency response of the medium and $G_{\ell}(f)$ is the frequency response of the crack (of length ℓ).

In other words, the return echo can be modeled validly as a linear function of the crack response if these assumptions are true.

Since the cracks are area-amplitude reflectors, the larger size cracks should produce larger reflections. Furthermore, all frequencies incident to the plane of the crack are reflected and received in phase at the transducer. Therefore, the return echo should be solely dependent on the size of the crack.

The assumptions of the characteristics of the transducer and the medium are too stringent to be realistic. The typical frequency response of a 10 MHz transducer would cover a bandwidth of approximately 8 MHz. Moreover, the frequency response of transducers differ even though they may be identically rated. The medium characteristics may also vary depending on the structural and the metallurgical properties of a local region. Hence, for either or both reasons, the response (Equation 6.2) will be altered for the same crack under different test conditions. On the other hand, one would desire the response of a particular size crack to be invariant, or at least relatively insensitive, to different operating conditions.

A signal preprocessing procedure was devised in this project to cope with these transducer and medium variabilities. It is derived as follows.

An inverse filtering operation can be performed to minimize the effects of the transducer and the medium. A reference signal can be recorded (similar to the scheme shown in Figure 6.1) by replacing the crack by a point source defect which has an all-pass characteristic. Therefore, $R_p(f)$ is recorded which is, from Equation 6.2,

$$R_p(f) = P(f)\, H^2(f)\, M^2(f) \tag{6.4}$$

The point source defect has unity response at all frequencies, and hence $G_\ell(f)$ does not appear explicitly in Equation 6.4. Deconvolving Equation 6.4 from Equation 6.2, which is division in the frequency domain, gives

$$F_d(f) = \frac{F(f)}{R_p(f)} = G_\ell(f) \tag{6.5}$$

That is, the recorded and deconvolved signal is characteristic solely of the crack.

If the reference signal is not obtained from a point source defect but from a standard size crack, $R_s(f)$ can be modeled as

$$R_s(f) = P(f)H^2(f)M^2(f)G_s(f) \tag{6.6}$$

where $G_s(f)$ is the frequency response of the standard size defect.

Deconvolving Equation 6.6 from Equation 6.2:

$$F_d(f) = \frac{F(f)}{R_s(f)} = \frac{G_\ell(f)}{G_s(f)} \tag{6.7}$$

where the deconvolved signal, although stripped of medium and transducer effects, still has the standard size defect characteristics imbedded within it.

The crack characteristics can still be exclusively extracted by homomorphic filtering procedures (Ref. 10) which convert a nonlinear operation such as multiplication or division into one of addition or subtraction. Specifically, the logarithm of both sides of Equation 6.7 is taken:

$$\log\{F_d(f)\} = \log\{G_\ell(f)\} - \log\{G_s(f)\} \tag{6.8}$$

and Equation 6.8 is rewritten as

$$F'_d(f) = G'_\ell(f) - G'_s(f) \tag{6.9}$$

where the primes indicate the log of the frequency transforms.

By the principle of linearity, the inverse transform of Equation 6.9 is

$$f'_d(t) = g'_\ell(t) - g'_s(t) \tag{6.10}$$

and the deconvolved signal in the time domain $f'_d(t)$ is a linear algebraic combination of the crack response and a standard size defect which does not vary from one crack to another. The signal $f'_d(t)$ is called the cepstrum of $F_d(f)$. In other words, the cepstral transform converts a nonlinear operation in the frequency domain (Equation 6.7) to a linear operation in the time domain (Equation 6.10).

Therefore, in summary, an ultrasonic signal from a subsurface defect can be modeled approximately as a linear system (under given assumptions) which consists of the transducer, medium, and the defect characteristics. To analyze the crack characteristics, one resorts to an inverse filtering operation to strip the medium and transducer effects from the recorded signal. In the case where a reference signal is not recorded from a point source defect, an inverse filtering operation can still be carried out by homomorphic techniques, which reduce a nonlinear operation such as multiplication of waveforms to a linear operation.

6.3 DECONVOLUTION OF PULSE ECHO SIGNALS

The six circularly scanned signals and the reference signal, described in Section 4.4, comprised a set of seven waveforms for a particular crack. Each of the six scanned signals consisted of 20.48 microseconds of data, sampled at 10 nanoseconds per point. The distance between the outer rim of the fastener hole and the transducer was known exactly, so the time of arrival of the reflection from it could be estimated accurately. The arrival time did not vary with changes in viewing angle or in crack size because the distance between the transducer and the fastener hole was fixed.

However, as explained above, the arrival time of the crack reflection changes with both viewing angle and crack size. As the viewing angle increases, the crack response tends to "creep up" on the hole response because one edge of the crack is encountered sooner than the other (Figure 4.2). If the crack size is smaller, the time duration of the crack response is lessened. Therefore, for either or both reasons, the time of arrival of the crack response could not be accurately estimated. It was thereby decided to use a data window that included both the hole and crack response for analysis. A 512-point window, containing the two responses, was isolated from the 2,048-point sampled signal for each of the six circularly scanned signals per specimen. The time axis location of the data window was established via visual examination of the data base.

The data window for the seventh, or reference signal, in each set of readings was recorded in the same way as the other six signals. The transducer was positioned away from the crack region of the hole. This signal consisted of the hole response alone and it occurred at the same instant that the hole response was observed in the other six signals. The reference signal is thus a function of the characteristics of the medium, the transducer, and a standard sized "defect"--the fastener hole in this case. From the theoretical development of Section 6.2, the reference signal can be used, in principle, to deconvolve the six circularly scanned signals in order to minimize medium and transducer effects.

Unfortunately, because all transducers are band-limited, Equation 6.7 cannot be fully realized. In practice, the only true frequencies in the deconvolved signal are resident in a limited band. The transducer was rated for 10 MHz with 3db cut-off frequencies at 6 and 14 MHz, so the data collected for the reference and the crack signal were also band-limited. Furthermore, the process of deconvolution introduces spurious frequencies beyond the 3db range of the transducer (due to dividing small numbers by other small numbers) and these had to be suppressed. The spurious frequencies were suppressed by filtering the deconvolved signal through a Gaussian band-pass filter, which had a sharp cut-off at the 3db frequencies. The advantage of using the Gaussian filter rather than the standard box filter is that, in the time domain, the tail of the former has fewer side lobes than does the latter.

Figure 6.2 outlines the sequence of operations to obtain the deconvolved signal for each of the six angular positions of the transducer. Figure 6.3 shows the resultant signals obtained, at each step in Figure 6.2, for a 279 mil crack viewed normal to the plane of the crack. The signal obtained after deconvolution (Figure 6.3(e)) has an all-pass characteristic in the frequency domain with the relevant information contained in the 6-14 MHz band (Figure 6.3(f)). After bandpass filtering, the deconvolved time waveform is plotted (Figure 6.3(g)) and, not surprisingly, the most prevalent frequencies are between 6-14 MHz, with a predominance around 10 MHz.

If the transducer were indeed not band-limited, the deconvolved time signal should have an impulse at about the instant when the hole response is observed and another set of impulses where the crack begins and terminates. The time between the latter two impulses is indicative of the length of the crack relative to the viewing angle of the transducer. However, because the transducer is band-limited, its convolution with the impulses produces the "ringing" effect as shown. The approximate positions of the impulses are indicated by arrows in Figure 6.3(g).

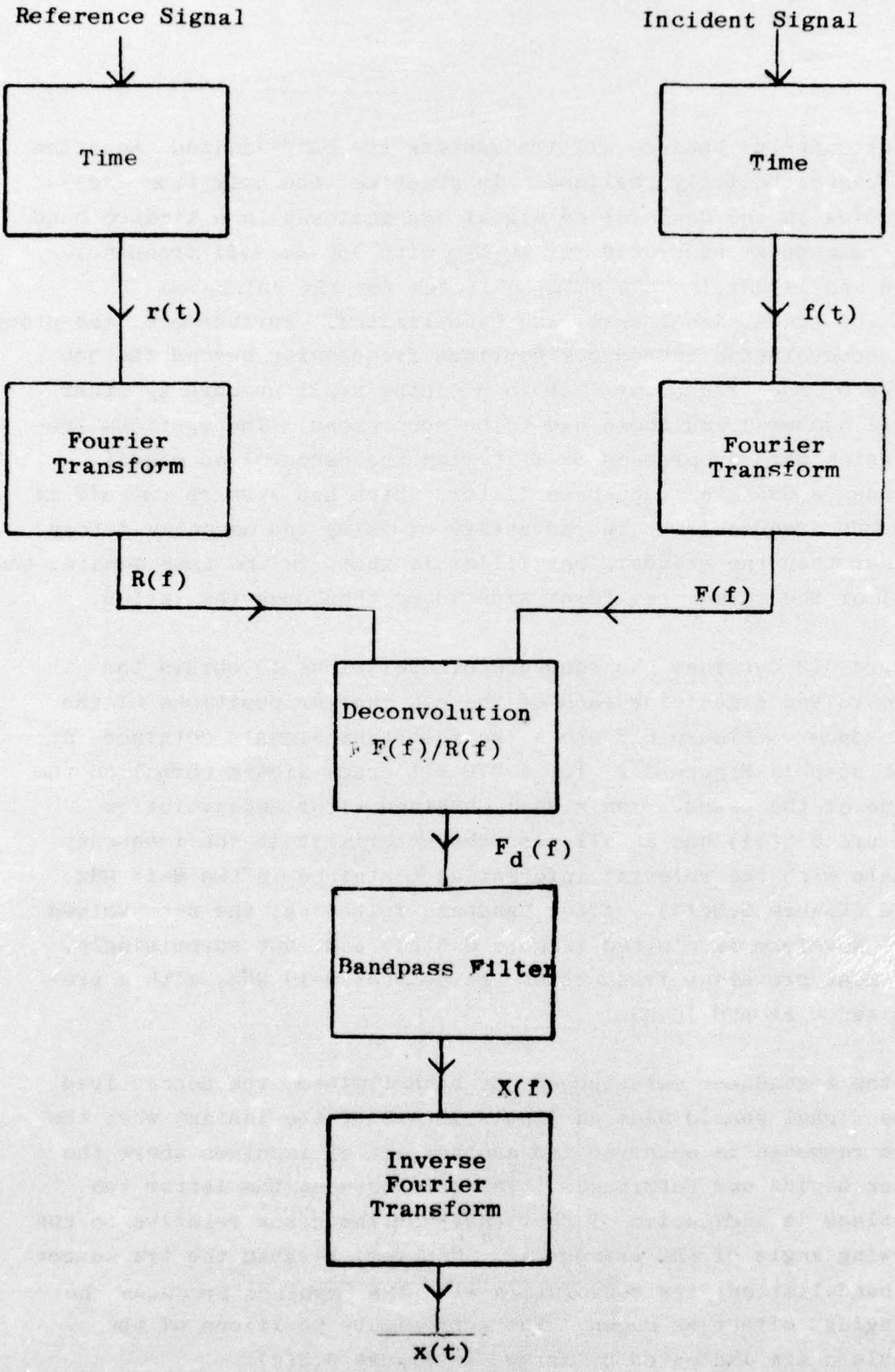


FIGURE 6.2: SCHEMATIC OF DECONVOLUTION OF CRACK RESPONSE FROM A REFERENCE SIGNAL

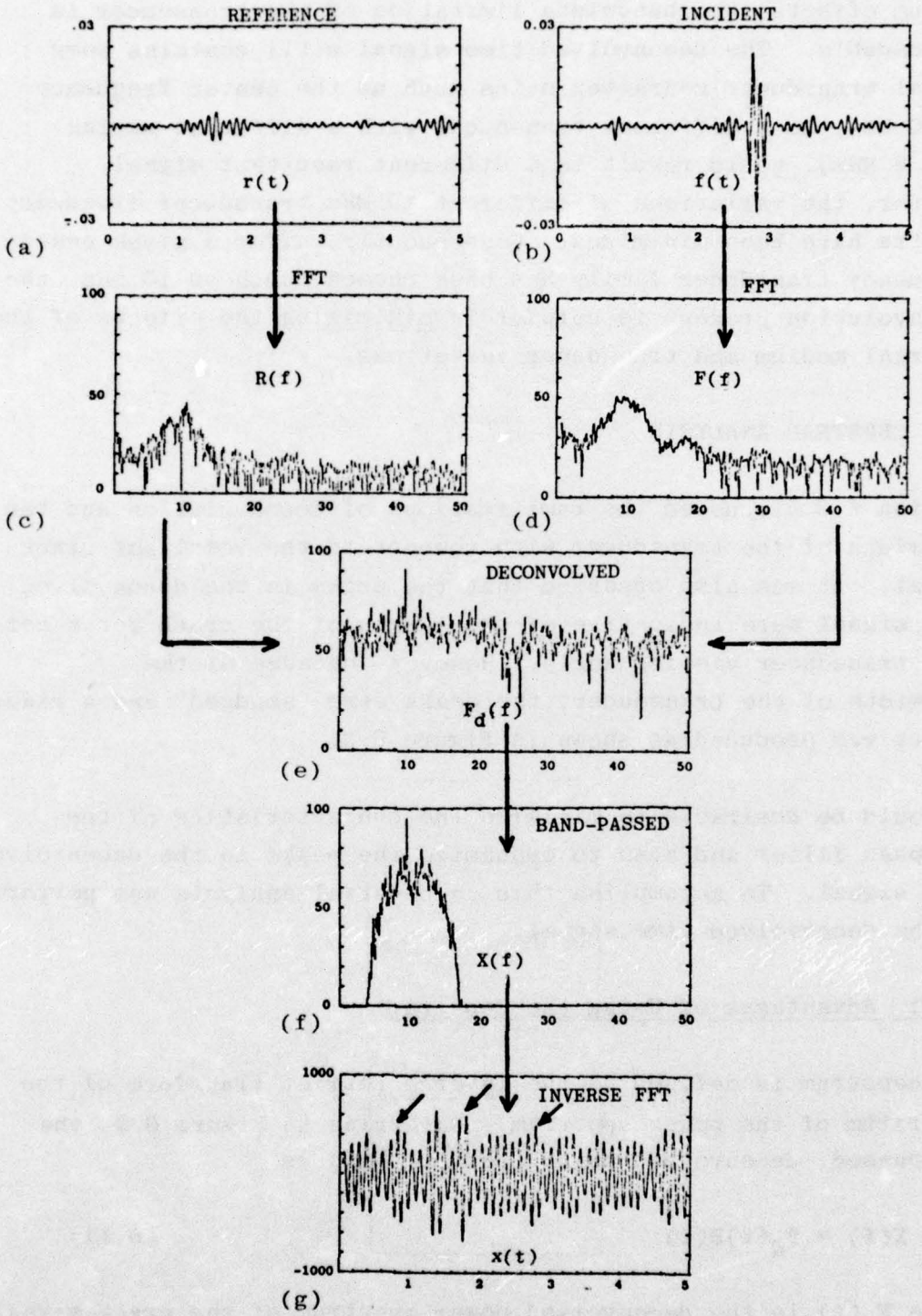


FIGURE 6.3: DECONVOLUTION OF 279 MIL CRACK (VIEWED AT 0^{o}) FROM A REFERENCE SIGNAL.

Although deconvolution is helpful in minimizing transducer and medium effects, the bandwidth limitation of the transducer is inescapable. The deconvolved time signal still contains some global transducer characteristics such as the center frequency of 10 MHz, so a different transducer with a different rating (say 5 MHz), would result in a different resultant signal. However, the variations of different 10 MHz transducer frequency spectra have been minimized. Consequently, after a given center frequency transducer family has been chosen, such as 10 MHz, the deconvolution process is helpful in minimizing the effects of the external medium and transducer variations.

6.4 CEPSTRAL ANALYSIS

Section 6.3 discussed the ramifications of deconvolution and the bandwidth of the transducer with respect to the resultant crack signal. It was also observed that the peaks in the deconvolved time signal were indicative of the length of the crack for a certain transducer viewing angle. However, because of the bandwidth of the transducer, the peaks were "smudged" and a ringing effect was produced as shown in Figure 6.3.

It would be desirable to minimize the characteristics of the bandpass filter and also to emphasize the peaks in the deconvolved time signal. To accomplish this, a cepstral analysis was performed on the deconvolved time signal.

6.4.1 Advantages of Using the Cepstrum

The cepstrum is defined as the inverse Fourier transform of the logarithm of the power spectrum. Referring to Figure 6.2, the bandpassed, deconvolved power spectrum X(f) is

$$X(f) = F_d(f)B(f) \qquad (6.11)$$

where $F_d(f)$ is the deconvolved power spectrum of the crack signal, and B(f) is the spectrum of the bandpass filter. Taking the log of

Equation 6.11 (as was done for Equation 6.8) reduces it to an additive process, i.e.,

$$\log\{X(f)\} = \log\{F_d(f)\} + \log\{B(f)\} \qquad (6.12)$$

or

$$X'(f) = F_d'(f) + B'(f) \qquad (6.13)$$

where the primes indicate the log transform of the respective frequency response.

By taking the inverse Fourier transform of the left hand side of Equation 6.13, and using the principle of linearity, the time response is

$$x'(t) = f_d'(t) + b'(t) \qquad (6.14)$$

where the lower case letters are the individual inverse Fourier transforms. In other words, the cepstrum of X(f) is a sum of the cepstra of $F_d(f)$, which is a characteristic of the crack and the viewing angle, and of B(f), which is a characteristic of the bandpass filter, and does not change from one experiment to another.

The signal $f_d(t)$ is not used alone because it is noise prone beyond the 3 db frequencies of the transducer. The filter response $b'(t)$ has the effect of suppressing these frequencies and still retaining the linear relationship between the resultant signal, $x'(t)$, and the deconvolved signal, $f_d'(t)$.

Therefore the cepstral signal $f_d'(t)$ bears important information about the crack length and the viewing angle.

6.4.2 Detection of Time Delayed Events

The cepstrum has historically been used to detect echoes in radar and sonar signal systems. For this project, the crack response signal is

composed of the response from the hole and the crack. Ideally, it should consist of three impulses as shown in Figure 6.4(a), where t_h, t_b, and t_e indicate the instant of occurence of the reflections from the hole, the beginning of the crack and the end of the crack, respectively. The time t_h is independent of the size of the crack, whereas t_b and t_e change with transducer viewing angle and crack size.

The crack response to a band-limited signal would resemble Figure 6.4(b), and has the effect of "smudging" the impulses. The narrower the bandwidth of the transducer, the broader the smudging. Nevertheless, the same phenomenon is manifest at t_h, t_b, and t_e. After computing the cepstrum of the response of Figure 6.4(b), peaks are manifest clearly at instant t_b-t_h, t_e-t_b and t_e-t_h as shown in Figure 6.4(c), and they are functions of crack length and viewing angle. As the transducer viewing angle is varied, t_b begins to creep up on t_h, which remains fixed, and t_e remains approximately the same. If the crack size were different, t_b and t_e would be different; for smaller cracks t_b and t_e would decrease.

Therefore, the positions of the peaks in the cepstrum are indicative of the size of the crack and the viewing angle of the transducer. Since the viewing angle is known, the crack size is thus potentially inferable.

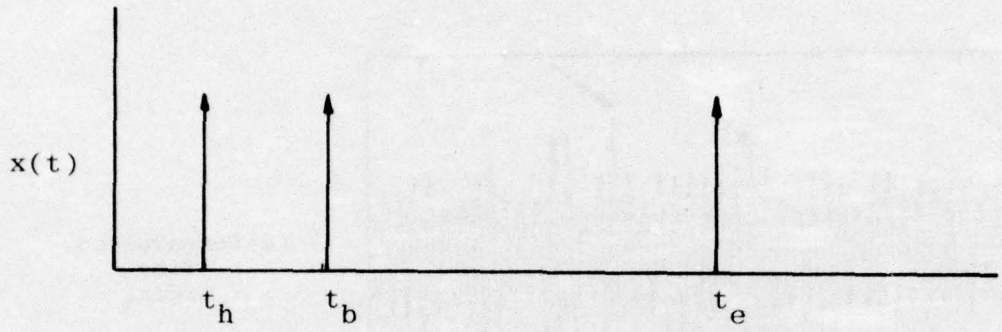
Unfortunately, in the actual physical environment, the resolution of the cepstral peaks is not very clear due to three main factors:

(1) The system is not linear.

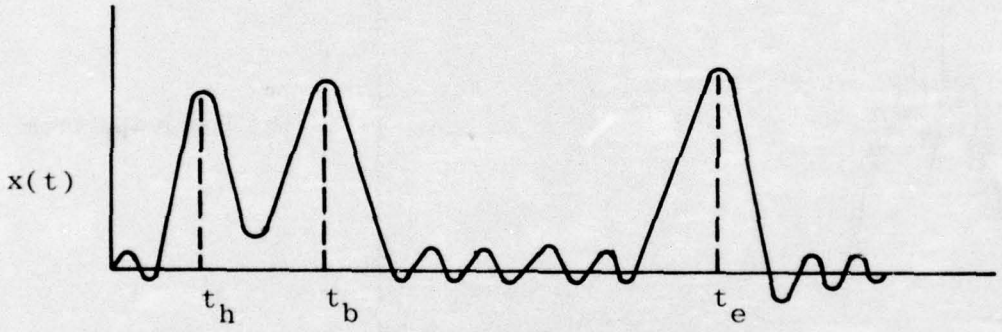
(2) There are multipath reflections which have not been treated in the analysis.

(3) The limited bandwidth of the transducer has the effect of smudging the peaks in the deconvolved time signal.

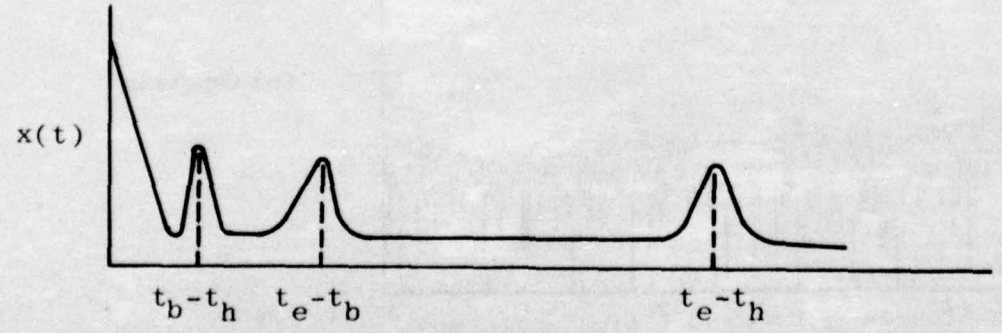
Figure 6.5 shows the deconvolved time signal for a 279 mil crack viewed at 0°. The corresponding power spectrum and the cepstrum are shown in Figures 6.5(b) and 6.5(c). The most probable location of t_h, t_b, and t_e are 0.25, 2.25, and 3.25 microseconds, respectively,



(a) Crack Response For Ideal Transducer



(b) Response For Band-Limited Transducer



(c) Cepstrum Of Response Of Band-Limited Transducer

FIGURE 6.4: CRACK RESPONSE UNDER DIFFERENT TRANSDUCER CONDITIONS

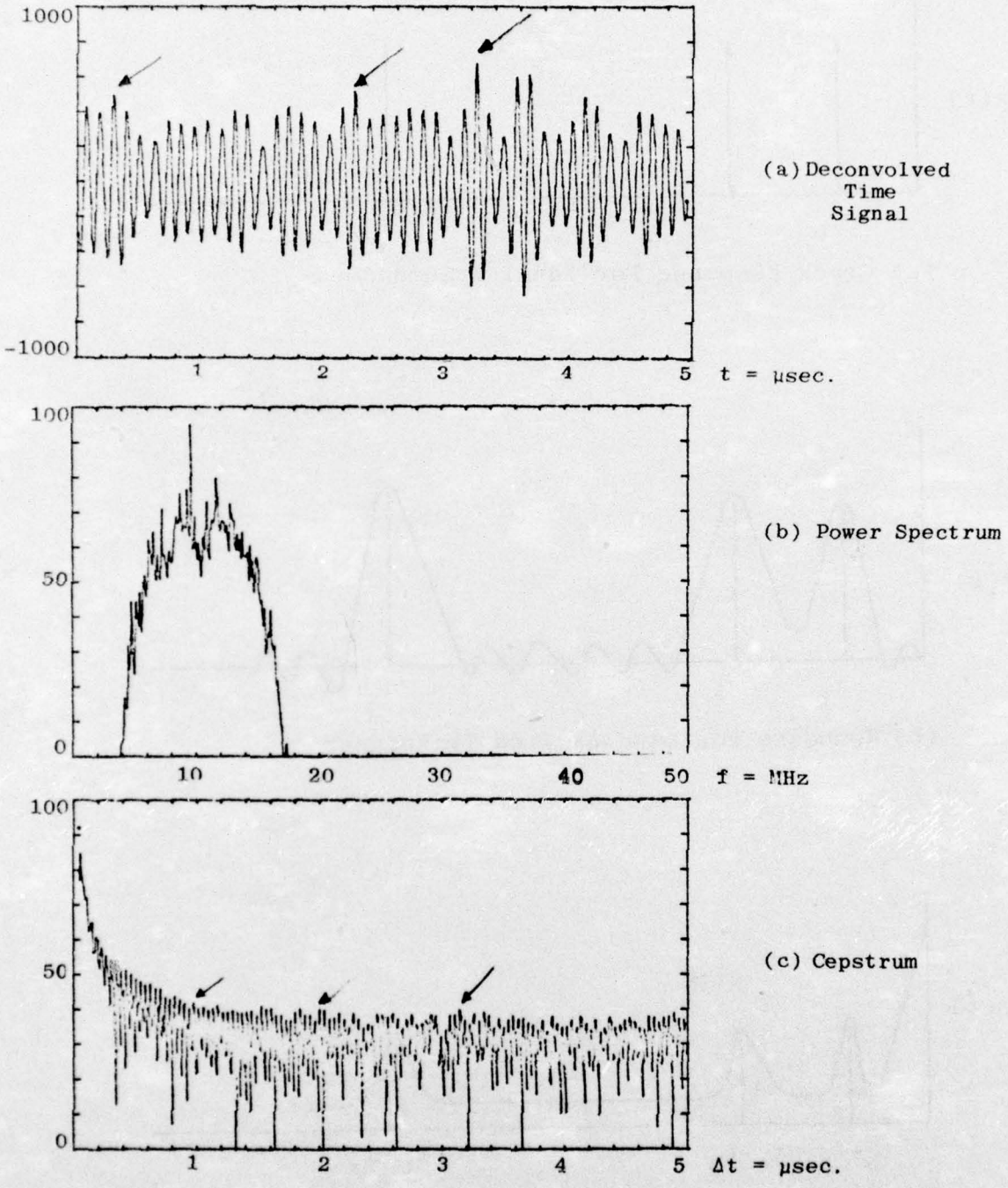


FIGURE 6.5: WAVEFORM PREPROCESSING FOR 279 MIL CRACK

and are shown by arrows in Figure 6.5(a). The impulses, as should be expected, are really sampling functions (i.e., sin x/x) because of the finite bandwidth of the transducer. The cepstrum should reveal peaks around the various time differences $t_e - t_b$, $t_b - t_h$, and $t_e - t_h$, i.e., 1, 2, and 3 microseconds. At the corresponding points in the cepstrum, local maxima can be observed (arrows) in Figure 6.5(c). However, the peaks are not clearly resolved, and once again, a statistical procedure of counting the peaks in certain bands of the cepstrum must be employed. This procedure is described in the parameterization procedures in Section 7.

The major revelation of the data of Figure 6.5 is that the physical environment -- transducer, medium and other geometrical factors in the defect zone -- will make correlations between simple waveform features (such as a peak) and defect size nearly impossible to find. Instead, in almost all NDE applications, effort should be spent in using theoretical analyses such as that above as a guide to methods for signal preprocessing steps, and then using parameters computed from these steps in linear and nonlinear combinations to infer defect characteristics.

6.5 THE SPATIAL TRANSFORM

6.5.1 Theoretical Considerations

The deconvolved crack response discussed in Section 6.3 was helpful in analyzing the characteristics of the crack, stripped of medium and transducer characteristics. However, for a particular crack, its response will change with different viewing angles of the transducer. In other words, a family of crack responses in time was available -- each member of the family corresponding to a particular viewing angle. Thus the crack response was sampled both in time (512 points at 10 nanoseconds/point) and space (six viewing angles from 0 to 27.5°, in 5.5° increments). Time and space represent two independent bases to evaluate the crack characteristics. As explained above, there were changes in the time response due to changes in the

viewing angle (i.e., interference effects). The next step was to establish a procedure that unified the variations in time and space in order to deduce a global description of the characteristics of the crack.

The following analysis shows that a spatial transform can be defined to describe crack characteristics in time as well as space. Its practical use and limitations are also discussed.

Consider a planar crack of length ℓ_o which is ultrasonically illuminated by a transducer at a fixed distance from the center of the fastener hole (Figure 4.4). The main wavefront emanating from the transducer is at an angle θ with respect to the normal to the crack plane.

The excess distance needed for an ultrasonic wave of wavelenth λ to travel to B relative to A, is $2\ell_o \sin\theta$, and the phase shift, ϕ, at the transducer relative to a frequency f is

$$\phi(f,\ell_o,\theta) = \frac{4\pi\ell_o \sin\theta}{\lambda} = \frac{(4\pi\ell_o \sin\theta)f}{c} \qquad (6.15)$$

where c is the ultrasonic shear wave velocity in the material.

If the transducer has an impulse response $A(f)\exp(j\gamma_f)$ at frequency f, the return signal from the crack can be described as

$$R(f) = k\, A(f)\exp\{j(\gamma_f + \phi(f,\ell_o,\theta)\} \qquad (6.16)$$

where k, a fraction, is the reflectance coefficient and it is a property of the material; and $\phi(f,\ell_o,\theta)$ is defined in Equation 6.15. Dividing Equation 6.16 by the impulse response of the transducer, the deconvolved response is obtained as

$$D(f) = k\exp\{j\phi(f,\ell_o,\theta)\} \qquad (6.17)$$

A spatial variable, Ω, can be defined as:

$$\Omega = \frac{4\pi f \sin\theta}{c} \tag{6.18}$$

which has units of inverse length (i.e., $1/\ell$). Therefore, Equation 6.17 becomes

$$D(\Omega) = k \exp(j\Omega\ell_o) \tag{6.19}$$

If the transducer has frequencies, f, extending from 0 to ∞, then Ω has the same range (from Equation 6.18) and $D(\Omega)$ is defined as in Equation 6.19 but with

$$D(\Omega) = k \exp(j\Omega\ell_o), \quad 0 < \Omega < \infty, \tag{6.20}$$

which is a sinusoidal function of Ω with frequency ℓ_o.

The inverse Fourier transform of $D(\Omega)$, defined as $S(\ell)$, is:

$$S(\ell) = \int_0^\infty D(\Omega) \exp(-j\Omega\ell) d\Omega \ , \ (0 < \ell < \infty) \tag{6.21}$$

$$= k \int_0^\infty \exp(j\Omega\ell_o) \exp(-j\Omega\ell) d\Omega \tag{6.22}$$

$$= k\, \delta(\ell - \ell_o) \tag{6.23}$$

which is an impulse of height k, at $\ell = \ell_o$ in the ℓ-space. Therefore, in theory, the complex frequency spectrum at any particular viewing angle can be deconvolved from the complex frequency spectrum at 0^o viewing angle and, by an appropriate transformation into the Ω-space, the deconvolved spectrum in the Ω-space can be inverse transformed to reveal an impulse in the ℓ-space at ℓ_o, the crack length.

The function $S(\ell)$ is defined to be the spatial transform and it consists of an impulse at ℓ_o in the ℓ-space. Notice that Ω can be varied by either changing the frequency f or the angle θ, or both. Hence, the term "spatial transform" is used to denote the function S.

6.5.2 Practical Considerations

The fatigue crack experimental apparatus consisted of collecting the reflected time signal from a crack at six viewing angles, including the normal position ($\theta = 0^{o}$) as described in Section 5. The complex Fourier transform at each viewing angle was band-limited both in the frequency f, because of the transducer limitations, and consequently in the spatial frequency, Ω (Equation 6.18).

One can still compute a band-limited spatial transform $S(\ell)$ but, unfortunately, even though the frequency sampling f is equally spaced, the sampling in the Ω-space is uneven because of the non-linear transformation of frequency f and of angle θ in Equation 6.18. However, a family of spatial transforms can still be derived for each viewing angle θ -- each one having a bandwidth in the Ω-space which is a function of: (1) the viewing angle, and (2) the frequency bandwidth of the transducer.

Because of the finite sampling interval in the time domain (10 nano-seconds) and because of the finite length of the complex transform in the f-domain, the sampling interval $d\Omega(\theta)$ in the Ω-space is finite:

$$d\Omega(\theta) = \frac{4\pi \sin\theta}{c} df \qquad (6.24)$$

and it increases with θ. Consequently, by the Nyquist criteria, the largest crack which can be detected by the spatial transform $S(\ell)$ in the ℓ-space varies inversely with θ; the larger the viewing angle θ, the smaller the maximum crack length that can be detected.

Table 6.1 shows the maximum and minimum values in the Ω-space and the corresponding maximum and minimum values in the ℓ-space for the six viewing angles. The frequency bandwidth of the transducer lies between 6-14 MHz; the sampling interval is 10 nanoseconds in the time domain with a frequency resolution of 0.195 MHz. The approximate velocity of an ultrasonic shear wave in aluminum is 3200 meters/second. The lowest and highest spatial frequencies, Ω_ℓ and Ω_h in columns 3 and 4, are computed by substituting the lowest and highest frequencies, f_ℓ and f_h, into Equation 6.18.

The $\theta=0^o$ position is used as the deconvolution signal as per Equation 6.17 because the relative phase shift $\phi(f,\ell,0)$ is zero at all frequencies.

6.5.3 Limitation Due to Spatial Sampling

It is clear from Table 6.1 that the largest crack which can be resolved is 268 mils when the transducer is at the 5.5^o position. The maximum detectable crack progressively becomes smaller as the transducer is moved from 0^o to 27.5^o. At 27.5^o, the largest crack which can be resolved is 55.6 mils. Therefore, many of the larger cracks (279 mils, 192 mils, etc.) are too infrequently sampled in the Ω-space to be detected in the ℓ-space.

However, one can imagine the inverse problem -- knowing the location of the impulse in the ℓ-space (i.e., the size of the crack), can it be predicted where the impulse will occur if it is insufficiently sampled in the Ω-space? The answer is yes, because an aliased version of the impulse will appear in the low frequency range of the ℓ-space, and its location can be computed exactly from the Nyquist sampling theorem. In fact, the crack can be as large as possible, and it will still appear in the limited range of $S(\ell)$ -- only the number of "fold-overs" has to be computed to determine its exact location in the ℓ-space.

TABLE 6.1

MAXIMUM AND MINIMUM SPATIAL FREQUENCIES AND THE MAXIMUM AND MINIMUM CRACK LENGTHS WHICH CAN BE RESOLVED AT EACH VIEWING ANGLE

Angle		Spatial Frequency		Spatial Sampling Rate	Crack Length Resolution (Mils)	
θ	Sin θ	Lowest (Ω_ℓ)	Highest (Ω_h)	$d\Omega$	Lowest $1/\Omega_h - \Omega_\ell$	Highest $1/2d\Omega$
0	0	0	0	I N D E T E R M I N A T E		
5.5	0.0958	0.0574	0.1338	0.0019	13.075	268.0
11^o	0.1908	0.1142	0.2665	0.0039	6.6	134.7
16.5	0.2840	0.1700	0.3966	0.0055	4.41	90.5
22.0	0.3746	0.2242	0.5231	0.0073	3.3	68.6
27.5	0.4617	0.2763	0.6448	0.0090	2.7	55.6

Figure 6.6 illustrates the problem when a sinusoidal function in the Ω-space is insufficiently sampled. Figure 6.6(a) shows the high frequency wave $D(\Omega)$ in the Ω domain, which extends from 0 to .04 per mil. The period of the wave is .0035/mil which corresponds to a frequency of 285.7 mils. This wave is sampled at .003/mil which is less than twice this frequency. The sampled wave, shown as a bold line in Figure 6.6(a), has a period of .023/mil, which is a frequency of 43.5 mils. The spatial transforms of the actual wave and the sampled wave are shown in Figure 6.6(b). The former is an impulse at 285 mils and the latter -- the aliased impulse -- is at 43.5 mils. The largest crack which can be detected is half the sampling rate, i.e., 166.7 mils. The aliased impulse at 43.5 mils is a mirror image of the actual impulse at 285 mils with 166.7 mils as the center, i.e., 285-166.7 $\simeq$ 166.7-43.5. In other words, if one knew a priori that the crack is larger than 166.7 mils, the aliased impulse can be correctly interpreted as the true impulse simply by folding it over the Nyquist frequency (167 mils) in the ℓ-space.

Therefore, the existence of an impulse in any one of the spatial transform curves is assured, and one needs only to interpret its location correctly regarding whether it is a true or an aliased version of the impulse, depending on whether the crack size is within or without the range of the sampled ℓ-space.

The a priori estimate of the true crack length can be very coarse. For example, for a viewing angle of 5.5°, a true 300 mil crack will appear as an aliased impulse at 236 mils in its spatial transform $S(\ell)$, because 268-236 $\simeq$ 300-268. If the crack length were known a priori to lie between 268 mils and 536 mils (range of -12 percent to +79 percent in error), the impulse could be accurately interpreted because the correct harmonic cycle is exactly known.

Therefore, in spite of the Nyquist sampling restriction in the Ω-space, in theory any crack can be detected as long as an a priori estimate of the true crack length is available. Additionally, the estimate need not be very accurate; it can be in error up to 70 to 80 percent of the true crack length.

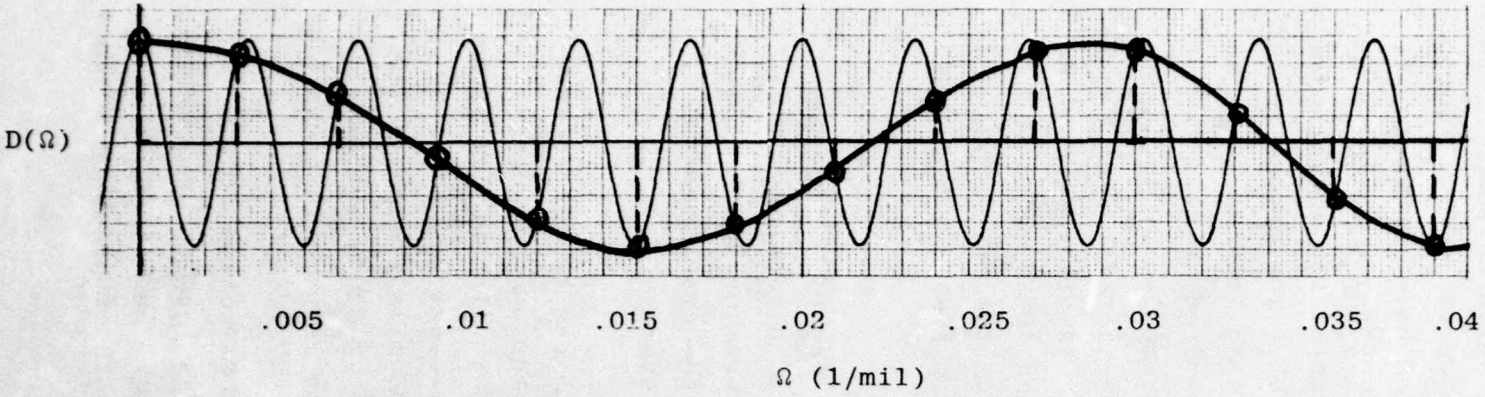


FIGURE 6.6(a): D(Ω) in ℓ-space, insufficiently sampled.

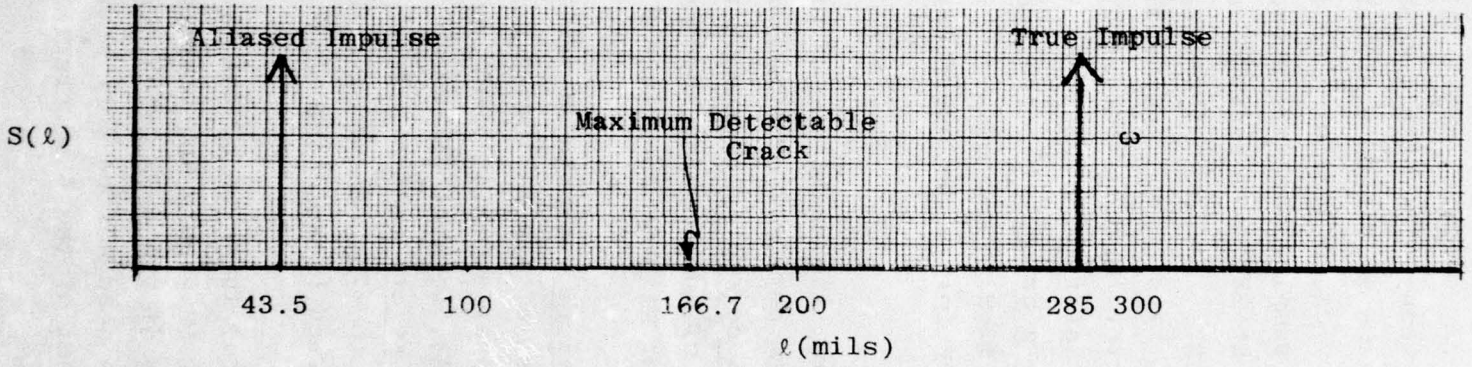


FIGURE 6.6(b) Spatial transform of sampled values.

FIGURE 6.6: ILLUSTRATION OF HIGH FREQUENCY IMPERSONATING A LOW FREQUENCY

6.5.4 Bandwidth Limitation of the Transducer and Other Practical Considerations

There are four main reasons why the spatial transform $S(\ell)$ (Equation 6.23) in the ℓ-space will not be an impulse:

(1) The fatigue crack is not a perfect reflector and multipath reflections cannot be precluded.

(2) The deconvolution step (Equation 6.7) is a noise-inducing process.

(3) The 0^{o} viewing angle is used to deconvolve the other five signals in the deconvolution step (Equation 6.17); all frequencies might not be reflected in phase for the 0^{o} signal.

(4) In the discrete ℓ-space an impulse function is manifest as a sampling function (sin x/x type); the aliasing of a function other than an impulse is more complicated.

For all of these reasons, an impulse distribution will be obtained rather than a single impulse in the ℓ-space for each fatigue crack. Therefore, a statistic of the spatial transform curve is computed. The closest statistical approximation to the location of an impulse is the expected value of the spatial transform curve.

Therefore, to use this technique, one constructs the spatial transform as in Equation 6.21, but in the discrete domain. A coarse estimate of the true-crack length is needed to determine if the spatial transform $S(\ell)$ curve contains aliased frequencies in the ℓ-space. The estimate is further used to compute the number of fold-overs of the spatial transform curve, and then its expected value is computed to be an estimate of the crack length.

6.6 SUMMARY AND DISCUSSION

The material in this section has dealt with both the theoretical and practical aspects of ultrasonic NDE signal processing. Under certain assumptions, the magnitude of the reflected signal and its energy content are directly correlated with the length of the crack (Equation 6.3). The deconvolution of the reflected signal from a reference signal was introduced to render the signal analyses relatively invariant under different transducers and media conditions (Equation 6.5). In fact, previous work in the crack detection problem has hinged on the amplitude variations of the reflection signal to indicate the size of the crack. The theoretical analysis in Section 6.2 leads to the same conclusion -- the total amount of reflected energy is directly correlated to the length of the crack (Equation 6.5). This is <u>not</u> the case in practice, however.

Figure 6.7 is a plot of the total energy in the reflected signal, after deconvolution, versus the crack length. Although there is a trend -- larger cracks tend to have larger amounts of reflected energy -- in no way can it be described as linear, i.e., monotonic.

Moreover, by changing the test conditions of Series 1 via changing the transducer wedge angle, the Series 2 trend is entirely different (a dotted line in Figure 6.7). So for example, a 54 mil crack in Series 2 resembles a 27 mil crack in Series 1, and a 93 mil crack in Series 1 appears larger than a 279 mil crack in Series 2, based on total spectral energy. The assumption of linearity is clearly insufficient in resolving crack sizes with any degree of accuracy.

The peaks and shape of the cepstrum were shown to yield important information about crack size, although the detection of the cepstral peaks must be resolved by a statistical procedure.

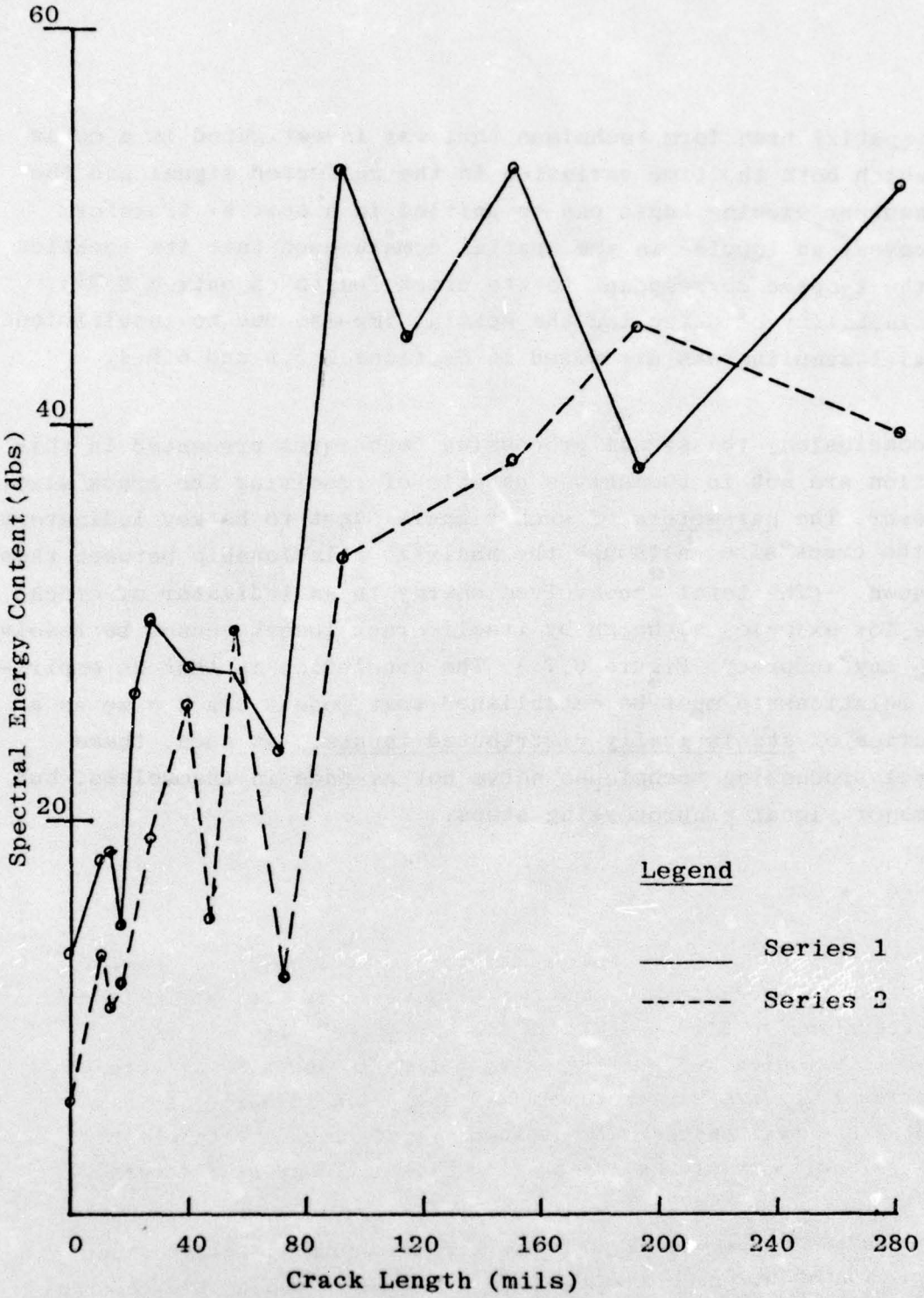


FIGURE 6.7: PLOT OF DECONVOLVED TOTAL SPECTRAL ENERGY VERSUS CRACK LENGTH

The spatial transform technique that was investigated is a means by which both the time variation in the reflected signal and the transducer viewing angle can be unified in a spatial transform to reveal an impulse in the spatial domain such that its location in the ℓ-space corresponds to the crack length (Equation 6.21). The inability of detecting the spatial impulse due to insufficient spatial sampling was discussed in Sections 6.5.3 and 6.5.4.

In conclusion, the signal processing techniques presented in this section are not in themselves capable of resolving the crack size. However, the parameters of such signals ought to be key indicators of the crack size, although the analytic relationship between them is unknown. (The total deconvolved energy is an indicator of crack size, for example, although by itself crack length cannot be resolved with any accuracy; Figure 6.7.) The conclusion is that an empirical relationship must be established that models crack size as a function of statistically distributed inputs. As such, these signal processing techniques serve not as ends in themselves, but as major signal preprocessing steps.

7. PULSE ECHO WAVEFORM PARAMETERIZATION

Based on the developments presented in Section 6, the following parameters were computed as candidate inputs to the Adaptive Learning Network (ALN) model.

The parameters extracted from the power spectrum consisted of the relative power in 1 MHz bands between 6 to 14 MHz, and the total power in the 6-14 MHz band. The relative power in a particular 1 MHz band is defined as the ratio between the actual power in that band and the total power in the 6-14 MHz band. The power spectra of small cracks have larger high frequency content than do large cracks, due to the interaction of small wavelengths with small cracks, so the ratio of high frequency power to low frequency power should be high for small cracks and low for large cracks. The relative power parameters should reflect this trend.

One additional "spatial" parameter was computed from the power spectrum and it relates to the discussion in Section 6.5. The expected value of the spatial transform was found to be an indicator of the crack size (Section 6.5.4) and it is a linear transformation of the power spectrum divided by the bandwidth of the spatial frequency. This ratio, in turn, is proportional to the transducer bandwidth, the viewing angle, and the velocity of ultrasound in the material (Equation 6.18). This parameter was computed by dividing the total power in the 6-14 MHz band by the spatial bandwidth, $\Omega_h - \Omega_\ell$.

Thus, there were a total of 10 parameters from the power spectrum -- eight relative powers in 1 MHz band from 6-14 MHz, the total power in the 6-14 MHz band, and the average spatial power.

The cepstral waveform was parameterized to reflect both its shape and peak distribution because both are informative of crack size geometry (Section 6.4). The abscissa of the cepstrum has the units of time, although it is termed "quefrency," and the

locations of the peaks along the abscissa are the relevant time delays (i.e., phase information). These are a function of the viewing angle and the crack geometry (Section 6.5).

It was decided that time delays (peaks) which were manifest beyond half the window length (of 5.12 microseconds) were artifactual. This was so because a time delay of 1 nanosecond corresponded to a crack length of 0.126 mils, and therefore a delay of 2.5 microseconds corresponded to 315 mils -- which was greater than the largest crack in the sample set. Therefore, the peak distribution as well as the overall cepstral waveform shap in the 0-2.7 microsecond range were considered to lie in an appropriate interval for parameterization.

The range 0-2.7 microseconds was divided into 10 equal bands of 0.27 microsecond width and the number of local maxima as well as the area in each band were computed. Initially, the locations of all the peaks within a band of interest were computed. A local maximum was determined by that candidate peak which was greater than its three neighboring peaks. In this fashion, the total number of local maxima was computed. The area of the cepstrum in the band of interest was computed by integrating over the band.

A total of 20 parameters was computed from the cepstrum -- 10 relating to the area and 10 relating to the number of local maxima in the 0 to 2.7 microsecond interval.

The sine of the transducer viewing angle was the final parameter.

Table 7.1 shows the 31 parameters that served as candidate inputs to the ALN. Table 7.2 lists the character of the parameter list compiled for each experiment. Table 7.2 has, in addition, three items of header information: (1) the test identification number, (2) the nominal crack size, and (3) the viewing angle.

TABLE 7.1
ALN INPUT PARAMETERS

Waveform	Number	Description
Power Spectrum	9	Fractional power in 1 MHz bands in range 6 to 14 MHz; total power
Spatial Power	1	Total power divided by width of spatial range
Cepstrum	20	Number of peaks observed in 10 equally spaced bands between 0-2,700 nanoseconds; total cepstral values in the 10 bands
Transducer Orientation	1	Sin θ

TOTAL: 31

TABLE 7.2

PARAMETER LIST USED AS INPUT TO THE ALN
FATIGUE CRACK LENGTH ESTIMATION MODEL

Variable Number	Description
1	Test number.
2	Crack size in mils.
3	Viewing angle with respect to the normal to the plane of the crack in degrees.
4	Fractional deconvolved power in the 6-7 MHz band.
5	Fractional deconvolved power in the 7-8 MHz band.
6	Fractional deconvolved power in the 8-9 MHz band.
7	Fractional deconvolved power in the 9-10 MHz band.
8	Fractional deconvolved power in the 10-11 MHz band.
9	Fractional deconvolved power in the 11-12 MHz band.
10	Fractional deconvolved power in the 12-13 MHz band.
11	Fractional deconvolved power in the 13-14 MHz band
12	Total deconvolved power in the 6-14 MHz band.
13	Total number of peaks in the 1-270 nanoseconds band of the cepstrum.
14	Total number of peaks in the 271-540 nanoseconds band of the cepstrum.
15	Total number of peaks in the 541-810 nanoseconds band of the cepstrum.
16	Total number of peaks in the 811-1,080 nanoseconds band of the cepstrum.
17	Total number of peaks in the 1,081-1,350 nanoseconds band of the cepstrum.
18	Total number of peaks in the 1,351-1,620 nanoseconds band of the cepstrum.
19	Total number of peaks in the 1,621-1,890 nanoseconds band of the cepstrum.
20	Total number of peaks in the 1,891-2,160 nanoseconds band of the cepstrum.
21	Total number of peaks in the 2,161-2,430 nanoseconds band of the cepstrum.
22	Total number of peaks in the 2,431-2,700 nanoseconds band of the cepstrum.
23	Area of the cepstrum in the 1-270 nanoseconds band.
24	Area of the cepstrum in the 271-540 nanoseconds band.
25	Area of the cepstrum in the 541-810 nanoseconds band.
26	Area of the cepstrum in the 811-1,080 nanoseconds band.
27	Area of the cepstrum in the 1,081-1,350 nanoseconds band.
28	Area of the cepstrum in the 1,351-1,620 nanoseconds band.
29	Area of the cepstrum in the 1,621-1,890 nanoseconds band.
30	Area of the cepstrum in the 1,891-2,160 nanoseconds band.
31	Area of the cepstrum in the 2,161-2,430 nanoseconds band.
32	Area of the cepstrum in the 2,431-2,700 nanoseconds band.
33	Total spatial power in the 6-14 MHz band. (Function of parameter 12).
34	Sine of the viewing angle.

Finally, Figure 7.1 is a schematic of the entire waveform preprocessing and parameterization procedures carried out for each experiment to generate the parameter list shown in Table 7.2. The pulse echoes collected by the transient recorder were first corrected for base line shift, gain, and damping induced by the electronic data gathering system. The appropriate window of data was gated to isolate the region of interest (i.e., the hole and crack responses). The six circularly scanned waveforms and the reference waveform were then transformed into the frequency domain by an FFT algorithm.

Each of the six frequency domain signals was deconvolved from the reference signal and bandpass filtered to isolate only the frequencies of interest. The power spectrum and cepstrum were generated and the parameters extracted by the method discussed in this section. The 31-component parameter vector, $X = (x_4, x_5, \ldots, x_{34})$, was the input to the ALN.

The synthesis of the final link, i.e., the ALN model and its performance, are discussed in the next section.

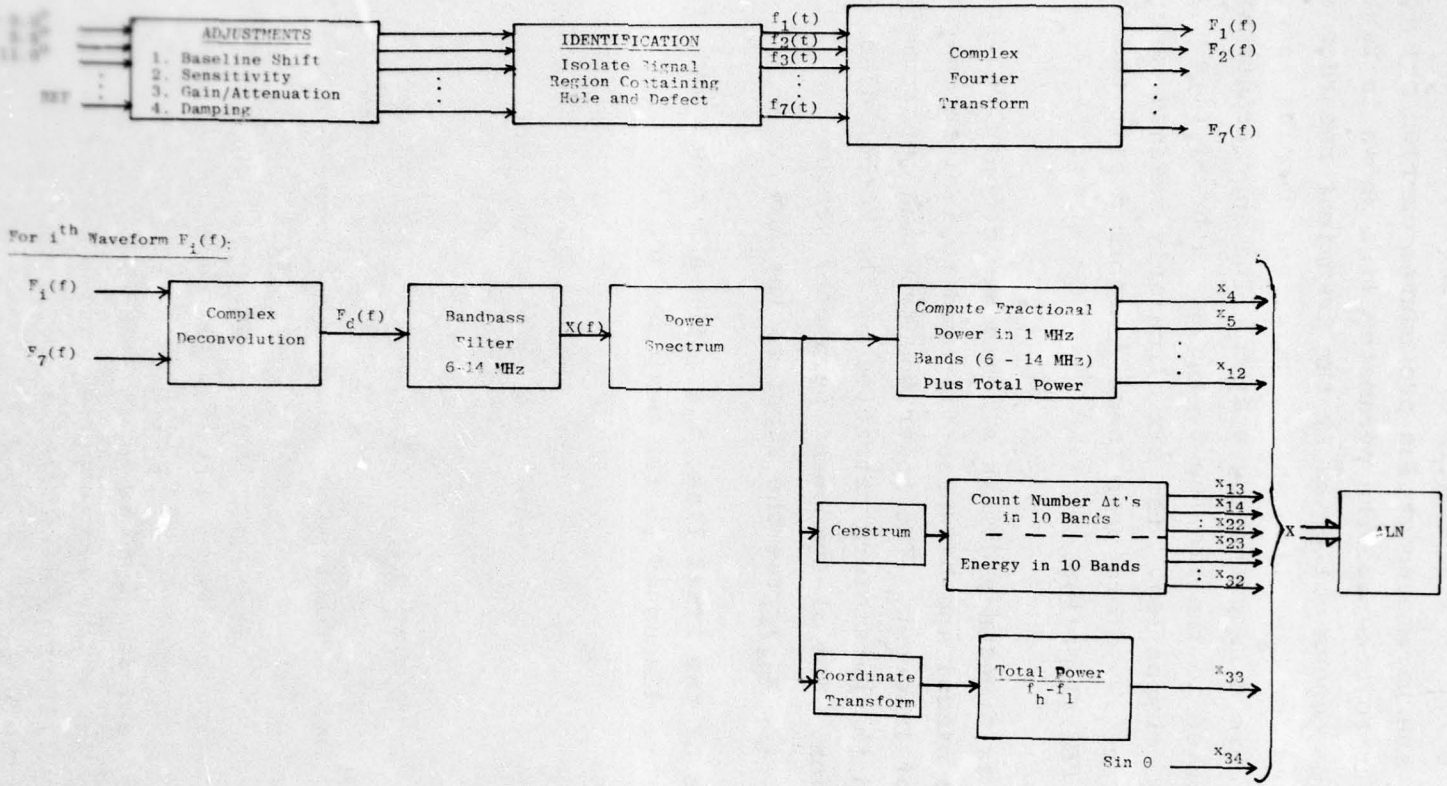


FIGURE 7.1: FATIGUE CRACK LENGTH SIGNAL PREPROCESSING STEPS

8. SYNTHESIS AND PERFORMANCE OF ADAPTIVE LEARNING NETWORK (ALN) SUBSURFACE FATIGUE CRACK MEASUREMENT MODEL

8.1 ALN SYNTHESIS PROCEDURE

Each of the time signals was preprocessed and 31 parameters were computed from its power spectrum and cepstrum (Section 7). Series 1 was recorded in July 1975. Series 2, with minor changes in the experimental arrangement, was recorded in August 1975. The latter series of data was recorded with a shear wave refracted angle of 60^{o} as opposed to the 70^{o} refracted angle used in the first series. Thus each crack specimen was recorded under two different experimental conditions and circularly scanned at six different viewing angles to yield a total of 12 time signals per specimen. The 12 time signals were treated as independent entities because, at each viewing angle, only a component of the plane of the crack is perpendicular to the longitudinal axis of the transducer -- the largest component corresponding to the case when the viewing angle is perpendicular to the plane of the crack and it is equal to the nominal crack length. So a total of 192 time signals (16 cracks x 12 signals/crack), each of which contained 512 points sampled at 10 nanoseconds/point, were parameterized (Section 7) to produce a data base consisting of 192 records with 31 independent parameters. The 32nd variable was the dependent variable, ℓ, the crack length.

For purposes of modeling, the 192 records were divided into three groups -- the fitting, selection, and evaluation subsets. Table 8.1 shows the distribution of data in the three subsets. The fitting and selection subset each consisted of 72 records of 12 crack specimens from either Series 1 or Series 2. The evaluation subset consisted of 48 records from four specimen cracks -- 192 mils, 93 mils, 39 mils and 14 mils. The fitting and selection subsets of data were used to synthesize the model to measure crack length and the evaluation subset was used to infer its generalizing capabilities to new crack specimens that had not been used in designing the model.

TABLE 8.1

DISTRIBUTION OF THE 192 DATA RECORDS

AMONG THE THREE DATA SUBSETS

Specimen	DATA SUBSET		
	Fitting	Selection	Evaluation
15-279	6 (I)	6 (II)	
14-192			6 (I), 6 (II)
13-150	6 (II)	6 (I)	
12-113	6 (I)	6 (II)	
11-093			6 (I), 6 (II)
10-073	6 (II)	6 (I)	
09-054	6 (I)	6 (II)	
08-048	6 (II)	6 (I)	
07-039			6 (I), 6 (II)
06-027	6 (I)	6 (II)	
05-022	6 (II)	6 (I)	
04-018	6 (I)	6 (II)	
03-014			6 (I), 6 (II)
02-011	6 (II)	6 (I)	
01-000	6 (I)	6 (II)	
00-000	6 (II)	6 (I)	
TOTAL RECORDS	72	72	48

I - Series 1 Records

II - Series 2 Records

By design, most of the crack sample specimens were in the smaller size range (50 percent of them were below 48 mils) because accuracy in this range was of prime importance. Therefore, the goal was to create a model that could discriminate between smaller sized cracks as accurately as between larger sized cracks.

One way to implement this bias is to train the model to estimate the logarithm of the crack length, rather than the crack length itself. The log function has the desirable property of rapid changes for small values of the argument because its derivative is inversely proportional to ℓ. However, these changes occur near 0 mils, where the derivative is infinite, whereas the modeling requirement calls for rapid changes at a higher value -- such as 30 mils. Consequently, it was decided to train the model to measure a variable y, where:

$$y = \text{Ln}\left(\frac{\ell'}{30}\right) \tag{8.1}$$

and

$$\ell' = \ell(1-\sin\theta) \tag{8.2}$$

where ℓ = nominal crack length in mils
θ = transducer viewing angle in degrees

Equation (8.1) is a function of the transducer viewing angle θ as well as ℓ. It was assumed that the crack length "visible" to the transducer at angle θ was proportional to (1-sin θ); hence, Equation 8.2.

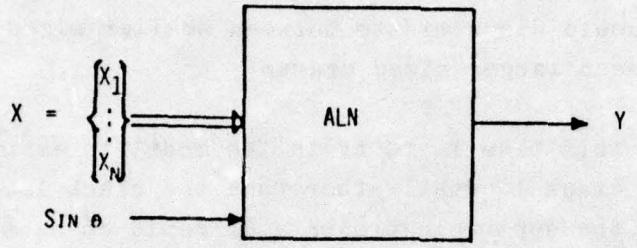
Figure 8.1(a) outlines the model synthesis procedure. It shows a plot of y (from Equation 8.1) versus crack length ℓ. Notice that the crossover point is ℓ=30 for a 0^{o} viewing angle. The crossover point increases for increases in viewing angle. The slope of Equation 8.1 is

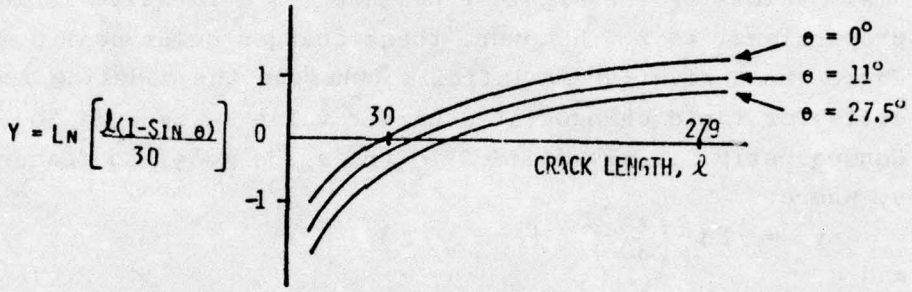
$$\frac{\partial y}{\partial \ell} = 1/\ell \tag{8.3}$$

(a) MODEL SYNTHESIS

INPUTS = NDE WAVEFORM PARAMETERS = $X_1, \ldots, X_N$, SIN θ

OUTPUT = $Y = \text{LN}\left[\frac{\ell(1-\text{SIN }\theta)}{30}\right]$





(b) MODEL USAGE

INPUTS = NDE WAVEFORM PARAMETERS = $X_1, \ldots, X_N$, SIN θ

OUTPUT = $\hat{\ell}$ = ESTIMATED CRACK LENGTH

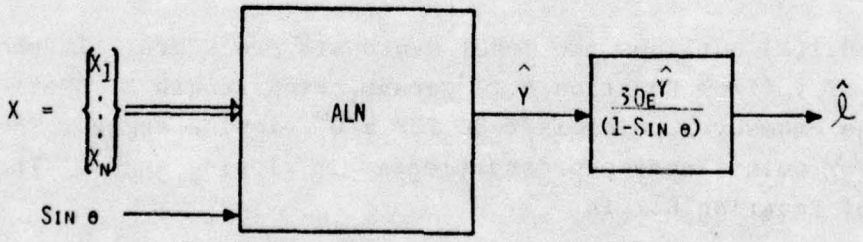


FIGURE 8.1: QUANTITATIVE SURFACE/SUBSURFACE FATIGUE CRACK LENGTH MEASUREMENT SYSTEM

which is large for small values of ℓ and progressively decreases for increases in crack length ℓ. This greatly penalizes the model for small errors in the range (0-30 mils), where a model output could be in error by several percentage points from its nominal value, whereas the corresponding error in the larger range (30 mils and above) is not so severely penalized.

It must be stressed that the model has been trained to recognize a function of the nominally characterized crack length, which is based on measurements detailed in Section 3. The agreement between nominally characterized crack lengths and actual crack lengths can only be verified by destructively testing the sample specimens. This information regarding the true crack length was not available at the time of writing.

After model synthesis, the estimate for new (i.e., previously unseen) data is processed through an inverse function of Equations (8.1) and (8.2) to yield the estimated measured crack size,[1/] i.e.,

$$\hat{\ell} = \frac{30\, e^{\hat{y}}}{(1-\sin\theta)} \qquad (8.4)$$

where:

$\hat{y}$ = estimate computed by the ALN model

$\hat{\ell}$ = measured crack length obtained from $\hat{y}$

θ = viewing angle.

Figure 8.1(b) shows how $\hat{\ell}$ is obtained. The relevant 31 parameters are computed by the methods of Section 7 and are input to the ALN model. Its output, $\hat{y}$, is processed through a system which realizes Equation 8.4, thereby producing the measured crack size, $\hat{\ell}$.

[1/] The carat above a variable (e.g., $\hat{y}$) denotes an estimated quantity.

If data of the same unknown crack are available at different viewing angles, additional measurements of the crack can be made. These measurements can be combined (by averaging, for example) to yield a composite measurement of the crack length. This was the procedure adopted in this project. Therefore, the composite crack length estimate for a given fastener hole, $\hat{\ell}$, was the average of the six ALN model outputs for each of the six viewing angles:

$$\hat{\ell} = 1/6\,[\hat{\ell}(\theta = 0^{o}) + \hat{\ell}(\theta = 5.5^{o}) + \hat{\ell}(\theta = 11^{o}) + \hat{\ell}(\theta = 16.5^{o}) + \hat{\ell}(\theta = 22^{o}) + \hat{\ell}(\theta = 27.5^{o})] \qquad (8.5)$$

8.2 RESULTANT ALN SUBSURFACE FATIGUE CRACK MEASUREMENT MODEL

A unique capability exists for synthesizing nonlinear multivariate models that can infer flaw geometry with very high accuracy. This approach is called the nonlinear adaptive learning network (ALN) and the ALN synthesis methodology is outlined in Appendix A of this project's interim report (Ref. 6) and in References 1, 5, 7, 8, and 9. In summary, an ALN model consists of a multinomial (a polynomial in many variables) that has been synthesized in such a manner as to discover adaptively the pertinent parameters and their linear and nonlinear combinations.

An ALN was trained via the methods summarized in the above references using the data from the 12 sample crack specimens (Table 8.1) and the parameters described in Section 7. The data from the 12 crack specimens consisted of 144 vectors in the 31-parameter space. The model output variable, y, was the function realized by Equation (8.1). Thus the information used for each experiment was:

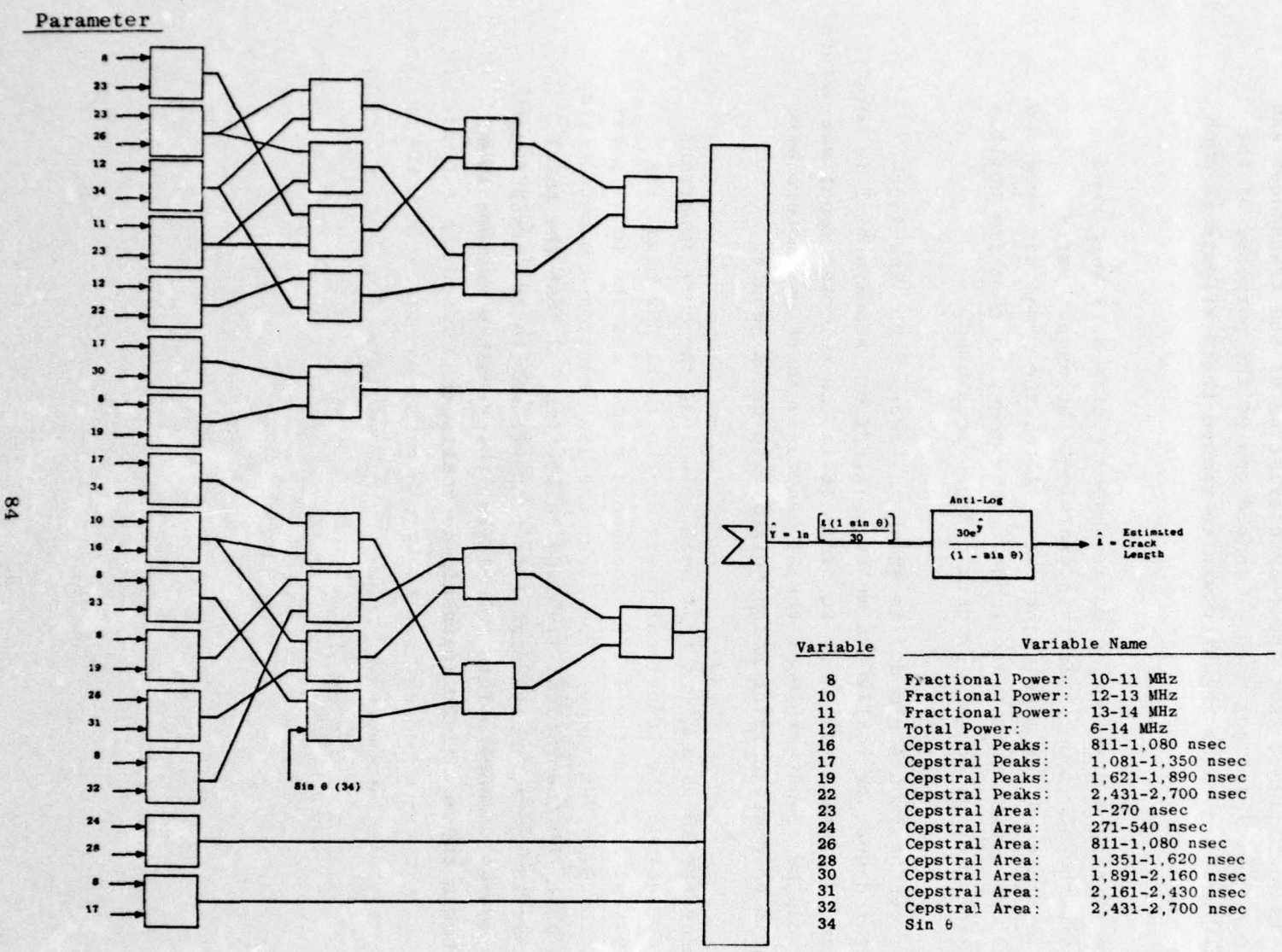
- Input variables -- 31 parameters of the recorded pulse echo in Table 7.2.
- Output variable -- a function of the crack length as per Equation 8.1.

It is significant that the characteristics of the transducer and the material are not used -- indeed one of the purposes of the waveform preprocessing step was to remove their effects as much as possible.

The fitting and selection data subsets (Table 8.1) were used to train the ALN model. In this exercise, the output variable was used for model synthesis. After the model was obtained, the evaluation subset was input to the model to test its ability to infer crack length for data not previous used.

The synthesized ALN model is shown in Figure 8.2. The four-layered network realizes a multinomial (i.e., a polynomial in more than two variables) of up to order 16 in the selected input parameters. It can be seen that 16 of the 31 candidate input parameters were found to contain information relative to crack length.

Among the 16 parameters that were selected, the more important ones include the fractional power in the 10-11 MHz band, the cepstral area in the 1-270 nanosecond range, and the total power in the 6-14 MHz range. The first and last mentioned substantiate, in part, the theoretical findings in Section 6.2 that the total power in the reflected signal is proportional to the crack length. Of course, theory points to a linear relationship between them, whereas the actual relationship is nonlinear.



Variable	Variable Name	
8	Fractional Power:	10-11 MHz
10	Fractional Power:	12-13 MHz
11	Fractional Power:	13-14 MHz
12	Total Power:	6-14 MHz
16	Cepstral Peaks:	811-1,080 nsec
17	Cepstral Peaks:	1,081-1,350 nsec
19	Cepstral Peaks:	1,621-1,890 nsec
22	Cepstral Peaks:	2,431-2,700 nsec
23	Cepstral Area:	1-270 nsec
24	Cepstral Area:	271-540 nsec
26	Cepstral Area:	811-1,080 nsec
28	Cepstral Area:	1,351-1,620 nsec
30	Cepstral Area:	1,891-2,160 nsec
31	Cepstral Area:	2,161-2,430 nsec
32	Cepstral Area:	2,431-2,700 nsec
34	Sin θ	

FIGURE 8.2: ALN SUBSURFACE FATIGUE CRACK MEASUREMENT MODEL

8.3 DISCUSSION OF RESULTS

Table 8.2 and Figure 8.3 show the performance of the ALN classifier in measuring subsurface fatigue cracks. The mean absolute percentage error, which is a measure of how close the model output is to the nominal crack length, i.e.,

$$e = \left| \frac{\ell - \hat{\ell}}{\ell} \right| \times 100\% \qquad (8.6)$$

is 33.4 percent for both Series 1 and Series 2. If the average of the two estimates from Series 1 and 2 is computed (last column in Table 8.2), the mean absolute percentage error is 30.3 percent. The largest errors are committed in classifying a 14 mil crack in Series 1, a 39 mil crack and a 93 mil crack in Series 2. It was mentioned in Sections 5.3 and 5.7 that four sample specimens -- the three aforementioned and sample 14-192 -- were used in most of the early experimentation in the data collection phase. A total of 176 experiments was conducted on these four sample specimens (see Appendix B2) to determine the optimum signal averaging procedures along with the feasibility of removing the fastener bolt prior to the recording of Series 1 and 2 data. There were enough anomalies in the reflected signals from these four sample specimens during the Series 1 and 2 experimentation to warrant a destructive examination of them. The results of the impending destructive test could show some effects of the early experimentation on these specimens. If the largest errors are omitted, the mean absolute percentage error is 19.2 percent for Series 1 and 19.6 percent for Series 2.

TABLE 8.2

PERFORMANCE OF ALN MODEL IN MEASURING
CRACK SIZE FROM ULTRASONIC NDE WAVEFORM PARAMETERS

True Crack Length ℓ (mils)	Series 1		Series 2		Average of Series 1 & 2	
	Estimated Length $\hat{\ell}$	Percent Error	Estimated Length $\hat{\ell}$	Percent Error	Estimated Length $\hat{\ell}$	Percent Error
279	278.7	0.1	311.7	-11.7	295.2	-5.8
192	178.6	7.0	159.6	16.9	169.1	11.9
150	137.3	8.5	122.6	18.3	130.0	13.4
113	84.5	25.2	81.8	27.6	83.2	26.4
93	75.6	18.7	26.4	71.6	51.0	45.2
73	48.6	33.4	34.8	52.3	41.7	42.9
54	56.6	-4.8	64.9	-20.2	60.8	-12.5
48	30.4	36.7	43.2	10.0	36.8	23.3
39	40.3	-3.3	96.7	-147.4	68.5	-75.6
27	47.3	75.2	20.0	25.9	33.7	-24.6
22	21.5	-2.3	18.4	16.4	20.0	9.3
18	18.7	-3.9	21.6	-20.0	20.2	-11.9
14	42.6	204.3	11.5	17.9	27.1	-93.2
11	15.9	44.5	12.2	-10.9	14.1	-27.7
0	3.8	-	5.3	-	4.6	-
0	5.5	-	17.7	-	11.6	-
	Mean % Error:	31.4	Mean % Error:	3.3	Mean % Error:	-5.6
	Mean Absolute % Error:	33.4	Mean Absolute % Error:	33.4	Mean Absolute % Error:	30.3

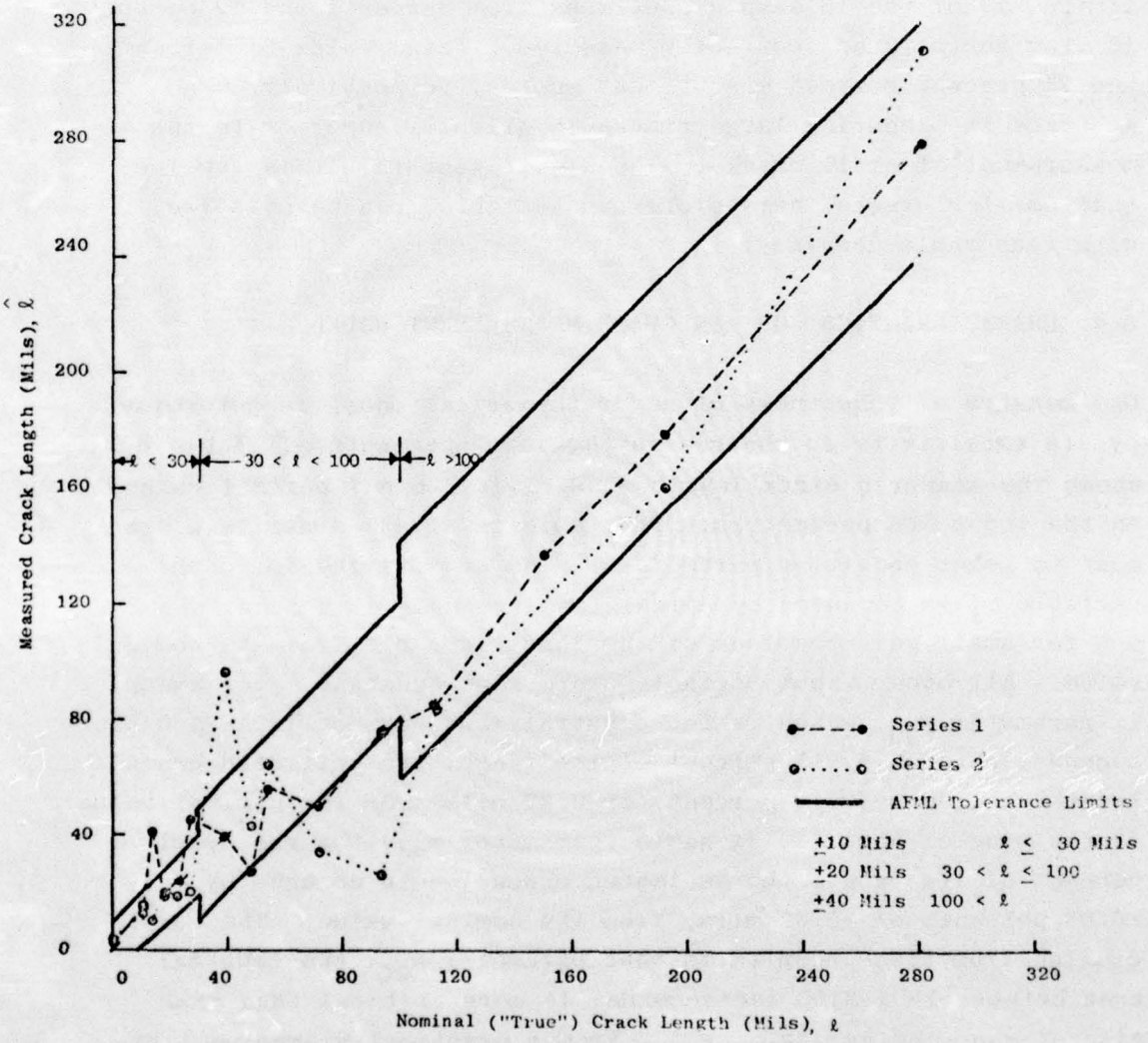


FIGURE 8.3: PERFORMANCE OF ALN QUANTITATIVE SURFACE/SUBSURFACE FATIGUE CRACK LENGTH MEASUREMENT SYSTEM

The AFML tolerance limit for cracks above 100 mils is ± 40 mils, for cracks between 30 and 100 mils is ± 20 mils, and for cracks less than 30 mils is ± 20 mils. With respect to these limits, 13 of the 16 sample specimens from Series 1 and 12 of the 16 from Series 2 are correctly measured. This yields 81 percent and 75 percent correct measurement scores, respectively. The accuracy in measuring large cracks is slightly superior to the measurement of small cracks. The significant result is the fact that smaller cracks, heretofore undetectable, can be measured with reasonable accuracy.

8.4 CHARACTERISTICS OF ALN CRACK MEASUREMENT MODEL

One measure of robustness of any mathematical model is determined by its sensitivity to changes in the input parameters. Table 8.3 shows the measured crack length sensitivity to a 1 percent change in the input NDE parameters. The table is a rank-ordering of the most to least sensitive parameters. The sensitivity for each variable x_i is computed by calculating the change in model output for small perturbations of the input variable from its nominal value. All other input variables were kept constant. For example, if parameter x_{30}, which is the cepstral area between 1891-2160 nanoseconds, changes by +1 percent of its range, the estimated crack length changes by 3.19 percent, or 2.87 mils from its nominal value. If the sine of the viewing angle (parameter x_{34}) changes by +1 percent of its range, the estimated crack length changes by only -0.08 percent, or -0.07 mils, from its nominal value. The conclusion from these results is that parameter x_{30}, the cepstral area between 1891-2160 nanoseconds, is more critical than the sine of the viewing angle, x_{34}. From a practical viewpoint, this is a highly desirable result since very accurate angular measurements are not predicted to be necessary for accurate crack estimates using this system.

Another important function of a robust mathematical model is the agreement between its empirically implemented input-output relationship and the underlying physical phenomena. Examining the table, parameters x_8, x_{23}, and x_{10}, the fractional power in the 10-11 MHz range, cepstral area in the 1-270 nanosecond interval, and the fractional power in the 12-13 MHz band, respectively, have been negatively correlated with the crack length by the model. It is known from physical principles that the power spectra of the reflected signals from large and small cracks differ in that the former has higher low-frequency content than the latter. At the frequencies 10-13 MHz, the wavelengths vary from 12.6 mils to 9.7 mils which are too small to interact with large cracks (279 mils, etc.) Thus, any increase in the energy content in these bands is an indication of a smaller crack. The sensitivity table indicates the same trend -- a 1 percent increase in parameters x_8 and x_{10}, leads to 0.29 mil and 0.17 mil decrease in crack length. An increase in cepstral area in the 1-270 nanosecond region (x_{23}) is an indication of increase in the time delays due to small cracks in the 0-34 mil range. Therefore, larger cracks will have a smaller value of x_{23}. The sensitivity table indicates the same trend. A one percent increase in x_{23} causes a 0.21 mil decrease in the estimated crack length.

Finally, parameters x_{30}, x_{12} and x_{31} -- which are the cepstral area in 1891-2160 nanoseconds region, the total power in the 6-14 MHz band and the cepstral area in the 2161-2430 nanosecond band, respectively -- have been positively correlated with the crack length by the model. Parameter x_{12}, the total power reflected from a crack, is known to increase with increase in crack length and, in previous investigations, was the sole indicator of crack length. Parameters x_{30} and x_{31} are time delays associated with cracks ranging from 238-306 mils. An increase in these values is an indication of a large crack. The crack length increases by an estimated 2.87 mils and 1.10 mils for 1 percent changes in x_{30} and x_{31}, respectively.

AD-A031 464 ADAPTRONICS INC MCLEAN VA F/G 20/1
ADAPTIVE NONLINEAR SIGNAL PROCESSING FOR CHARACTERIZATION OF UL--ETC(U)
JUN 76 R SHANKAR, A N MUCCIARDI, D CLEVELAND F33615-74-C-5122
UNCLASSIFIED 687 AFML-TR-76-44 NL

2 OF 2
AD A031464



END

DATE FILMED
12-76

TABLE 8.3

CRACK LENGTH SENSITIVITY TO CHANGES
IN NDE ULTRASONIC PARAMETERS

VARIABLE NAME* (X_i)	AVERAGE CRACK LENGTH CHANGE PER 1% CHANGE IN VARIABLE X_i	
	MILS	%
CEPSTRAL AREA: 1891-2160 NSEC BAND (X_{30})	2.87	3.19
TOTAL POWER: 6-14 MHz BAND (X_{12})	1.44	1.60
CEPSTRAL AREA: 2161-2430 NSEC BAND (X_{31})	1.10	1.23
CEPSTRAL AREA: 271-540 NSEC BAND (X_{24})	0.33	0.36
CEPSTRAL AREA: 811-1080 NSEC BAND (X_{26})	0.32	0.35
FRACTIONAL POWER: 10-11 MHz BAND (X_8)	-0.29	-0.33
CEPSTRAL AREA: 1-270 NSEC BAND (X_{23})	-0.21	-0.23
CEPSTRAL PEAKS: 811-1080 NSEC BAND (X_{16})	0.18	0.20
FRACTIONAL POWER: 12-13 MHz BAND (X_{10})	-0.17	-0.19
CEPSTRAL AREA: 1351-1620 NSEC BAND (X_{28})	0.09	0.10
SINE OF VIEWING ANGLE (X_{34})	-0.07	-0.08
CEPSTRAL PEAKS: 1621-1890 NSEC BAND (X_{19})	0.05	0.06
CEPSTRAL AREA: 2431-2700 NSEC BAND (X_{32})	-0.02	-0.03
CEPSTRAL PEAKS: 2431-2700 NSEC BAND (X_{22})	0.02	0.02
CEPSTRAL PEAKS: 1081-1350 NSEC BAND (X_{17})	-0.01	-0.02
FRACTIONAL POWER: 13-14 MHz BAND (X_{11})	0.01	0.01

* POWER SPECTRUM AND CEPSTRUM HAVE BEEN DECONVOLVED AND BAND-PASS FILTERED

$\ell = ct = (0.126 \text{ mils/nsec})\ t$

Δt, nsec	$\Delta \ell$, mils
1-270	0.1-34
271-540	34-68
811-1,080	102-136
1,081-1,350	136-170
1,351-1,620	170-204
1,621-1,890	204-238
1,891-2,160	238-272
2,161-2,430	272-306
2,431-2,000	306-340

9. RECOMMENDATIONS

It has been shown that subsurface fatigue crack geometries can be modeled from parameters of the reflected ultrasonic signals with good accuracy over a range of 0-279 mils. For each specimen, reflections were observed at different transducer angular positions, θ, and θ varied from 0^{o} to 27.5^{o}, in 5.5^{o} increments. It was found that the frequency response varied considerably with changes in the angular position, probably due to interference effects. As a consequence, a spatial transform was introduced in an attempt to derive global characteristics of the reflection from a crack as a function of Ω, a spatial variable which, in turn, is a function of both the frequency, f, and θ (Equation 6.18). Unfortunately, Ω was insufficiently sampled in the θ-space, (although it was sampled sufficiently in f-space) to obtain any meaningful global description of the crack characteristics. Consequently, it is recommended that an array of transducers be placed around the periphery of the defect to obtain a larger number of time signals as functions of θ. A spatial transform of the signals should contain more defect discriminatory information since sufficient samples will exist in both time and space (i.e., angular positions).

To obtain a meaningful spatial transform, the amplitude versus time signal data obtained at the various angles must be correctly phased. The time of occurrence of the hole response was invariant as long as the physical distance between the transducer and the fastener hole was fixed. Therefore, the time of occurrence of the hole response in each of the signals can be used as the leading edge of the data window to assist in correctly phasing the reflected signals received at each transducer position in the array.

Another advantage of ultrasonically interrogating a defect with an array of transducers is that each time signal, recorded under different angular conditions, can be considered an independent evaluation of the crack characteristics. If, as the geometry suggests, only a component of the crack length is available at different viewing angles, an ALN can be trained to measure that component of crack length. A global estimate of the crack length can be computed by combining the individual estimates from each viewing angle. Thus, there are more independent estimates of the crack length, which should lead to a more accurate global estimate.

One drawback in using a ring of transducers is that each transducer in the array will have different characteristics. (Of course an array of transducers can be simulated by stepping one transducer through various angular positions as was done in this project. However, to scan over 360^{o} in 5.5^{o} increments requires measurements at 65 positions.) Thus, each reflected signal will have to be deconvolved, in software, from the characteristics of its parent transducer. It was found that the deconvolution process was noise inducing and efforts to bandpass filter tend to reinforce the characteristics of the transducer back into the deconvolute. Further research in the area of inverse filtering procedures is highly recommended.

The effect of deconvolution could be mitigated if one used a chirped continuous wave (CW) input instead of a pulsed input to the transducer. The pulse is broadband and each transducer distorts it depending on individual characteristics. If the chirping frequency range extends over a determined bandwidth, which is a common characteristic to all the constitutent transducers in the array, the existence of spurious frequencies in the deconvolute beyond the transducer dynamic range, is minimized.

It was assumed that the crack length visible to the transducer was porportional to $1-\sin\theta$. This relationship was used to construct the six values of the dependent quantity as a function of the six angular positions for crack specimen: $y(\theta) = \text{Ln}\,[\ell(1-\sin\theta)/30]$ (Equation 8.1). The ALN model that was obtained (Figure 8.2) along with its crack estimates (Figures 1.2 and 8.3) was intentionally biased by this assumption. Further study has revealed that the proper form for $y(\theta)$ is a quadratic in ℓ and θ. This function has a minimum at approximately $\theta = 11^{o}$, which approaches zero as ℓ decreases. Since each value in Figures 1.2 and 8.3 is an average of six estimates, it is conceivable that the scatter could be reduced by retraining the ALN model with a more appropriate form of the dependent variable, $y(\theta)$. The accuracy of the new model should exceed the 70 percent value obtained above. It is recommended that such further training be performed.

10. REFERENCES

1. Barron, R.L., "Theory and Application of Cybernetic Systems: An Overview," Proc. IEEE 1974 National Aerospace Electronics Conference (NAECON '74), Dayton, Ohio, May 13-15, pp. 107-118.

2. Bergland, G. D., "A Guided Tour of the Fast Fourier Transform," IEEE Spectrum, 6, July 1969, pp. 41-52.

3. Boeing Commercial Airplane Company, Detection of Cracks Under Installed Fasteners, AFML-TR-74-50, April 1974.

4. Frederick, J. R. and J. A. Seydel, "Improved Discontinuity Detection Using Computer-Aided Ultrasonic Pulse-Echo Techniques," Welding Research Council Bulletin 185, June 1973, pp. 1-23.

5. Gilstrap, L. O., Jr., "Keys to Developing Machines with High-Level Artificial Intelligence," Proc. ASME Design Engineering Conference, New York, New York, April 19-22, 1971.

6. Mucciardi, A. N., Shankar, R., et.al., Adaptive Nonlinear Signal Processing for Characterization of Ultrasonic NDE Waveforms; TASK 1: Inference of Flat-Bottom Hole Size, Interim Project Report under Contract F33615-74-C-5122, AFML-TR-75-24, February 1975.

7. Mucciardi, A. N., Shankar, and M.J. Buckley, "Applications of Adaptive Learning Networks to Nondestructive Evaluation Technology," Proc. IEEE 1975 National Aerospace Electronics Conference (NAECON '75), Dayton, Ohio, pp. 460-469.

8. Mucciardi, A. N. and E. E. Gose, "An Automatic Clustering Algorithm and Its Properties in High-Dimensional Spaces," IEEE Trans. on Systems, Man, and Cybernetics, Vol. SMC-2, No. 2, April 1972, pp. 247-254.

9. Mucciardi, A. N., "Adaptive Nonlinear Modeling for Ultrasonic Signal Processing," Proc. Interdisciplinary Workshop for Quantitative Flaw Definition, June 1974, D. O. Thompson, (ed.) AFML-TR-74-238, pp. 194-212.

10. Oppenheim, A. V., et.al., "Nonlinear Filtering of Multiplied and Convolved Signals," Proc. IEEE, Vol. 56, pp. 1264-1291, August 1968.

PRECEDING PAGE BLANK-NOT FILMED

APPENDIX A

PREPARATION OF FATIGUE CRACKED FASTENER SPECIMENS

PREPARATION OF FATIGUE CRACKED FASTENER SPECIMENS

Metcut Report 1449-21640-1

for

Adaptronics, Inc.
McLean, Virginia 22101

METCUT RESEARCH ASSOCIATES INC.

February 18, 1975

John B. Kohls, Project Engineer

Approved:

William J. Stross, Supervisor
Materials Testing Laboratory

PRECEDING PAGE BLANK-NOT FILMED

At the request of Mr. Roger L. Barron, President of Adaptronics, Inc., Metcut Research manufactured 16 cracked fatigue specimens. The specimens were manufactured in general conformance to ASTM Specification E127-64 from 5/8 x 3 in. 7075-T651 Aluminum plate. The aluminum conforms to Federal Specification QQ-A-250/13 and was ultrasonically inspected per American Aluminum Association FBH C1. AA 3/64 in. by Conam Inspection of Columbus, Ohio, A Division of Automation Industries, Inc. Certification of material as to mechanical property and ultrasonic inspection is given in the Appendix.

The specimens were low stress ground on all surfaces with a single drilled and reamed hole located at one end. Specimen configuration is shown in Figure 1. Specimens were then loaded into the precracking fixture shown in Figure 2. The precracking was performed in four-point bending on a SF01 Sonntag fatigue machine. This is a constant force machine and has a cycle rate of 1800 cpm. The specimens were cycled at a surface bending stress of 20 ksi and an A ratio of 0.90 ($\sigma_{dyn.} / \sigma_{stat.} = 0.9\%$). Crack initiation occurred between 20,000 and 50,000 cycles with no specimens seeing more than 400,000 cycles (initiation plus growth).

A table showing crack length versus specimen identification is presented in Table I. The cracked surface is identified in the sketch at the bottom of Table I. Holding the specimen in a manner to enable you to read the specimen number, the crack will be on the lower surface, see sketch, Table I.

To insure precracking location and to avoid double crack initiation, an EDM starter notch was used on all specimens except 15-279. The depth and width dimensions of the EDM notches are given in Table I.

One of the initial concerns in the manufacture of the specimens was to grow a crack with a length-to-depth ratio of approximately 1:1. To verify this ratio, four specimens were precracked and broken apart to observe the crack shape and also the relation of actual crack length to the observed crack length prior to failure. Table II gives the crack lengths for the four specimens and Figure 3 shows photographs of the crack area at a magnification of 10X.

After manufacturing and precracking, 1/4 - 28 aircraft quality fasteners were installed in the specimens. The fasteners were installed with a hardened steel washer under both the nut and the head of the fastener, and torqued to a value of 20 ft.-lbs.

The sealant applied to the fastener assembly was a 3-M product - EC-1675, Class B - which is equivalent to MIL-S-8802. A sketch of the installed fastener is shown at the bottom of Table I.

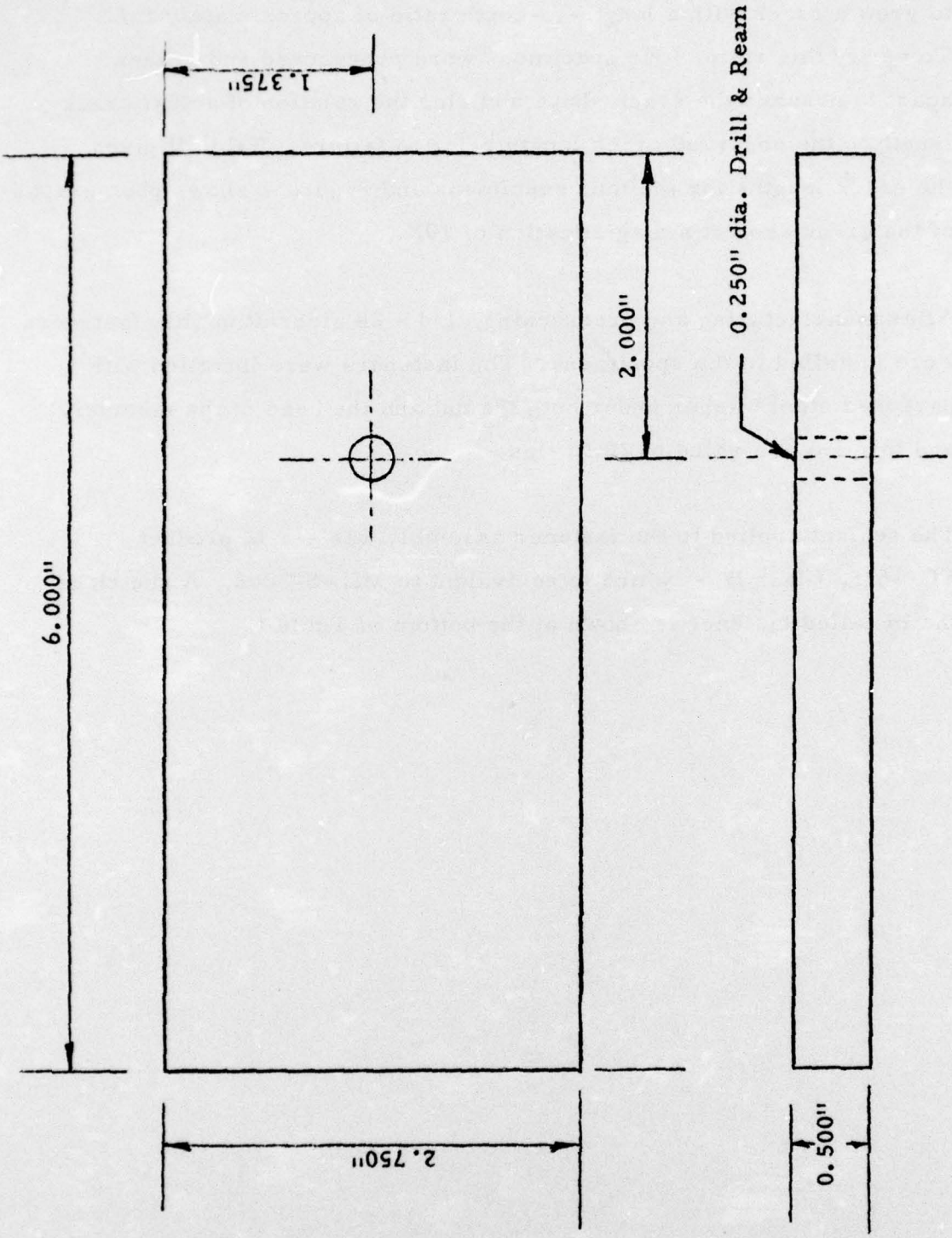


FIGURE 1 - FATIGUE CRACK SPECIMEN

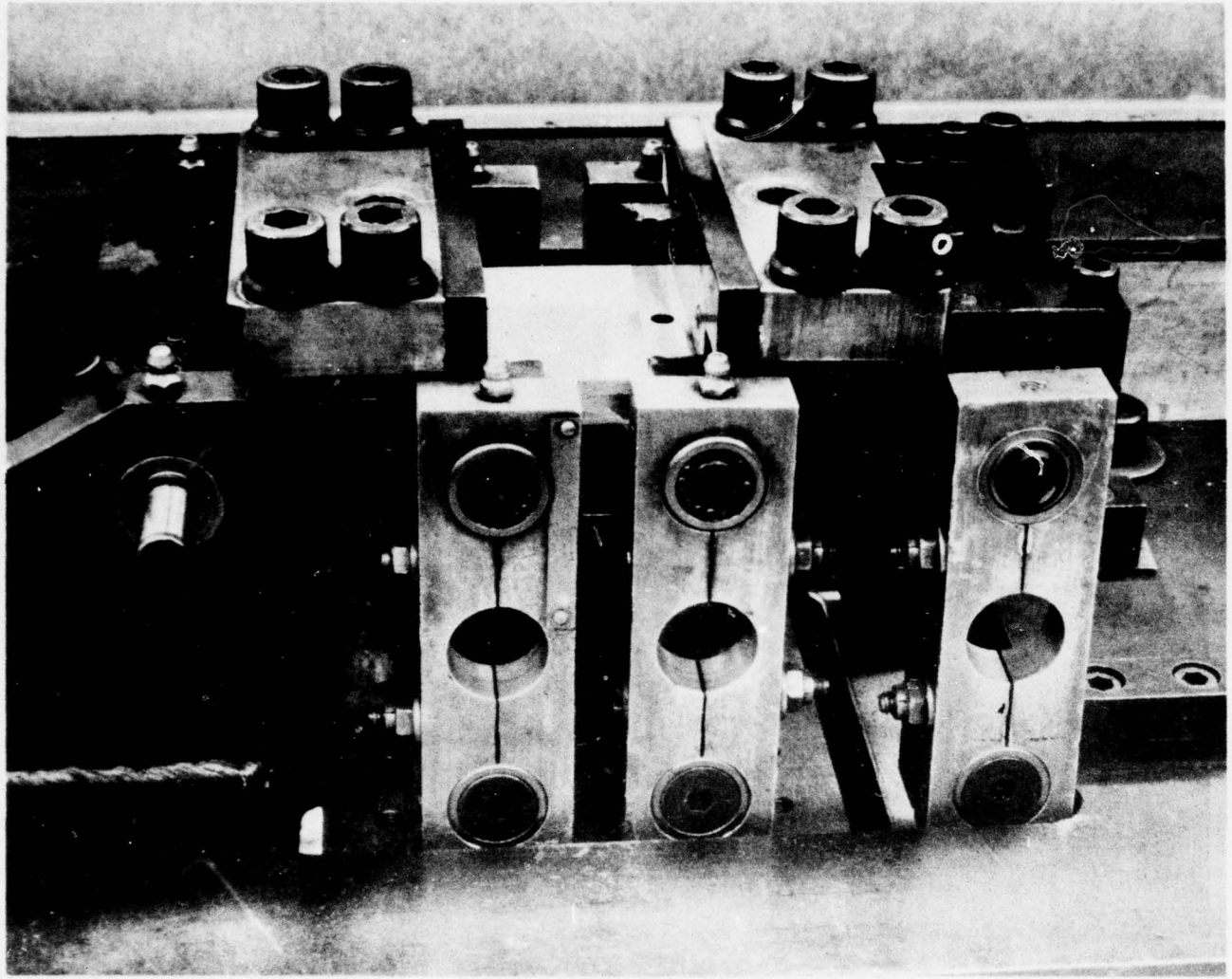
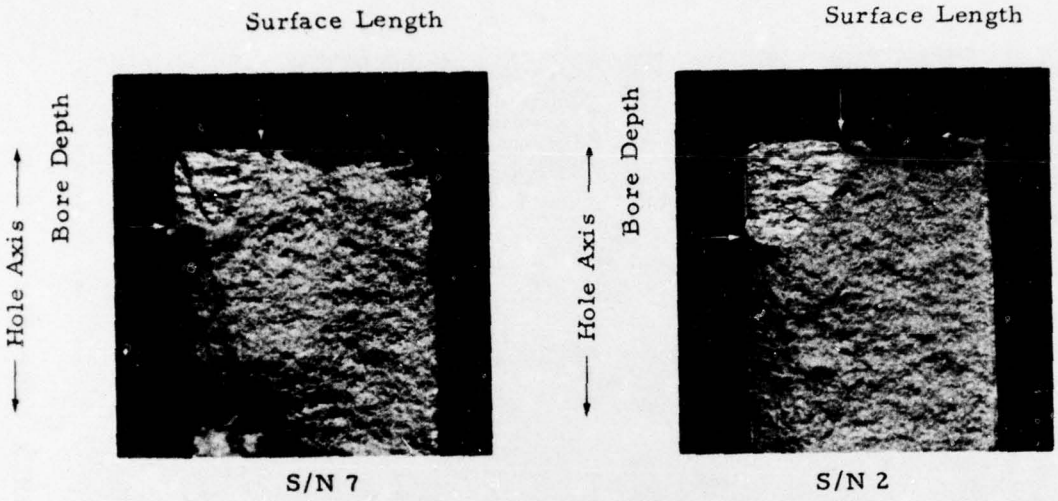
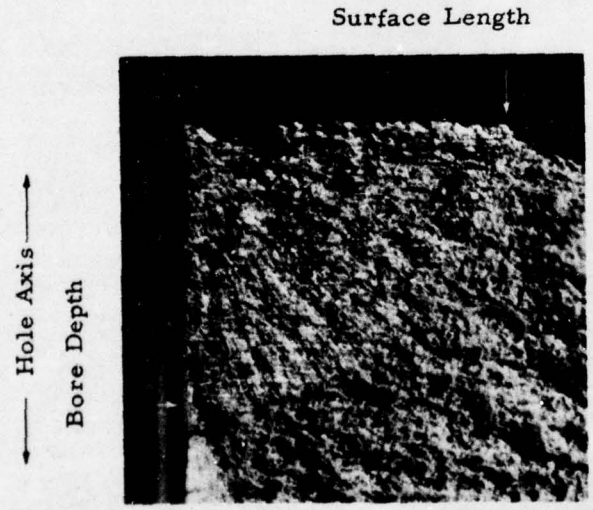


FIGURE 2: PRECRACKING FIXTURE LOADED WITH SPECIMEN (See Figure 3.2)





Ref. Table 3.2.

Mag. 10X

FIGURE 3: PHOTOMACROGRAPHS SHOWING FATIGUE CRACK DEPTH (See Figure 3.3)

APPENDIX

CERTIFICATE OF MATERIAL

ULTRASONIC INSPECTION

CERTIFICATE OF INSPECTION

Report No. 74-811

Date 11-13-74

AUTOMATION INDUSTRIES, INC.
CONAM Inspection
4000 LOCKBOURNE ROAD • COLUMBUS, OHIO 43207 • AC 614 491-3000

ustomer Metcut Research Associates Inc.

Cust. P. O. No. 59035

ttn. John Kohls

☐ PENETRANT ☐ MAGNETIC PARTICLE

treet Address 3980 Rosslyn Drive

☒ ULTRASONIC ☐ EDDY CURRENT

ity & State Cincinnati, Ohio 45209

SPEC No. Am. Alum. Assoc. FBH Cl. AA 3/64"

ort No./Dwg No. 5/8" x 3" Bars

Procedure No.

aterial 7075-T651

No. of Parts or Area of Test 3

est Equipt.
725 Immerscope S/N 7042, Pulser/Receiver S/N 8042, lithium sulphate transducer S/N 13044 15MHz.

t Up Data
Set up on 3/64" flat bottom hole at various depth at 80% minimum amplitude.

chnique
Longitudinal at 10MHz.

ST RESULTS:

3 PCS INSPECTED AND ACCEPTED.

No Reportable Indications Detected

ASNT - TC - 1A LEVEL III	DATE	TECHNICIAN	OBSERVER/APPROVED	DATE
Dale T. Fister	11-13-74	Charles Frazier	C. H. Frazier	11-13-74

I HEREBY CERTIFY THE PARTS LISTED HAVE BEEN TESTED IN CONFORMANCE WITH THE SPECIFICATION NOTED. THIS REPORT REPRESENTS AUTOMATION INDUSTRIES, INC. INTERPRETATION OF THE RESULTS OBTAINED FROM THE TEST AND IS NOT TO BE CONSTRUED AS A GUARANTY OR WARRANTY OF THE CONDITION OF THE MATERIALS TESTED. AUTOMATION INDUSTRIES, INC. SHALL NOT BE HELD LIABLE FOR MISINTERPRETATION OF CONDITIONS, LOSS, DAMAGE, INJURY OR DEATH ARISING FROM OR ATTRIBUTABLE TO DELAY PRECEDING A TEST, OR SUBSEQUENT TO PERFORMANCE OF A TEST.

TABLE I

CRACK LENGTHS OF SPECIMEN

Specimen No.	EDM Starter Notch Depth *	EDM Starter Notch Width **	Crack Length
00-000	---	---	0
01-000	---	---	0
02-011	.0026	.0022	.011
3-014	.0016	.0020	.014
4-018	.0016	.0019	.018
5-022	.0035	.0020	.022
6-027	.0020	.0020	.027
7-039	.0014	.0018	.039
8-048	.0019	.0020	.048
9-054	.0016	.0018	.054
10-073	.0019	.0021	.073
11-093	.0020	.0021	.093
12-113	.0024	.0019	.113
13-150	.0015	.0019	.150
14-192	.0017	.0018	.192
15-279	---	---	.279

* Depth along hole radius

** Width tangent to hole circumference

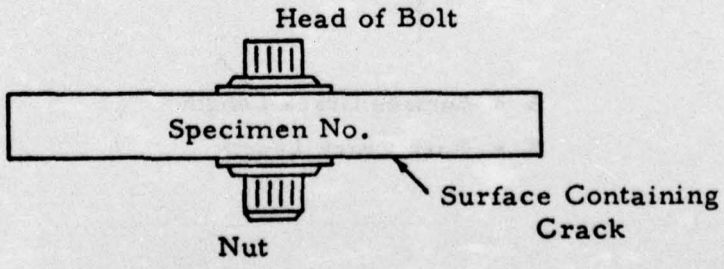
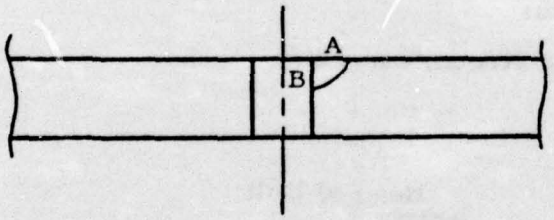


TABLE II

RELATION OF OBSERVED CRACK LENGTH

TO ACTUAL SURFACE LENGTH AND BORE DEPTH

Specimen No.	Surface Crack Length (A) Observed on Surface	Surface Crack Length (A) After Failure	Bore Crack Length (B) After Specimen Failure
7	.057	.055	.035
2	.054	.060	.067
3	.197	.198	.180
10	.196	.201	.185



A = Surface Crack Length

B = Bore Crack Length

(A PENNSYLVANIA CORPORATION)
901 PENNSYLVANIA AVENUE PITTSBURGH, PA. 15233

Certificate of Aluminum Analysis

To: METCUTT RESEARCH
3980 Rosslyn Drive
Cincinnati, OH 45209

October 25, 1974

DISTRIBUTOR
ALCOA

OMERS ORDER NO.	WILLIAMS AND COMPANY, INC. ORDER NO.
58983 Partial	B 071902-103

MATERIAL FURNISHED — DESCRIPTION	WEIGHT	CONFORMS TO
7075-T651 Aluminum Plate 5/8 in x 3 in x RDM	20' 46#	QQ-A-250/13

CHEMICAL COMPOSITION LIMITS OF WROUGHT ALUMINUM ALLOYS

Aluminum Alloy	Silicon	Iron	Copper	Manganese	Magnesium	Chromium	Zinc	Ti	Other Each	Other Total	Aluminum	Tests – Minimum Tensile	Yield	Elong
EC											99.45 MIN			
1100	1.0 Si	+ Fe	0.05-0.20	0.05			0.10		0.05	0.15	99.00 MIN			
2014	0.50-1.2	0.7	3.9-5.0	0.40-1.2	0.20-0.8	0.10	0.25	0.15	0.05	0.15	Remainder			
2017	0.8	0.7	3.5-4.5	0.40-1.0	0.20-0.8	0.10	0.25		0.05	0.15	Remainder			
2024	0.50	0.50	3.8-4.9	0.30-0.9	1.2-1.8	0.10	0.25		0.05	0.15	Remainder			
3003	0.6	0.7	0.05-0.20	1.0-1.5			0.10		0.05	0.15	Remainder			
5005	0.40	0.7	0.20	0.20	0.50-1.1	0.10	0.25		0.05	0.15	Remainder			
5050	0.40	0.7	0.20	0.10	1.1-1.8	0.10	0.25		0.05	0.15	Remainder			
5052	0.45 Si	+ Fe	0.10	0.10	2.2-2.8	0.15-0.35	0.10		0.05	0.15	Remainder			
5083	0.40	0.40	0.10	0.30-1.0	4.0-4.9	0.05-0.25	0.25	0.15	0.05	0.15	Remainder			
5086	0.40	0.50	0.10	0.20-0.7	3.5-4.5	0.05-0.25	0.25	0.15	0.05	0.15	Remainder			
5252	0.08	0.10	0.10	0.10	2.2-2.8				0.03	0.10	Remainder			
5454	0.40 Si	+ Fe	0.10	0.50-1.0	2.4-3.0	0.05-0.20	0.25	0.20	0.05	0.15	Remainder			
5456	0.40 Si	+ Fe	0.10	0.50-1.0	4.7-5.5	0.05-0.20	0.25	0.20	0.05	0.15	Remainder			
5457	0.08	0.10	0.20	0.15-0.45	0.8-1.2				0.03	0.10	Remainder			
5657	0.08	0.10	0.10	0.03	0.6-1.0		0.03		0.02	0.05	Remainder			
6061	0.40-0.80	0.7	0.15-0.40	0.15	0.8-1.2	0.04-0.35	0.25	0.15	0.05	0.15	Remainder			
pe 200	0.40-0.80	0.7	0.15-0.40	0.15	0.8-1.2	0.15-0.35	0.25	0.15	0.05	0.15	Remainder			
6063	0.20-0.6	0.35	0.10	0.10	0.45-0.9	0.10	0.10	0.10	0.05	0.15	Remainder			
6101	0.30-0.7	0.50	0.10	0.03	0.35-0.8	0.03	0.10		0.03	0.10	Remainder			
6262	0.40-0.8	0.7	0.15-0.40	0.15	0.8-1.2	0.04-0.14	0.25	0.15	0.05	0.15	Remainder			
* 7075	0.40	0.50	1.2-2.0	0.30	2.1-2.9	0.18-0.35	5.1-6.1	0.20	0.05	0.15	Remainder	Tensile	85.4	85.3ksi
ad 2024 Clad	0.7 Si	+ Fe	0.10	0.05			0.10		0.05		99.30 MIN	Yield	76.6	76.6 ksi
Core	0.50	0.50	3.8-4.9	0.30-0.9	1.2-1.8	0.10	0.25		0.05	0.15	Remainder	Elong	11.4	11.4
ad 7075 Clad	0.7 Si	+ Fe	0.10	0.10	0.10		0.8-1.3		0.05	0.15	Remainder			
Core	0.50	0.7	1.2-2.0	0.30	2.1-2.9	0.18-0.40	5.1-6.1	0.20	0.05	0.15	Remainder			

nposition in percent maximum, unless shown as a range or minimum.

This report indicates the chemical analysis range to which the items listed were manufactured. Based on certificate of compliance furnished to us by the producer, we certify them to be within the limits shown, and will conform to specification:

QQ-A-250/13

BY Mildred Donnelly
CERTIFIED AGENT

Mildred Donnelly/lap
WILLIAMS AND COMPANY, INC.

WILLIAMS OTHER LOCATIONS

sburgh, Pa. 15233
Pennsylvania Ave.
412-237-2211

Cleveland, Ohio 44125
5301 Grant Ave.
216-441-1000

Cincinnati, Ohio 45237
7640 Reinhold Dr.
513-821-5555

umbus, Ohio 43212
00 Williams Ave.
614-294-4898

Toledo, Ohio 43612
946 Kane St.
419-476-7800

Louisville, Ky. 40203
1109 S. Preston St.
502-582-3321

Charleston, W. Va. 25303
1010 F. St.
304-744-5363

Buffalo, New York 14227
495 Kennedy Road
716-897-2000

APPENDIX B-1

ULTRASONIC TEST DATA LISTED BY TEST NUMBER

ULTRASONIC TEST DATA
LISTED BY TEST NUMBER

THE FOLLOWING HEADING DATA IS COMMON TO ALL TESTS:

LINE NUMBER	DESCRIPTION		
20	BABCOCK AND WILCOX CO		
30	LYNCHBURG RESEARCH CENTER		
330	XDUCER	PANAMETRI NOM FREQ	10 MHZ
400	SAMPLE	ALUMINUM MFG	METCUT
510	P/R	PANAMETRICS	5052PR
520	P/R	PULSER RECVR	1
530	P/R	REP RATE	4
540	P/R	ENERGY	3
550	P/R	DAMPING	8.0
560	P/R	ATTENUATION/GAIN	-0/+40 DB
610	B6100	CH A COUPLING	DC DC
630	B6100	CH A INPUT OFFSET	PLUS .00
710	B6100	CH B INPUT/OFF	OFF
810	B6100	ARM FROM	NONE
820	B6100	ARM DELAY	0.00 K SAMPLES
830	B6100	ARM SOURCE	EXT
840	B6100	ARM INTERNAL	CH A
870	B6100	ARM LEVEL	0 X FS INPUT
910	B6100	TRIGGER FROM	5052PR SYNC
930	B6100	TRIGGER SOURCE	EXT
940	B6100	TRIGGER INTERNAL	CH A
950	B6100	TRIGGER SLOPE	PLUS
960	B6100	TRIGGER COUPLING	DC
970	B6100	TRIGGER LEVEL	PLUS .10 X FS
1010	B6100	TIME BASE SAMPLE INTERV	.01 US
1020	B6100	TIME BASE SOURCE	INTERNAL
1040	B6100	RECORD MODE	NORMAL
1200	COMMENT	COUPLANT	HAMIKLEER

THE FOLLOWING HEADING DATA CORRESPONDS TO THE TEST DATA TABULATED BELOW.
THE LINE NUMBER IS GIVEN ABOVE THE APPROPRIATE COLUMN.

LINE NUMBER	DESCRIPTION
310	XDUCER PANAMETRIC SERIAL NUMBER
320	XDUCER PANAMETRIC DIAMETER(INCHES)/ANGLE(DEGREES)
340	XDUCER POSITION X (INCHES)
350	XDUCER POSITION Y (INCHES)
360	XDUCER DIRECTION CCW THETA (DEGREES)
410	SAMPLE NUMBER
620	B6100 CH A INPUT RANGE FULL SCALE + OR - (VOLTS)
920	B6100 TRIGGER TIME BASE DELAY INCREMENTS (X 1000)

NOTES:

1. THE LAST COLUMN HEADED "NR RDG" CONTAINS THE NUMBER OF READINGS AVERAGED FOR THE TEST.
   THE NUMBER IN THE COLUMN HEADINGS REFER TO THE LINE NUMBERS ABOVE.
2. THE NOMINAL FREQUENCY FOR THIS TRANSDUCER (LINE 330) IS 5 MHZ.
   THE DAMPING OF THE 5052 PR (LINE 550) WAS SET AT 7.5 FOR THIS TEST.
3. THE ATTENUATION/GAIN (LINE 560) WAS SET AT -6/+40 FOR THIS TEST.
4. THIS TEST WAS INCURRECTLY NUMBERED 340 INSTEAD OF 313.

PRECEDING PAGE BLANK-NOT FILMED

ULTRASONIC TEST DATA LISTED BY TEST NUMBER, CONTINUED

TEST NR	SERIAL NUMBER 310	XDUCER D/ANGLE 320	XDUCER POSITION X-IN 340	Y-IN 350	THETA 360	SAMPLE NUMBER 410	VOLT +-FS 620	DELAY X1000 920	RDGS AVGD	NOTES
201	5354	0.25/45				15-279	0.50	2.0	1	NOTES 2 & 3
202	5354	0.25/45				14-192	0.50	0.0	1	NOTE 2
203	5354	0.25/45				13-150	0.50	0.0	1	NOTE 2
204	5354	0.25/45				12-113	0.20	0.0	1	NOTE 2
205	4081	0.25/60				15-279	0.10	2.0	1	
206	4081	0.25/60				14-192	0.10	2.0	1	
207	4081	0.25/60				13-150	0.10	2.0	1	
208	4081	0.25/60				12-113	0.10	2.0	1	
209	4081	0.25/60				11-093	0.10	2.0	1	
210	4081	0.25/60				10-073	0.05	2.0	1	
211	4081	0.25/60				09-054	0.05	2.0	1	
212	4081	0.25/60				09-054	0.05	2.0	1	
213	4081	0.25/60				08-048	0.05	2.0	1	
214	4081	0.25/60				07-039	0.05	2.0	1	
215	4081	0.25/60				06-027	0.05	2.0	1	
216	4081	0.25/60				05-022	0.05	2.0	1	
217	4081	0.25/60				04-016	0.05	2.0	1	
218	4081	0.25/60				04-016	0.05	2.0	1	
219	4081	0.25/60				03-014	0.05	2.0	1	
220	4081	0.25/60				02-011	0.05	2.0	1	
221	4081	0.25/60				02-011	0.05	2.0	1	
222	4081	0.25/60				01-000	0.05	2.0	1	
223	4081	0.25/60				00-000	0.05	2.0	1	
224	4081	0.25/60				14-192	0.20	1.5	1	
225	4081	0.25/60				11-093	0.20	1.5	1	
226	4081	0.25/60				14-192	0.20	1.5	1	
227	4081	0.25/60				11-093	0.10	1.0	1	
228	4081	0.25/60	1.24	2.64	88.0	14-192	0.20	1.5	1	
229	4081	0.25/60	1.31	2.68	86.0	11-093	0.20	1.5	1	
230	4081	0.25/60	1.25	2.67	83.3	07-039	0.05	1.5	1	
231	4081	0.25/60	0.94	2.70	65.5	03-014	0.05	1.5	1	
232	4081	0.25/60	1.36	2.70	93.0	14-192	0.20	1.5	10	
233	4081	0.25/60	1.26	2.72	83.5	11-093	0.10	1.5	10	
234	4081	0.25/60	1.33	2.69	86.0	07-039	0.50	1.5	10	
235	4081	0.25/60	1.37	2.68	87.0	03-014	0.50	1.5	10	
236	4081	0.25/70	1.22	2.50	86.5	14-192	0.05	1.5	10	
237	4081	0.25/70	1.24	2.48	84.0	11-093	0.05	1.5	10	
238	4081	0.25/70	1.37	2.38	85.5	07-039	0.05	1.5	25	
239	4081	0.25/70	1.22	2.43	81.0	03-014	0.05	1.5	25	
240	4081	0.25/70	1.42	2.44	91.0	14-192	0.10	1.5	10	
241	4081	0.25/70	2.75	3.25	150.0	14-192	0.10	1.5	10	
242	4081	0.25/70	2.75	4.80	210.0	14-192	0.10	1.5	10	
243	4081	0.25/70	1.42	5.56	270.0	14-192	0.10	1.5	10	
244	4081	0.25/70	0.00	4.75	330.0	14-192	0.10	1.5	10	
245	4081	0.25/70	-.05	3.33	30.0	14-192	0.10	1.5	10	
246	4081	0.25/70	0.93	2.50	71.0	14-192	0.10	1.5	10	
247	4081	0.25/70	1.42	2.43	91.0	11-093	0.10	1.5	10	
248	4081	0.25/70	2.75	3.25	150.0	11-093	0.10	1.5	10	
249	4081	0.25/70	2.75	4.84	210.0	11-093	0.10	1.5	10	
250	4081	0.25/70	1.45	5.55	270.0	11-093	0.10	1.5	10	
251	4081	0.25/70	0.00	4.75	330.0	11-093	0.10	1.5	10	
252	4081	0.25/70	0.05	3.20	30.0	11-093	0.10	1.5	10	
253	4081	0.25/70	0.89	2.53	72.0	11-093	0.10	1.5	10	
254	4081	0.25/70	1.42	2.44	91.0	07-039	0.05	1.5	10	

ULTRASONIC TEST DATA LISTED BY TEST NUMBER, CONTINUED

TEST NR	SERIAL NUMBER 310	XDUCER D/ANGLE 320	XDUCER POSITION X-IN 340	Y-IN 350	THETA 360	SAMPLE NUMBER 410	VOLT +-FS 620	DELAY X1000 920	RDGS AVGD	NOTES
255	4081	0.25/70	2.75	3.25	150.0	07-039	0.05	1.5	10	
256	4081	0.25/70	2.72	4.77	210.0	07-039	0.05	1.5	10	
257	4081	0.25/70	1.37	5.55	270.0	07-039	0.05	1.5	10	
258	4081	0.25/70	0.05	4.75	330.0	07-039	0.05	1.5	10	
259	4081	0.25/70	0.05	3.18	30.0	07-039	0.05	1.5	10	
260	4081	0.25/70	0.87	2.54	70.0	07-039	0.05	1.5	10	
261	4081	0.25/70	1.38	2.44	91.5	03-014	0.05	1.5	10	
262	4081	0.25/70	2.75	3.25	150.0	03-014	0.05	1.5	10	
263	4081	0.25/70	2.72	4.80	210.0	03-014	0.05	1.5	10	
264	4081	0.25/70	1.34	5.55	270.0	03-014	0.05	1.5	10	
265	4081	0.25/70	0.03	4.78	330.0	03-014	0.05	1.5	10	
266	4081	0.25/70	0.03	3.19	30.0	03-014	0.05	1.5	10	
267	4081	0.25/70	0.87	3.19	70.0	03-014	0.05	1.5	10	
268	4081	0.25/70	0.87	3.19	70.0	03-014	0.05	1.5	1	
269	4081	0.25/70	1.17	5.53	276.5	03-014	0.05	1.5	10	
270	4081	0.25/70	1.35	2.43	86.5	14-192	0.05	1.5	10	
271	4081	0.25/70	1.35	2.43	85.5	14-192	0.05	1.5	10	
272	4081	0.25/70	1.35	2.43	85.5	11-093	0.05	1.5	10	
273	4081	0.25/70	1.35	2.43	85.5	11-093	0.05	1.5	10	
274	4081	0.25/70	1.47	2.43	90.0	07-039	0.05	1.5	10	
275	4081	0.25/70	1.47	2.43	90.0	07-039	0.05	1.5	10	
276	4081	0.25/70	1.39	2.42	87.5	03-014	0.05	1.5	10	
277	4081	0.25/70	1.39	2.42	87.5	03-014	0.05	1.5	10	
278	4081	0.25/70	1.32	2.42	84.5	14-192	0.05	1.5	10	
279	4081	0.25/70	1.35	2.43	85.5	14-192	0.05	1.5	10	
280	4081	0.25/70	1.35	2.43	85.5	14-192	0.05	1.5	10	
281	4081	0.25/70	1.35	2.43	85.5	11-093	0.05	1.5	10	
282	4081	0.25/70	1.35	2.43	85.5	11-093	0.05	1.5	10	
283	4081	0.25/70	1.35	2.43	85.5	11-093	0.05	1.5	10	
284	4081	0.25/70	1.47	2.43	90.0	07-039	0.05	1.5	10	
285	4081	0.25/70	1.47	2.43	90.0	07-039	0.05	1.5	10	
286	4081	0.25/70	1.39	2.42	87.5	03-014	0.05	1.5	10	
287	4081	0.25/70	1.39	2.42	87.5	03-014	0.05	1.5	10	
288	4081	0.25/70	1.56	2.53	90.0	00-000	0.05	1.5	1	
289	4081	0.25/70	1.60	2.46	90.5	02-011	0.05	1.5	1	
290	4081	0.25/70	1.45	2.52	86.5	15-279	0.05	1.5	1	
291	4081	0.25/70	1.23	2.47	80.5	14-192	0.05	1.5	10	
292	4081	0.25/70	1.23	2.47	80.5	14-192	0.05	1.5	10	
293	4081	0.25/70	1.17	2.50	75.0	14-192	0.05	1.5	10	
294	4081	0.25/70	0.91	2.54	70.0	14-192	0.05	1.5	10	
295	4081	0.25/70	0.77	2.60	64.0	14-192	0.05	1.5	10	
296	4081	0.25/70	0.64	2.65	58.0	14-192	0.05	1.5	10	
297	4081	0.25/70	0.53	2.72	52.5	14-192	0.05	1.5	10	
298	4081	0.25/70	2.72	2.71	121.0	14-192	0.05	1.5	10	
299	4081	0.25/70	1.36	2.47	86.5	11-093	0.05	1.5	10	
300	4081	0.25/70	1.22	2.48	81.0	11-093	0.05	1.5	10	
301	4081	0.25/70	1.09	2.50	75.5	11-093	0.05	1.5	10	
302	4081	0.25/70	0.95	2.52	70.0	11-093	0.05	1.5	10	
303	4081	0.25/70	0.81	2.57	64.5	11-093	0.05	1.5	10	
304	4081	0.25/70	0.68	2.64	59.0	11-093	0.05	1.5	10	
305	4081	0.25/70	2.72	3.32	149.0	11-093	0.05	1.5	10	
306	4081	0.25/70	1.44	2.48	90.0	07-039	0.05	1.5	10	
307	4081	0.25/70	1.32	2.48	84.5	07-039	0.05	1.5	10	
308	4081	0.25/70	1.17	2.49	79.0	07-039	0.05	1.5	10	

ULTRASONIC TEST DATA LISTED BY TEST NUMBER, CONTINUED

TEST NR	SERIAL NUMBER	XDUCER D/ANGLE	XDUCER POSITION X-IN	Y-IN	THETA	SAMPLE NUMBER	VOLT +-FS	DELAY X1000	RDGS AVGD	NOTES
	310	320	340	350	360	410	620	920		
309	4081	0.25/70	1.03	2.50	73.5	07-039	0.05	1.5	10	
310	4081	0.25/70	0.88	2.54	68.0	07-039	0.05	1.5	10	
311	4081	0.25/70	0.86	2.59	62.5	07-039	0.05	1.5	10	
312	4081	0.25/70	2.60	3.09	141.0	07-039	0.05	1.5	10	
313	4081	0.25/70	1.50	2.47	92.0	03-014	0.05	1.5	10	NOTE 4
314	4081	0.25/70	1.37	2.47	86.5	03-014	0.05	1.5	10	
315	4081	0.25/70	1.24	2.47	81.0	03-014	0.05	1.5	10	
316	4081	0.25/70	1.08	2.50	75.5	03-014	0.05	1.5	10	
317	4081	0.25/70	0.95	2.52	70.0	03-014	0.05	1.5	10	
318	4081	0.25/70	0.79	2.57	64.5	03-014	0.05	1.5	10	
319	4081	0.25/70	2.57	3.06	139.5	03-014	0.05	1.5	10	
320	4078	0.25/70	1.45	2.53	90.0	07-039	0.05	1.5	1	
321	4078	0.25/70	1.45	2.53	90.0	07-039	0.05	1.5	2	
322	4078	0.25/70	1.45	2.53	90.0	07-039	0.05	1.5	4	
323	4078	0.25/70	1.45	2.53	90.0	07-039	0.05	1.5	8	
324	4078	0.25/70	1.45	2.53	90.0	07-039	0.05	1.5	16	
325	4078	0.25/70	1.45	2.53	90.0	07-039	0.05	1.5	32	
326	4078	0.25/70	1.45	2.53	90.0	07-039	0.05	1.5	64	
327	4078	0.25/70	1.45	2.53	90.0	07-039	0.05	1.5	128	
328	4078	0.25/70	1.45	2.53	90.0	07-039	0.05	1.5	255	
329	4078	0.25/70	1.24	2.60	87.0	15-279	0.05	1.5	32	
330	4078	0.25/70	1.10	2.60	81.5	15-279	0.05	1.5	32	
331	4078	0.25/70	0.98	2.63	75.5	15-279	0.05	1.5	32	
332	4078	0.25/70	0.88	2.69	70.4	15-279	0.05	1.5	32	
333	4078	0.25/70	0.72	2.76	64.5	15-279	0.05	1.5	32	
334	4078	0.25/70	0.61	2.81	59.0	15-279	0.05	1.5	32	
335	4078	0.25/70	0.00	3.72	12.0	15-279	0.05	1.5	32	
336	4081	0.25/70	1.27	2.50	87.0	14-192	0.05	1.5	32	
337	4081	0.25/70	1.09	2.52	81.5	14-192	0.05	1.5	32	
338	4081	0.25/70	0.97	2.54	76.0	14-192	0.05	1.5	32	
339	4081	0.25/70	0.83	2.59	71.0	14-192	0.05	1.5	32	
340	4081	0.25/70	0.70	2.65	65.0	14-192	0.05	1.5	32	
341	4081	0.25/70	0.56	2.73	59.5	14-192	0.05	1.5	32	
342	4081	0.25/70	0.00	3.35	27.0	14-192	0.05	1.5	32	
343	4081	0.25/70	1.33	2.50	90.0	13-150	0.05	1.5	32	
344	4081	0.25/70	1.18	2.51	84.5	13-150	0.05	1.5	32	
345	4081	0.25/70	1.03	2.54	79.0	13-150	0.05	1.5	32	
346	4081	0.25/70	0.92	2.58	73.5	13-150	0.05	1.5	32	
347	4081	0.25/70	0.78	2.63	68.0	13-150	0.05	1.5	32	
348	4081	0.25/70	0.65	2.69	62.5	13-150	0.05	1.5	32	
349	4081	0.25/70	0.00	3.40	25.5	13-150	0.05	1.5	32	
350	4081	0.25/70	1.39	2.49	91.5	12-113	0.05	1.5	32	
351	4081	0.25/70	1.25	2.50	86.0	12-113	0.05	1.5	32	
352	4081	0.25/70	1.10	2.52	80.5	12-113	0.05	1.5	32	
353	4081	0.25/70	0.95	2.57	75.0	12-113	0.05	1.5	32	
354	4081	0.25/70	0.81	2.61	69.5	12-113	0.05	1.5	32	
355	4081	0.25/70	0.68	2.68	74.0	12-113	0.05	1.5	32	
356	4081	0.25/70	0.00	3.40	25.0	12-113	0.05	1.5	32	
357	4078	0.25/70	1.34	2.50	91.0	11-093	0.05	1.5	32	
358	4078	0.25/70	1.25	2.51	85.5	11-093	0.05	1.5	32	
359	4078	0.25/70	1.08	2.53	80.0	11-093	0.05	1.5	32	
360	4078	0.25/70	0.93	2.57	74.5	11-093	0.05	1.5	32	
361	4078	0.25/70	0.80	2.62	69.0	11-093	0.05	1.5	32	
362	4078	0.25/70	0.67	2.68	63.5	11-093	0.05	1.5	32	

ULTRASONIC TEST DATA LISTED BY TEST NUMBER, CONTINUED

TEST NR	SERIAL NUMBER	XDUCER D/ANGLE	XDUCER POSITION X-IN	Y-IN	THETA	SAMPLE NUMBER	VOLT +-FS	DELAY X1000	RDGS AVGD	NOTES
	310	320	340	350	360	410	620	920		
363	4078	0.25/70	0.00	3.38	25.0	11-093	0.05	1.5	32	
364	4078	0.25/70	1.47	2.43	92.0	10-073	0.05	1.5	32	
365	4078	0.25/70	1.33	2.43	86.5	10-073	0.05	1.5	32	
366	4078	0.25/70	1.19	2.44	81.0	10-073	0.05	1.5	32	
367	4078	0.25/70	1.03	2.48	75.5	10-073	0.05	1.5	32	
368	4078	0.25/70	0.90	2.51	70.0	10-073	0.05	1.5	32	
369	4078	0.25/70	0.75	2.57	64.5	10-073	0.05	1.5	32	
370	4078	0.25/70	0.00	3.30	24.0	10-073	0.05	1.5	32	
371	4081	0.25/70	1.49	2.43	93.0	09-054	0.05	1.5	32	
372	4081	0.25/70	1.33	2.43	87.5	09-054	0.05	1.5	32	
373	4081	0.25/70	1.20	2.46	82.0	09-054	0.05	1.5	32	
374	4081	0.25/70	0.99	2.49	75.5	09-054	0.05	1.5	32	
375	4081	0.25/70	0.86	2.53	70.0	09-054	0.05	1.5	32	
376	4081	0.25/70	0.71	2.58	64.5	09-054	0.05	1.5	32	
377	4081	0.25/70	0.60	2.66	59.0	09-054	0.05	1.5	32	
378	4081	0.25/70	0.00	3.28	28.0	09-054	0.05	1.5	32	
379	4081	0.25/60	1.32	2.70	87.0	15-279	0.10	1.5	32	
380	4081	0.25/60	1.20	2.72	81.5	15-279	0.10	1.5	32	
381	4081	0.25/60	1.08	2.78	76.0	15-279	0.10	1.5	32	
382	4081	0.25/60	0.94	2.78	70.5	15-279	0.10	1.5	32	
383	4081	0.25/60	0.82	2.82	65.0	15-279	0.10	1.5	32	
384	4081	0.25/60	0.71	2.88	59.5	15-279	0.05	1.5	32	
385	4081	0.25/60	0.14	3.56	18.0	15-279	0.05	1.5	32	
386	4081	0.25/60	1.44	2.66	93.0	14-192	0.10	1.5	32	
387	4081	0.25/60	1.30	2.67	87.5	14-192	0.10	1.5	32	
388	4081	0.25/60	1.20	2.68	82.0	14-192	0.10	1.5	32	
389	4081	0.25/60	1.08	2.70	76.5	14-192	0.05	1.5	32	
390	4081	0.25/60	0.95	2.74	71.0	14-192	0.05	1.5	32	
391	4081	0.25/60	0.83	2.78	65.5	14-192	0.05	1.5	32	
392	4081	0.25/60	0.17	3.43	23.0	14-192	0.05	1.5	32	
393	4081	0.25/60	1.38	2.68	91.0	13-150	0.10	1.5	32	
394	4081	0.25/60	1.27	2.69	85.5	13-150	0.10	1.5	32	
395	4081	0.25/60	1.16	2.69	80.0	13-150	0.05	1.5	32	
396	4081	0.25/60	1.03	2.71	74.5	13-150	0.05	1.5	32	
397	4081	0.25/60	0.90	2.76	69.0	13-150	0.05	1.5	32	
398	4081	0.25/60	0.80	2.82	63.5	13-150	0.05	1.5	32	
399	4081	0.25/60	0.16	3.42	25.0	13-150	0.05	1.5	32	
400	4081	0.25/60	1.30	2.68	86.5	12-113	0.05	1.5	32	
401	4081	0.25/60	1.20	2.70	81.0	12-113	0.05	1.5	32	
402	4081	0.25/60	1.05	2.72	75.5	12-113	0.05	1.5	32	
403	4081	0.25/60	0.92	2.76	70.0	12-113	0.05	1.5	32	
404	4081	0.25/60	0.80	2.80	64.5	12-113	0.05	1.5	32	
405	4081	0.25/60	0.70	2.86	59.0	12-113	0.05	1.5	32	
406	4081	0.25/60	0.16	3.43	25.5	12-113	0.05	1.5	32	
407	4081	0.25/60	1.28	2.68	86.0	11-093	0.10	1.5	32	
408	4081	0.25/60	1.16	2.68	80.5	11-093	0.10	1.5	32	
409	4081	0.25/60	1.05	2.71	75.0	11-093	0.05	1.5	32	
410	4081	0.25/60	0.92	2.75	69.5	11-093	0.05	1.5	32	
411	4081	0.25/60	0.81	2.79	64.0	11-093	0.05	1.5	32	
412	4081	0.25/60	0.70	2.85	58.5	11-093	0.05	1.5	32	
413	4081	0.25/60	0.17	3.43	25.0	11-093	0.05	1.5	32	
414	4081	0.25/60	1.32	2.68	87.0	10-073	0.05	1.5	32	
415	4081	0.25/60	1.18	2.69	81.5	10-073	0.05	1.5	32	
416	4081	0.25/60	1.05	2.71	76.0	10-073	0.05	1.5	32	

ULTRASONIC TEST DATA LISTED BY TEST NUMBER, CONTINUED

TEST NR	SERIAL NUMBER 310	XDUCER D/ANGLE 320	XDUCER POSITION X-IN 340	Y-IN 350	THETA 360	SAMPLE NUMBER 410	VOLT +-FS 620	DELAY X1000 920	RDGS AVGD	NOTES
417	4081	0.25/60	0.94	2.74	70.5	10-073	0.05	1.5	32	
418	4081	0.25/60	0.84	2.79	65.0	10-073	0.05	1.5	32	
419	4081	0.25/60	0.73	2.86	59.5	10-073	0.05	1.5	32	
420	4081	0.25/60	0.17	3.40	26.0	10-073	0.05	1.5	32	
421	4081	0.25/60	1.34	2.66	89.0	09-054	0.05	1.5	32	
422	4081	0.25/60	1.23	2.68	83.5	09-054	0.05	1.5	32	
423	4081	0.25/60	1.20	2.70	78.0	09-054	0.05	1.5	32	
424	4081	0.25/60	1.00	2.73	72.5	09-054	0.05	1.5	32	
425	4081	0.25/60	0.87	2.77	67.0	09-054	0.05	1.5	32	
426	4081	0.25/60	0.77	2.83	61.5	09-054	0.05	1.5	32	
427	4081	0.25/60	0.17	3.43	25.0	09-054	0.05	1.5	32	
428	4081	0.25/60	1.21	2.69	82.0	08-048	0.05	1.5	32	
429	4081	0.25/60	1.08	2.71	76.5	08-048	0.05	1.5	32	
430	4081	0.25/60	0.95	2.73	71.0	08-048	0.05	1.5	32	
431	4081	0.25/60	0.84	2.78	65.5	08-048	0.05	1.5	32	
432	4081	0.25/60	0.72	2.84	60.0	08-048	0.05	1.5	32	
433	4081	0.25/60	0.61	2.92	54.5	08-048	0.05	1.5	32	
434	4081	0.25/60	0.17	3.42	26.0	08-048	0.05	1.5	32	
435	4081	0.25/60	1.24	2.68	83.5	07-039	0.05	1.5	32	
436	4081	0.25/60	1.12	2.69	78.0	07-039	0.05	1.5	32	
437	4081	0.25/60	1.00	2.73	72.5	07-039	0.05	1.5	32	
438	4081	0.25/60	0.86	2.78	67.0	07-039	0.05	1.5	32	
439	4081	0.25/60	0.74	2.83	61.5	07-039	0.05	1.5	32	
440	4081	0.25/60	0.64	2.88	56.0	07-039	0.05	1.5	32	
441	4081	0.25/60	0.19	3.41	26.0	07-039	0.05	1.5	32	
442	4081	0.25/60	1.31	2.68	87.5	06-027	0.05	1.5	32	
443	4081	0.25/60	1.20	2.68	82.0	06-027	0.05	1.5	32	
444	4081	0.25/60	1.09	2.70	76.5	06-027	0.05	1.5	32	
445	4081	0.25/60	0.96	2.74	71.0	06-027	0.05	1.5	32	
446	4081	0.25/60	0.84	2.79	65.5	06-027	0.05	1.5	32	
447	4081	0.25/60	0.73	2.84	60.0	06-027	0.05	1.5	32	
448	4081	0.25/60	0.17	3.43	26.0	06-027	0.05	1.5	32	
449	4081	0.25/60	1.38	0.68	90.5	05-022	0.05	1.5	32	
450	4081	0.25/60	1.25	0.68	85.0	05-022	0.05	1.5	32	
451	4081	0.25/60	1.13	0.70	79.5	05-022	0.05	1.5	32	
452	4081	0.25/60	1.02	0.72	74.0	05-022	0.05	1.5	32	
453	4081	0.25/60	0.88	0.76	68.5	05-022	0.05	1.5	32	
454	4081	0.25/60	0.77	0.82	63.0	05-022	0.05	1.5	32	
455	4081	0.25/60	0.17	1.42	26.0	05-022	0.05	1.5	32	
456	4081	0.25/60	1.30	2.66	85.5	04-016	0.05	1.5	32	
457	4081	0.25/60	1.17	2.69	80.0	04-016	0.05	1.5	32	
458	4081	0.25/60	1.03	2.71	74.5	04-016	0.05	1.5	32	
459	4081	0.25/60	0.92	2.75	69.0	04-016	0.05	1.5	32	
460	4081	0.25/60	0.80	2.80	63.5	04-016	0.05	1.5	32	
461	4081	0.25/60	0.69	2.86	58.0	04-016	0.05	1.5	32	
462	4081	0.25/60	0.17	3.42	26.0	04-016	0.05	1.5	32	
463	4081	0.25/60	1.30	2.67	88.0	03-014	0.05	1.5	32	
464	4081	0.25/60	1.20	2.68	82.5	03-014	0.05	1.5	32	
465	4081	0.25/60	1.07	2.69	77.0	03-014	0.05	1.5	32	
466	4081	0.25/60	0.95	2.72	71.5	03-014	0.05	1.5	32	
467	4081	0.25/60	0.83	2.77	66.0	03-014	0.05	1.5	32	
468	4081	0.25/60	0.73	2.84	60.5	03-014	0.05	1.5	32	
469	4081	0.25/60	0.17	3.43	25.0	03-014	0.05	1.5	32	
470	4081	0.25/60	1.60	2.68	99.5	02-011	0.05	1.5	32	

ULTRASONIC TEST DATA LISTED BY TEST NUMBER, CONTINUED

TEST NR	SERIAL NUMBER	XDUCER D/ANGLE	XDUCER POSITION X-IN	Y-IN	THETA	SAMPLE NUMBER	VOLT +-FS	DELAY X1000	RDGS AVGD	NOTES
	310	320	340	350	360	410	620	920		
471	4081	0.25/60	1.45	2.68	94.0	02-011	0.05	1.5	32	
472	4081	0.25/60	1.34	2.67	88.5	02-011	0.05	1.5	32	
473	4081	0.25/60	1.21	2.68	83.0	02-011	0.05	1.5	32	
474	4081	0.25/60	1.10	2.70	77.5	02-011	0.05	1.5	32	
475	4081	0.25/60	0.94	2.73	72.0	02-011	0.05	1.5	32	
476	4081	0.25/60	0.17	3.43	25.0	01-000	0.05	1.5	32	
477	4081	0.25/60	1.39	2.66	90.0	01-000	0.05	1.5	32	
478	4081	0.25/60	1.24	2.67	84.5	01-000	0.05	1.5	32	
479	4081	0.25/60	1.13	2.69	79.0	01-000	0.05	1.5	32	
480	4081	0.25/60	1.00	2.72	73.5	01-000	0.05	1.5	32	
481	4081	0.25/60	0.87	2.77	68.0	01-000	0.05	1.5	32	
482	4081	0.25/60	0.76	2.83	62.5	01-000	0.05	1.5	32	
483	4081	0.25/60	0.15	3.44	24.0	01-000	0.05	1.5	32	
484	4081	0.25/60	1.39	2.67	91.0	00-000	0.05	1.5	32	
485	4081	0.25/60	1.28	2.68	85.5	00-000	0.05	1.5	32	
486	4081	0.25/60	1.14	2.69	80.0	00-000	0.05	1.5	32	
487	4081	0.25/60	1.03	2.73	74.5	00-000	0.05	1.5	32	
488	4081	0.25/60	0.92	2.76	69.0	00-000	0.05	1.5	32	
489	4081	0.25/60	0.79	2.82	63.5	00-000	0.05	1.5	32	
490	4081	0.25/60	0.17	3.43	26.0	00-000	0.05	1.5	32	
491	4081	0.25/60	1.32	2.70	87.0	15-279	0.05	1.5	32	
492	4081	0.25/60	1.19	2.71	81.5	15-279	0.05	1.5	32	
493	4081	0.25/60	1.07	2.73	76.0	15-279	0.05	1.5	32	
494	4081	0.25/60	0.95	2.76	70.5	15-279	0.05	1.5	32	
495	4081	0.25/60	0.84	2.82	65.0	15-279	0.05	1.5	32	
496	4081	0.25/60	0.73	2.86	59.5	15-279	0.05	1.5	32	
497	4081	0.25/60	2.65	3.74	167.0	15-279	0.05	1.5	32	
498	4081	0.25/60	1.46	2.70	93.5	14-192	0.10	1.5	32	
499	4081	0.25/60	1.34	2.70	88.0	14-192	0.10	1.5	32	
500	4081	0.25/60	1.20	2.70	82.5	14-192	0.10	1.5	32	
501	4081	0.25/60	1.08	2.73	77.0	14-192	0.05	1.5	32	
502	4081	0.25/60	0.97	2.76	71.5	14-192	0.05	1.5	32	
503	4081	0.25/60	0.85	2.80	66.0	14-192	0.05	1.5	32	
504	4081	0.25/60	2.63	3.71	164.5	14-192	0.05	1.5	32	
505	4081	0.25/60	1.59	2.72	99.5	13-150	0.05	1.5	32	
506	4081	0.25/60	1.44	2.68	94.0	13-150	0.05	1.5	32	
507	4081	0.25/60	1.33	2.68	88.5	13-150	0.05	1.5	32	
508	4081	0.25/60	1.22	2.70	83.0	13-150	0.05	1.5	32	
509	4081	0.25/60	1.10	2.72	77.5	13-150	0.05	1.5	32	
510	4081	0.25/60	0.97	2.76	72.0	13-150	0.05	1.5	32	
511	4081	0.25/60	2.63	3.67	166.0	13-150	0.05	1.5	32	
512	4081	0.25/60	1.34	2.70	87.5	12-113	0.05	1.5	32	
513	4081	0.25/60	1.20	2.70	82.0	12-113	0.05	1.5	32	
514	4081	0.25/60	1.10	2.73	76.5	12-113	0.05	1.5	32	
515	4081	0.25/60	0.97	2.77	71.0	12-113	0.05	1.5	32	
516	4081	0.25/60	0.83	2.81	65.5	12-113	0.05	1.5	32	
517	4081	0.25/60	0.73	2.87	60.0	12-113	0.05	1.5	32	
518	4081	0.25/60	2.62	3.59	160.5	12-113	0.05	1.5	32	
519	4081	0.25/60	1.27	2.69	85.5	11-093	0.05	1.5	32	
520	4081	0.25/60	1.16	2.70	80.0	11-093	0.05	1.5	32	
521	4081	0.25/60	1.03	2.73	74.5	11-093	0.05	1.5	32	
522	4081	0.25/60	0.91	2.77	69.0	11-093	0.05	1.5	32	
523	4081	0.25/60	0.80	2.82	63.5	11-093	0.05	1.5	32	
524	4081	0.25/60	0.68	2.89	58.0	11-093	0.05	1.5	32	

ULTRASONIC TEST DATA LISTED BY TEST NUMBER, CONTINUED

TEST NR	SERIAL NUMBER 310	XDUCER D/ANGLE 320	XDUCER POSITION X-IN 340	Y-IN 350	THETA 360	SAMPLE NUMBER 410	VOLT +-FS 620	DELAY X1000 920	RDGS AVGD	NOTES
525	4081	0.25/60	2.62	3.64	161.0	11-093	0.05	1.5	32	
526	4081	0.25/60	1.64	2.72	101.0	10-073	0.05	1.5	32	
527	4081	0.25/60	1.53	2.68	95.5	10-073	0.05	1.5	32	
528	4081	0.25/60	1.38	2.70	90.0	10-073	0.05	1.5	32	
529	4081	0.25/60	1.27	2.70	84.5	10-073	0.05	1.5	32	
530	4081	0.25/60	1.14	2.72	79.0	10-073	0.05	1.5	32	
531	4081	0.25/60	1.03	2.74	73.5	10-073	0.05	1.5	32	
532	4081	0.25/60	2.67	3.78	169.0	10-073	0.05	1.5	32	
533	4081	0.25/60	1.43	2.69	91.0	09-054	0.05	1.5	32	
534	4081	0.25/60	1.29	2.70	85.5	09-054	0.05	1.5	32	
535	4081	0.25/60	1.17	2.72	80.0	09-054	0.05	1.5	32	
536	4081	0.25/60	1.03	2.74	74.5	09-054	0.05	1.5	32	
537	4081	0.25/60	0.91	2.78	69.0	09-054	0.05	1.5	32	
538	4081	0.25/60	0.82	2.92	63.5	09-054	0.05	1.5	32	
539	4081	0.25/60	2.64	3.61	162.5	09-054	0.05	1.5	32	
540	4081	0.25/60	1.30	2.70	86.0	08-048	0.05	1.5	32	
541	4081	0.25/60	1.16	2.72	80.5	08-048	0.05	1.5	32	
542	4081	0.25/60	1.03	2.73	75.0	08-048	0.05	1.5	32	
543	4081	0.25/60	0.90	2.77	69.5	08-048	0.05	1.5	32	
544	4081	0.25/60	0.81	2.82	64.0	08-048	0.05	1.5	32	
545	4081	0.25/60	0.76	2.90	58.5	08-048	0.05	1.5	32	
546	4081	0.25/60	2.62	3.57	160.5	08-048	0.05	1.5	32	
547	4081	0.25/60	1.28	2.68	86.0	07-039	0.05	1.5	32	
548	4081	0.25/60	1.17	2.71	80.5	07-039	0.05	1.5	32	
549	4081	0.25/60	1.04	2.74	75.0	07-039	0.05	1.5	32	
550	4081	0.25/60	0.92	2.78	69.5	07-039	0.05	1.5	32	
551	4081	0.25/60	0.82	2.82	64.0	07-039	0.05	1.5	32	
552	4081	0.25/60	0.71	2.87	58.5	07-039	0.05	1.5	32	
553	4081	0.25/60	2.63	3.66	164.0	07-039	0.05	1.5	32	
554	4081	0.25/60	1.56	2.70	97.0	06-027	0.05	1.5	32	
555	4081	0.25/60	1.43	2.70	91.5	06-027	0.05	1.5	32	
556	4081	0.25/60	1.31	2.70	86.0	06-027	0.05	1.5	32	
557	4081	0.25/60	1.18	2.70	80.5	06-027	0.05	1.5	32	
558	4081	0.25/60	1.06	2.73	75.0	06-027	0.05	1.5	32	
559	4081	0.25/60	0.93	2.77	69.5	06-027	0.05	1.5	32	
560	4081	0.25/60	2.64	3.69	163.0	06-027	0.05	1.5	32	
561	4081	0.25/60	1.23	0.70	83.0	05-022	0.05	1.5	32	
562	4081	0.25/60	1.10	0.72	77.5	05-022	0.05	1.5	32	
563	4081	0.25/60	1.00	0.74	72.0	05-022	0.05	1.5	32	
564	4081	0.25/60	0.89	0.77	66.5	05-022	0.05	1.5	32	
565	4081	0.25/60	0.77	0.86	61.0	05-022	0.05	1.5	32	
566	4081	0.25/60	0.67	0.89	55.5	05-022	0.05	1.5	32	
567	4081	0.25/60	2.62	1.58	161.5	05-022	0.05	1.5	32	
568	4081	0.25/60	1.53	2.72	96.0	04-018	0.05	1.5	32	
569	4081	0.25/60	1.41	2.68	90.5	04-018	0.05	1.5	32	
570	4081	0.25/60	1.30	2.69	85.0	04-018	0.05	1.5	32	
571	4081	0.25/60	1.17	2.70	79.5	04-018	0.05	1.5	32	
572	4081	0.25/60	1.03	2.73	74.0	04-018	0.05	1.5	32	
573	4081	0.25/60	0.92	2.77	68.5	04-018	0.05	1.5	32	
574	4081	0.25/60	2.61	3.55	160.0	04-018	0.05	1.5	32	
575	4081	0.25/60	1.32	2.68	87.0	03-014	0.05	1.5	32	
576	4081	0.25/60	1.19	2.70	81.5	03-014	0.05	1.5	32	
577	4081	0.25/60	1.08	2.72	76.0	03-014	0.05	1.5	32	
578	4081	0.25/60	0.94	2.75	70.5	03-014	0.05	1.5	32	

ULTRASONIC TEST DATA LISTED BY TEST NUMBER, CONTINUED

TEST NR	SERIAL NUMBER 310	XDUCER D/ANGLE 320	XDUCER POSITION X-IN 340	Y-IN 350	THETA 360	SAMPLE NUMBER 410	VOLT +-FS 620	DELAY X1000 920	RDGS AVGD	NOTES
579	4081	0.25/60	0.83	2.80	65.0	03-014	0.05	1.5	32	
580	4081	0.25/60	0.71	2.87	59.5	03-014	0.05	1.5	32	
581	4081	0.25/60	2.61	3.57	159.0	03-014	0.05	1.5	32	
582	4081	0.25/60	1.55	2.69	97.0	02-011	0.05	1.5	32	
583	4081	0.25/60	1.43	2.68	91.5	02-011	0.05	1.5	32	
584	4081	0.25/60	1.31	2.68	86.0	02-011	0.05	1.5	32	
585	4081	0.25/60	1.18	2.70	80.5	02-011	0.05	1.5	32	
586	4081	0.25/60	1.07	2.72	75.0	02-011	0.05	1.5	32	
587	4081	0.25/60	0.94	2.75	69.5	02-011	0.05	1.5	32	
588	4081	0.25/60	2.64	3.65	163.5	02-011	0.05	1.5	32	
589	4081	0.25/60	1.41	2.68	91.0	01-000	0.05	1.5	32	
590	4081	0.25/60	1.29	2.69	85.5	01-000	0.05	1.5	32	
591	4081	0.25/60	1.16	2.71	80.0	01-000	0.05	1.5	32	
592	4081	0.25/60	1.05	2.73	74.5	01-000	0.05	1.5	32	
593	4081	0.25/60	0.93	2.77	69.0	01-000	0.05	1.5	32	
594	4081	0.25/60	0.81	2.82	63.5	01-000	0.05	1.5	32	
595	4081	0.25/60	2.62	3.57	160.0	01-000	0.05	1.5	32	
596	4081	0.25/60	1.54	2.68	97.0	00-000	0.05	1.5	32	
597	4081	0.25/60	1.42	2.68	91.5	00-000	0.05	1.5	32	
598	4081	0.25/60	1.31	2.68	86.0	00-000	0.05	1.5	32	
599	4081	0.25/60	1.18	2.70	80.5	00-000	0.05	1.5	32	
600	4081	0.25/60	1.05	2.72	75.0	00-000	0.05	1.5	32	
601	4081	0.25/60	0.94	2.74	69.5	00-000	0.05	1.5	32	
602	4081	0.25/60	2.64	3.63	163.0	00-000	0.05	1.5	32	

APPENDIX B-2

ULTRASONIC TEST DATA LISTED BY SAMPLE NUMBER

PRECEDING PAGE BLANK-NOT FILMED

ULTRASONIC TEST DATA
LISTED BY SAMPLE NUMBER

THE FOLLOWING HEADING DATA IS COMMON TO ALL TESTS:

LINE NUMBER	DESCRIPTION			
20	BABCOCK AND WILCOX CO			
30	LYNCHBURG RESEARCH CENTER			
330	XDUCER	PANAMETRI NOM FREQ		10 MHZ
400	SAMPLE	ALUMINUM MFG		METCUT
510	P/R	PANAMETRICS		5052PR
520	P/R	PULSER RECVR		1
530	P/R	REP RATE		4
540	P/R	ENERGY		3
550	P/R	DAMPING		8.0
560	P/R	ATTENUATION/GAIN		-0/+40 DB
610	88100	CH A	COUPLING	DC DC
630	88100	CH A	INPUT OFFSET	PLUS .00
710	88100	CH B	INPUT/OFF	OFF
810	88100	ARM	FROM	NONE
820	88100	ARM	DELAY	0.00 K SAMPLES
830	88100	ARM	SOURCE	EXT
840	88100	ARM	INTERNAL	CH A
870	88100	ARM	LEVEL	0 X FS INPUT
910	88100	TRIGGER	FROM	5052PR SYNC
930	88100	TRIGGER	SOURCE	EXT
940	88100	TRIGGER	INTERNAL	CH A
950	88100	TRIGGER	SLOPE	PLUS
960	88100	TRIGGER	COUPLING	DC
970	88100	TRIGGER	LEVEL	PLUS .10 X FS
1010	88100	TIME BASE	SAMPLE INTERV	.01 US
1020	88100	TIME BASE	SOURCE	INTERNAL
1040	88100		RECORD MODE	NORMAL
1200	COMMENT	COUPLANT		HAMIKLEER

THE FOLLOWING HEADING DATA CORRESPONDS TO THE TEST DATA TABULATED BELOW.
THE LINE NUMBER IS GIVEN ABOVE THE APPROPRIATE COLUMN.

LINE NUMBER	DESCRIPTION
310	XDUCER PANAMETRIC SERIAL NUMBER
320	XDUCER PANAMETRIC DIAMETER(INCHES)/ANGLE(DEGREES)
340	XDUCER POSITION X (INCHES)
350	XDUCER POSITION Y (INCHES)
360	XDUCER DIRECTION CCW THETA (DEGREES)
410	SAMPLE NUMBER
620	88100 CH A INPUT RANGE FULL SCALE + OR - (VOLTS)
920	88100 TRIGGER TIME BASE DELAY INCREMENTS (X 1000)

NOTES:

1. THE LAST COLUMN HEADED "NR RDG" CONTAINS THE NUMBER OF READINGS AVERAGED FOR THE TEST.
   THE NUMBER IN THE COLUMN HEADINGS REFER TO THE LINE NUMBERS ABOVE.
2. THE NOMINAL FREQUENCY FOR THIS TRANSDUCER (LINE 330) IS 5 MHZ.
   THE DAMPING OF THE 5052 PR (LINE 550) WAS SET AT 7.5 FOR THIS TEST.
3. THE ATTENUATION/GAIN (LINE 560) WAS SET AT -6/+40 FOR THIS TEST.
4. THIS TEST WAS INCORRECTLY NUMBERED 340 INSTEAD OF
5. FOR TESTS 217,218, AND 456 THROUGH 462, THE SAMPLE NUMBER SHOULD BE 04-018, NOT 04-016 AS SHOWN.

PRECEDING PAGE BLANK-NOT FILMED

ULTRASONIC TEST DATA LISTED BY SAMPLE NUMBER, CONTINUED

TEST NR	SERIAL NUMBER 310	XDUCER D/ANGLE 320	XDUCER POSITION X-IN 340	Y-IN 350	THETA 360	SAMPLE NUMBER 410	VOLT +-FS 620	DELAY X1000 920	RDGS AVGD	NOTES
223	4081	0.25/60				00-000	0.05	2.0	1	
288	4081	0.25/70	1.56	2.53	90.0	00-000	0.05	1.5	1	
484	4081	0.25/60	1.39	2.67	91.0	00-000	0.05	1.5	32	
485	4081	0.25/60	1.28	2.68	85.5	00-000	0.05	1.5	32	
486	4081	0.25/60	1.14	2.69	80.0	00-000	0.05	1.5	32	
487	4081	0.25/60	1.03	2.73	74.5	00-000	0.05	1.5	32	
488	4081	0.25/60	0.92	2.76	69.0	00-000	0.05	1.5	32	
489	4081	0.25/60	0.79	2.82	63.5	00-000	0.05	1.5	32	
490	4081	0.25/60	0.17	3.43	26.0	00-000	0.05	1.5	32	
596	4081	0.25/60	1.54	2.68	97.0	00-000	0.05	1.5	32	
597	4081	0.25/60	1.42	2.68	91.5	00-000	0.05	1.5	32	
598	4081	0.25/60	1.31	2.68	86.0	00-000	0.05	1.5	32	
599	4081	0.25/60	1.18	2.70	80.5	00-000	0.05	1.5	32	
600	4081	0.25/60	1.05	2.72	75.0	00-000	0.05	1.5	32	
601	4081	0.25/60	0.94	2.74	69.5	00-000	0.05	1.5	32	
602	4081	0.25/60	2.64	3.63	163.0	00-000	0.05	1.5	32	
222	4081	0.25/60				01-000	0.05	2.0	1	
476	4081	0.25/60	0.17	3.43	25.0	01-000	0.05	1.5	32	
477	4081	0.25/60	1.39	2.66	90.0	01-000	0.05	1.5	32	
478	4081	0.25/60	1.24	2.67	84.5	01-000	0.05	1.5	32	
479	4081	0.25/60	1.13	2.69	79.0	01-000	0.05	1.5	32	
480	4081	0.25/60	1.00	2.72	73.5	01-000	0.05	1.5	32	
481	4081	0.25/60	0.87	2.77	68.0	01-000	0.05	1.5	32	
482	4081	0.25/60	0.76	2.83	62.5	01-000	0.05	1.5	32	
483	4081	0.25/60	0.15	3.44	24.0	01-000	0.05	1.5	32	
589	4081	0.25/60	1.41	2.68	91.0	01-000	0.05	1.5	32	
590	4081	0.25/60	1.29	2.69	85.5	01-000	0.05	1.5	32	
591	4081	0.25/60	1.16	2.71	80.0	01-000	0.05	1.5	32	
592	4081	0.25/60	1.05	2.73	74.5	01-000	0.05	1.5	32	
593	4081	0.25/60	0.93	2.77	69.0	01-000	0.05	1.5	32	
594	4081	0.25/60	0.81	2.82	63.5	01-000	0.05	1.5	32	
595	4081	0.25/60	2.62	3.57	160.0	01-000	0.05	1.5	32	
220	4081	0.25/60				02-011	0.05	2.0	1	
221	4081	0.25/60				02-011	0.05	2.0	1	
289	4081	0.25/70	1.60	2.46	90.5	02-011	0.05	1.5	1	
470	4081	0.25/60	1.60	2.68	99.5	02-011	0.05	1.5	32	
471	4081	0.25/60	1.45	2.68	94.0	02-011	0.05	1.5	32	
472	4081	0.25/60	1.34	2.67	88.5	02-011	0.05	1.5	32	
473	4081	0.25/60	1.21	2.68	83.0	02-011	0.05	1.5	32	
474	4081	0.25/60	1.10	2.70	77.5	02-011	0.05	1.5	32	
475	4081	0.25/60	0.94	2.73	72.0	02-011	0.05	1.5	32	
582	4081	0.25/60	1.55	2.69	97.0	02-011	0.05	1.5	32	
583	4081	0.25/60	1.43	2.68	91.5	02-011	0.05	1.5	32	
584	4081	0.25/60	1.31	2.68	86.0	02-011	0.05	1.5	32	
585	4081	0.25/60	1.18	2.70	80.5	02-011	0.05	1.5	32	
586	4081	0.25/60	1.07	2.72	75.0	02-011	0.05	1.5	32	
587	4081	0.25/60	0.94	2.75	69.5	02-011	0.05	1.5	32	
588	4081	0.25/60	2.64	3.65	163.5	02-011	0.05	1.5	32	
219	4081	0.25/60				03-014	0.05	2.0	1	
231	4081	0.25/60	0.94	2.70	65.5	03-014	0.05	1.5	1	
235	4081	0.25/60	1.37	2.68	87.0	03-014	0.50	1.5	10	

ULTRASONIC TEST DATA LISTED BY SAMPLE NUMBER, CONTINUED

TEST NR	SERIAL NUMBER 310	XDUCER D/ANGLE 320	XDUCER POSITION X-IN 340	Y-IN 350	THETA 360	SAMPLE NUMBER 410	VOLT +-FS 620	DELAY X1000 920	RDGS AVGD	NOTES
239	4081	0.25/70	1.22	2.43	81.0	03-014	0.05	1.5	25	
261	4081	0.25/70	1.36	2.44	91.5	03-014	0.05	1.5	10	
262	4081	0.25/70	2.75	3.25	150.0	03-014	0.05	1.5	10	
263	4081	0.25/70	2.72	4.60	210.0	03-014	0.05	1.5	10	
264	4081	0.25/70	1.34	5.55	270.0	03-014	0.05	1.5	10	
265	4081	0.25/70	0.03	4.78	330.0	03-014	0.05	1.5	10	
266	4081	0.25/70	0.03	3.19	30.0	03-014	0.05	1.5	10	
267	4081	0.25/70	0.87	3.19	70.0	03-014	0.05	1.5	10	
268	4081	0.25/70	0.87	3.19	70.0	03-014	0.05	1.5	1	
269	4081	0.25/70	1.17	5.53	276.5	03-014	0.05	1.5	10	
276	4081	0.25/70	1.39	2.42	87.5	03-014	0.05	1.5	10	
277	4081	0.25/70	1.39	2.42	87.5	03-014	0.05	1.5	10	
286	4081	0.25/70	1.39	2.42	87.5	03-014	0.05	1.5	10	
287	4081	0.25/70	1.39	2.42	87.5	03-014	0.05	1.5	10	
313	4081	0.25/70	1.50	2.47	92.0	03-014	0.05	1.5	10	NOTE 4
314	4081	0.25/70	1.37	2.47	86.5	03-014	0.05	1.5	10	
315	4081	0.25/70	1.24	2.47	81.0	03-014	0.05	1.5	10	
316	4081	0.25/70	1.08	2.50	75.5	03-014	0.05	1.5	10	
317	4081	0.25/70	0.95	2.52	70.0	03-014	0.05	1.5	10	
318	4081	0.25/70	0.79	2.57	64.5	03-014	0.05	1.5	10	
319	4081	0.25/70	2.57	3.06	139.5	03-014	0.05	1.5	10	
463	4081	0.25/60	1.30	2.67	88.0	03-014	0.05	1.5	32	
464	4081	0.25/60	1.20	2.68	82.5	03-014	0.05	1.5	32	
465	4081	0.25/60	1.07	2.69	77.0	03-014	0.05	1.5	32	
466	4081	0.25/60	0.95	2.72	71.5	03-014	0.05	1.5	32	
467	4081	0.25/60	0.83	2.77	66.0	03-014	0.05	1.5	32	
468	4081	0.25/60	0.73	2.84	60.5	03-014	0.05	1.5	32	
469	4081	0.25/60	0.17	3.43	25.0	03-014	0.05	1.5	32	
575	4081	0.25/60	1.32	2.68	87.0	03-014	0.05	1.5	32	
576	4081	0.25/60	1.19	2.70	81.5	03-014	0.05	1.5	32	
577	4081	0.25/60	1.08	2.72	76.0	03-014	0.05	1.5	32	
578	4081	0.25/60	0.94	2.75	70.5	03-014	0.05	1.5	32	
579	4081	0.25/60	0.83	2.80	65.0	03-014	0.05	1.5	32	
580	4081	0.25/60	0.71	2.87	59.5	03-014	0.05	1.5	32	
581	4081	0.25/60	2.61	3.57	159.0	03-014	0.05	1.5	32	
217	4081	0.25/60				04-016	0.05	2.0	1	NOTE 5
218	4081	0.25/60				04-016	0.05	2.0	1	NOTE 5
456	4081	0.25/60	1.30	2.66	85.5	04-016	0.05	1.5	32	NOTE 5
457	4081	0.25/60	1.17	2.69	80.0	04-016	0.05	1.5	32	NOTE 5
458	4081	0.25/60	1.03	2.71	74.5	04-016	0.05	1.5	32	NOTE 5
459	4081	0.25/60	0.92	2.75	69.0	04-016	0.05	1.5	32	NOTE 5
460	4081	0.25/60	0.80	2.80	63.5	04-016	0.05	1.5	32	NOTE 5
461	4081	0.25/60	0.69	2.86	58.0	04-016	0.05	1.5	32	NOTE 5
462	4081	0.25/60	0.17	3.42	26.0	04-016	0.05	1.5	32	NOTE 5
568	4081	0.25/60	1.53	2.72	96.0	04-018	0.05	1.5	32	
569	4081	0.25/60	1.41	2.68	90.5	04-018	0.05	1.5	32	
570	4081	0.25/60	1.30	2.69	85.0	04-018	0.05	1.5	32	
571	4081	0.25/60	1.17	2.70	79.5	04-018	0.05	1.5	32	
572	4081	0.25/60	1.03	2.73	74.0	04-018	0.05	1.5	32	
573	4081	0.25/60	0.92	2.77	68.5	04-018	0.05	1.5	32	
574	4081	0.25/60	2.61	3.55	160.0	04-018	0.05	1.5	32	

ULTRASONIC TEST DATA LISTED BY SAMPLE NUMBER, CONTINUED

TEST NR	SERIAL NUMBER 310	XDUCER D/ANGLE 320	XDUCER POSITION X-IN 340	Y-IN 350	THETA 360	SAMPLE NUMBER 410	VOLT +-FS 620	DELAY X1000 920	RDGS AVGD	NOTES
216	4081	0.25/60				05-022	0.05	2.0	1	
449	4081	0.25/60	1.38	0.68	90.5	05-022	0.05	1.5	32	
450	4081	0.25/60	1.25	0.68	85.0	05-022	0.05	1.5	32	
451	4081	0.25/60	1.13	0.70	79.5	05-022	0.05	1.5	32	
452	4081	0.25/60	1.02	0.72	74.0	05-022	0.05	1.5	32	
453	4081	0.25/60	0.88	0.76	68.5	05-022	0.05	1.5	32	
454	4081	0.25/60	0.77	0.82	63.0	05-022	0.05	1.5	32	
455	4081	0.25/60	0.17	1.42	26.0	05-022	0.05	1.5	32	
561	4081	0.25/60	1.23	0.70	83.0	05-022	0.05	1.5	32	
562	4081	0.25/60	1.10	0.72	77.5	05-022	0.05	1.5	32	
563	4081	0.25/60	1.00	0.74	72.0	05-022	0.05	1.5	32	
564	4081	0.25/60	0.89	0.77	66.5	05-022	0.05	1.5	32	
565	4081	0.25/60	0.77	0.86	61.0	05-022	0.05	1.5	32	
566	4081	0.25/60	0.67	0.89	55.5	05-022	0.05	1.5	32	
567	4081	0.25/60	2.62	1.58	161.5	05-022	0.05	1.5	32	
215	4081	0.25/60				06-027	0.05	2.0	1	
442	4081	0.25/60	1.31	2.68	87.5	06-027	0.05	1.5	32	
443	4081	0.25/60	1.20	2.68	82.0	06-027	0.05	1.5	32	
444	4081	0.25/60	1.09	2.70	76.5	06-027	0.05	1.5	32	
445	4081	0.25/60	0.96	2.74	71.0	06-027	0.05	1.5	32	
446	4081	0.25/60	0.84	2.79	65.5	06-027	0.05	1.5	32	
447	4081	0.25/60	0.73	2.84	60.0	06-027	0.05	1.5	32	
448	4081	0.25/60	0.17	3.43	26.0	06-027	0.05	1.5	32	
554	4081	0.25/60	1.56	2.70	97.0	06-027	0.05	1.5	32	
555	4081	0.25/60	1.43	2.70	91.5	06-027	0.05	1.5	32	
556	4081	0.25/60	1.31	2.70	86.0	06-027	0.05	1.5	32	
557	4081	0.25/60	1.18	2.70	80.5	06-027	0.05	1.5	32	
558	4081	0.25/60	1.06	2.73	75.0	06-027	0.05	1.5	32	
559	4081	0.25/60	0.93	2.77	69.5	06-027	0.05	1.5	32	
560	4081	0.25/60	2.64	3.69	163.0	06-027	0.05	1.5	32	
320	4078	0.25/70	1.45	2.53	90.0	07-039	0.05	1.5	1	
321	4078	0.25/70	1.45	2.53	90.0	07-039	0.05	1.5	2	
322	4078	0.25/70	1.45	2.53	90.0	07-039	0.05	1.5	4	
323	4078	0.25/70	1.45	2.53	90.0	07-039	0.05	1.5	8	
324	4078	0.25/70	1.45	2.53	90.0	07-039	0.05	1.5	16	
325	4078	0.25/70	1.45	2.53	90.0	07-039	0.05	1.5	32	
326	4078	0.25/70	1.45	2.53	90.0	07-039	0.05	1.5	64	
327	4078	0.25/70	1.45	2.53	90.0	07-039	0.05	1.5	128	
328	4078	0.25/70	1.45	2.53	90.0	07-039	0.05	1.5	255	
214	4081	0.25/60				07-039	0.05	2.0	1	
230	4081	0.25/60	1.25	2.67	83.3	07-039	0.05	1.5	1	
234	4081	0.25/60	1.33	2.69	86.0	07-039	0.50	1.5	10	
238	4081	0.25/70	1.37	2.38	85.5	07-039	0.05	1.5	25	
254	4081	0.25/70	1.42	2.44	91.0	07-039	0.05	1.5	10	
255	4081	0.25/70	2.75	3.25	150.0	07-039	0.05	1.5	10	
256	4081	0.25/70	2.72	4.77	210.0	07-039	0.05	1.5	10	
257	4081	0.25/70	1.37	5.55	270.0	07-039	0.05	1.5	10	
258	4081	0.25/70	0.05	4.75	330.0	07-039	0.05	1.5	10	
259	4081	0.25/70	0.05	3.18	30.0	07-039	0.05	1.5	10	
260	4081	0.25/70	0.87	2.54	70.0	07-039	0.05	1.5	10	
274	4081	0.25/70	1.47	2.43	90.0	07-039	0.05	1.5	10	
275	4081	0.25/70	1.47	2.43	90.0	07-039	0.05	1.5	10	

ULTRASONIC TEST DATA LISTED BY SAMPLE NUMBER, CONTINUED

TEST NR	SERIAL NUMBER	XDUCER D/ANGLE	XDUCER POSITION X-IN	Y-IN	THETA	SAMPLE NUMBER	VOLT +-FS	DELAY X1000	RDGS AVGD	NOTES
	310	320	340	350	360	410	620	920		
284	4081	0.25/70	1.47	2.43	90.0	07-039	0.05	1.5	10	
285	4081	0.25/70	1.47	2.43	90.0	07-039	0.05	1.5	10	
306	4081	0.25/70	1.44	2.48	90.0	07-039	0.05	1.5	10	
307	4081	0.25/70	1.32	2.48	84.5	07-039	0.05	1.5	10	
308	4081	0.25/70	1.17	2.49	79.0	07-039	0.05	1.5	10	
309	4081	0.25/70	1.03	2.50	73.5	07-039	0.05	1.5	10	
310	4081	0.25/70	0.88	2.54	68.0	07-039	0.05	1.5	10	
311	4081	0.25/70	0.86	2.59	62.5	07-039	0.05	1.5	10	
312	4081	0.25/70	2.60	3.09	141.0	07-039	0.05	1.5	10	
435	4081	0.25/60	1.24	2.68	83.5	07-039	0.05	1.5	32	
436	4081	0.25/60	1.12	2.69	78.0	07-039	0.05	1.5	32	
437	4081	0.25/60	1.00	2.73	72.5	07-039	0.05	1.5	32	
438	4081	0.25/60	0.86	2.78	67.0	07-039	0.05	1.5	32	
439	4081	0.25/60	0.74	2.83	61.5	07-039	0.05	1.5	32	
440	4081	0.25/60	0.64	2.88	56.0	07-039	0.05	1.5	32	
441	4081	0.25/60	0.19	3.41	26.0	07-039	0.05	1.5	32	
547	4081	0.25/60	1.28	2.68	86.0	07-039	0.05	1.5	32	
548	4081	0.25/60	1.17	2.71	80.5	07-039	0.05	1.5	32	
549	4081	0.25/60	1.04	2.74	75.0	07-039	0.05	1.5	32	
550	4081	0.25/60	0.92	2.78	69.5	07-039	0.05	1.5	32	
551	4081	0.25/60	0.82	2.82	64.0	07-039	0.05	1.5	32	
552	4081	0.25/60	0.71	2.87	58.5	07-039	0.05	1.5	32	
553	4081	0.25/60	2.63	3.66	164.0	07-039	0.05	1.5	32	
213	4081	0.25/60				08-048	0.05	2.0	1	
428	4081	0.25/60	1.21	2.69	82.0	08-048	0.05	1.5	32	
429	4081	0.25/60	1.08	2.71	76.5	08-048	0.05	1.5	32	
430	4081	0.25/60	0.95	2.73	71.0	08-048	0.05	1.5	32	
431	4081	0.25/60	0.84	2.78	65.5	08-048	0.05	1.5	32	
432	4081	0.25/60	0.72	2.84	60.0	08-048	0.05	1.5	32	
433	4081	0.25/60	0.61	2.92	54.5	08-048	0.05	1.5	32	
434	4081	0.25/60	0.17	3.42	26.0	08-048	0.05	1.5	32	
540	4081	0.25/60	1.30	2.70	86.0	08-048	0.05	1.5	32	
541	4081	0.25/60	1.16	2.72	80.5	08-048	0.05	1.5	32	
542	4081	0.25/60	1.03	2.73	75.0	08-048	0.05	1.5	32	
543	4081	0.25/60	0.90	2.77	69.5	08-048	0.05	1.5	32	
544	4081	0.25/60	0.81	2.82	64.0	08-048	0.05	1.5	32	
545	4081	0.25/60	0.76	2.90	58.5	08-048	0.05	1.5	32	
546	4081	0.25/60	2.62	3.57	160.5	08-048	0.05	1.5	32	
211	4081	0.25/60				09-054	0.05	2.0	1	
212	4081	0.25/60				09-054	0.05	2.0	1	
371	4081	0.25/70	1.49	2.43	93.0	09-054	0.05	1.5	32	
372	4081	0.25/70	1.33	2.43	87.5	09-054	0.05	1.5	32	
373	4081	0.25/70	1.20	2.46	82.0	09-054	0.05	1.5	32	
374	4081	0.25/70	0.99	2.49	75.5	09-054	0.05	1.5	32	
375	4081	0.25/70	0.86	2.53	70.0	09-054	0.05	1.5	32	
376	4081	0.25/70	0.71	2.58	64.5	09-054	0.05	1.5	32	
377	4081	0.25/70	0.60	2.66	59.0	09-054	0.05	1.5	32	
378	4081	0.25/70	0.00	3.28	28.0	09-054	0.05	1.5	32	
421	4081	0.25/60	1.34	2.66	89.0	09-054	0.05	1.5	32	
422	4081	0.25/60	1.23	2.68	83.5	09-054	0.05	1.5	32	
423	4081	0.25/60	1.20	2.70	78.0	09-054	0.05	1.5	32	
424	4081	0.25/60	1.00	2.73	72.5	09-054	0.05	1.5	32	

ULTRASONIC TEST DATA LISTED BY SAMPLE NUMBER, CONTINUED

TEST NR	SERIAL NUMBER	XDUCER D/ANGLE	XDUCER POSITION X-IN	Y-IN	THETA	SAMPLE NUMBER	VOLT +-FS	DELAY X1000	RDGS AVGD	NOTES
	310	320	340	350	360	410	620	920		
425	4081	0.25/60	0.87	2.77	67.0	09-054	0.05	1.5	32	
426	4081	0.25/60	0.77	2.83	61.5	09-054	0.05	1.5	32	
427	4081	0.25/60	0.17	3.43	25.0	09-054	0.05	1.5	32	
533	4081	0.25/60	1.43	2.69	91.0	09-054	0.05	1.5	32	
534	4081	0.25/60	1.29	2.70	85.5	09-054	0.05	1.5	32	
535	4081	0.25/60	1.17	2.72	80.0	09-054	0.05	1.5	32	
536	4081	0.25/60	1.03	2.74	74.5	09-054	0.05	1.5	32	
537	4081	0.25/60	0.91	2.78	69.0	09-054	0.05	1.5	32	
538	4081	0.25/60	0.82	2.92	63.5	09-054	0.05	1.5	32	
539	4081	0.25/60	2.64	3.61	162.5	09-054	0.05	1.5	32	
364	4078	0.25/70	1.47	2.43	92.0	10-073	0.05	1.5	32	
365	4078	0.25/70	1.33	2.43	86.5	10-073	0.05	1.5	32	
366	4078	0.25/70	1.19	2.44	81.0	10-073	0.05	1.5	32	
367	4078	0.25/70	1.03	2.48	75.5	10-073	0.05	1.5	32	
368	4078	0.25/70	0.90	2.51	70.0	10-073	0.05	1.5	32	
369	4078	0.25/70	0.75	2.57	64.5	10-073	0.05	1.5	32	
370	4078	0.25/70	0.00	3.30	24.0	10-073	0.05	1.5	32	
210	4081	0.25/60				10-073	0.05	2.0	1	
414	4081	0.25/60	1.32	2.68	87.0	10-073	0.05	1.5	32	
415	4081	0.25/60	1.18	2.69	81.5	10-073	0.05	1.5	32	
416	4081	0.25/60	1.05	2.71	76.0	10-073	0.05	1.5	32	
417	4081	0.25/60	0.94	2.74	70.5	10-073	0.05	1.5	32	
418	4081	0.25/60	0.84	2.79	65.0	10-073	0.05	1.5	32	
419	4081	0.25/60	0.73	2.86	59.5	10-073	0.05	1.5	32	
420	4081	0.25/60	0.17	3.40	26.0	10-073	0.05	1.5	32	
526	4081	0.25/60	1.64	2.72	101.0	10-073	0.05	1.5	32	
527	4081	0.25/60	1.53	2.68	95.5	10-073	0.05	1.5	32	
528	4081	0.25/60	1.38	2.70	90.0	10-073	0.05	1.5	32	
529	4081	0.25/60	1.27	2.70	84.5	10-073	0.05	1.5	32	
530	4081	0.25/60	1.14	2.72	79.0	10-073	0.05	1.5	32	
531	4081	0.25/60	1.03	2.74	73.5	10-073	0.05	1.5	32	
532	4081	0.25/60	2.67	3.78	169.0	10-073	0.05	1.5	32	
357	4078	0.25/70	1.34	2.50	91.0	11-093	0.05	1.5	32	
358	4078	0.25/70	1.25	2.51	85.5	11-093	0.05	1.5	32	
359	4078	0.25/70	1.08	2.53	80.0	11-093	0.05	1.5	32	
360	4078	0.25/70	0.93	2.57	74.5	11-093	0.05	1.5	32	
361	4078	0.25/70	0.80	2.62	69.0	11-093	0.05	1.5	32	
362	4078	0.25/70	0.67	2.68	63.5	11-093	0.05	1.5	32	
363	4078	0.25/70	0.00	3.38	25.0	11-093	0.05	1.5	32	
209	4081	0.25/60				11-093	0.10	2.0	1	
225	4081	0.25/60				11-093	0.20	1.5	1	
227	4081	0.25/60				11-093	0.10	1.0	1	
229	4081	0.25/60	1.31	2.68	86.0	11-093	0.20	1.5	1	
233	4081	0.25/60	1.26	2.72	83.5	11-093	0.10	1.5	10	
237	4081	0.25/70	1.24	2.48	84.0	11-093	0.05	1.5	10	
247	4081	0.25/70	1.42	2.43	91.0	11-093	0.10	1.5	10	
248	4081	0.25/70	2.75	3.25	150.0	11-093	0.10	1.5	10	
249	4081	0.25/70	2.75	4.84	210.0	11-093	0.10	1.5	10	
250	4081	0.25/70	1.45	5.55	270.0	11-093	0.10	1.5	10	
251	4081	0.25/70	0.00	4.75	330.0	11-093	0.10	1.5	10	
252	4081	0.25/70	0.05	3.20	30.0	11-093	0.10	1.5	10	
253	4081	0.25/70	0.89	2.53	72.0	11-093	0.10	1.5	10	

ULTRASONIC TEST DATA LISTED BY SAMPLE NUMBER, CONTINUED

TEST NR	SERIAL NUMBER	XDUCER D/ANGLE	XDUCER POSITION X-IN	Y-IN	THETA	SAMPLE NUMBER	VOLT +-FS	DELAY X1000	RDGS AVGD	NOTES
	310	320	340	350	360	410	620	920		
272	4081	0.25/70	1.35	2.43	85.5	11-093	0.05	1.5	10	
273	4081	0.25/70	1.35	2.43	85.5	11-093	0.05	1.5	10	
281	4081	0.25/70	1.35	2.43	85.5	11-093	0.05	1.5	10	
282	4081	0.25/70	1.35	2.43	85.5	11-093	0.05	1.5	10	
283	4081	0.25/70	1.35	2.43	85.5	11-093	0.05	1.5	10	
299	4081	0.25/70	1.36	2.47	86.5	11-093	0.05	1.5	10	
300	4081	0.25/70	1.22	2.48	81.0	11-093	0.05	1.5	10	
301	4081	0.25/70	1.09	2.50	75.5	11-093	0.05	1.5	10	
302	4081	0.25/70	0.95	2.52	70.0	11-093	0.05	1.5	10	
303	4081	0.25/70	0.81	2.57	64.5	11-093	0.05	1.5	10	
304	4081	0.25/70	0.68	2.64	59.0	11-093	0.05	1.5	10	
305	4081	0.25/70	2.72	3.32	149.0	11-093	0.05	1.5	10	
407	4081	0.25/60	1.29	2.68	86.0	11-093	0.10	1.5	32	
408	4081	0.25/60	1.16	2.68	80.5	11-093	0.10	1.5	32	
409	4081	0.25/60	1.05	2.71	75.0	11-093	0.05	1.5	32	
410	4081	0.25/60	0.92	2.75	69.5	11-093	0.05	1.5	32	
411	4081	0.25/60	0.81	2.79	64.0	11-093	0.05	1.5	32	
412	4081	0.25/60	0.70	2.85	58.5	11-093	0.05	1.5	32	
413	4081	0.25/60	0.17	3.43	25.0	11-093	0.05	1.5	32	
519	4081	0.25/60	1.27	2.69	85.5	11-093	0.05	1.5	32	
520	4081	0.25/60	1.16	2.70	80.0	11-093	0.05	1.5	32	
521	4081	0.25/60	1.03	2.73	74.5	11-093	0.05	1.5	32	
522	4081	0.25/60	0.91	2.77	69.0	11-093	0.05	1.5	32	
523	4081	0.25/60	0.80	2.82	63.5	11-093	0.05	1.5	32	
524	4081	0.25/60	0.66	2.89	58.0	11-093	0.05	1.5	32	
525	4081	0.25/60	2.62	3.64	161.0	11-093	0.05	1.5	32	
208	4081	0.25/60				12-113	0.10	2.0	1	
350	4081	0.25/70	1.39	2.49	91.5	12-113	0.05	1.5	32	
351	4081	0.25/70	1.25	2.50	86.0	12-113	0.05	1.5	32	
352	4081	0.25/70	1.10	2.52	80.5	12-113	0.05	1.5	32	
353	4081	0.25/70	0.95	2.57	75.0	12-113	0.05	1.5	32	
354	4081	0.25/70	0.81	2.61	69.5	12-113	0.05	1.5	32	
355	4081	0.25/70	0.68	2.68	74.0	12-113	0.05	1.5	32	
356	4081	0.25/70	0.00	3.40	25.0	12-113	0.05	1.5	32	
400	4081	0.25/60	1.30	2.68	86.5	12-113	0.05	1.5	32	
401	4081	0.25/60	1.20	2.70	81.0	12-113	0.05	1.5	32	
402	4081	0.25/60	1.05	2.72	75.5	12-113	0.05	1.5	32	
403	4081	0.25/60	0.92	2.76	70.0	12-113	0.05	1.5	32	
404	4081	0.25/60	0.80	2.80	64.5	12-113	0.05	1.5	32	
405	4081	0.25/60	0.70	2.86	59.0	12-113	0.05	1.5	32	
406	4081	0.25/60	0.16	3.43	25.5	12-113	0.05	1.5	32	
512	4081	0.25/60	1.34	2.70	87.5	12-113	0.05	1.5	32	
513	4081	0.25/60	1.20	2.70	82.0	12-113	0.05	1.5	32	
514	4081	0.25/60	1.10	2.73	76.5	12-113	0.05	1.5	32	
515	4081	0.25/60	0.97	2.77	71.0	12-113	0.05	1.5	32	
516	4081	0.25/60	0.83	2.81	65.5	12-113	0.05	1.5	32	
517	4081	0.25/60	0.73	2.87	60.0	12-113	0.05	1.5	32	
518	4081	0.25/60	2.62	3.59	160.5	12-113	0.05	1.5	32	
204	5354	0.25/45				12-113	0.20	0.0	1	NOTE 2
207	4081	0.25/60				13-150	0.10	2.0	1	
343	4081	0.25/70	1.33	2.50	90.0	13-150	0.05	1.5	32	
344	4081	0.25/70	1.18	2.51	84.5	13-150	0.05	1.5	32	

ULTRASONIC TEST DATA LISTED BY SAMPLE NUMBER, CONTINUED

TEST NR	SERIAL NUMBER	XDUCER D/ANGLE	XDUCER X-IN	XDUCER Y-IN	POSITION THETA	SAMPLE NUMBER	VOLT +-FS	DELAY X1000	RDGS AVGD	NOTES
	310	320	340	350	360	410	620	920		
345	4081	0.25/70	1.03	2.54	79.0	13-150	0.05	1.5	32	
346	4081	0.25/70	0.92	2.58	73.5	13-150	0.05	1.5	32	
347	4081	0.25/70	0.78	2.63	68.0	13-150	0.05	1.5	32	
348	4081	0.25/70	0.65	2.69	62.5	13-150	0.05	1.5	32	
349	4081	0.25/70	0.00	3.40	25.5	13-150	0.05	1.5	32	
393	4081	0.25/60	1.38	2.68	91.0	13-150	0.10	1.5	32	
394	4081	0.25/60	1.27	2.69	85.5	13-150	0.10	1.5	32	
395	4081	0.25/60	1.16	2.69	80.0	13-150	0.05	1.5	32	
396	4081	0.25/60	1.03	2.71	74.5	13-150	0.05	1.5	32	
397	4081	0.25/60	0.90	2.76	69.0	13-150	0.05	1.5	32	
398	4081	0.25/60	0.80	2.82	63.5	13-150	0.05	1.5	32	
399	4081	0.25/60	0.16	3.42	25.0	13-150	0.05	1.5	32	
505	4081	0.25/60	1.59	2.72	99.5	13-150	0.05	1.5	32	
506	4081	0.25/60	1.44	2.68	94.0	13-150	0.05	1.5	32	
507	4081	0.25/60	1.33	2.68	88.5	13-150	0.05	1.5	32	
508	4081	0.25/60	1.22	2.70	83.0	13-150	0.05	1.5	32	
509	4081	0.25/60	1.10	2.72	77.5	13-150	0.05	1.5	32	
510	4081	0.25/60	0.97	2.76	72.0	13-150	0.05	1.5	32	
511	4081	0.25/60	2.63	3.67	166.0	13-150	0.05	1.5	32	
203	5354	0.25/45				13-150	0.50	0.0	1	NOTE 2
206	4081	0.25/60				14-192	0.10	2.0	1	
224	4081	0.25/60				14-192	0.20	1.5	1	
226	4081	0.25/60				14-192	0.20	1.5	1	
228	4081	0.25/60	1.24	2.64	88.0	14-192	0.20	1.5	1	
232	4081	0.25/60	1.36	2.70	93.0	14-192	0.20	1.5	10	
236	4081	0.25/70	1.22	2.50	86.5	14-192	0.05	1.5	10	
240	4081	0.25/70	1.42	2.44	91.0	14-192	0.10	1.5	10	
241	4081	0.25/70	2.75	3.25	150.0	14-192	0.10	1.5	10	
242	4081	0.25/70	2.75	4.80	210.0	14-192	0.10	1.5	10	
243	4081	0.25/70	1.42	5.56	270.0	14-192	0.10	1.5	10	
244	4081	0.25/70	0.00	4.75	330.0	14-192	0.10	1.5	10	
245	4081	0.25/70	-.05	3.33	30.0	14-192	0.10	1.5	10	
246	4081	0.25/70	0.93	2.50	71.0	14-192	0.10	1.5	10	
270	4081	0.25/70	1.35	2.43	86.5	14-192	0.05	1.5	10	
271	4081	0.25/70	1.35	2.43	85.5	14-192	0.05	1.5	10	
278	4081	0.25/70	1.32	2.42	84.5	14-192	0.05	1.5	10	
279	4081	0.25/70	1.35	2.43	85.5	14-192	0.05	1.5	10	
280	4081	0.25/70	1.35	2.43	85.5	14-192	0.05	1.5	10	
291	4081	0.25/70	1.23	2.47	80.5	14-192	0.05	1.5	10	
292	4081	0.25/70	1.23	2.47	80.5	14-192	0.05	1.5	10	
293	4081	0.25/70	1.17	2.50	75.0	14-192	0.05	1.5	10	
294	4081	0.25/70	0.91	2.54	70.0	14-192	0.05	1.5	10	
295	4081	0.25/70	0.77	2.60	64.0	14-192	0.05	1.5	10	
296	4081	0.25/70	0.64	2.65	58.0	14-192	0.05	1.5	10	
297	4081	0.25/70	0.53	2.72	52.5	14-192	0.05	1.5	10	
298	4081	0.25/70	2.72	2.71	121.0	14-192	0.05	1.5	10	
336	4081	0.25/70	1.27	2.50	87.0	14-192	0.05	1.5	32	
337	4081	0.25/70	1.09	2.52	81.5	14-192	0.05	1.5	32	
338	4081	0.25/70	0.97	2.54	76.0	14-192	0.05	1.5	32	
339	4081	0.25/70	0.83	2.59	71.0	14-192	0.05	1.5	32	
340	4081	0.25/70	0.70	2.65	65.0	14-192	0.05	1.5	32	
341	4081	0.25/70	0.56	2.73	59.5	14-192	0.05	1.5	32	
342	4081	0.25/70	0.00	3.35	27.0	14-192	0.05	1.5	32	

ULTRASONIC TEST DATA LISTED BY SAMPLE NUMBER, CONTINUED

TEST NR	SERIAL NUMBER	XDUCER D/ANGLE	XDUCER POSITION X-IN	Y-IN	THETA	SAMPLE NUMBER	VOLT +-FS	DELAY X1000	RDGS AVGD	NOTES
	310	320	340	350	360	410	620	920		
386	4081	0.25/60	1.44	2.66	93.0	14-192	0.10	1.5	32	
387	4081	0.25/60	1.30	2.67	87.5	14-192	0.10	1.5	32	
388	4081	0.25/60	1.20	2.68	82.0	14-192	0.10	1.5	32	
389	4081	0.25/60	1.08	2.70	76.5	14-192	0.05	1.5	32	
390	4081	0.25/60	0.95	2.74	71.0	14-192	0.05	1.5	32	
391	4081	0.25/60	0.83	2.78	65.5	14-192	0.05	1.5	32	
392	4081	0.25/60	0.17	3.43	23.0	14-192	0.05	1.5	32	
498	4081	0.25/60	1.46	2.70	93.5	14-192	0.10	1.5	32	
499	4081	0.25/60	1.34	2.70	88.0	14-192	0.10	1.5	32	
500	4081	0.25/60	1.20	2.70	82.5	14-192	0.10	1.5	32	
501	4081	0.25/60	1.08	2.73	77.0	14-192	0.05	1.5	32	
502	4081	0.25/60	0.97	2.76	71.5	14-192	0.05	1.5	32	
503	4081	0.25/60	0.85	2.80	66.0	14-192	0.05	1.5	32	
504	4081	0.25/60	2.63	3.71	164.5	14-192	0.05	1.5	32	
202	5354	0.25/45				14-192	0.50	0.0	1	NOTE 2
329	4078	0.25/70	1.24	2.60	87.0	15-279	0.05	1.5	32	
330	4078	0.25/70	1.10	2.60	81.5	15-279	0.05	1.5	32	
331	4078	0.25/70	0.98	2.63	75.5	15-279	0.05	1.5	32	
332	4078	0.25/70	0.88	2.69	70.4	15-279	0.05	1.5	32	
333	4078	0.25/70	0.72	2.76	64.5	15-279	0.05	1.5	32	
334	4078	0.25/70	0.61	2.81	59.0	15-279	0.05	1.5	32	
335	4078	0.25/70	0.00	3.72	12.0	15-279	0.05	1.5	32	
205	4081	0.25/60				15-279	0.10	2.0	1	
290	4081	0.25/70	1.45	2.52	86.5	15-279	0.05	1.5	1	
379	4081	0.25/60	1.32	2.70	87.0	15-279	0.10	1.5	32	
380	4081	0.25/60	1.20	2.72	81.5	15-279	0.10	1.5	32	
381	4081	0.25/60	1.08	2.78	76.0	15-279	0.10	1.5	32	
382	4081	0.25/60	0.94	2.78	70.5	15-279	0.10	1.5	32	
383	4081	0.25/60	0.82	2.82	65.0	15-279	0.10	1.5	32	
384	4081	0.25/60	0.71	2.88	59.5	15-279	0.05	1.5	32	
385	4081	0.25/60	0.14	3.56	18.0	15-279	0.05	1.5	32	
491	4081	0.25/60	1.32	2.70	87.0	15-279	0.05	1.5	32	
492	4081	0.25/60	1.19	2.71	81.5	15-279	0.05	1.5	32	
493	4081	0.25/60	1.07	2.73	76.0	15-279	0.05	1.5	32	
494	4081	0.25/60	0.95	2.76	70.5	15-279	0.05	1.5	32	
495	4081	0.25/60	0.84	2.82	65.0	15-279	0.05	1.5	32	
496	4081	0.25/60	0.73	2.86	59.5	15-279	0.05	1.5	32	
497	4081	0.25/60	2.65	3.74	167.0	15-279	0.05	1.5	32	
201	5354	0.25/45				15-279	0.50	2.0	1	NOTES 2 & 3

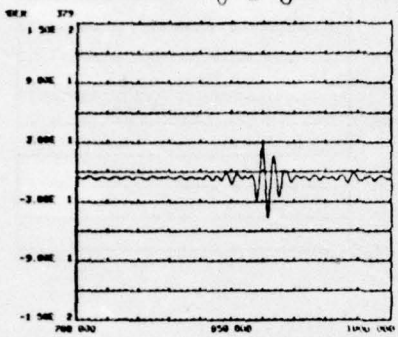
APPENDIX C

AMPLITUDE VERSUS TIME PLOTS OF SERIES 1 AND 2 DATA

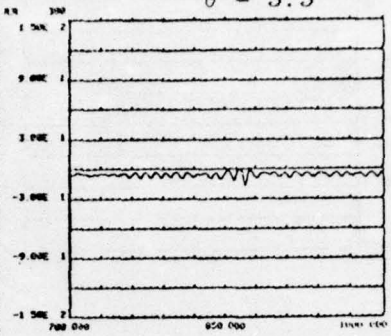
Time waveforms recorded for each specimen crack at the six angular positions and the reference signal for Series 1 and Series 2 are shown. The viewing angles increase from left to right and top to bottom in 5.5° increments, starting with 0° in the top left hand corner. The bottom most figure is the reference signal for the particular specimen.

Sample specimens are labeled xx-yyy, where xx is the 16-sample set identification number (xx = 0, 1, ..., 15) and yyy is the crack length in mils. For example, 15-279 denotes specimen number 15, which contains a 279 mil crack.

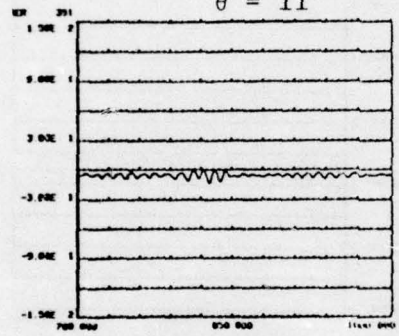
$\theta = 0^{o}$



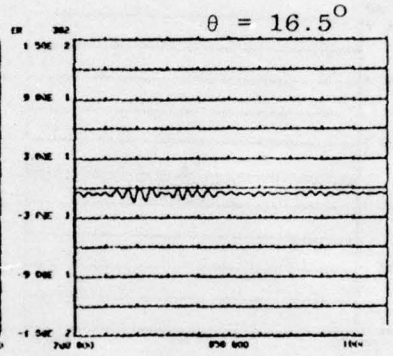
$\theta = 5.5^{o}$



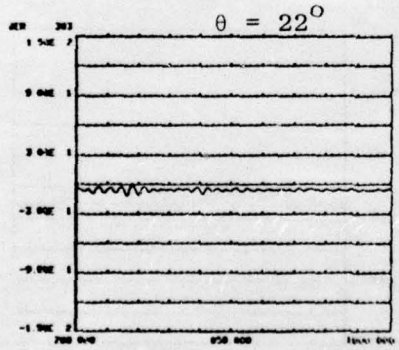
$\theta = 11^{o}$



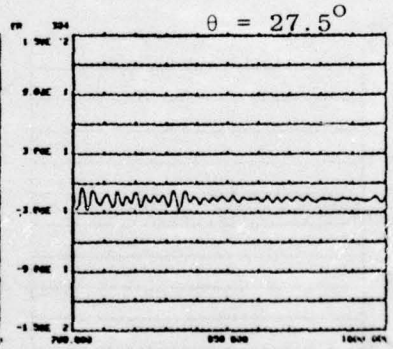
$\theta = 16.5^{o}$



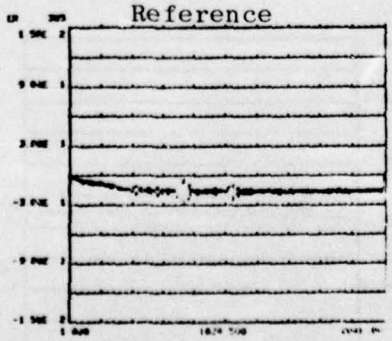
$\theta = 22^{o}$



$\theta = 27.5^{o}$

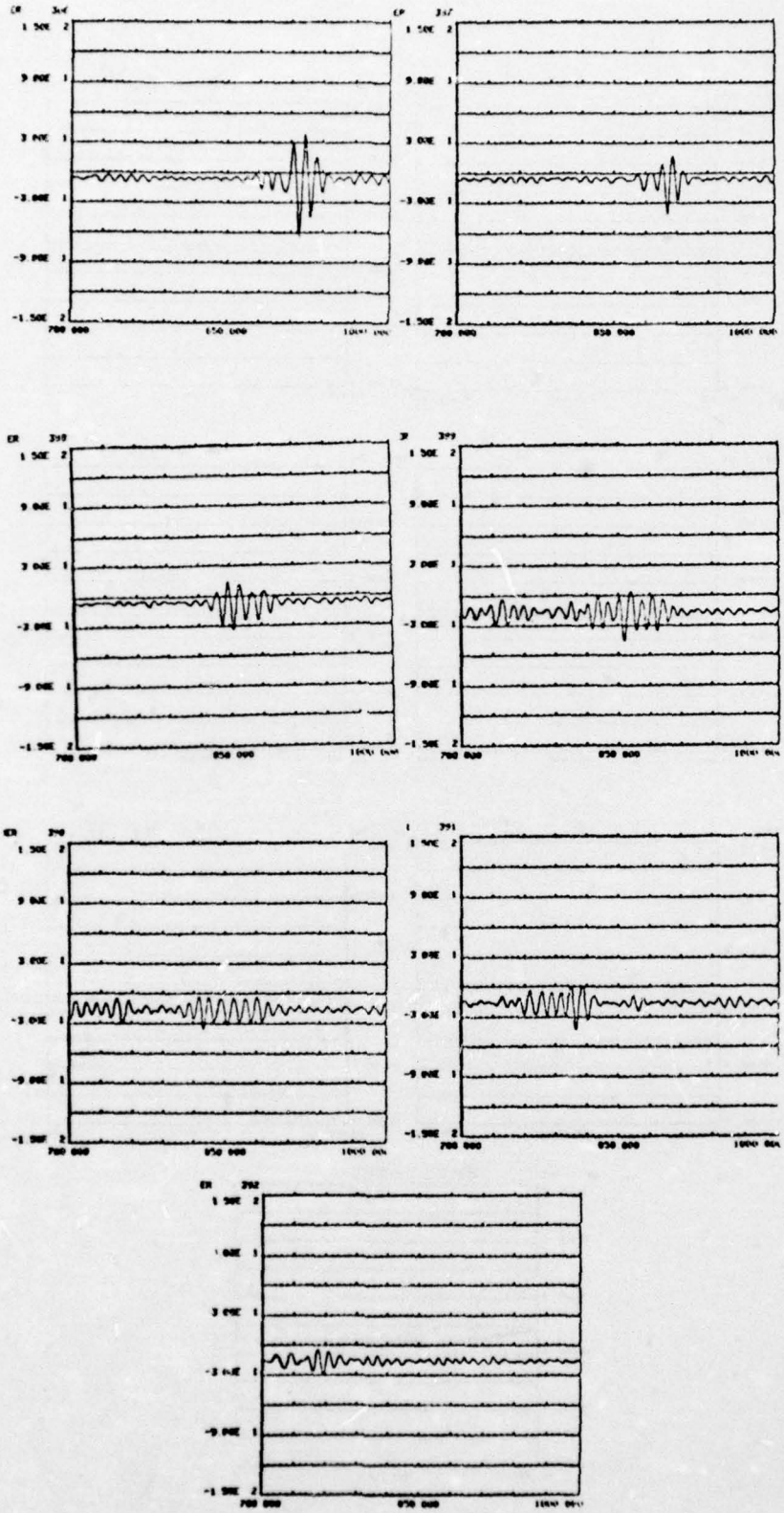


Reference

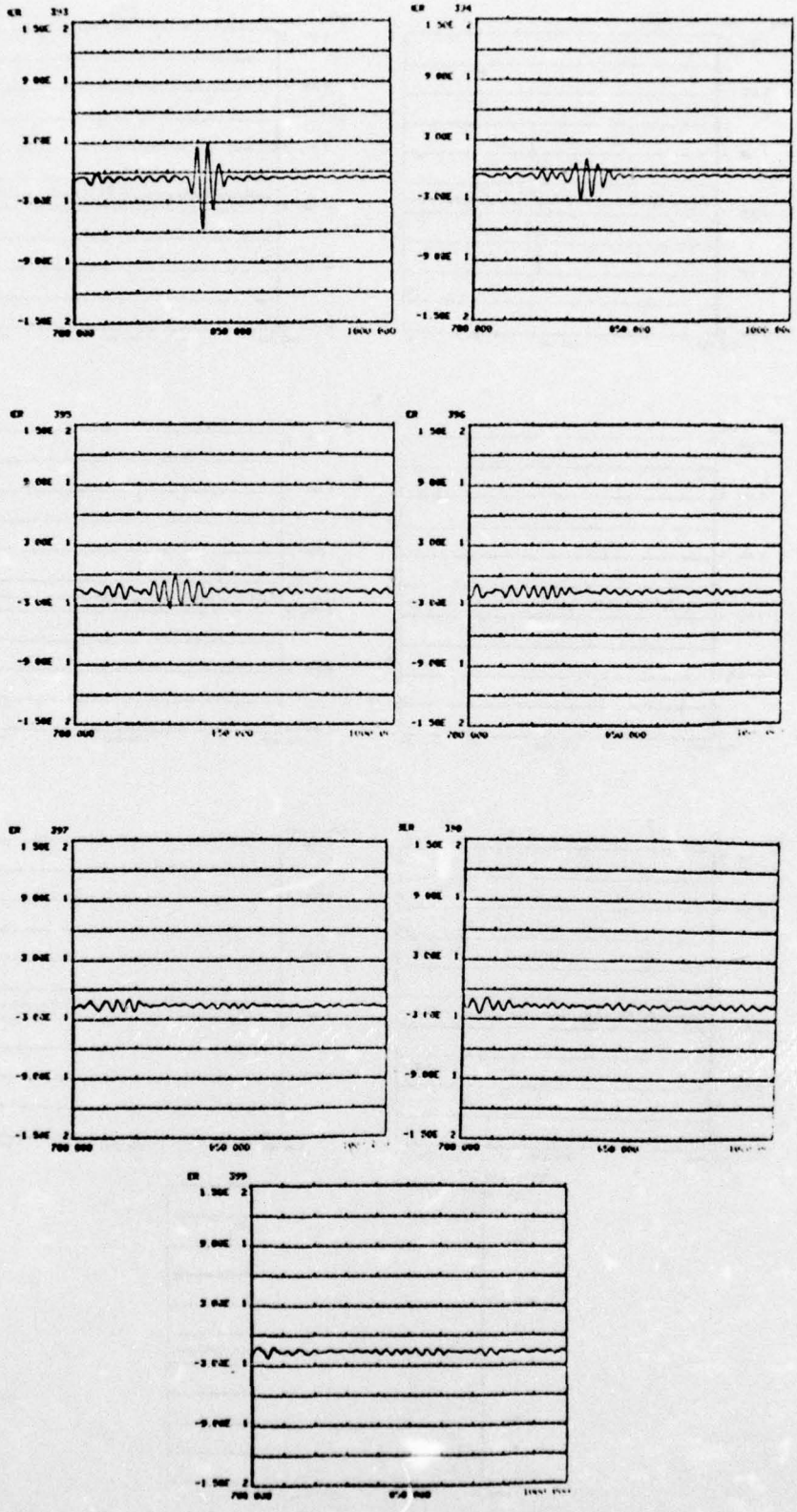


Specimen 15-279: Series 1

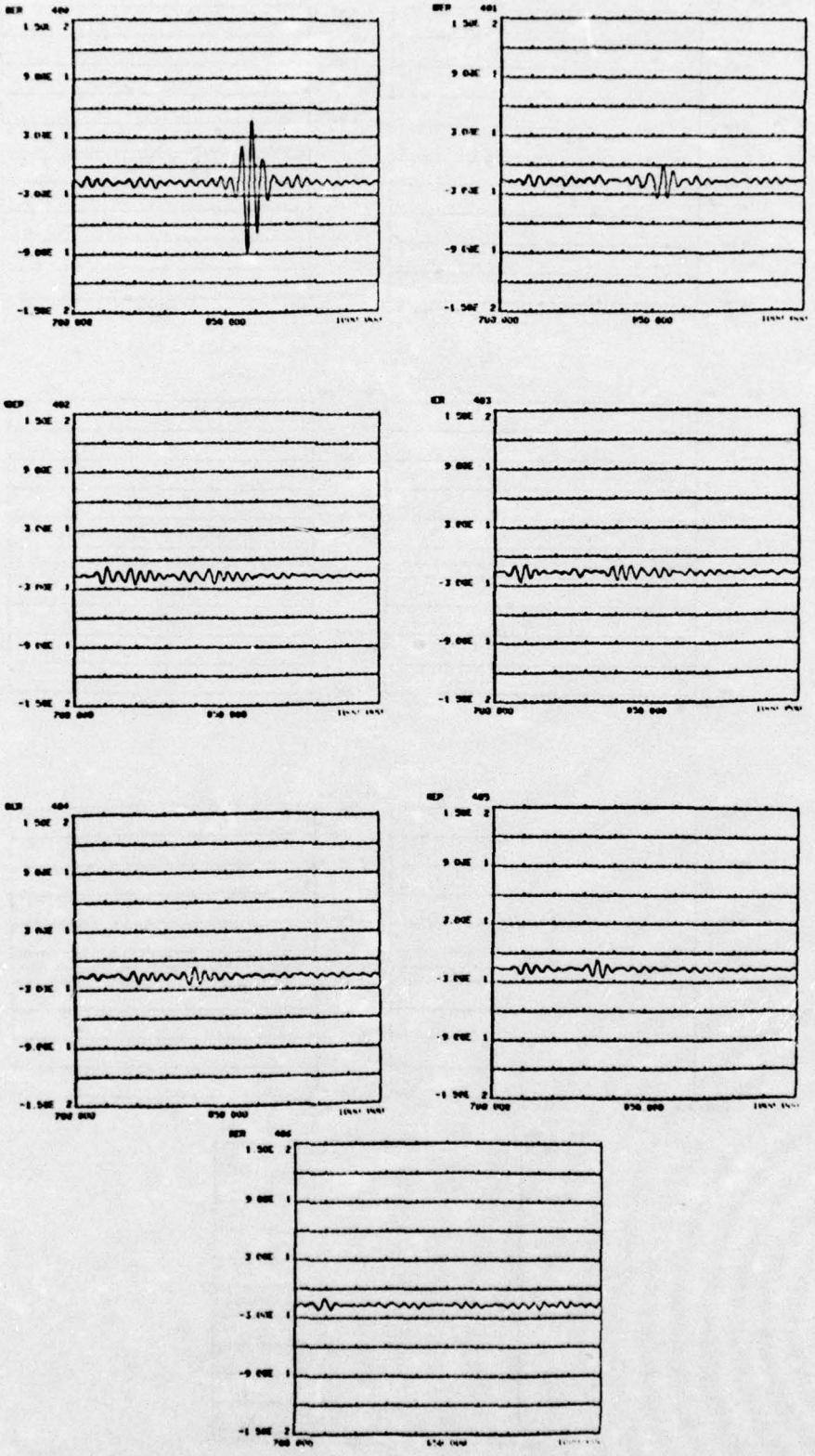
PRECEDING PAGE BLANK-NOT FILMED



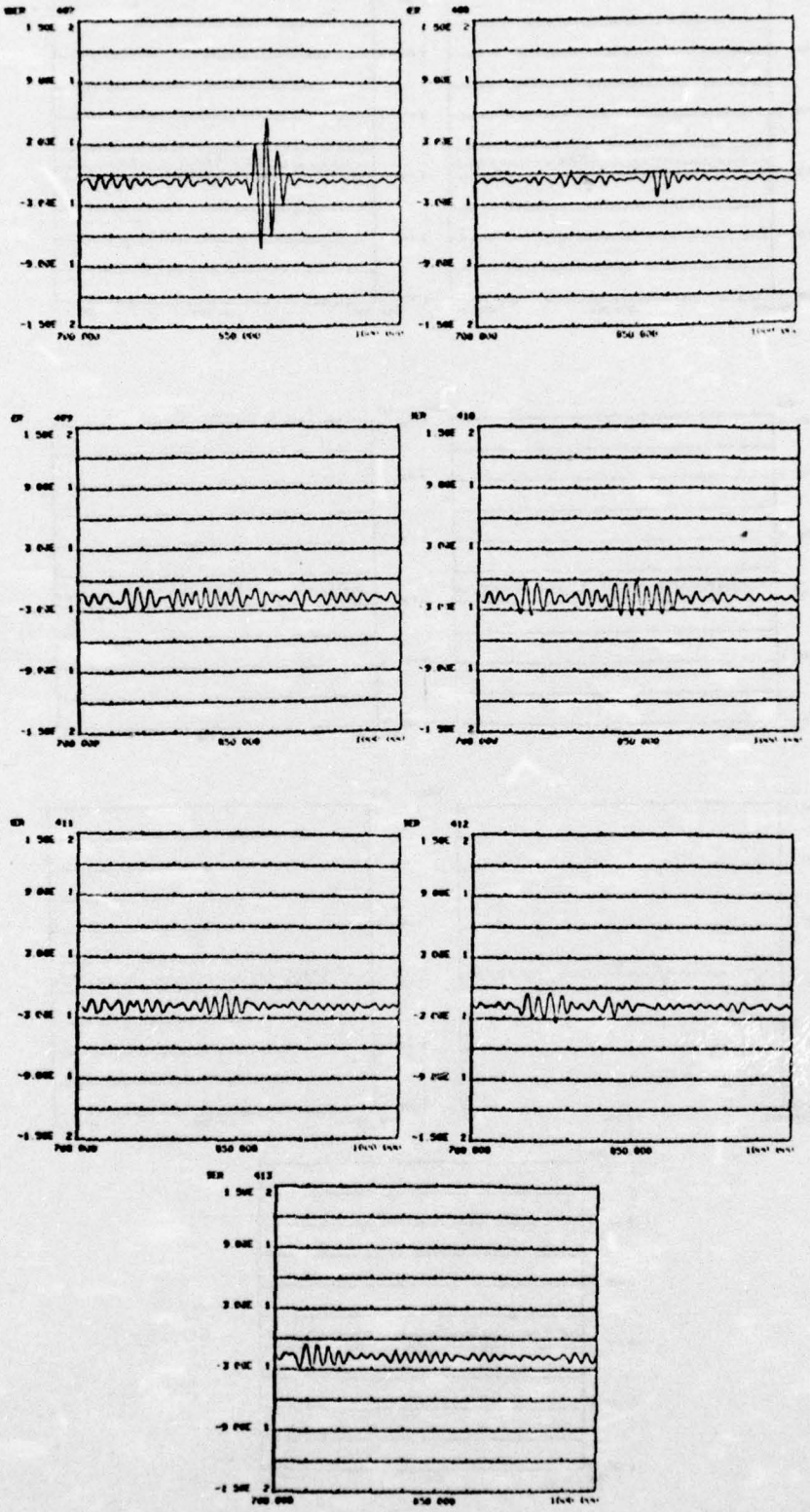
Specimen 14-192: Series 1
C-4



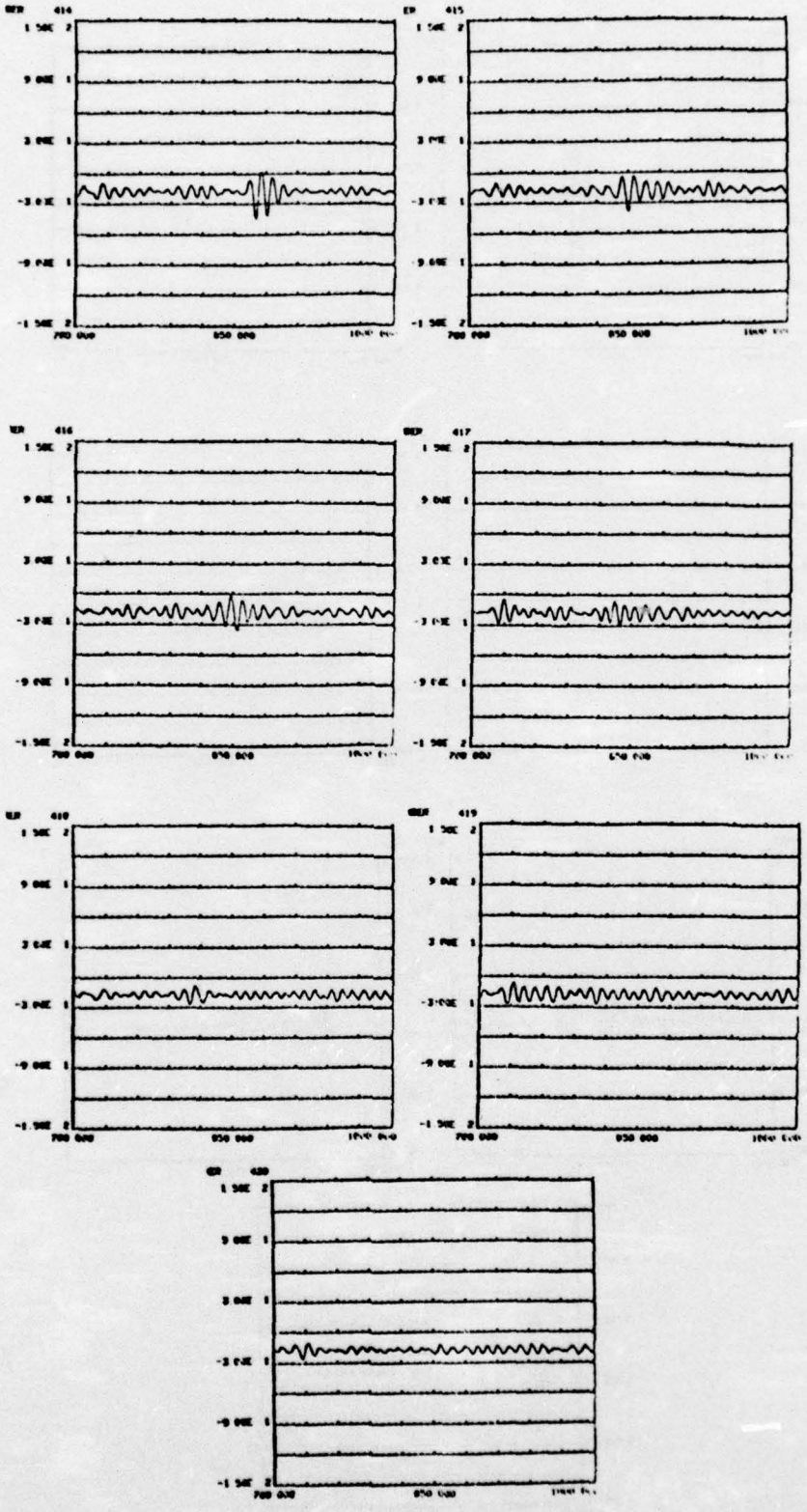
Specimen 13-150: Series 1
C-5



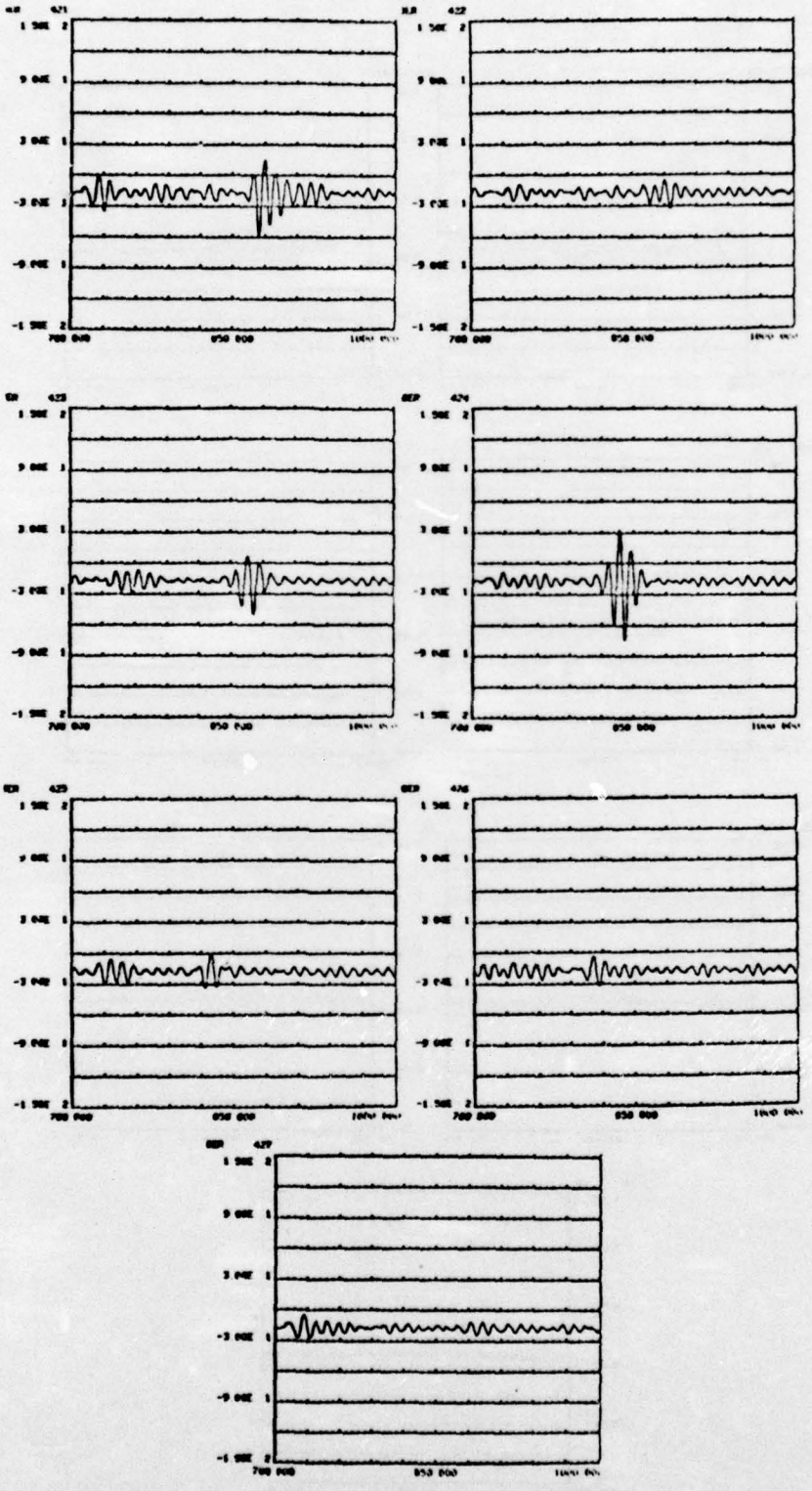
Specimen 12-113: Series 1
C-6



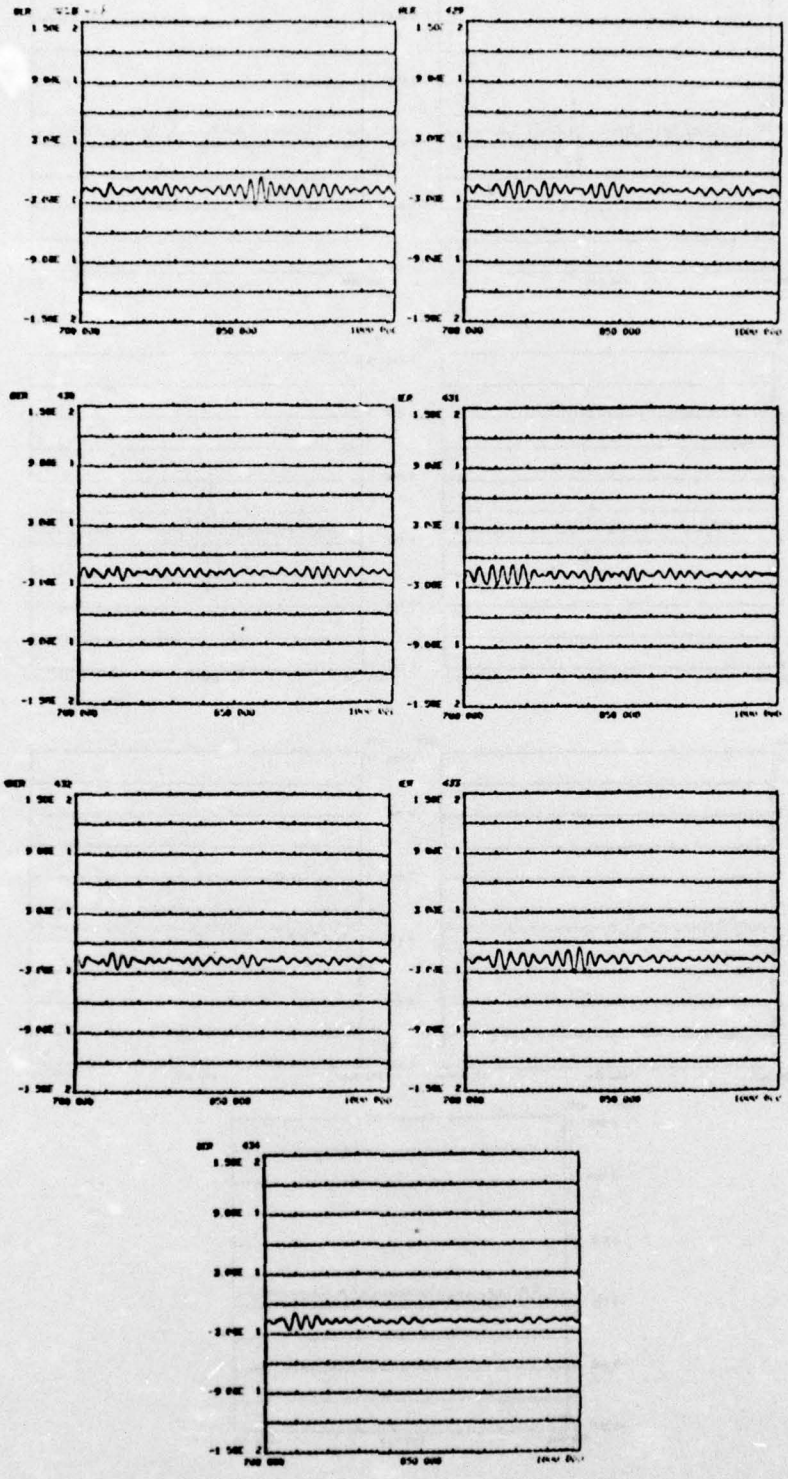
Specimen 11-093: Series 1
C-7



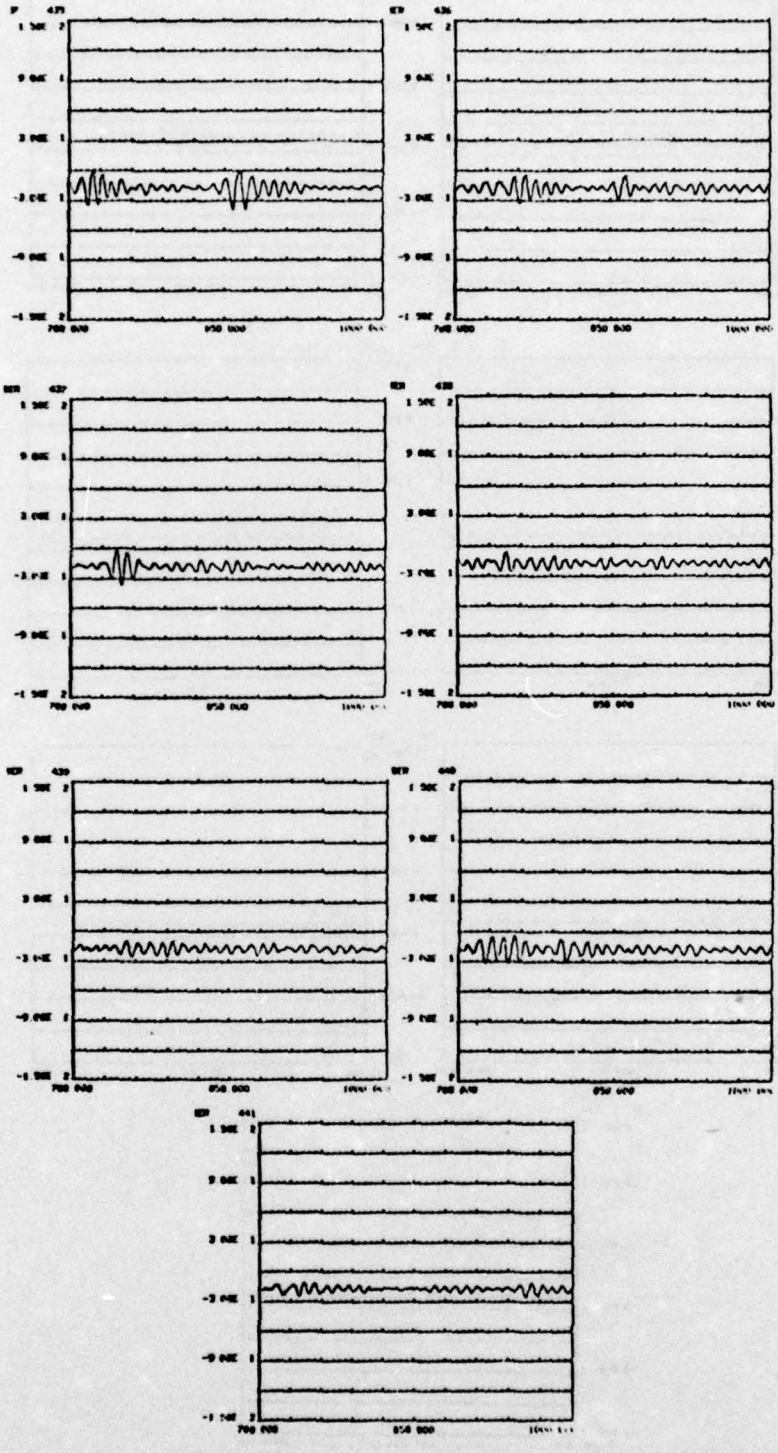
Specimen 10-073: Series 1



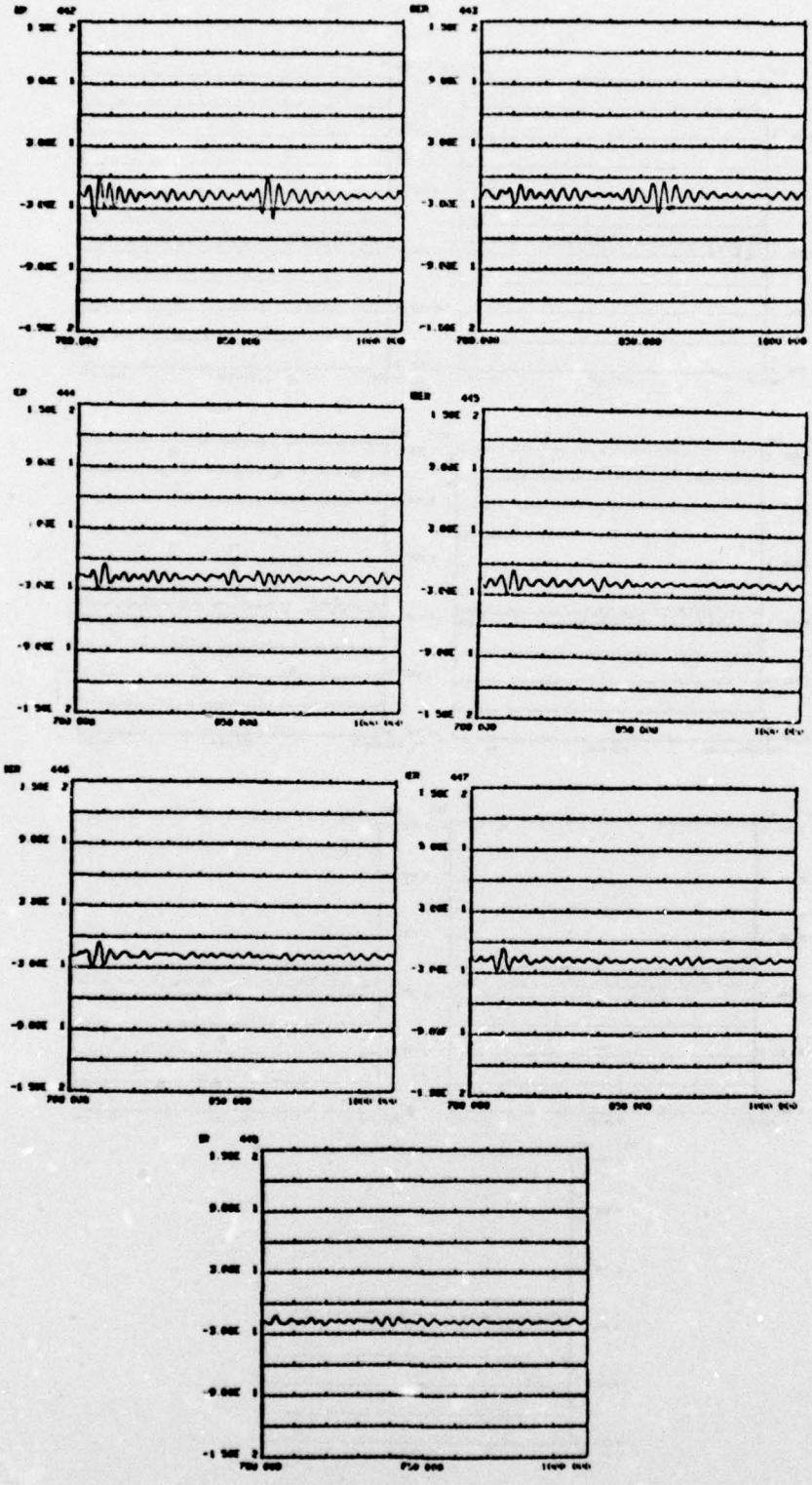
Specimen 09-054: Series 1



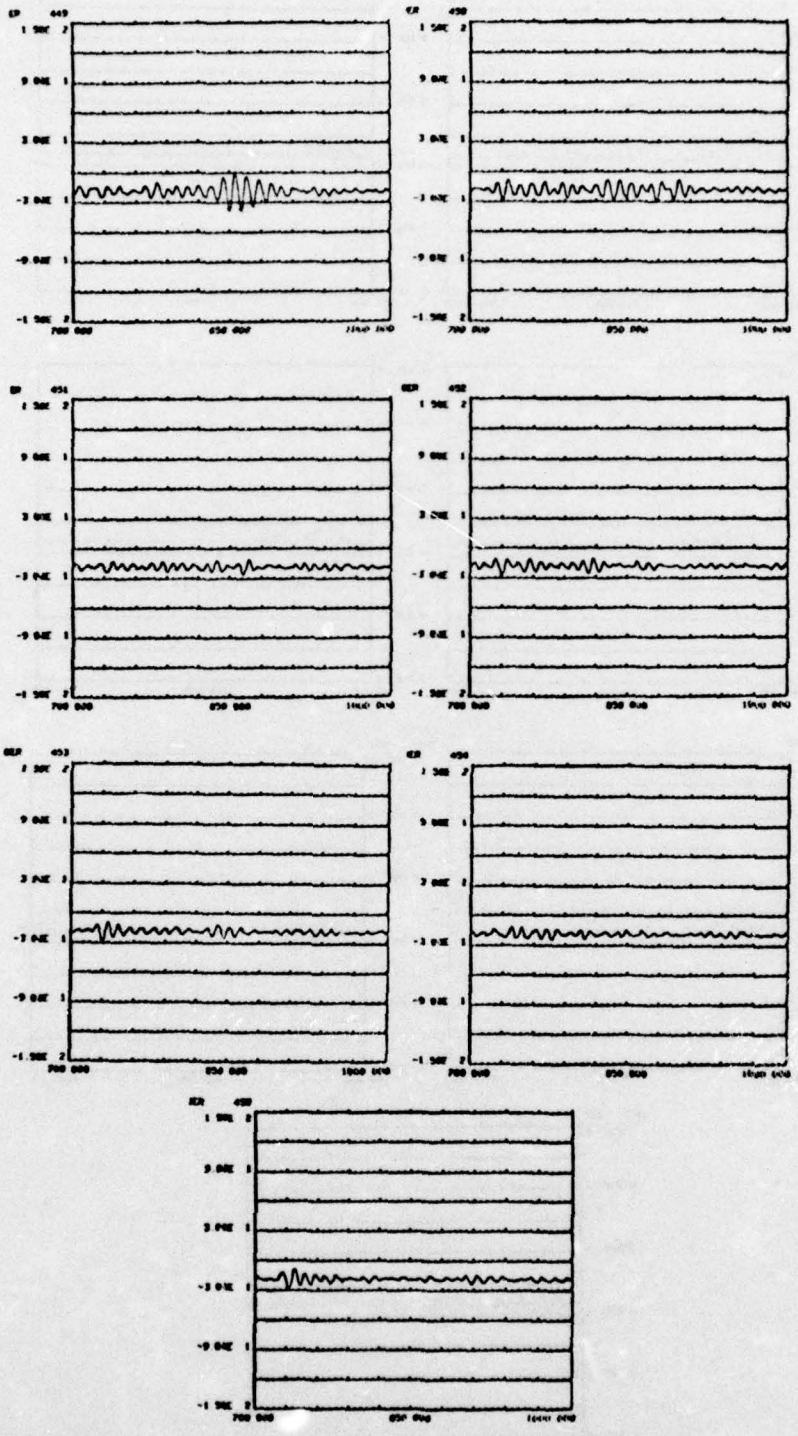
Specimen 08-048: Series 1



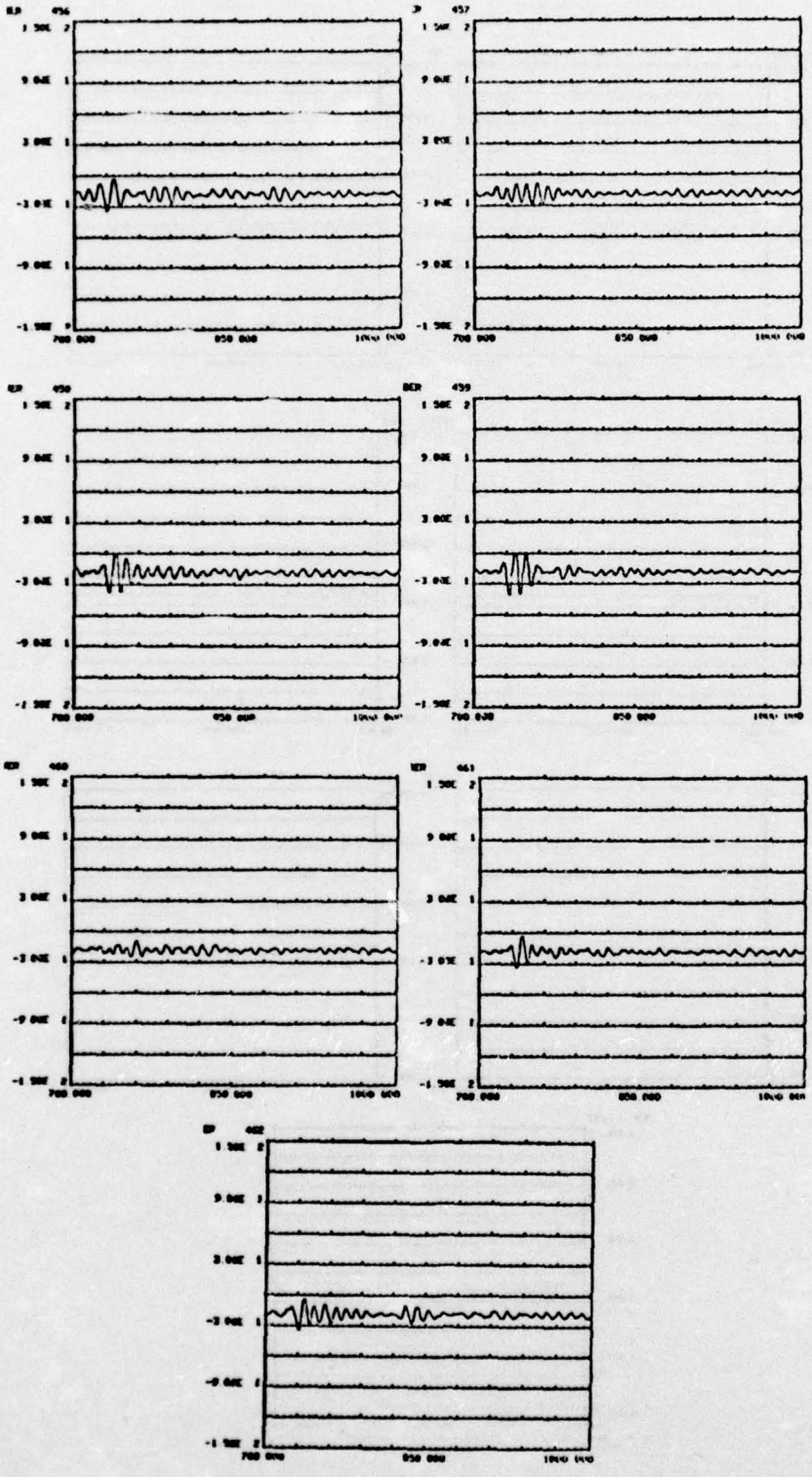
Specimen 07-039: Series 1



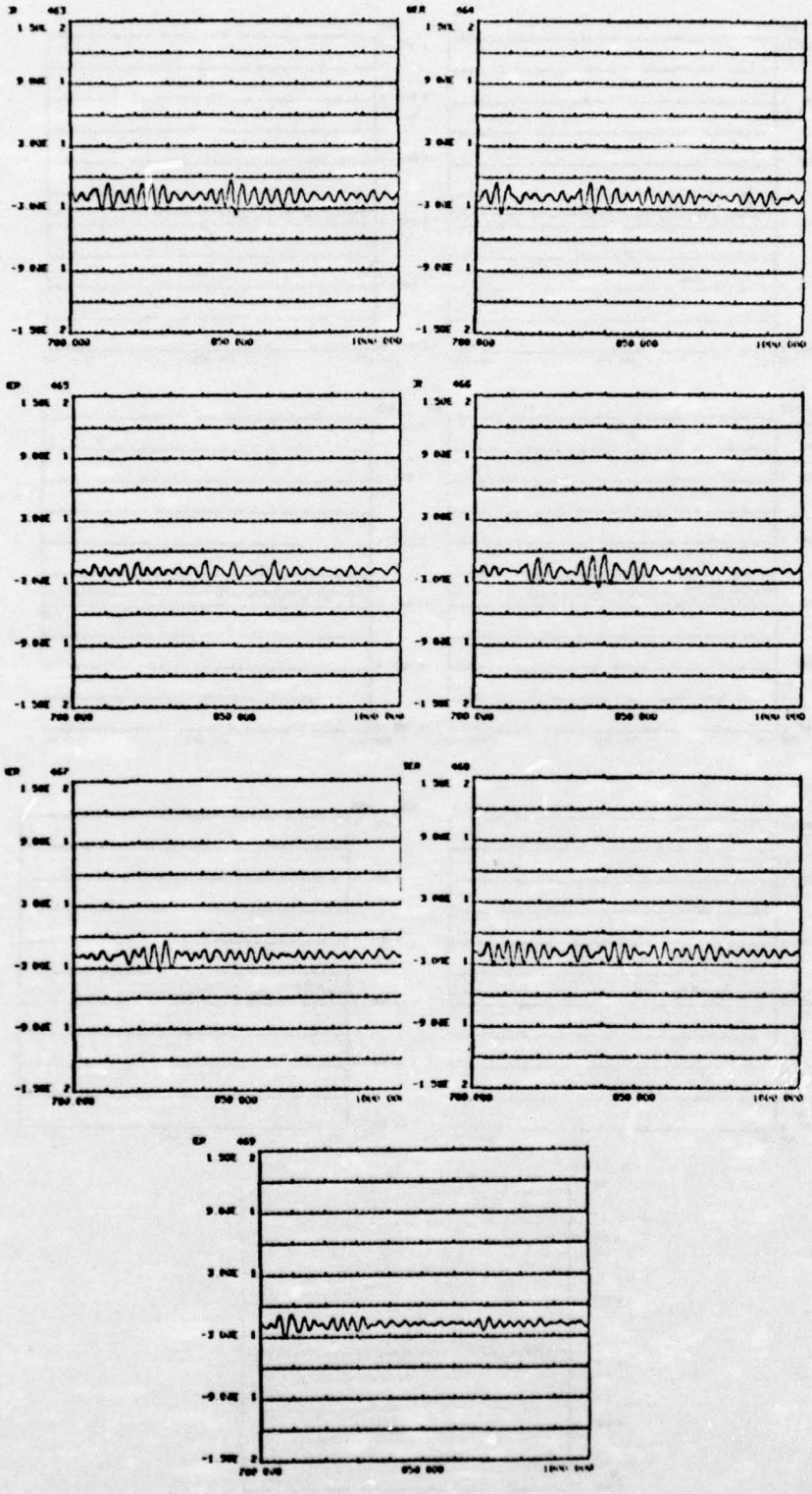
Specimen 06-027: Series 1



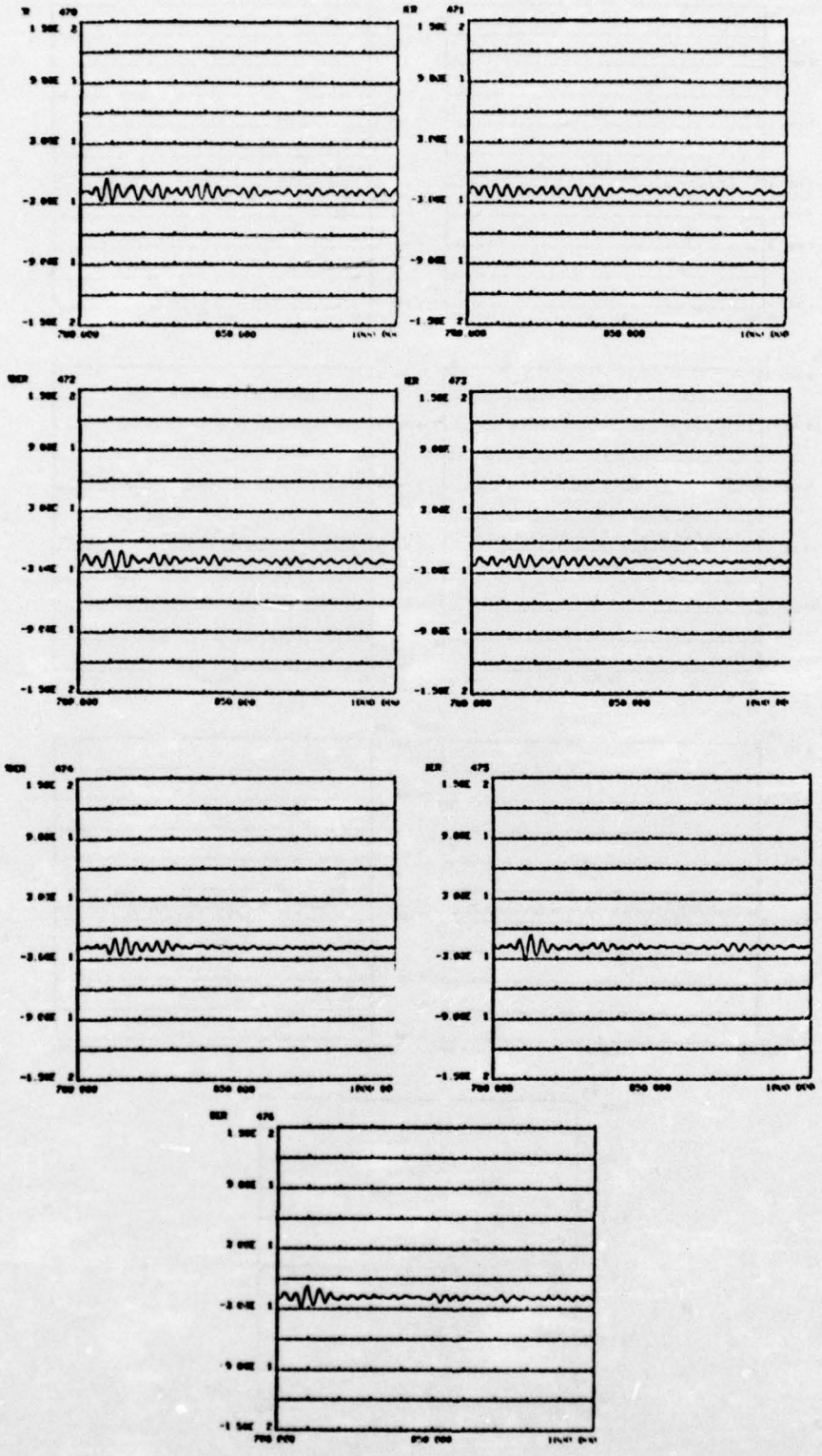
Specimen 05-022: Series 1
C-13



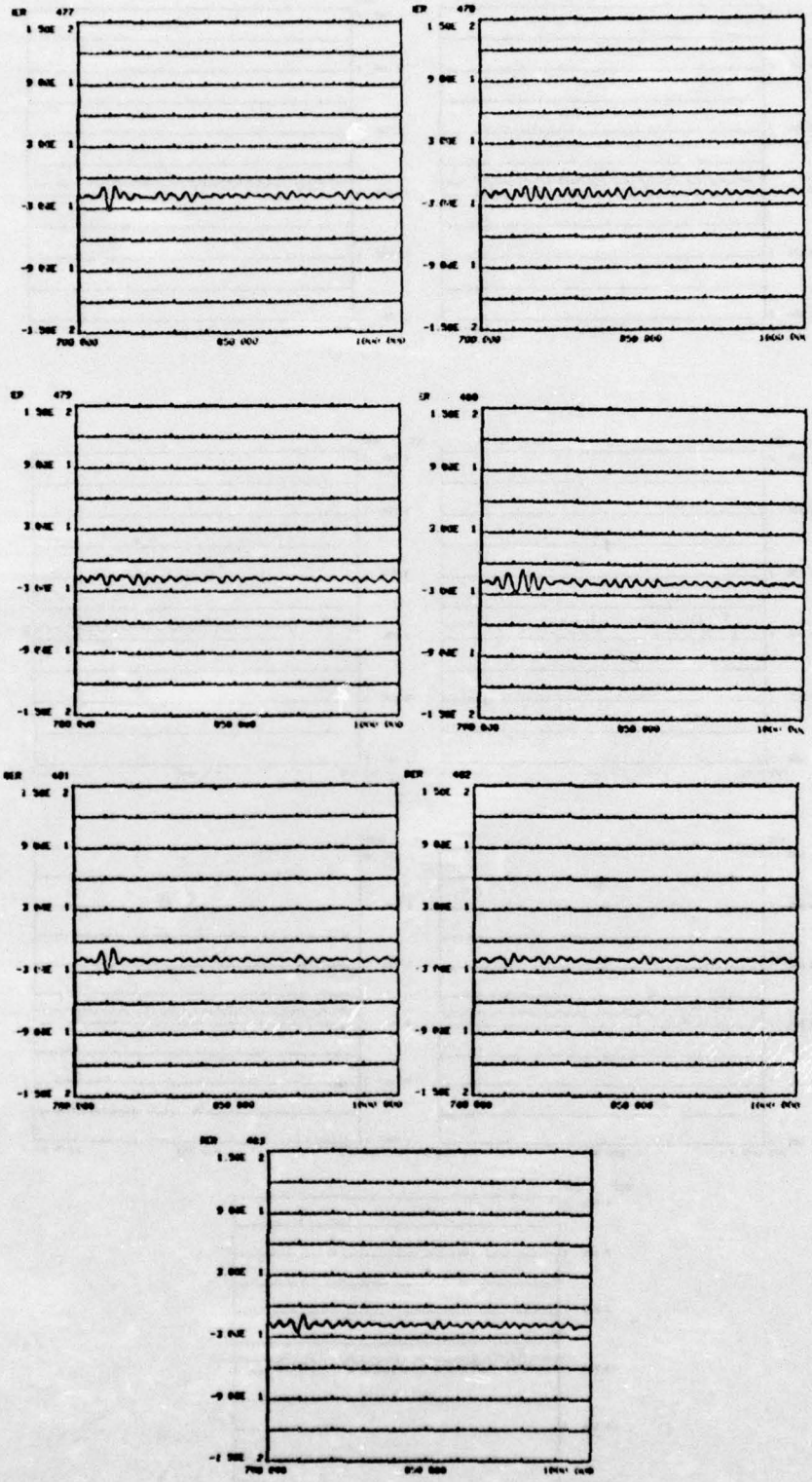
Specimen 04-018: Series 1



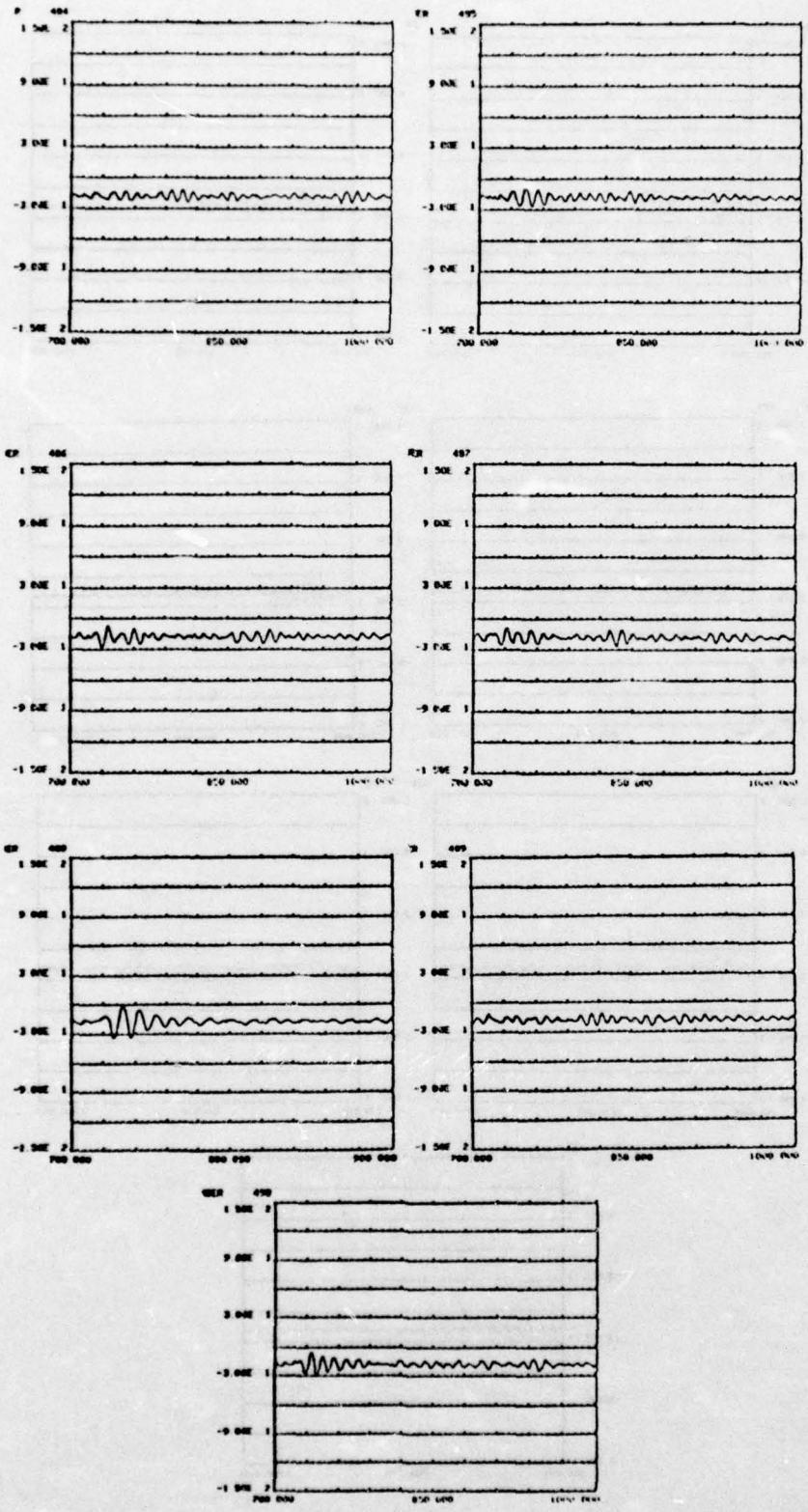
Specimen 03-014: Series 1



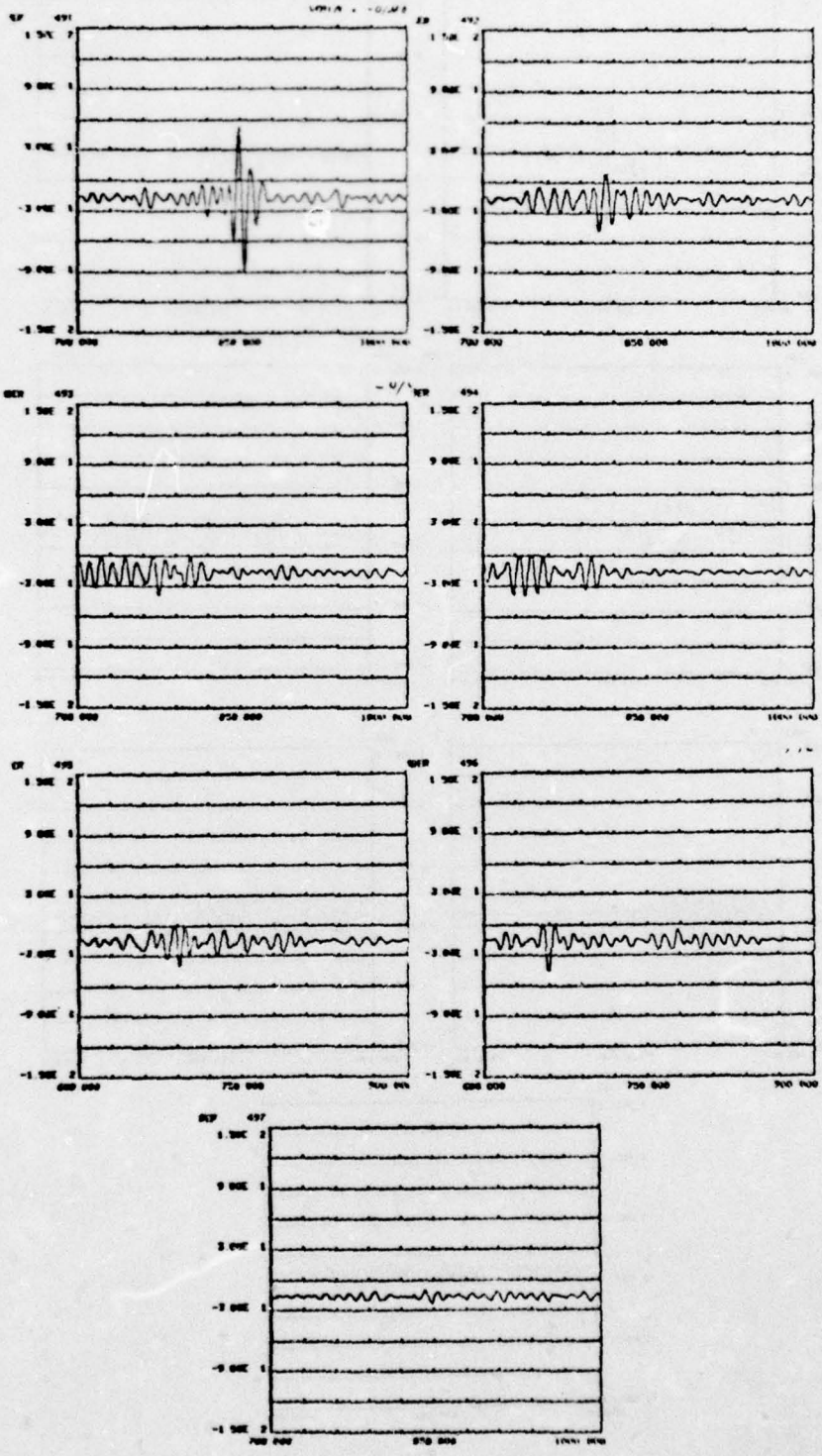
Specimen 02-011: Series 1



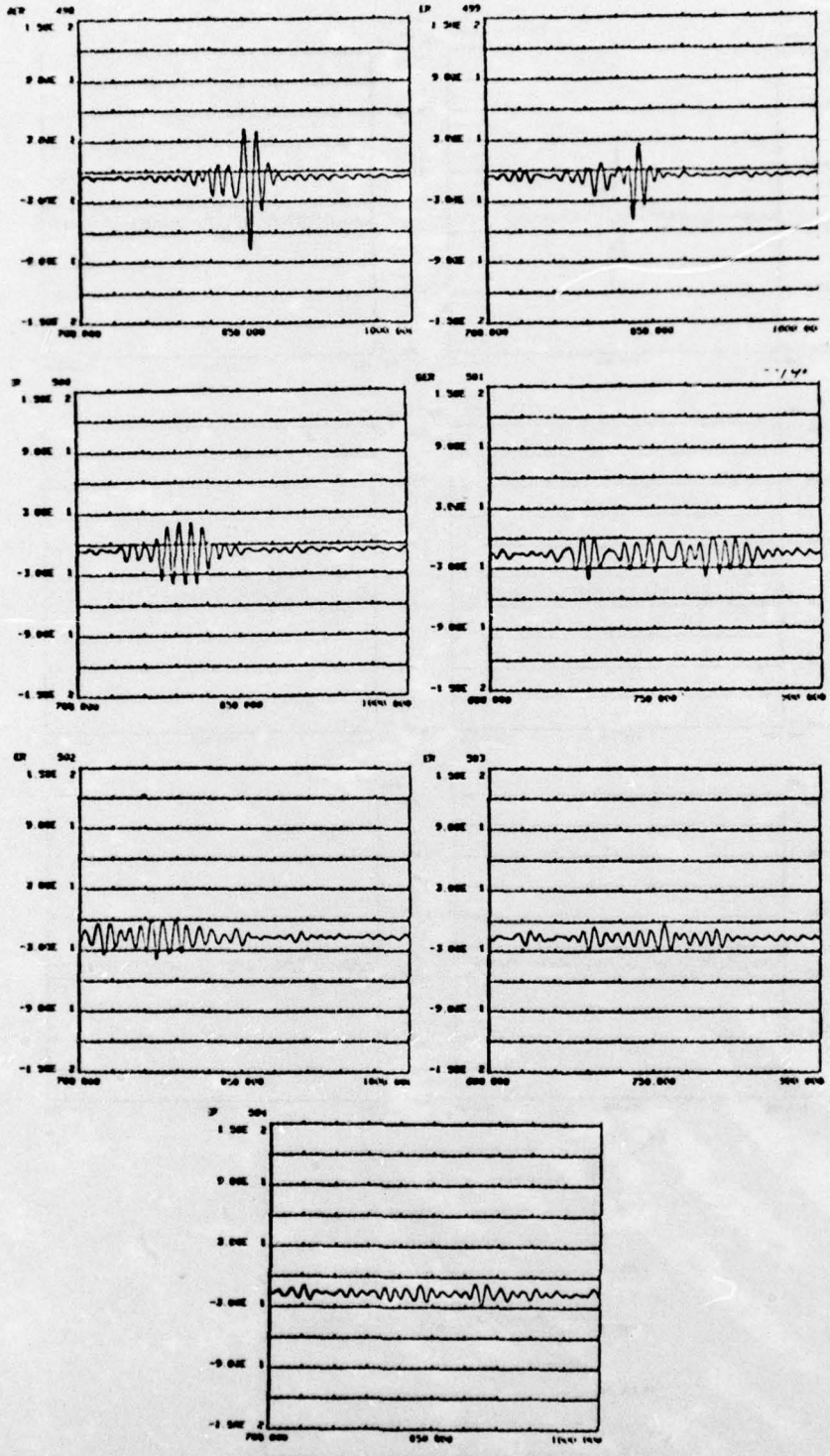
Specimen 01-000: Series 1



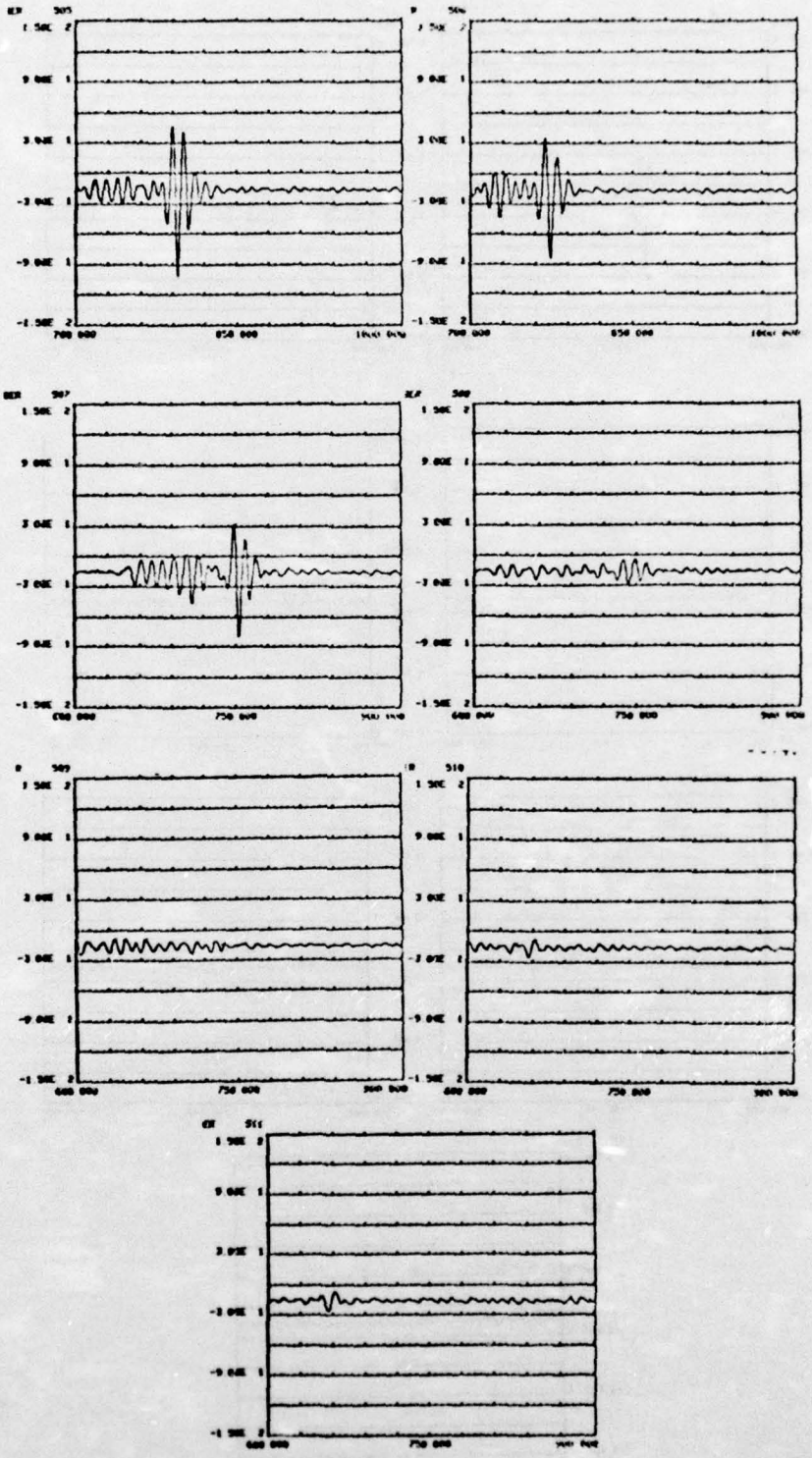
Specimen 00-000: Series 1



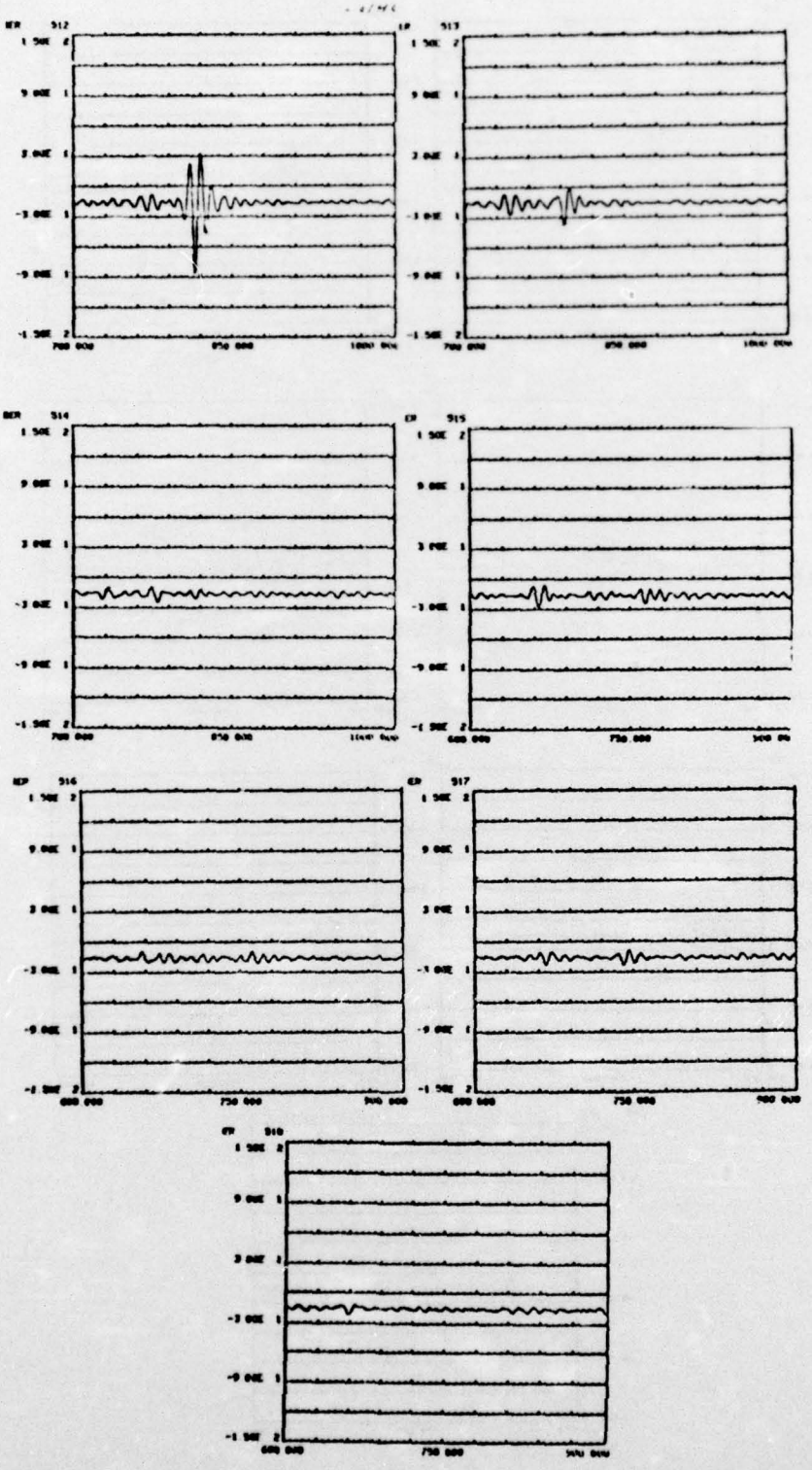
Specimen 15-270: Series 2



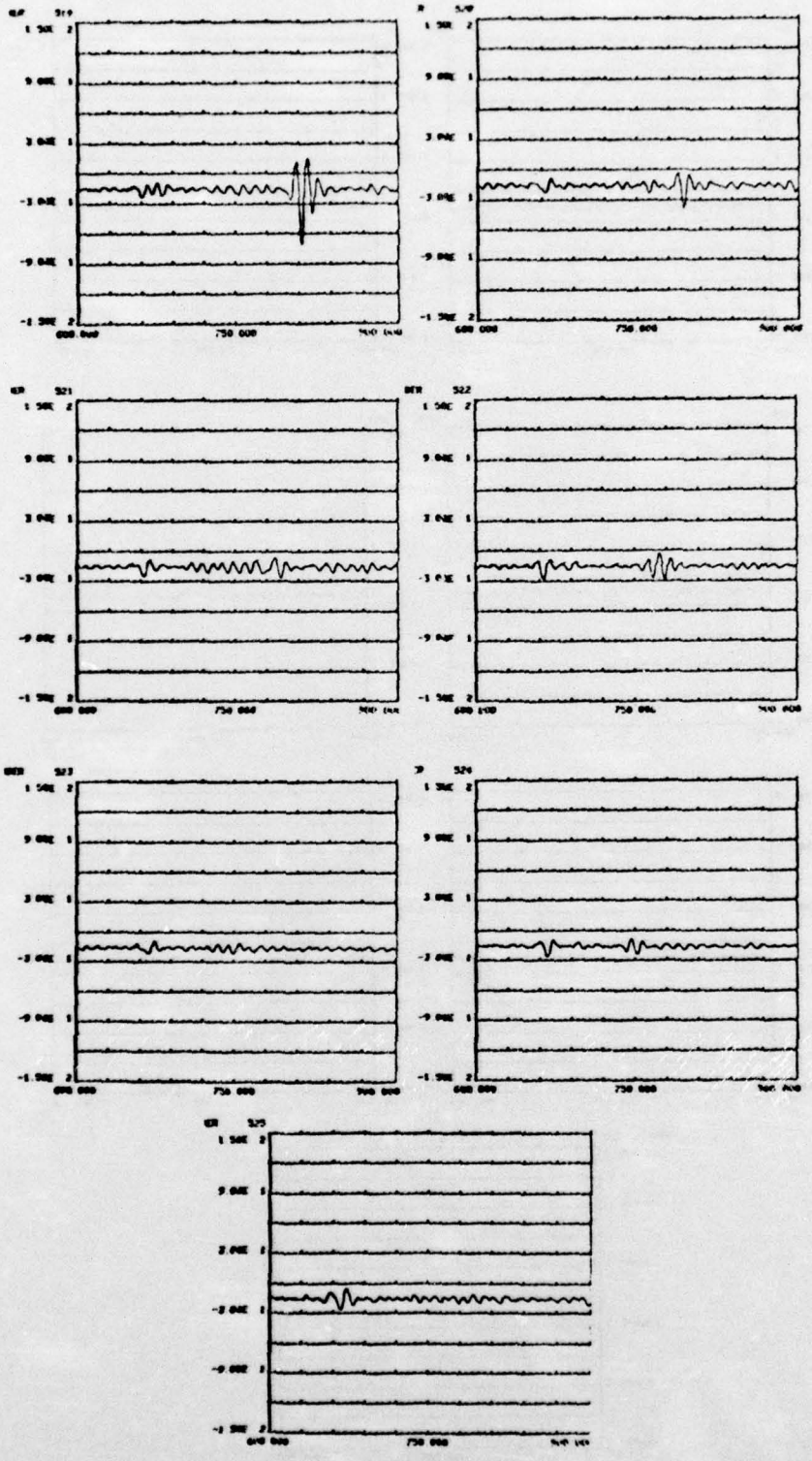
Specimen 14-192: Series 2



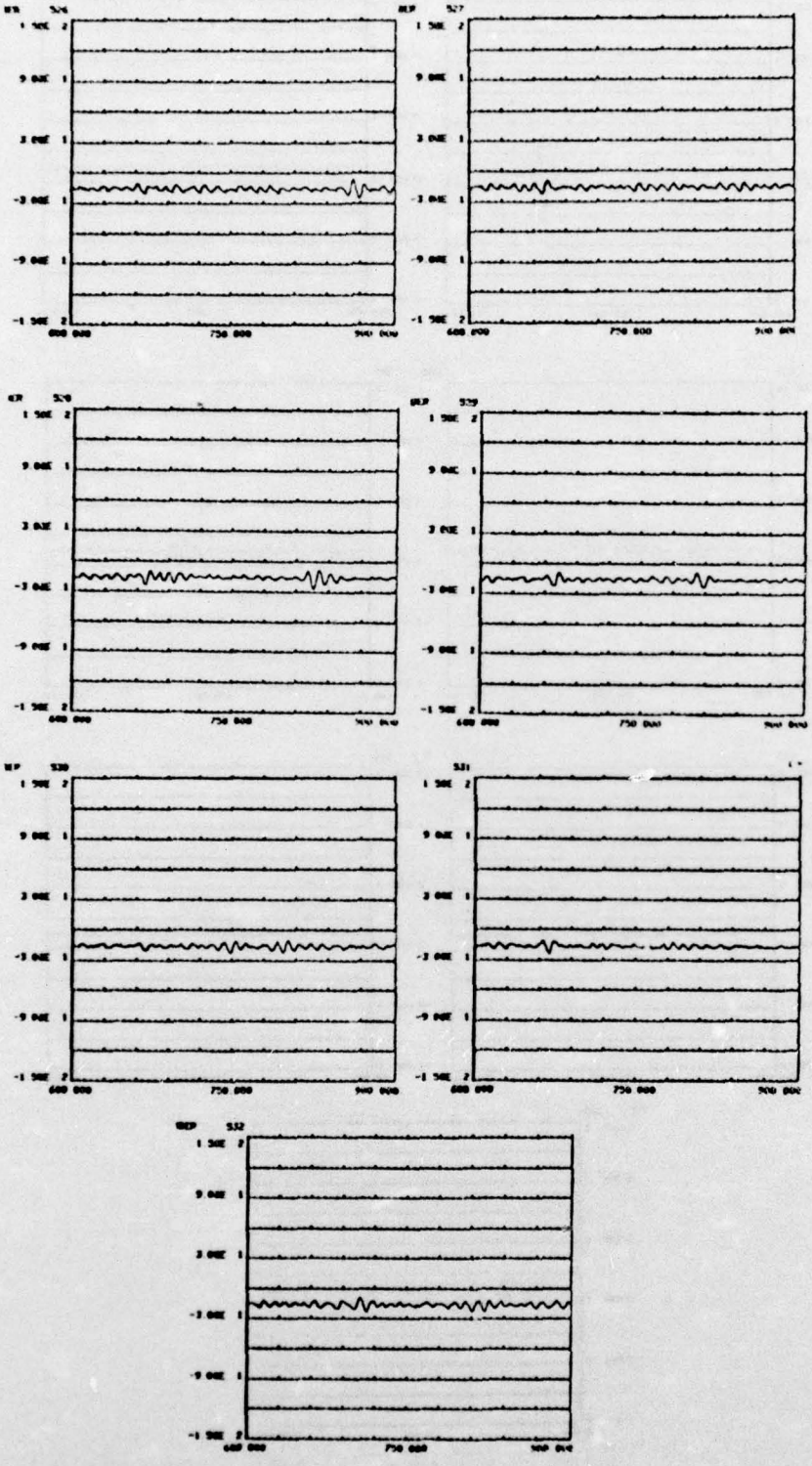
Specimen 13-150: Series 2



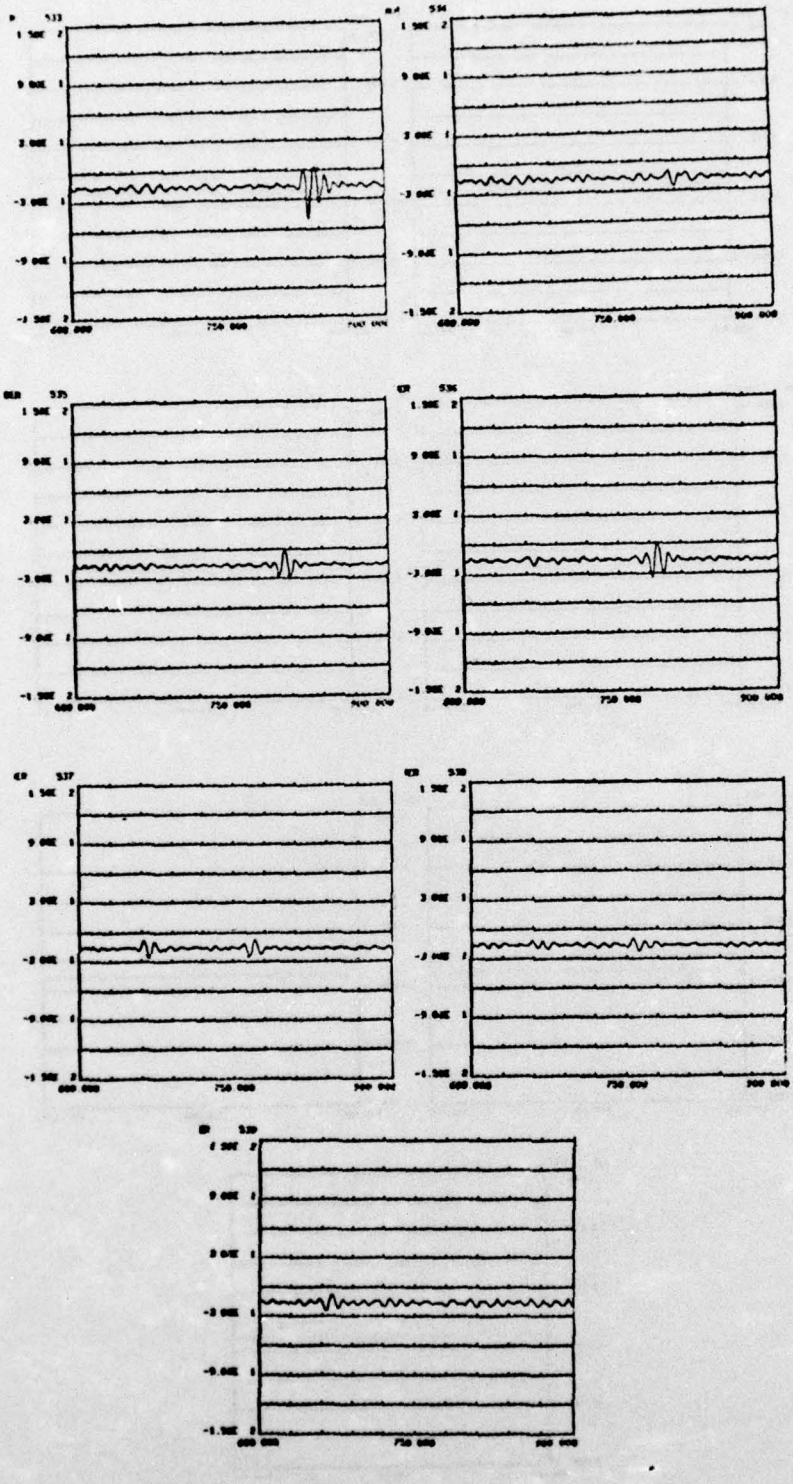
Specimen 12-113: Series 2



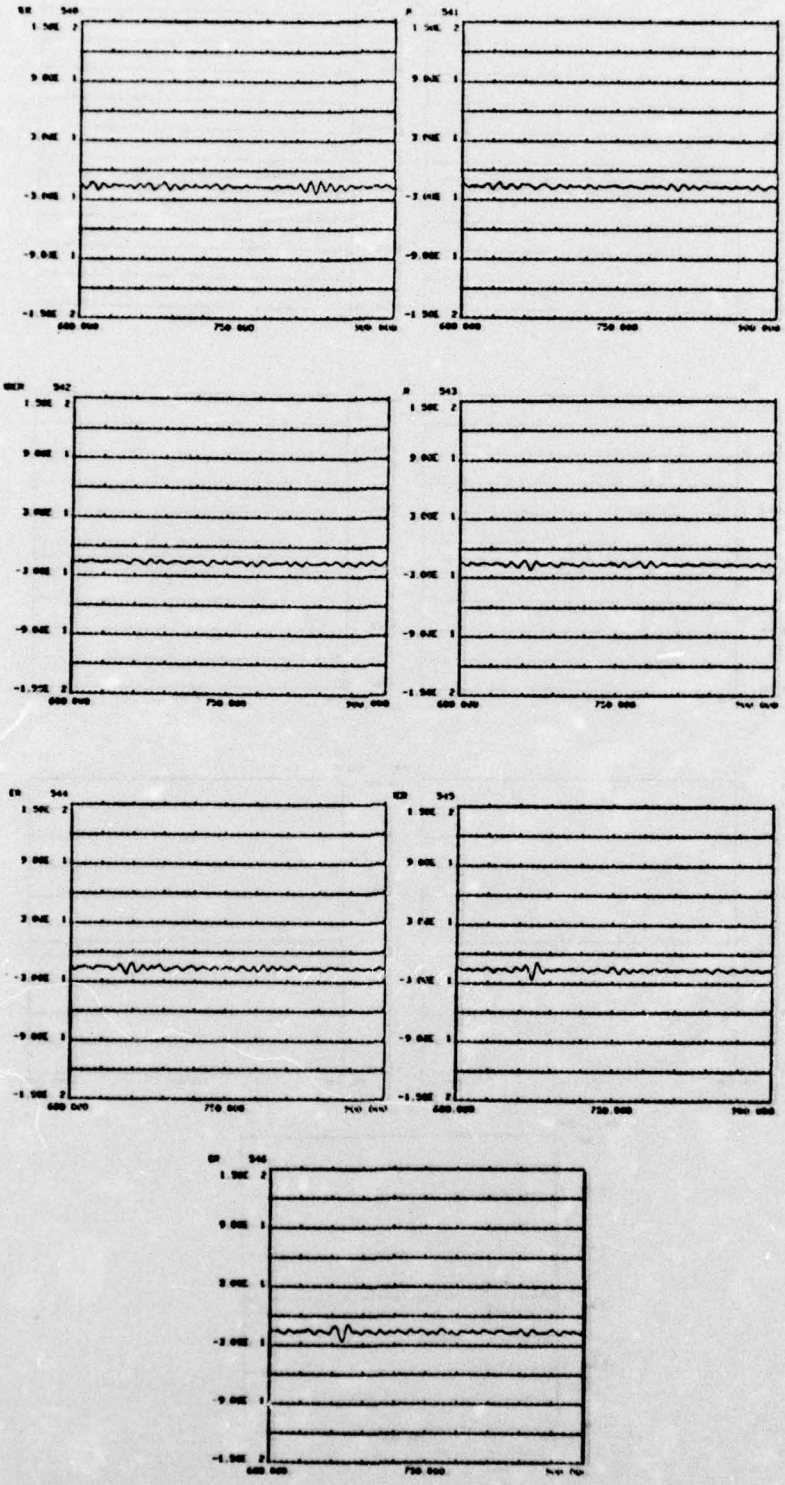
Specimen 11-093: Series 2



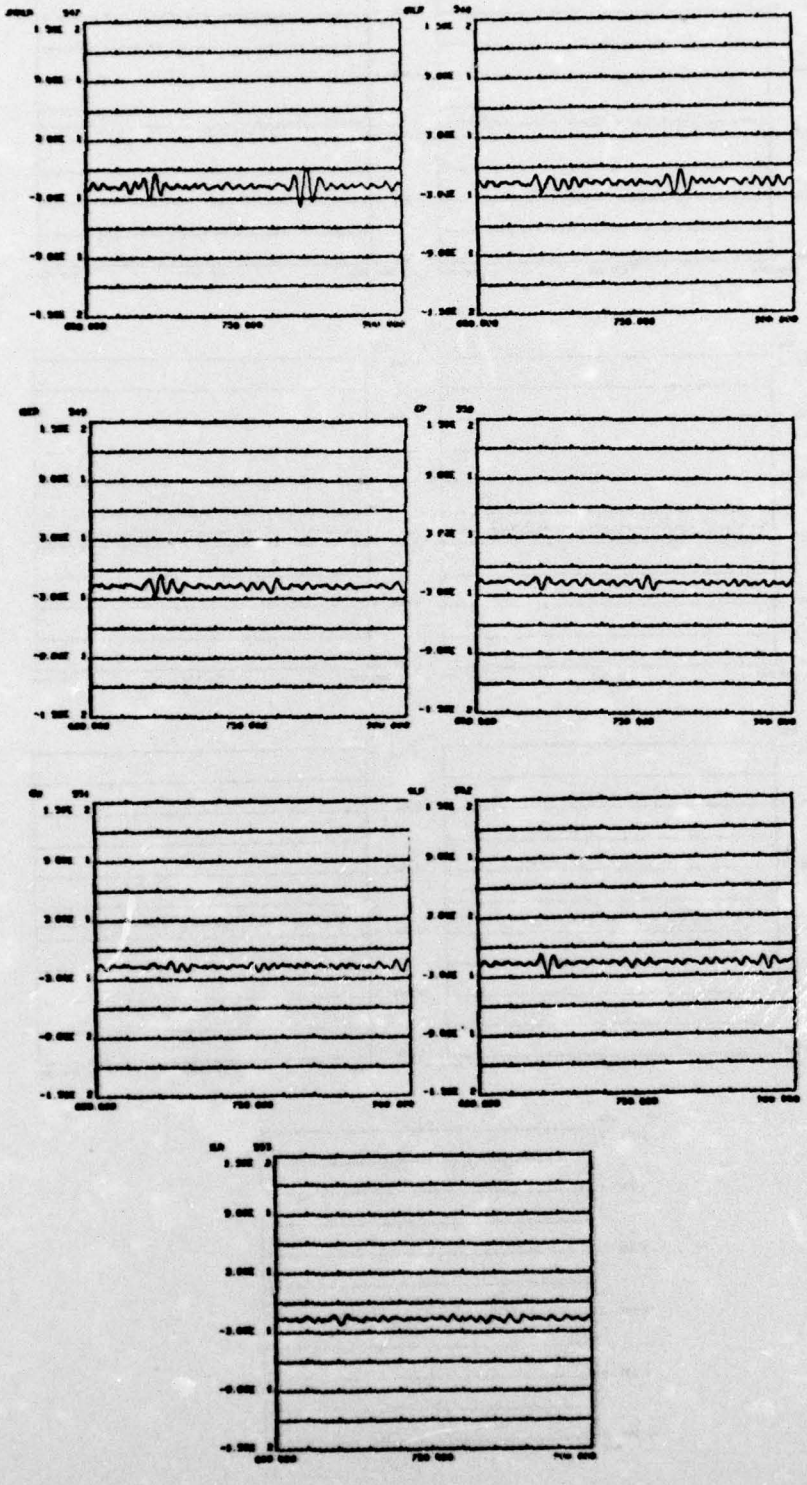
Specimen 10-073: Series 2



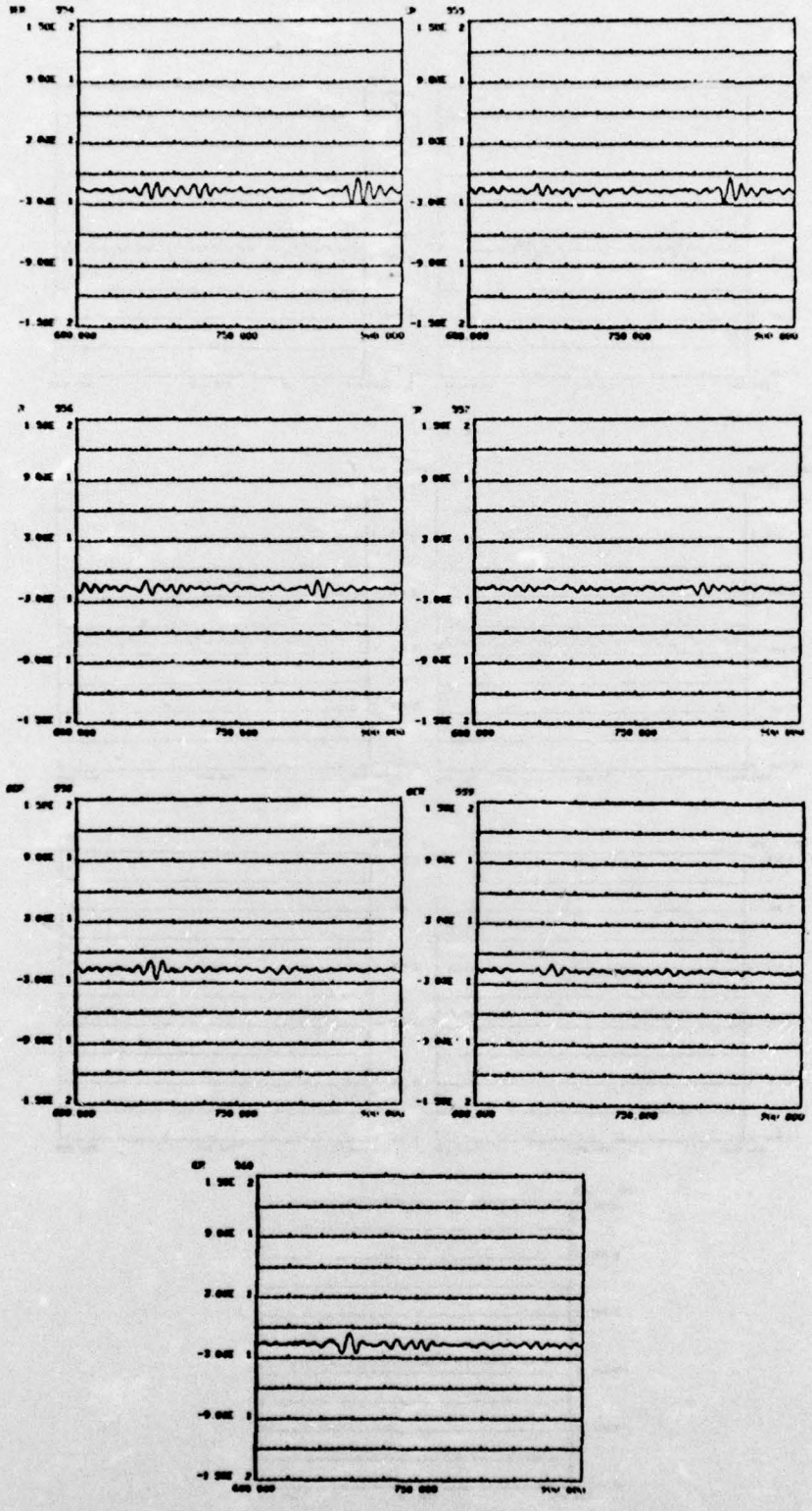
Specimen 09-054: Series 2



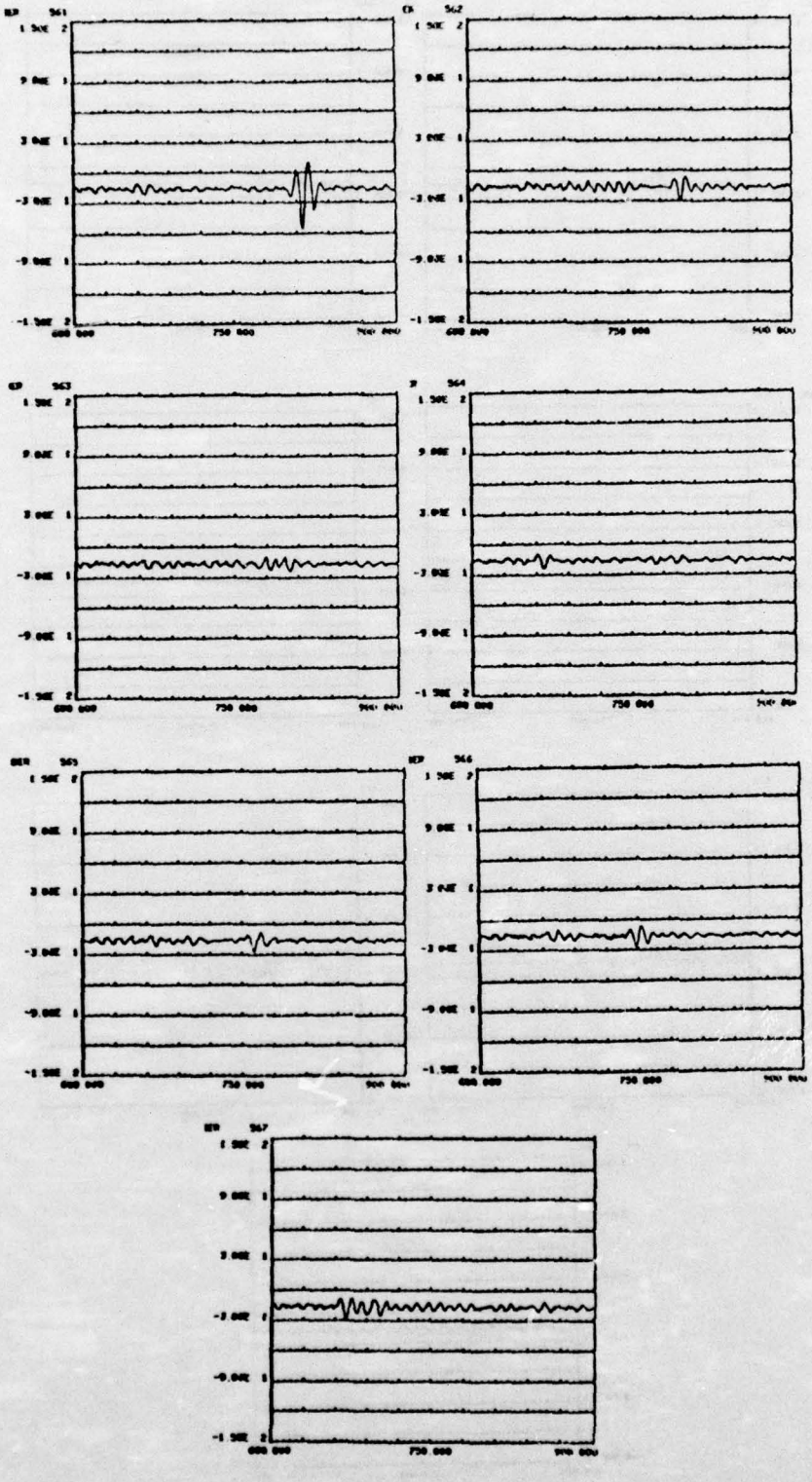
Specimen 08-048: Series 2



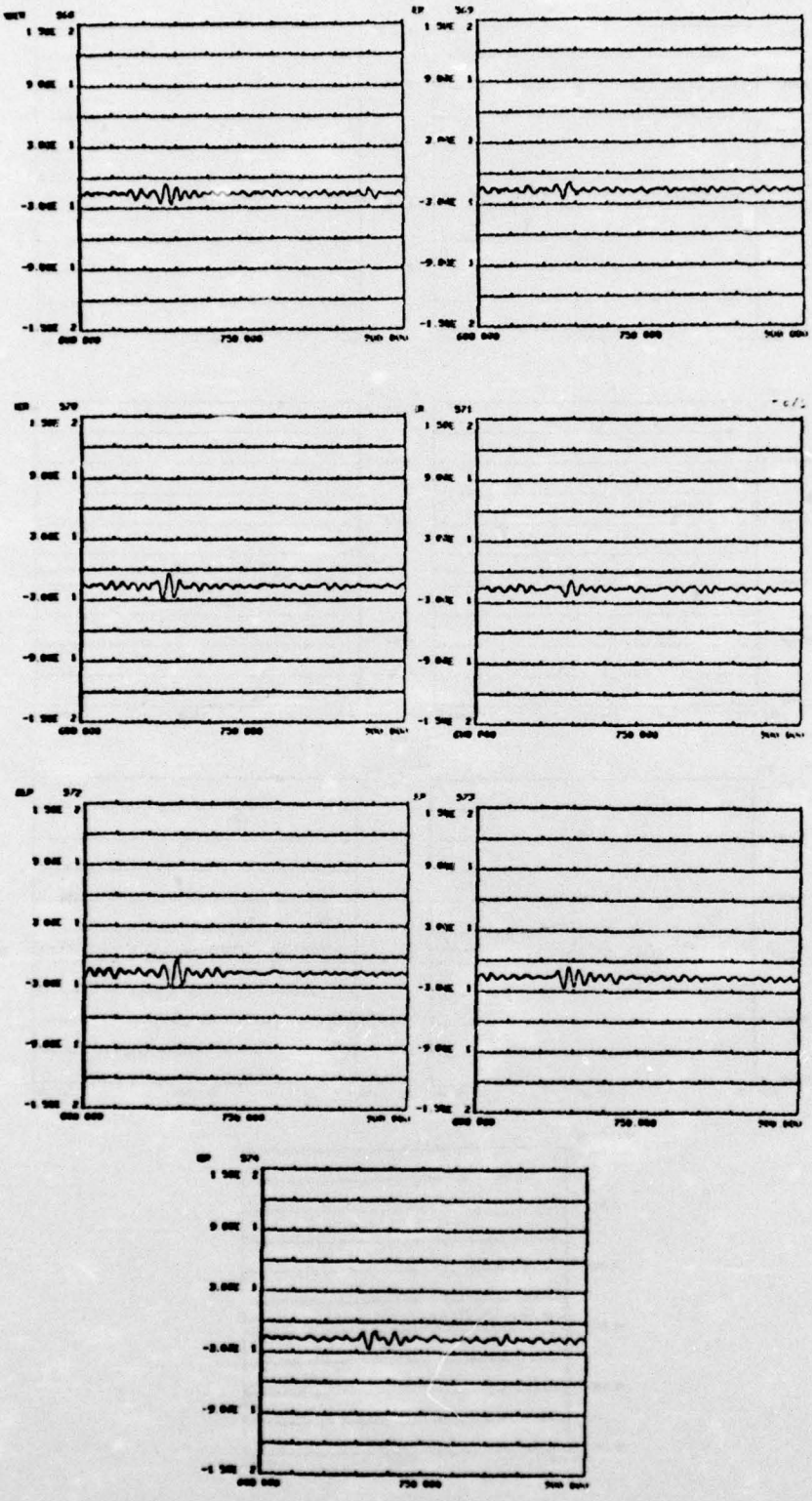
Specimen 07-039: Series 2



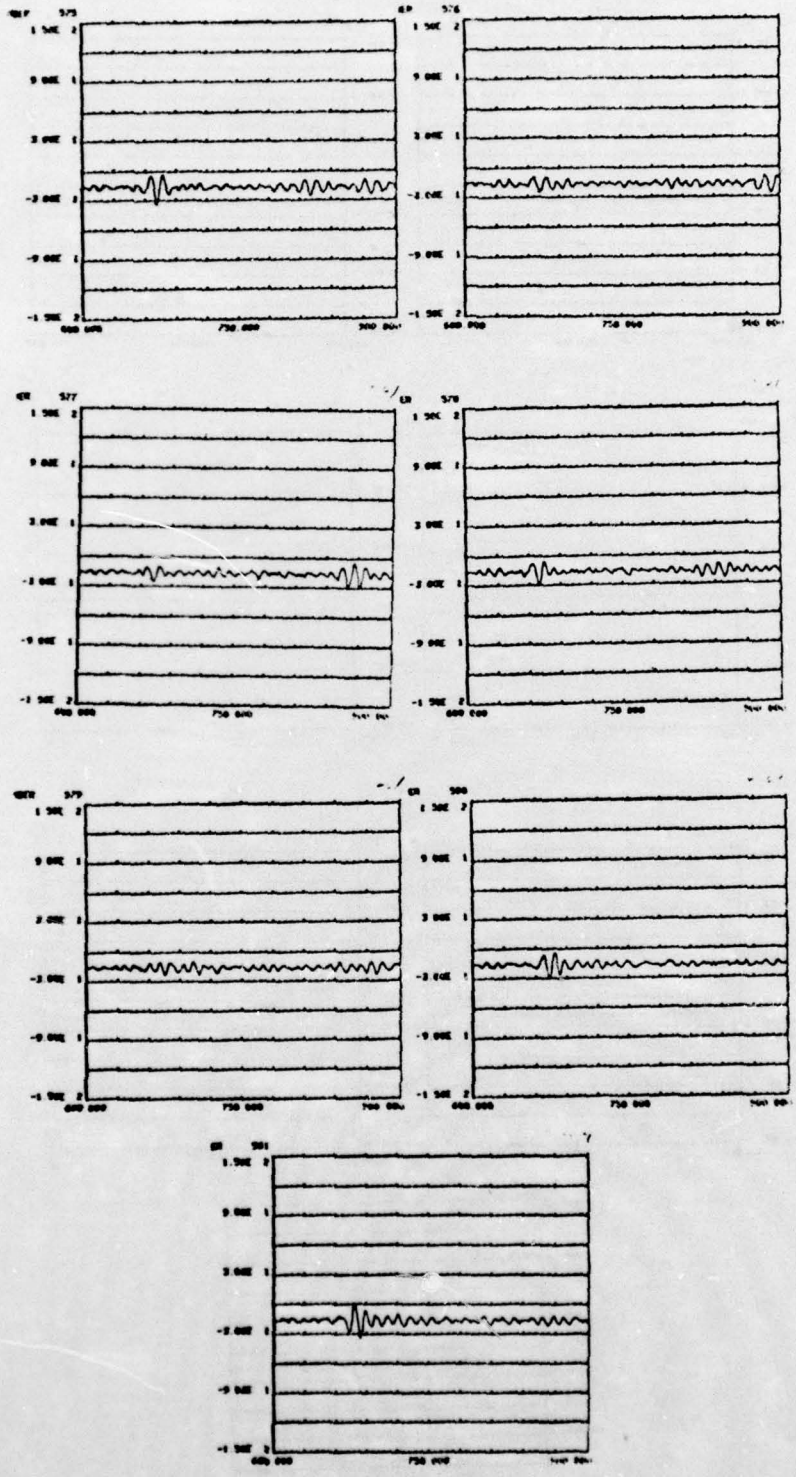
Specimen 06-027: Series 2
C-28



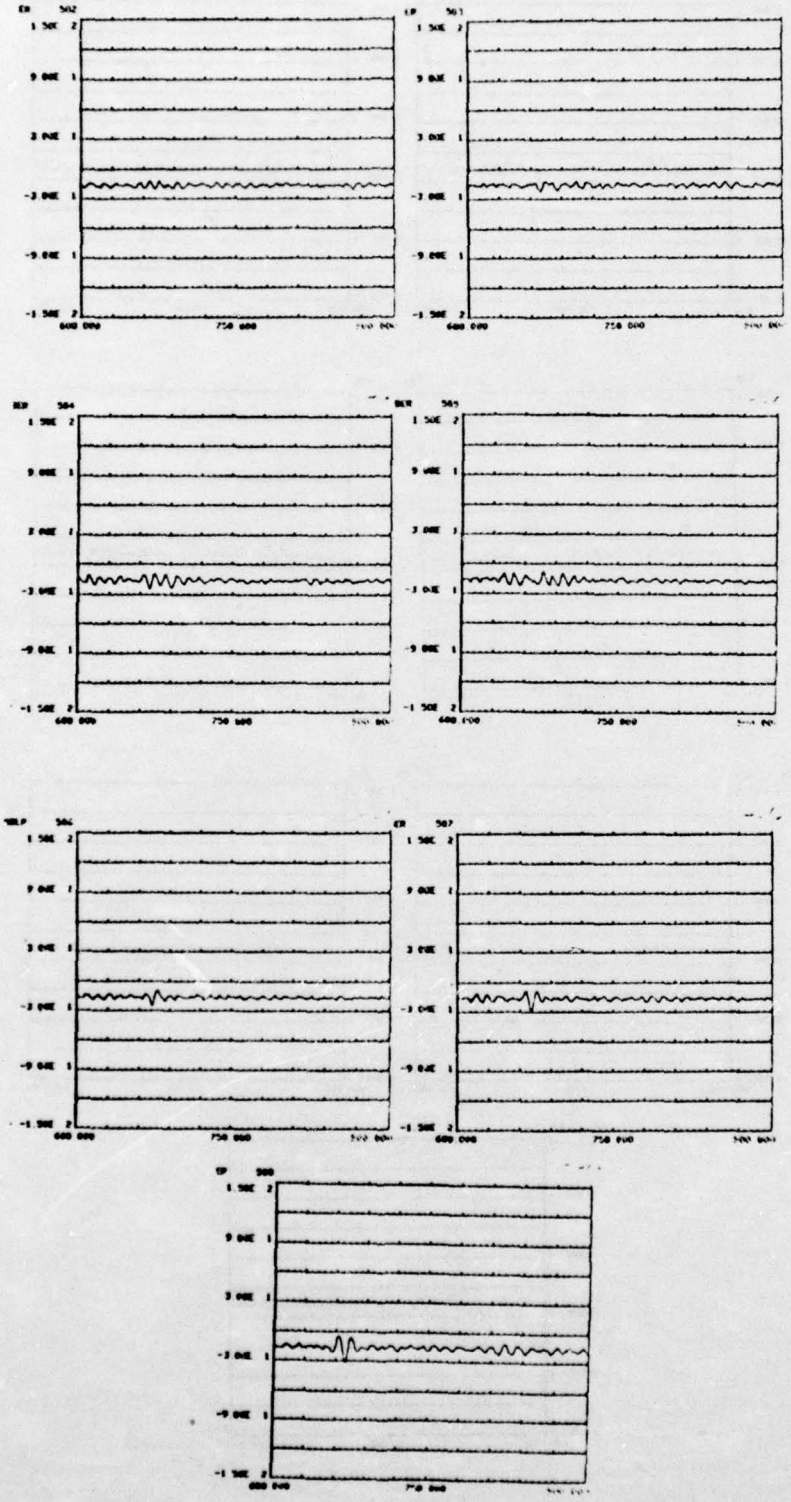
Specimen 05-022: Series 2



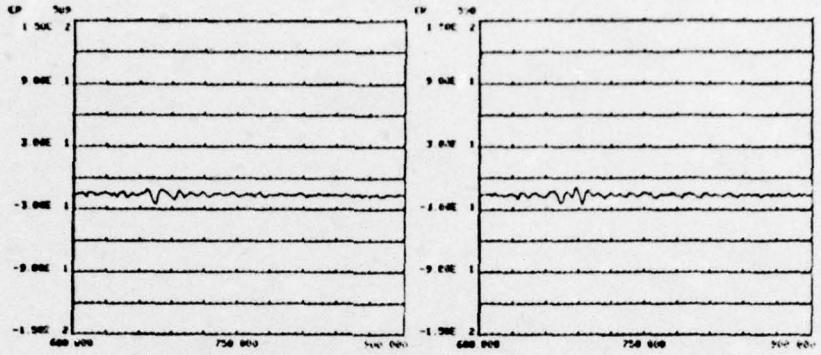
Specimen 04-018: Series 2
C-30

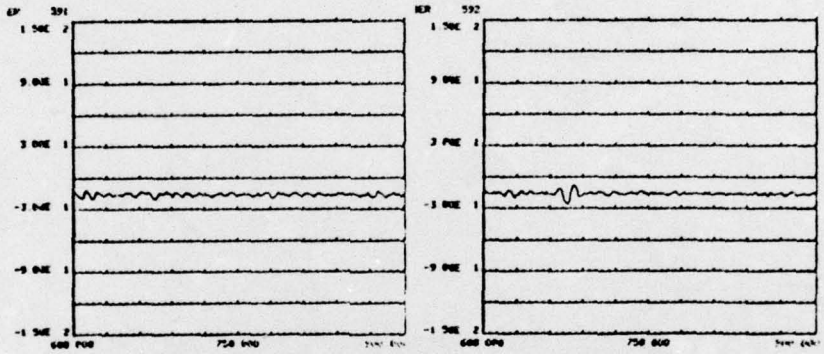


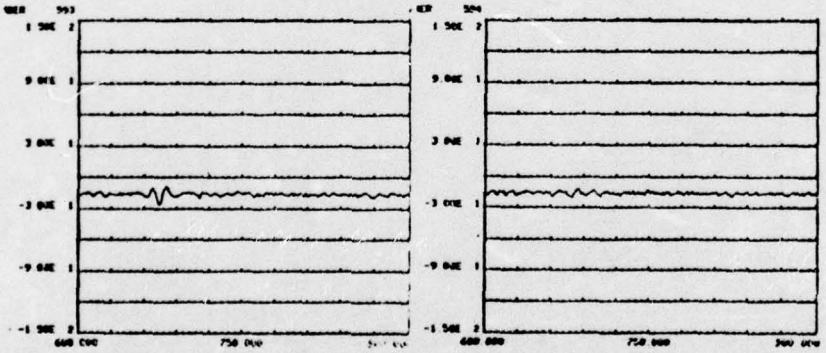
Specimen 03-014: Series 2

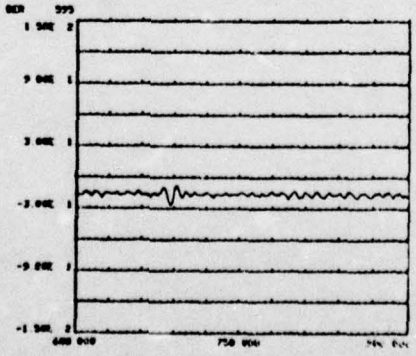


Specimen 02-011: Series 2









Specimen 01-000: Series 2

☆ U. S. GOVERNMENT PRINTING OFFICE: 1976 — 657-630/914